Duplex Emulsions for Healthy Foods

by

Aleksandra Pawlik

A thesis submitted to
The University of Birmingham
for the degree of
DOCTOR OF ENGINEERING

Department of Chemical Engineering
School of Engineering
The University of Birmingham
May 2012

Abstract

Clear scientific links between major diseases and diet are the main reasons for a change in food processing technology and products. In that sense, novel food structures such as duplex emulsions offer the possibility of reduction of the fat content, and also encapsulation of bio-components and their targeted delivery within the human body. Nevertheless, there are many stability problems associated with the manufacture of duplex emulsions. In this work the formulation and production/processing of food grade $W_1/O/W_2$ duplex emulsions were investigated in relation to emulsion's stability.

Initially, experiments were carried out to determine the formulation space and process parameters for the primary W_1/O emulsions. Stable emulsions with polyglycerol polyricinoleate could be produced when salt was contained in the internal water phase. The addition of salt alters the interactions between surfactant molecules in the adsorbed film resulting in visco-elastic film properties. These simple emulsions were then processed to construct duplex $W_1/O/W_2$ emulsions with and without balancing osmotic pressures with glucose. When the osmotic pressures were balanced, there was still a release of salt in storage. The extent and rate of release was proportional to glucose concentration over a storage period of 60 days.

Duplex emulsions are shear-sensitive and high shear stresses during the secondary emulsification could lead to their damage and hence release of the encapsulated ingredients. To investigate how the emulsification process influences the droplet size and stability of duplex $W_1/O/W_2$ emulsions, three techniques have been used for the secondary emulsification: Shirasu Porous Glass (SPG) cross-flow membranes, SPG rotating membrane and high-shear mixer. Duplex emulsion droplet size and salt encapsulation were both

investigated by modifying the emulsification conditions inherent for each technique: cross-flow velocity (CFV) and trans-membrane pressure (TMP) for the cross-flow membrane, rotational velocity (RV) and TMP for the rotating membrane, and mixing time for the high-shear mixer. The droplet size increased with TMP and decreased with both CFV and RV. It was shown that the amount of salt released during storage depends on the emulsification technique (up to ~20 % for the cross-flow membrane, ~13 % for the high-shear mixer and ~8 % for the rotating membrane). The differences in salt release were explained in terms of emulsions droplet size and interfacial properties of adsorbed surfactant molecules.

The SPG rotating membrane was identified as a promising tool for the secondary emulsification step in the production of duplex emulsions, therefore more detailed work was performed to investigate the potential of this technique. Droplet sizes of simple oil-in-water emulsions were independent of the dispersed phase volume, increasing with the viscosity of the continuous phase, size of the membrane pores and TMP. It was also shown that droplet size could be controlled by the concentration and properties of an emulsifier.

Acknowledgements

I am very grateful to Professor Ian Norton, my supervisor, for encouraging, teaching and motivating me throughout these years. I want to thank Prof Steve Moore, Dr Phil Cox, Dr Richard Greenwood, Dr Fotis Spyropoulous and Dr Shad Siddiqui for their scientific contribution towards this thesis and for correcting my endless drafts.

I am very thankful to EPSRC, the University of Birmingham and Unilever Ltd. for giving me the opportunity to carry out this work. I have greatly benefited from this experience in so many ways.

I would also like to thank all my Colleagues for their support and for letting me to pick their brains. And for the fun I had working with them.

Special thank you to my Friends in Poland and those, whom I have met here in the UK. I owe them a lot for all the great moments we had together and their constant encouragement.

Thank you to Roman for his great help, support and putting up with me while completing this work.

Dziękuję również moim kochanym Rodzicom i Braciom za wiarę we mnie, nieustające wsparcie i zainteresowanie tym co robię.

Table of Content

List of Figures

List of Tables

Nomenclature

Symbols

Symbol	Unit	Definition
A	m^2	Interfacial area
A_m	m^2	Membrane surface area
C_g	M	Concentration of glucose
C_{Na+}	M	Concentration of Na^+ ions
C_{Cl-}	M	Concentration of Cl^- ions
$D_{3,2}$	m	Surface-weighted (Sauter) droplet diameter
D_m	$m^2 \cdot s^{-1}$	Diffusion coefficient
D_h	m	Hydraulic diameter of the cross-flow membrane annulus
D	m	Diameter of the impeller
d_d	m	Diameter of the droplet
d_p	m	Diameter of membrane pore
f_F	-	Fanning friction factor
ΔG	J	Gibbs free energy
J_d	$m \cdot s^{-1}$, $L \cdot m^{-2} \cdot h^{-1}$	Dispersed phase flux
k_B	$m^2 \cdot kg \cdot s^{-2} \cdot K^{-1}$	Boltzmann constant
k_c	$S \cdot cm^{-1}$	Conductivity of the continuous phase
k_d	$S \cdot cm^{-1}$	Conductivity of the dispersed phase
k_e	$S \cdot cm^{-1}$	Conductivity of emulsion
M_t	g	Total mass of salt originally encapsulated in the internal water
M_r	g	Mass of salt that migrated to the external water phase
n	mole	Number of moles
N_m	-	Number of molecules
P_c	Pa	Critical pressure
P_L	Pa	Laplace pressure
Q_d	$kg \cdot h^{-1}$	Mass flow rate of the dispersed phase
r	m	Radius of a diffusing particle
R	m	Radius of a spherical droplet
R_i	m	Radius of the rotating membrane
R_o	m	Radius of the emulsification cylinder
T	K	Absolute temperature
v	$m \cdot s^{-1}$	Cross-flow velocity

Greek letters

Symbol	Unit	Definition
α	-	Contact angle
γ	$J \cdot m^{-2}$ or $N \cdot m^{-1}$	Interfacial tension
$\dot{\gamma}$	s^{-1}	Shear rate
δ	m	Width of the gap
η_c	Pa·s	Continuous phase viscosity
η_d	Pa·s	Dispersed phase viscosity
π	-	Pi number
ρ_c	$kg \cdot m^{-3}$	Continuous phase density
ρ_d	$kg \cdot m^{-3}$	Dispersed phase density
τ	Pa	Shear stress
τ_w	Pa	Wall shear stress
υ	$m^2 \cdot s^{-1}$	Kinematic viscosity
φ	-	Dispersed phase volume fraction
ω	$rad \cdot s^{-1}$	Angular velocity

Abbreviations

Abbreviation	Definition
CFV	Cross-flow velocity
CMC	Critical micelle concentration
CTMP	Critical trans-membrane pressure
HLB	Hydrophilic-lipophilic balance
ME	Membrane emulsification
O/W	Oil-in-water emulsion
O/W/O	Oil-in-water-in-oil emulsion
PGPR	Polyglycerol polyricinoleate
Re	Reynolds number
RV	Rotational velocity
SB	Soybean oil
SF	Sunflower oil
SPG	Shirasu porous glass
TMP	Trans-membrane pressure
WPI	Whey protein isolate
W/O	Water-in-oil emulsion
W/O/W	Water-in-oil-in-water emulsion
XG	Xanthan gum

1 Introduction

1.1 Motivation and purpose

Obesity is now a global problem. World Health Organisation states, that currently the majority of the world's population lives in a country where overweight and obesity kills more people than being underweight. Globally, there are 1 billion overweight adults and 300 million obese with estimated 2.6 million deaths annually as a result of obesity related diseases (WHO, 2010). A fundamental cause of obesity and overweight state in people is an energy imbalance between calories consumed and expended. Thus, the demand for a balanced diet but with low energy density and functional food products, that address specific health benefits, is a pressing issue. With health and well-being as major drivers of the modern food industry, it is currently the consumers who tell food manufacturers what they prefer to eat; healthy, nutritionally balanced food with all of the taste and convenience of presently produced unhealthy food products. In this respect, it is a part of food structuring to provide structures that are generally acceptable and stable enough to resist changes during the shelf life of the product. Food engineers aim at generating products of desired properties from materials, whose individual properties are understood, and to do this in a cost effective way (Aguilera,1999).

Production of low energy density, nutritionally enriched food-grade delivery systems can be achieved through microstructuring of a product's matrix (Palzer, 2009). One such way to do this is with duplex emulsions. Duplex emulsions, also termed double or multiple emulsions, are emulsions with a complex microstructure, where dispersed droplets contain even smaller droplets inside. For example, the use of duplex water-in-oil-in-water ($W_1/O/W_2$) emulsions

allows for a substantial fat reduction as the dispersed oil phase is made up by water contained in the internal aqueous phase. Therefore, a reduction in fat without a change of droplet size or phase content can be made. Moreover, these systems can also be used to encapsulate and protect bioactive components, whilst delivering them to specific sites within the human body (*e.g.* mouth, stomach, small intestine *etc*.) (Lesmes & McClements, 2009).

Duplex emulsions are normally prepared in a two-step emulsification process. The primary emulsion is typically prepared under intense homogenisation conditions, in order to transform two immiscible fluids into an emulsion (Garti, 1997a), or to reduce the size of a pre-existing emulsion. In the food industry, this process is usually carried out using mechanical devices (*e.g*. high speed blenders, high-pressure homogenizers, colloid mills), where the dispersed phase is broken up by turbulent shear stresses. On the contrary, the secondary emulsification step has to be carried out under mild shear conditions, in order to avoid the rupture of the internal droplets (Dickinson & Akhtar, 2001; McClements, 2005). In the conventional turbulence based emulsification techniques (such as these used for the primary emulsification step) the repeated breakup of the emulsion droplets may lead to a considerable loss of the internal phase carrying the encapsulated ingredient. Using membranes for the secondary emulsification process offers the possibility of: (i) good control over droplet size and droplet size distributions, (ii) low energy consumption, and most importantly (iii) mildness of the process (important for temperature sensitive components and economic savings, Schadler & Windhab, 2006). It has been suggested (Aserin, 2008), that membrane emulsification enables high encapsulation yields of the internal droplets in the final product. Even though much work has been done (Mine *et al.*, 1996; Vladisavljević & Schubert, 2003; Vladisavljević *et al*., 2004; Scherze *et al.*, 2005; van der Graaf *et al.*, 2005; Vladisavljević *et al.*, 2006b), investigation of the influence of membrane emulsification parameters on the droplet size and

droplet size distribution in $W_1/O/W_2$ duplex emulsions, the encapsulation and release of marker compounds from these, remains scarcely explored (Okochi & Nakano, 1997; Scherze *et al.*, 2005; Vladisavljević *et al.*, 2006b). These issues will be addressed in this work, where a high-shear mixer and two membrane techniques (cross-flow and rotating membranes) are compared in a comprehensive study of duplex $W_1/O/W_2$ emulsions encapsulation properties.

Rotating membrane emulsification is a relatively new technique and there have been only a small number of publications on this subject (Aryanti *et al.*, 2006; Schadler & Windhab, 2006; Yuan *et al.*, 2009a). All the reported research focuses on stainless steel rotating membranes, which were successfully used in the manufacture of simple (and mostly coarse, Aryanti *et al.*, 2006 & Yuan *et al.*, 2009a) O/W emulsions, where processing parameters, membrane characteristics and emulsion composition were analysed in relation to the microstructure of the emulsion. In this work, potential advantages of SPG rotating membranes for the production of duplex $W_1/O/W_2$ and simple O/W emulsions are investigated.

Duplex emulsions are thermodynamically unstable and frequently a large part of the encapsulated inner phase is lost during emulsions processing or/and storage. It has also been reported that the overall stability of these structures essentially depends on the stability of the primary emulsion (Su *et al.*, 2006), which in turn is determined by the type and concentration of the emulsifiers used, the nature of the fat phase and any entrapped materials (encapsulant). This is particularly true if possible encapsulants are or include small electrolyte molecules that can rapidly diffuse across the oil layer (Dickinson *et al.*, 1994). This work focuses on factors determining the stability of the primary W_1/O emulsion as a prerequisite for the subsequent formation of stable duplex $W_1/O/W_2$ emulsions.

Mass transfer rates in $W_1/O/W_2$ emulsions for the migration of water and/or water-soluble materials through the oil film are dominated by two major release mechanisms: (i) the "swelling-breakdown" mechanism and (ii) diffusion/permeation through the oil membrane. In the second mechanism, the molecules either pass through thin lamellae of surfactant which partially form in the oil layer due to fluctuations in its thickness, or diffuse across the oil layer *via* incorporation in "reverse micelles" (Cheng *et al.*, 2007a). It is also believed, that any osmotic pressure imbalance provides a driving force for the flux of water and water soluble material between the two aqueous compartments (Mezzenga *et al.*, 2004). Such mass transfer could lead to emulsion destabilisation, but for certain food applications controlled release of encapsulated substance can be considered beneficial. However, up to date there is a lack of understanding of how different formulation parameters of duplex emulsions affect the kinetics of destabilisation and what effect the presence and extent of the osmotic pressure has (Aserin, 2008). This work investigates how osmotic pressure imbalance affects transport of water and encapsulated electrolyte across the oil membrane in duplex $W_1/O/W_2$ emulsions.

1.2 Objectives

As discussed throughout this Chapter, duplex emulsions have the potential to be used for the formulation of novel healthy foods. Therefore, the need to understand the formulation and processing of these complex structures is the major driving force for this research. This is in line with Unilever's mission "to meet the everyday needs of people everywhere for tasty, healthy and nutritious food", which includes developing new products that have clear and positive health benefits, and are pleasant to eat (Unilever, 2012). Duplex emulsions have the potential to be such products, therefore obtaining better control over parameters controlling their stability and exploring alternative production methods for these complex structures, may result in a commercial production of duplex-emulsion-based-healthy-foods.

The overall purpose of this study was to investigate the parameters that impact the stability and encapsulation efficiency of $W_1/O/W_2$ duplex emulsions as potential food products. Specifically, to build a mechanistic understanding that underpins the following processes:

- Production of duplex $W_1/O/W_2$ emulsions using food grade materials,
- Formulation and processing parameters determining stability of the primary W_1/O emulsions,
- Formulation of duplex $W_1/O/W_2$ emulsions with structured water phases (*e.g.* to induce an osmotic pressures imbalance) to study the release of the encapsulated marker compound during processing and storage (*i.e.* under usage conditions),
- Influence of the secondary emulsification process on the short- and long-term stability of duplex emulsions (*i.e.* stability that is measured by changes in emulsions droplet size and encapsulation properties); high-shear mixer and two membrane techniques as a probe,
- Novel routes for the production of emulsions; membrane emulsification.

1.3 Thesis layout

Chapter 2 gives a theoretical background of the research area enclosed in this thesis. Additionally, relevant work conducted so far in the area of duplex emulsions and emulsification methods have been critically reviewed, emphasising main ideas behind the applied research directions in this thesis.

Chapter 3 presents detailed information on the materials and methods used in the experimental work. Also analytical methods used for the characterisation of samples' microstructure are described.

In the first part of **Chapter 4,** the experiments to determine the formulation space and process parameters for primary water-in-oil (W_1/O) emulsions are presented. Next, the parameters that impact the stability and encapsulation efficiency of duplex $W_1/O/W_2$ emulsions containing the marker compound were investigated. The effect of osmotic pressure, emulsification time and surfactant concentration is highlighted.

The following **Chapter 5,** investigates the effects of the secondary emulsification step (*i.e.* rotor-stator method, cross-flow membrane emulsification and rotating membrane emulsification) on the droplet size, droplet size distribution, yield of encapsulation and prolonged release of salt from duplex $W_1/O/W_2$ emulsions.

In **Chapter 6** the rotating membrane technique is investigated in more details. The effect of membrane pore size, rotational velocity, trans-membrane pressure, viscosity of the continuous phase, concentration and type of emulsifier are highlighted.

Finally **Chapter 7** summarises the main findings presented in this thesis and gives suggestions for further/complimentary research.

The results obtained during this study have been published as follows:

Pawlik, A., Cox, P.W. and Norton, I.T. (2010). Food grade duplex emulsions designed and stabilised with different osmotic pressures, *Journal of Colloids and Interface Science*, 352, 59 – 67.

Pawlik, A. & Norton, I.T. (2012). Encapsulation stability of duplex emulsions prepared with SPG cross-flow membrane, SPG rotating membrane and rotor-stator techniques – a comparison, *Journal of Membrane Science*, 415-416, 459-467

Pawlik, A.K. & Norton, I.T. (2012). SPG rotating membrane technique for production of food grade emulsions. *Journal of Food Engineering, Accepted Manuscript*

The results obtained during this study have been presented as follows:

Pawlik, A., Moore, S. & Norton, I.T. (June 2009). Duplex emulsion stability during emulsification process; effect of glucose on salt migration, *5th International Symposium on Food Rheology and Structure*, ETH Zurich, Switzerland.

Pawlik, A., Moore, S. & Norton, I.T. (July 2009). Duplex emulsion stability during emulsification process; effect of glucose on salt migration, *Gums and Stabilisers for the Food Industry 15*, Wrexham, North Wales.

Pawlik, A., Cox, P.W. & Norton, I.T. (July 2010). Food grade duplex emulsions designed and stabilised with different osmotic pressures, *Formula VI*, Stockholm, Sweden.

Pawlik, A., Cox, P.W. & Norton, I.T. (October 2010). Duplex emulsions for healthy foods, *World Congress on Emulsions*, Lyon, France.

2 Literature Review

2.1 Emulsions

Emulsions are dispersions of two immiscible liquid phases, one of which is the continuous phase, while the other is the dispersed phase (Aguilera, 1999). Simple emulsions are of two different types: *direct emulsions* (*e.g.* milk, cream, mayonnaise, cake batter) are dispersions of oil into water (O/W), whereas *inverse emulsions* (*e.g.* margarine, butter) are dispersions of water into oil (W/O). More complex emulsions termed *multiple emulsions* have also been produced and investigated (Garti, 1997a). The simplest multiple emulsion - *duplex emulsion* is in fact a ternary system having either water-in-oil-in-water ($W_1/O/W_2$ in Figure 2-1 left) or oil-in-water-in-oil ($O_1/W/O_2$ in Figure 2-1 right) structures, whereby the dispersed droplets contain smaller droplets of a different phase.

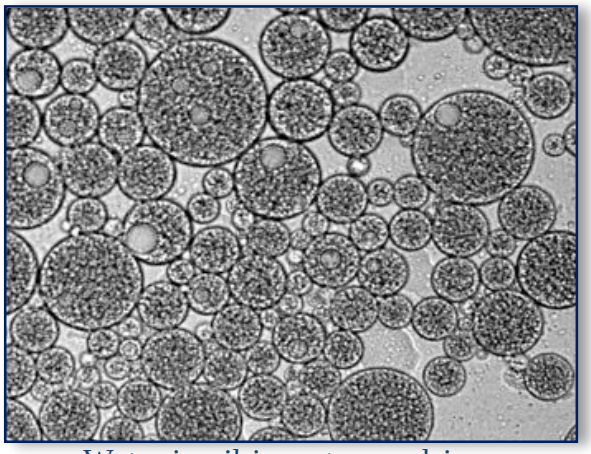

Water-in-oil-in-water emulsion
$W_1/O/W_2$

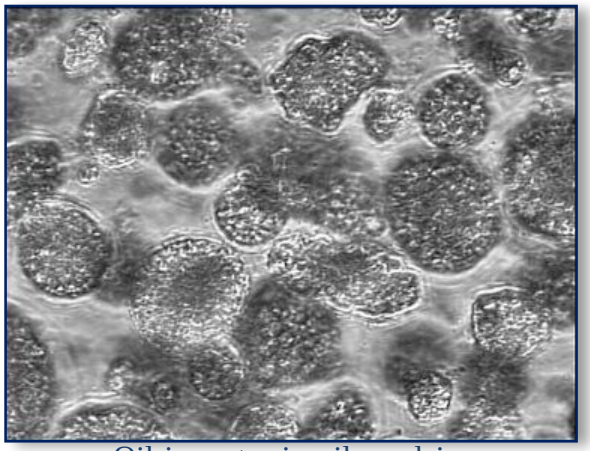

Oil-in-water-in-oil emulsion
$O_1/W/O_2$

Figure 2-1 Examples of: (Left) water-in-oil-in-water emulsion and (Right) oil-in-water-in-oil emulsion

2.2 Emulsifiers and interfacial phenomena

2.2.1 Interfacial tension

The interfacial region between the two immiscible phases has a significant impact on the bulk physicochemical and sensory properties of emulsions, and is characterised by interfacial composition, structure, electrical properties, energy and rheology (McClements, 2005). An *interface* is defined as a narrow region that separates two phases (*e.g.* two liquids, gas and solid, gas and liquid) (Walstra, 2003). The nature of the two-phase system is highly dynamic and its composition varies smoothly across the interfacial region, as the molecules intermingle with each other over a finite distance of few molecular diameters (Fennell & Wennerstrom, 1994). These interactions of molecules at the interface are strongly thermodynamically unfavourable because of the *hydrophobic effect* (Israelachvili, 2011). Consequently, an increase in the contact area (ΔA) between the two immiscible phases (*e.g.* during formation of emulsion droplets) gives a rise to the free energy of the system (ΔG):

$$\Delta G = \gamma \Delta A \qquad \text{Eq. 2-1}$$

where γ is the *interfacial tension*. An increase in the free energy of the system leads to an inherent emulsion instability as the system tends to its most thermodynamically favourable state – phase separation. Mechanisms of emulsions instabilities will be further discussed in Section 2.4.

2.2.2 Surface-active agents

An emulsifier is here defined as a surface-active agent that is capable of adsorbing at the oil-water interface. The main role of the emulsifier is to lower the interfacial tension during the

emulsification, which reduces the required mechanical energy input as well as decreases droplet coalescence.

Emulsifier molecules present in the emulsion system tend to accumulate at the interface if such process leads to a change in the interaction energies and lowers the free energy of the system (Hiemenz, 1977). This change in interaction energies comes from: (i) reduction of unfavourable contact between immiscible liquids and (ii) reduction of unfavourable contact between the part of the amphiphilic solute that is not soluble in the bulk with the bulk itself.

The most commonly used emulsifiers in the food industry can be divided into three main categories: low molecular weight surfactants, amphiphilic biopolymers and particles of colloidal size. A surfactant is a substance whose molecules are amphiphilic, *i.e.* one part of them is a hydrophobic chain (has affinity to nonpolar phase) and the other part is a hydrophilic head group (has affinity to the polar phase). Moreover, according to the type of the hydrophilic head group, surfactant can be divided into ionic (cationic and anionic) and non-ionic, depending on whether they dissociate in water.

Amphiphilic biopolymers are naturally occurring surface-active proteins and polysaccharides. Having both polar and nonpolar groups within their complex structure, biopolymers undergo conformational changes at the interface, leading to formation of strong viscoelastic membranes. Droplet stability against aggregation depends on the properties of such interfacial membrane, *e.g.* thickness, charge, reactive groups *etc*. (McClements, 2005).

It is well known that solid particles of colloidal size can be used to kinetically stabilise emulsions *via* a mechanism termed *Pickering stabilisation* (Binks, 2002). Such mechanism

differs fundamentally from surfactant stabilisation, as particles and surfactants, either in the bulk phase or at the interface, behave differently. For instance, particles do not aggregate to form micelles as surfactant molecules do (Binks, 2002). Moreover, unlike low molecular weight surfactants, solid particles in Pickering emulsions are thought to be irreversibly adsorbed at the oil-water interface, providing a mechanical barrier against coalescence (Arditty *et a*l., 2004) and, in some cases, Ostwald ripening (Timgren *et al.,* 2011). This is a consequence of a very high energy required to remove a spherical particle from the interface (~2750 *kT*), relative to thermal energy (Binks, 2002). Unlike surfactants and biopolymers, solid particles usually do not significantly influence the interfacial tension.

2.2.2.1 Adsorption and Critical Micelle Concentration

Driven by the need to minimise the free energy of the system and their amphiphilic nature, surfactant molecules tend to move to the interface and adsorb onto it. Due to the finite time of such processes the *dynamic interfacial tension* is used to describe the changes in the interfacial tension with time. This is different to the *equilibrium interfacial tension,* which is the numerical value taken at the end of the adsorption process.

At a certain concentration, surfactant molecules start to self-assemble into clusters called *micelles*. When a surfactant is dissolved in water, formation of micelles is driven by reduction in the free energy of the system, where the hydrophobic groups are directed toward the interior of the cluster and hydrophilic head groups directed towards water (Patist *et al*., 2002). The concentration at which micelles first form in solution, is termed the critical micelle concentration (CMC). At higher concentrations than CMC, interfacial/surface[*] tension does not change (Dickinson, 1992), since any new surfactant molecule added will either join the

[*] *Surface* tension is usually referred to a two-phase system, where one of the phases is air.

existing micelles or form a new one. As a result the chemical potential of the solution above the CMC does not change significantly (Fennell & Wennerstrom 1994). CMC value is usually taken at the point where a sharp break in the plot of interfacial/surface tension against surfactant concentration occurs, as shown in Figure 2-2.

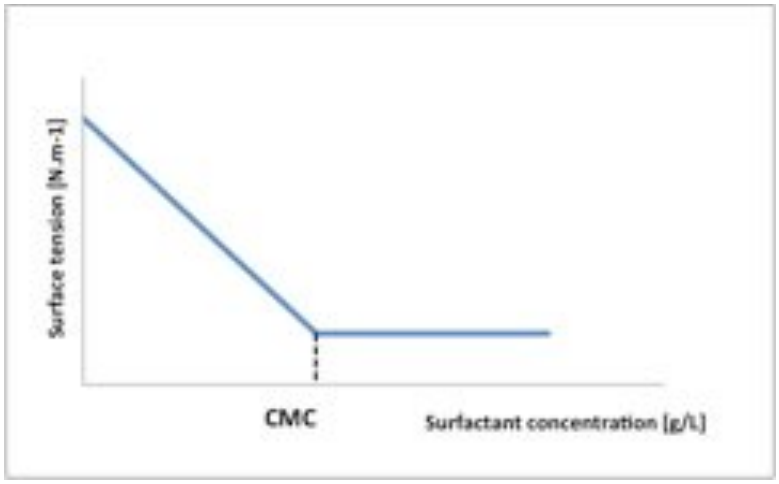

Figure 2-2 Determination of a critical micelle concentration (CMC).

The process of surfactant adsorption consists of: (i) transport of the surfactant molecules from the bulk phase towards the interface, and (ii) the actual adsorption at the interface. In the absence of bulk fluid motion, the surfactant will be transferred to the *sub-surface* (*i.e.* the region of the bulk phase, with a thickness of a few molecular diameters, immediately next to the interface, Ward & Tordai, 1946) by *molecular diffusion* (Miller & Kretzschmar, 1991; Wang & Wang, 2000). According to Fick's law, the rate of surfactant mass transport in a given direction is proportional to a mass concentration gradient in the said direction and the *molecular diffusion coefficient*. The value of the diffusion coefficient (D_m) is inversely proportional to the viscosity of the continuous phase (η_c) and the radius of a particle (r):

$$D_m = k_B T / 6 \pi \eta_c r \qquad \text{Eq. 2-2}$$

where k_B is Boltzmann constant and T is the absolute temperature. In the flowing fluid however, another major mass transport mechanism occurs due to the flow itself, *i.e*. *advective* transport. The magnitude of this transport in a given direction is proportional to fluid velocity in such direction and the concentration of a solute (Roberts & Webster, 2002). According to Walstra (1983), in highly dynamic emulsification process, transport of surfactant is dominated by advection.

Several processes can affect the rate of surfactant adsorption. To begin with, the rate of adsorption will slow down with increasing occupation of the interface until an adsorption-desorption dynamic equilibrium is established between the interface and the sub-surface. Additionally, in the system with surfactant solution above CMC, the effect of micellisation process on the adsorption dynamics must be taken into account (Patist *et al*., 2002). Micelles are in dynamic equilibrium with the concentration of the individual molecules and also micelles themselves constantly rearrange. It was reported that de-micellisation of a non-ionic surfactant can take relatively long time, therefore micellisation-de-micellisation rates must be considered when interpreting adsorption of non-ionic surfactants (Patist *et al.*, 2002).

2.2.3 Interfacial rheology

The interfacial rheology has been defined as the "study of the mechanical and flow properties of adsorbed layers at fluid interfaces" (Murray, 1996). In the emulsion system, where the surface to volume ratio is high, interfacial rheology becomes an important factor in the overall system's behaviour. It has been suggested that visco-elastic properties of films adsorbed at fluid interfaces in emulsions and foams are important for the stability of such emulsions with respect to film rupture and coalescence (Dickinson, 1992). In emulsions with monomolecular films of surfactants, coalescence is opposed by the elasticity and cohesiveness of the films

sandwiched between the two droplets when in contact. For these films to be effective, they must not thin out and break, therefore posses enough elasticity to maintain their integrity (Myers, 1992).

In mechanically agitated emulsions an interface can be deformed in two ways, by shearing and by dilatation (Walstra, 2003). Stresses acting on droplets in *shear deformation* cause different regions of the interface to move past each other and in *dilatational deformation* the droplet's interface area expands or contracts. Shear rheology is a measure of the mechanical strength of the adsorbed layers when the interface is subjected to a shear stress and the strain is recorded. Dilatational rheology is determined by measuring the change in the interfacial tension due to the specific change in the interfacial area (Jiao & Burgess, 2008). While shear properties may underpin the long term stability of emulsions and foams, dilatational rheology is generally considered to be more relevant for their stability during emulsification (Benjamins *et al*., 2006). Interfacial film characteristics can be described in terms of *viscous* (liquid-like) and *elastic* (solid-like) properties (Jiao & Burgess, 2008). In general, however, the deformation of the interface could produce a combination of responses termed *visco-elastic* properties.

2.2.3.1 Shear rheology

The measurements of shear rheology are performed in rotational rheometers, where shear deformations are generated in a thin surface/interface (Derkach *et al*., 2009), which is characterised by a constant concentration of surface active material (Walstra, 2003). It has been reported, that for layers of small-molecule surfactants the values of measured surface shear viscosity are generally immeasurably small (10^{-5} $N \cdot s \cdot m^{-1}$ or less) as compared to polymers where the values between 10^{-3} and 1 $N \cdot s \cdot m^{-1}$ have been reported (Walstra, 2003).

Interfacial shear elasticities of the range of Span surfactants have been measured by Opawale & Burgess (1998). They have demonstrated that the interfacial elasticity increased with the bulk concentration of surfactant, and at a relatively high surfactant concentration a rearrangement of molecules and/or a multilayer build-up at the interface probably occurred. They have also indicated that the effect of NaCl on the interfacial elasticity was surfactant specific (depends on the polarity of a molecule). For most investigated systems, the elasticity decreased with the increase in salt concentration and this lead to decreased interfacial film strength and subsequent limited emulsion stability.

2.2.3.2 Dilatational rheology

In dilatational rheology measurements, the determination of rheological properties of interfacial layers is based on measuring the dynamic interfacial tension during droplet oscillation at a certain frequency. In compression/expansion measurements, the interfacial dilatational modulus is defined as the ratio of a small change in the surface tension to the change in the surface area. When a relaxation process near or at the interface affects the interfacial tension within the timescale of the experiment, the interfacial dilatational viscosity can be also measured. If oscillatory methods are used to study interfaces, the dilatational modulus can be expressed as a sum of a storage modulus and a loss modulus contribution. In such case, the value of the dilatational modulus will depend on the oscillation frequency, thus reflecting relaxation properties of interfacial layers. Consequently, the viscous contribution is reflected in the measurable phase difference between the stress and strain.

The commercial instruments available to measure compression/expansion rheology are the bubble or droplet method (Leser *et al*., 2005). Both methods measure interfacial tension from the shape of the droplet (or bubble) *via* the Laplace equation (Eq. 2-3) and by applying

transient or harmonic oscillations, both methods can provide information on the dilatational rheology of the interfacial layer (Leser *et al.*, 2005). The hydrodynamic restrictions in oscillation frequency are caused by the deviation of the droplet profile from the theoretically expected shape (Derkach *et al.*, 2009). Consequently, in the droplet oscillation method the upper limit of frequency has been reported to be 1 Hz (Leser *et al.*, 2005). Due to the fact that diffusion in most cases is the slowest process and thus a controlling mechanism in the relaxation phenomenon (Li *et al.*, 2008), the characteristic observation time (reciprocal to the oscillation frequency) should be smaller than the characteristic diffusion time (Derkach *et al.*, 2009). As a result, very dilute surfactant solutions are normally used for measurements. This however, has a drawback of not posing exactly the same conditions as in "real" emulsions where the concentration of surfactant is much higher (Georgieva *et al.*, 2009).

2.3 Emulsion formation

Two immiscible liquids can be converted into an emulsion by the application of mechanical energy. Disruption of interfaces between the two phases is a critical step in emulsion formation (Walstra, 2003) and the ease of emulsion formation is measured by the energy that must be provided to form it (Aguilera, 1999).

At a droplet level, the stress acting towards droplet deformation (and subsequent breakup) is resisted by the Laplace pressure (ΔP_L), which originates from the pressure difference at the convex and concave side of the droplet interface:

$$\Delta P_L = 2\,\gamma / R \qquad \text{Eq. 2-3}$$

where γ is the interfacial tension and R is the radius of a spherical droplet. Therefore, the applied energy needs to be higher than the Laplace pressure to induce droplet disruption

and/or a suitable emulsifier is needed to lower the interfacial tension, and hence the Laplace pressure.

2.3.1 Conventional emulsifying techniques

Emulsions in the food industry are usually produced using devices which involve large energy consumption rates (van der Graaf *et al.*, 2005). As discussed by Walstra (1983), after the emulsion is formed, the interfacial area is much larger than before emulsification and so the free energy of the system increases by: $\gamma \Delta A$ (Eq. 2-1). During a typical emulsification process, however the actual energy supplied to make an emulsion is 1000 times the theoretical energy needed to create a given surface. The difference in energy is being dissipated as heat in the bulk phase.

One of the conventional emulsification methods is a *stirring method,* where the dispersed phase is broken up by the shear stress of turbulence. By addition of baffles and the design of the mixing head the efficiency of mixing can be modified (Fellows, 2000). In the *rotor-stator homogenisers* (*e.g.* colloid mill), the rapid rotation of the rotor generates shear stress in the gap between rotor and stator and this causes larger droplets to be broken up into smaller ones. The design of the surfaces in the gap defines whether the flow in the gap would be laminar (smooth surfaces) or turbulent (roughened or toothed surfaces) (Schubert & Engel, 2004). One of the drawbacks of this system is that the value of power density may greatly vary among sites in a typical rotor-stator apparatus (Walstra, 2003). Another example of high-shear homogenisation technique is *high-pressure homogenisation*. In this method a coarse emulsion made by other emulsification technique (*e.g.* high-speed mixer) is further processed to reduce the droplet size. The emulsion passes thorough a narrow orifice and by decreasing the gap

size in the homogenising valve, the pressure drop across the valve increases, thus causing the greater degree of droplet disruption and smaller droplet size.

There are number of problems associated with the described methods. Firstly, the droplet size and droplet size distribution cannot be easily controlled. Even if the mean droplet size can be obtained, the droplet size distribution is often wide and this affects the emulsion characteristics and stability (Williams *et al.*, 1998). Secondly, these are methods requiring high energy input (van der Graaf *et al*., 2005) yet with poor energy utilisation (Williams *et al*., 1998), thus greatly increasing manufacturing costs (McClements, 2005). And thirdly, reproducibility on a single piece of device is often poor and the quality of the product may differ from one manufacturing vessel design to another, even if the manufacturing scales are the same. This creates problems with scaling-up of the technique (Peng & Williams, 1998).

2.3.2 Novel emulsifying techniques

The disadvantages of high-shear emulsification techniques were the main drivers for the development of novel methods, where the droplets are formed individually and (allegedly) in a more controlled way. Amongst them are microfluidic, microcapillary, microchannel and membrane emulsification and these are described below.

2.3.2.1 Microfluidic, microcapillary and microchannel devices

A new *microfluidic device* has been proposed by Okushima *et al.* (2004). It has both hydrophobic and hydrophilic junctions positioned consecutively, which can be used for production of multi-phase systems with high reproducibility and narrow size distribution of the droplets. Furthermore, by adjusting the ratio between breakup rates at two junctions

(Figure 2-3), the number of included droplets can be precisely controlled. However, this type of device finds more application in areas where accuracy of the volume fraction is crucial (*e.g.* drug delivery systems), than in the industrial applications, where the production of the largest volume of material in the shortest amount of time is preferred.

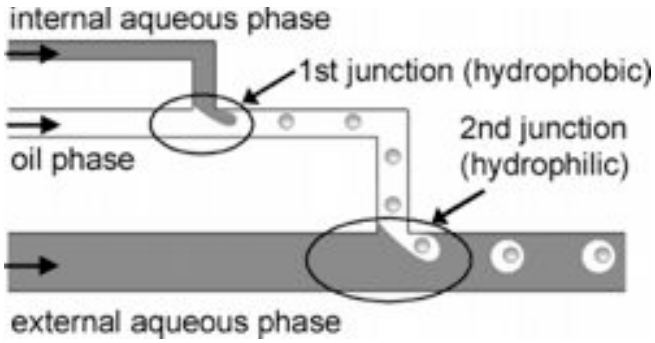

Figure 2-3 Basic concept for preparing duplex emulsions ($W_1/O/W_2$) using T-shaped microchannels (from Okushima *et al.*, 2004).

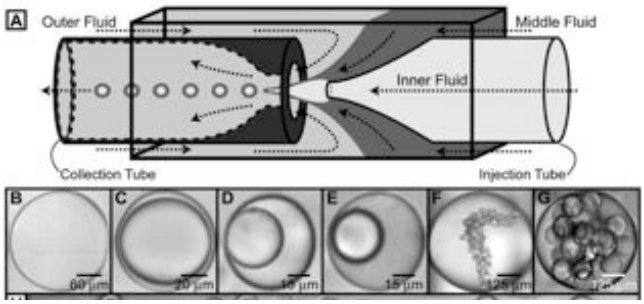

Figure 2-4 (A) Microcapillary geometry for manufacturing duplex emulsions; (B - G) Duplex emulsions with varying internal droplet number produced by microcapillary (from Utada *et al.*, 2005).

Utada *et al.* (2005) described a *microcapillary device*, that produces duplex emulsions in a single step, ensuring precision control of the outer and inner drop sizes, as well as the number of droplets included in each larger droplet. The device consists of cylindrical glass capillary tubes placed within the square glass tube (Figure 2-4).

In *microchannel emulsification* process, droplets are produced by forcing the to-be-dispersed phase through the microchannels in a silicone plate with well defined geometries (McClements, 2005). Droplets are formed spontaneously, as a result of different Laplace pressures on the terrace and in the well of the channel. This technique has been reported to be particularly useful in particle stabilised emulsions, as a gentle method involving no extensive mechanical shear, and thus no significant effect on the size of nanoparticle's aggregates during emulsification (Xu *et al.*, 2005). Low production rates make the technique disadvantageous for large scale practical applications, however Sugiura *et al.* (2004a) have argued that the microchannel emulsification could be scaled-up by using larger microchannel plates, straight-through microchannels and multiple microchannel plates.

2.3.2.2 Membrane emulsification

Membrane emulsification (ME) is a relatively new method of emulsion manufacture, offering the possibility of low energy consumption, better control of the droplet size distribution and reduced shear in the process (van der Graaf *et al.*, 2005). This method involves production of droplets individually (drop-by-drop), using an applied pressure to force the to-be-dispersed phase to permeate through a membrane into the continuous phase. The unique feature of ME is that the droplet size can be controlled primarily by the choice of the membrane and not by the generation of turbulent droplet breakup (Joscelyne & Trägårdh, 1999; Charcosset *et al*., 2004). Moreover, emulsion droplets formed are expected to be maintained as they are produced without any further breakup or coalescence (Yuan *et al.*, 2009b). Large part of this thesis focuses on membrane emulsification, therefore this technique is described in more detail in the following sections.

2.3.2.3 Principles and methods of membrane emulsification

There are different types of membrane emulsification (Figure 2-5): *dead-end* emulsification with spontaneous detachment of droplets (Kobayashi *et al.*, 2003), *cross-flow* system where the shear stress outside the membrane is generated to ensure regular droplet detachment before they reach the volume for spontaneous detachment (Nakashima *et al.*, 1991), *stirring* system, and the *rotating/vibrating* system where, in contrast to other membrane techniques, the dispersed phase volume allegedly does not influence the droplet size (Schadler & Windhab, 2006).

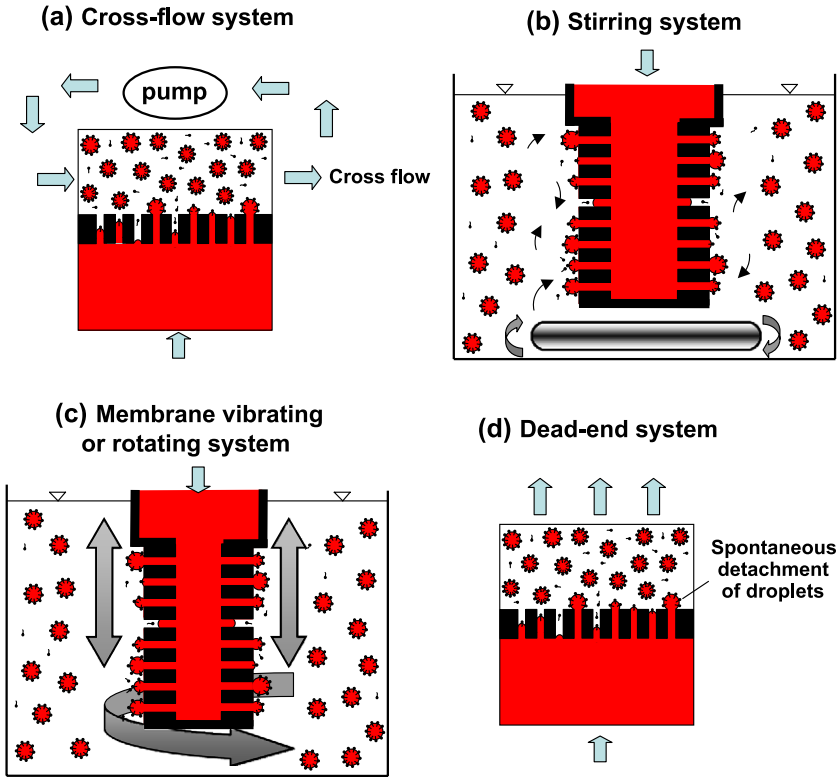

Figure 2-5 Different types of membrane emulsification (from Vladisavljević & Williams, 2005)

In *cross-flow* ME, the to-be-dispersed phase is pressed through a microporous membrane while the continuous phase flows along the membrane surface (direct ME). *Pre-mix* ME involves preparation of a coarse emulsion using conventional high-shear homogenisation and

then passing it through the membrane to reduce the diameter of the dispersed droplets. Pre-mix ME as compared to the direct method, is claimed to provide a relatively high flux of the dispersed phase (van der Graaf *et al*., 2005). The proposed advantages of the cross-flow system include: good control over droplet size and droplet size distribution, production of emulsions with shear sensitive components and with low energy consumption (Gijsbertsen-Abrahamse *et al*., 2004), simplicity of the design, easy scale-up and good reproducibility of data (Joscelyne & Trägårdh, 2000).

Rotating membranes are a relatively new technique, where the shear stress is generated by the rotation of the membrane and the to-be-dispersed phase passes radially through the micropores of the membrane and forms droplets moving into the continuous phase. The small number of publications on this subject mostly focuses on stainless steel rotating membranes, which were used in the production of simple (and mostly coarse, Aryanti *et al*., 2006 & Yuan *et al*., 2009a) O/W emulsions, where rotational velocity, trans-membrane pressure, width of the gap, membrane pore geometry and emulsion composition were analysed in relation to the microstructure of the emulsion. It has been suggested, that amongst membrane techniques, the rotating membrane offers the advantage of increased disperse phase fluxes which can be otherwise achieved by using an asymmetric membrane (Kukizaki & Goto, 2007).

The main challenge in ME remains in the prediction and explanation of the dependence of the droplet size on the membrane characteristics, process parameters and properties of used ingredients (Danov *et al.*, 2007; Lepercq-Bost *et al*., 2008). One of the main focuses of this thesis was to provide a better understanding of both the cross-flow and rotating membrane techniques in relation to the properties of simple and duplex emulsions.

2.3.2.3.1 Different membrane materials

Depending on the required characteristics of the final emulsion, different types of membranes can be used: SPG membranes (Nakashima *et al.*, 2000), polymer membranes (*e.g.* polypropylene, Vladisavljević *et a*l., 2002), ceramic membranes (Joscelyne & Trägårdh, 1999; Williams *et al.*, 1998) and metal membranes (*e.g.* stainless steel, Aryanti *et al.*, 2009). These membranes are characterised by various shapes, surface affinities, mean pore size and effective membrane areas (Vladisavljević *et al.*, 2005).

SPG is a type of glass obtained by phase separation of a primary CaO-Al_2O_3-B_2O_3-SiO_2 composition made of Shirasu[*]. Calcium carbonate and boric acid are added to a refined Shirasu ash in a fixed ratio and then mixed and heated up to 1350°C to obtain glass fusion. After a desired shape formation, the primary glass is heated to 650 – 750°C from several hours to tens of hours. This treatment causes glass decomposition into Al_2O_3-SiO_2 and CaO-B_2O_3. Phase separated glass is then treated with HCl to leach out calcium borate. The mean pore size is controlled by the time and temperature of the heat treatment (Nakashima *et al.*, 2000). SPG membranes contain cylindrical, tortuous pores forming a 3D interconnected network. Cross-sections of pores are not circular and this provides an additional factor in spontaneous droplet detachment (Kobayashi *et al.*, 2002). SPG membranes are widely available and have the advantage of a narrow pore size distribution, which has been claimed to be the most critical factor for the production of "monodisperse" emulsions (Joscelyne & Trägårdh, 2000; Peng & Williams, 1998). SPG membranes have wide range of available pore sizes (0.05 – 30 μm), high porosity (50 – 60 %, Charcosset *et al.*, 2004) and high thermal stability for practical use (Cheng *et al.*, 2008).

[*] Volcanic ash from the southern part of Kyushu Island in Japan.

2.3.2.3.2 Effect of membrane process parameters on droplet size

In general terms, growth of droplets and their detachment from the membrane pores is described by the *balance of forces* (Charcosset *et al.*, 2004; Timgren *et al.*, 2009), which is schematically shown in Figure 2-6. The interfacial tension force (F_I) and the drag of the continuous phase (F_D) are the main forces usually taken into account (Xu *et al.*, 2005) due to their range.

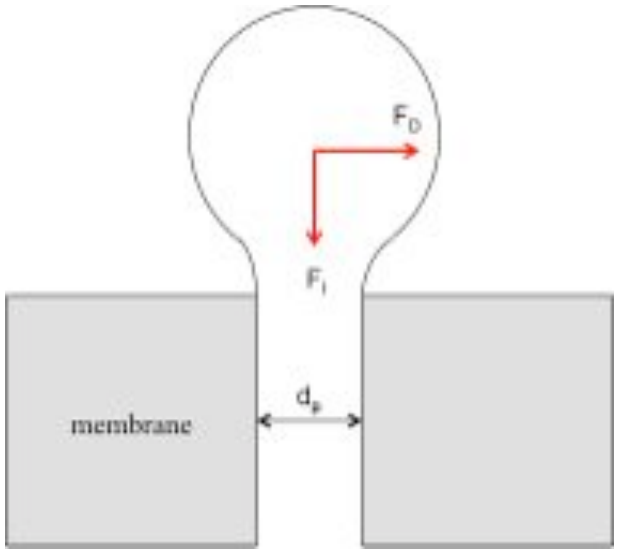

Figure 2-6 Schematic representation of the major forces acting on the droplet at the membrane surface. F_D – drag force, F_I – interfacial tension force, d_p – membrane pore diameter.

Droplets formed at the membrane surface are detached under the influence of the continuous phase flowing parallel to the membrane surface (in cross-flow ME) or the rotations of the membrane (in rotating ME). In cross-flow ME, the continuous phase flow is characterised by cross-flow velocity (Charcosset *et al*., 2004), while in rotating ME, rotational velocity is used as a parameter. Both create a hydrodynamic drag force that shears off the droplets from the membrane surface. Timgren *et al*. (2009) showed that the cross-flow velocity has the largest influence on the emulsion droplet size (relative to effect of the dispersed phase flux and the viscosity of the dispersed phase). Typically, the droplet size decreases with increasing the

cross-flow velocity (Charcosset *et al.*, 2004; Joscelyne & Trägårdh, 2000). For the rotating membrane, Schadler & Windhab (2006) found that the higher the rotational speed, the smaller are the droplets and narrower the size distribution.

In ME methods, a trans-membrane pressure (TMP) is used to force the to-be-dispersed phase to permeate through the membrane pores and into the continuous phase. TMP is defined as a difference between the pressure of the dispersed phase and the pressure of the continuous phase. When the TMP increases, the flux of the dispersed phase also increases, according to *Darcy's law*. This leads to a faster droplet inflation resulting in larger emulsion droplets being produced. There is an optimum range of the applied TMPs. The lower limit of TMP is determined by the critical trans-membrane pressure (CTMP), which is the minimum pressure difference over the pore to start producing droplets from this pore. The critical pressure (P_c) is inversely proportional to the pore diameter[*] (d_p):

$$P_c = 4\gamma \cos\alpha / d_p \qquad \text{Eq. 2-4}$$

This is essentially a capillary pressure equation, where γ is the interfacial tension, α is the contact angle of the dispersed phase to the membrane surface. The critical pressure also depends on tortuosities in the pores, irregular pore openings and significant effects of surface wettability. In principle, to achieve the highest production rate, the TMP should be maintained at the highest practicable level in the *non-jetting regime* (Peng & Williams, 1998). That is, the highest limit of TMP is the highest value at which droplets are still produced *via a dripping mechanism* (Vladisavljević *et al.,* 2007). However, there is no reliable theoretical approach

[*] For membranes with a pore distribution, the critical pressure will depend on the width of such distribution (Gijsbertsen-Abrahamse *et al.*, 2004)

estimating the practical maximum TMP and it has been suggested that an experimental approach has to be adopted for adjusting individual process conditions (Williams *et al.*, 1998).

2.3.2.3.3 Effect of membrane properties on the droplet size

Membrane properties play a crucial part in the control of emulsion properties. The most important factor affecting the droplet size and distribution however is the wall contact angle and pore size (Gijsbertsen-Abrahamse *et al.*, 2004).

The average emulsion droplet size (d_d) is mostly determined by the size of the pore opening (d_p) (Gijsbertsen-Abrahamse *et al.*, 2004), but also the shape of the opening. Kobayashi *et al.* (2002) showed that droplets produced with oblong straight-through microchannels are three times smaller than those produced with circular straight-through microchannels. Similarly, Yuan *et al.* (2009a) reported that pores of square and rectangular shape are beneficial to the formation of uniform droplets at low rotational velocity of the stainless steel rotating membrane. They also showed that at a given trans-membrane pressure and rotational velocity, horizontal pores yielded twice as high droplet formation rate as the vertical pores. It has been shown (Charcosset *et al.*, 2004) that in membrane emulsification, the average droplet diameter (d_d) increases with the average membrane pore size (d_p) in a linear manner.

Conceptually, the membrane should be wetted by the continuous phase, so the wall contact angle should be bigger than 90° (measured in the dispersed phase, as shown in Figure 2-7). The wetting properties of the membrane can be manipulated by pre-soaking in the continuous phase (Gijsbertsen-Abrahamse *et al.*, 2004).

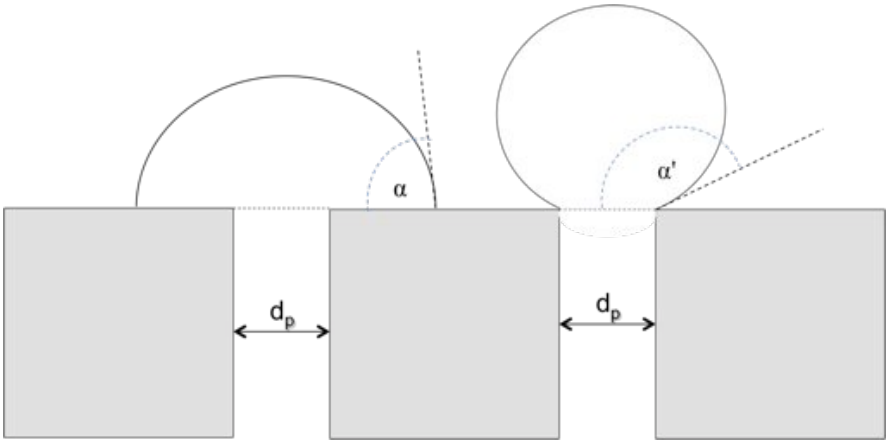

Figure 2-7 Wall contact angle measured in the dispersed phase. (Left) membrane wetted by the dispersed phase (α < 90°), (Right) membrane not wetted by the dispersed phase (α' > 90°).

2.3.2.3.4 Effect of formulation on droplet size

The emulsion droplet size depends on the type and concentration of emulsifier used and the viscosity ratio of both phases (Danov *et al.*, 2007). The oil–water interfacial tension is recognized to be the major retention force (F_I in Figure 2-6), which keeps the droplets attached to the membrane surface. Higher interfacial tension will lead to the production of bigger droplets (Christov *et al.*, 2002). It has been reported by Kukizaki (2009), that more concentrated solutions of Tween 20 caused a faster decrease in the interfacial tension resulting in the detachment of smaller droplets and also a narrower droplet size distribution due to better interfacial coverage and thus lower droplet tendency to coalescence. The author also claimed that the production of small droplets will depend on kinetics of surfactant adsorption and electrostatic interactions between the droplet and the membrane surface (in case of anionic emulsifiers). It has been suggested by Nakashima *et al*. (1991), that stable emulsions can be obtained with an extremely small quantity of added surfactant.

The viscosity of the continuous phase has been reported (Aryanti *et al.*, 2009) to have an effect on the droplet size of emulsions made with the rotating membrane. The hydrodynamic

drag force, being one of the major detaching forces in membrane emulsification, is directly proportional to the viscosity of the continuous phase. Therefore, at higher viscosity smaller droplet size could be expected. Wang & Wang (2000) postulated that when a wall shear stress is constant, the droplet size increases with the increase in the continuous phase viscosity. This was associated with slower reduction in interfacial tension. Kawakatsu *et al*. (2001) found that the average droplet size of a water-in-oil system decreases as the ratio of viscosity of the dispersed phase to continuous phase increases.

Existing data on the influence of viscosity on the droplet size of emulsions produced with the rotating membrane technique is scarce and the effect of viscosity is not interpreted explicitly. Aryanti *et al.* (2009) found that droplet size of O/W emulsions produced with a stainless steel rotating membrane decreases with an increase in the viscosity of the continuous phase. However this was attributed to both (i) an increase in the drag force, and (ii) interfacial properties and interactions of Carbomer (cross-linked polyacrylic acid polymer used to adjust the viscosity of the continuous phase) with surfactants. They observed that negatively charged Carbomer adsorbs onto the interface and this, on one hand facilitates the adsorption of non-ionic surfactant Tween 20, but on the other hand, hinders SDS adsorption by electrostatic repulsions. However, the authors did not suggest what is the mechanism that prevails in the reduction of droplet size. Dragosavac *et al.* (2008) reported that the droplet size decreases with viscosity of the continuous phase. However, this increase in viscosity was achieved by increasing the concentration of the emulsifier Pluronic F68 from 1 % (1.07 mPa·s) to 10 % (4.45 mPa·s). A result of such increase would be reduced dynamic interfacial tension and capillary force at the moment of droplet detachment.

2.3.2.3.5 Effect of membrane properties on the dispersed phase flux

One of the potential disadvantages of SPG membranes, for industrial applications, is low dispersed phase flux that has to be maintained to avoid the transition from a "size stable" to "continuous outflow" zone (Yasuno *et al*., 2002). Low dispersed phase flux in SPG membranes is caused by high membrane resistance arising from its thickness (Gijsbertsen-Abrahamse *et al.*, 2004) and small proportion of active pores (Vladisavljević & Schubert, 2003).

In order to lower the membrane resistance, Kukizaki & Goto (2007) designed asymmetric SPG membranes with a 0.67 μm skin and 4.7 μm support layer pore diameters. They found that the dispersed phase flux increased more than 20 times in the asymmetric membrane (between 11 and 39 $L \cdot m^{-2} \cdot h^{-1}$ at TMP of 35 – 120 kPa), as compared to the symmetric one. Additionally, the percentage of active pores increased from approximately 2.5 % for the symmetric membrane to around 4.5 % for the asymmetric membrane. Vladisavljević & Schubert (2002) reported the dispersed phase flux of 0.7 - 7 $L \cdot m^{-2} \cdot h^{-1}$ in the production of simple O/W emulsions. However, the applied TMPs were low (*i.e.* TMP = 1.1 × CTMP). Scherze *et al*. (1999) produced O/W emulsions stabilised with a milk protein, using a microporous glass membrane (d_p = 0.5 μm). Obtained dispersed phase fluxes were in order of 50 $L \cdot m^{-2} \cdot h^{-1}$ at 35 kPa TMP. Interestingly, Katoh *et al*. (1996) found that addition of an oil soluble emulsifier, in the manufacture of O/W emulsions, can increase the dispersed phase flux ten times, up to 30 $L \cdot m^{-2} \cdot h^{-1}$ (160 kPa TMP for a 0.57 μm SPG membrane).

Membrane systems have been reported to be easy scaled-up as it involves multiplication of small processes (*i.e.* adding more membranes to a device), rather than simple enlargement of the processing vessel (Charcosset, 2009; Vladisavljević & Williams, 2005). It has been shown

by Williams *et al*. (1998), that pilot scale cross-flow membrane emulsification can be used for the production of emulsions with controlled droplet size and droplet size distribution in both batch and continuous mode. To date however, there is only one food product manufactured using membrane technology ("Yes light", a very low fat spread, Moringa Milk Industry, Japan) (Nakashima *et al.*, 2000).

2.4 Emulsion (in)stability

2.4.1 Thermodynamic and kinetic (in)stability

Emulsions are thermodynamically unstable as their formation involves an increase in interfacial area between both phases, which is accompanied by an increase of the free energy (Eq. 2-1). Energy associated with the increase in the interfacial area in the emulsion overweighs the entropy of formation associated with the number of arrangements accessible to the droplet in the emulsified state as compared to bulk phase (Taylor, 1998). Thus the formation of an emulsion is always thermodynamically unfavourable.

The free energy change, although giving the *thermodynamic stability* estimate, will not specify the rate at which the properties of foods change over time, and that is why the term *kinetic stability* has been used (McClements, 2005). Conceptually, the kinetic stability (*metastability*) of an emulsion is the activation energy that has to be overcome before the emulsion can reach its most thermodynamically favourable state. Therefore, kinetically stable emulsions must have larger activation energy than thermal energy of the system (kT). The kinetic stability of emulsions is largely determined by their dynamic nature. Constant motion of particles, either due to intermolecular, or external forces, will induce particles interactions and trigger of instability mechanism(s).

The stability of emulsions can be considered on many levels: physical, chemical and microbiological. The emulsion is physically stable if its dispersed state does not change, meaning its droplet size stays constant, irrespective of the time and volume element observed (Schubert & Engel, 2004). The main processes leading to physical instability of emulsions include: gravitational separation, flocculation, coalescence and Ostwald ripening. Amongst chemical and biochemical reactions that have adverse effects on food emulsion quality, lipid oxidation (Kargar *et al*., 2010; McClements & Decker, 2000), biopolymer hydrolysis (van der Ven *et al.*, 2001), flavour or colour degradation are the most common (McClements, 2005). Various ways in which the state of dispersity may change (and be prevented from changing) are discussed in the following sections.

2.4.2 Gravitational separation

Due to differences in densities of emulsion components, the net gravitational force acting on both phases will lead to their gravitational movement. If the droplets have lower density than the surrounding medium then this movement is called *creaming*. If the opposite happens, and the droplets have higher density than the continuous phase, then *sedimentation* of droplets occurs. The rate of gravitational separation depends on the size of the settling unit and the density difference between two phases (Dickinson, 1992). Gravitational separation in emulsions can be controlled by: (i) minimising the density difference between the droplet and the surrounding media, (ii) reducing the droplet size, (iii) increasing viscosity of the continuous phase with either a thickening agent or with increased droplet concentration and (iv) altering droplet flocculation.

2.4.3 Droplet flocculation and coalescence

Droplets in emulsions continuously collide due to constant thermal motions, gravity and externally applied forces. After a collision, droplets may either move apart, or stay together (aggregate) due to coalescence, or flocculation. The strength of droplet aggregation depends on the relative magnitude of the attractive and repulsive colloidal interactions between droplets (Dickinson, 1992).

Flocculation is the aggregation of droplets in three-dimensional clusters without coalescence occurring, *i.e.* the droplets preserve their individual entities in the clusters (Tadros & Vincent, 1983). Flocculation can be either reversible (weak flocculation) or irreversible (strong flocculation also termed *coagulation*). In dilute systems, flocculation can increase the creaming rate; on the contrary in more concentrated systems, by forming a 3D network, flocculation can hinder gravitational droplet movements. The most efficient way to control the rate and extent of flocculation is to regulate colloidal interactions between droplets (*e.g.* electrostatic, steric *etc.*).

Coalescence occurs when droplets merge together to form a larger droplet (Kabalnov, 1998). When the two droplets come together and the external forces overcome droplets Laplace pressures, their surfaces flatten (Walstra, 2003). Whether the two droplets merge together, depends on the thin liquid film of the continuous phase between them. When such film thins and ruptures, the two droplets form a larger one. In O/W emulsions, coalescence results in faster creaming due to an increase in the droplet size, but also to further coalescence as larger droplets are more susceptible to coalescence (self-accelerating process) (Dickinson, 1992). Such progression will result in “oiling off”, *i.e.* separation of free oil on the surface of the sample. Inhibiting coalescence is the key issue in emulsion stabilisation processes. The most

appropriate methods are highly dependent on the type of the emulsifier used and the prevailing environmental conditions. Droplets may be physically stopped from colliding by increasing the viscosity of the continuous phase or its gelation. Using particles and polymeric emulsifiers can increase the interfacial tension and the rheological properties of the interfacial film layer. For example, proteins have been found to be effective at preventing coalescence in emulsions under quiescent conditions (Dickinson, 1992). This was associated with small sizes of produced droplets and formation of interfacial membrane that produced strong repulsive forces of electrostatic and steric origin.

2.4.4 Ostwald ripening

Ostwald ripening is a process where larger droplets grow at the expense of smaller ones. This occurs because the solubility of smaller droplets is higher than solubility of the larger ones. This is an effect of increased chemical potential in small particles resulting from the high surface curvature and surface/interfacial tension. Smaller liquid droplets (with higher surface curvature) exhibits a higher effective vapour pressure since the surface is larger with comparison to the volume. It has been reported, that Ostwald ripening is not effective in droplets above 10 μm (Walstra, 2003) and it is not significant in most food emulsions as the solubility of triacylglycerol in water is very low (Dickinson, 1992). Out of the instability mechanisms discussed, Ostwald ripening is the only change in dispersity that proceeds faster for smaller particles. A subsequent increase in the emulsion droplet size leads to an increase in the intermolecular attractions between droplets. In this sense Ostwald ripening can be the "trigger" mechanism of emulsion destabilisation (Kabalnov & Shchukin, 1992).

2.5 Duplex emulsions

Duplex (double) emulsions are complex systems also termed “emulsions of emulsions” or “emulsified emulsions”, as droplets of a dispersed liquid are further dispersed in another liquid. Multiple emulsions were first reported by Seifriz (1923).There are two main types of duplex emulsions: water-in-oil-in-water ($W_1/O/W_2$) and oil-in-water-in-oil ($O_1/W/O_2$). Other types such as oil-in-water-in-water ($O/W_1/W_2$) have also been prepared and investigated (Kim *et al.,* 2006). The main advantage of multiple emulsions over simple emulsions is a direct consequence of their complex microstructure. For example, such constructions could potentially act as microcarriers of active ingredients (hydrophilic or hydrophobic) that could be encapsulated in the internal droplets. These active ingredients could be then delivered in a controlled way during a specific process (Lesmes & McClements, 2009). This property of multiple emulsions was appreciated by the pharmaceutical, food, agrochemical and cosmetic industries (Muschiolik, 2007).

In food applications the possibility of salt reduction without compromising the taste of a product have been investigated (Malone *et al.,* 2003). Perception of saltiness in the food product increases with salt concentration in the water continuous phase. Reduction in the overall salt concentration in O/W emulsions can be done by increasing the concentration of the included phase while maintaining satisfactory, yet lower salt levels in the external water phase. With the duplex emulsion approach, the fat (included) volume increases only apparently, as the fat phase is an emulsion itself (*i.e.* W_1/O emulsion). This means that, the use of duplex $W_1/O/W_2$ emulsions allows for a substantial fat reduction, as the dispersed phase is made up by water contained in the internal aqueous phase (W_1). Therefore, a volumetric reduction in fat without a change of droplet size or phase content can be made. Another potential benefit of duplex emulsions over the conventional emulsions is taste

masking of certain ingredients or additives, for example fish oils, bitter peptides *etc.* (Leal-Calderon *et al.*, 2007).

The increasing application of duplex emulsions in foods is likely to sustain due to their potential advantages over conventional emulsions (Garti, 1997b). Nevertheless, despite the potential usefulness, the application of duplex emulsion technology has been so far hindered due to many forms of inherent instabilities of their structures (Jiao & Burgess, 2008) and also intensive processing conditions (during manufacture and storage), which could lead to breakdown of a duplex structure.

2.5.1 Formations of duplex emulsions

Duplex emulsions are typically prepared in a two-step emulsification process (Garti, 1997a). As discussed earlier (Section 1), the primary emulsion is usually made under intense homogenisation conditions (Garti, 1997a), using high speed blenders, high-pressure homogenizers, colloid mills *etc*. The smallest possible primary emulsion droplets should be obtained, as such emulsions are more stable during the subsequent secondary emulsification. Additionally, small primary droplets are favoured as they are incorporated into duplex emulsions which preferably would be smaller than 20 μm due to the undesirable sensory properties (Norton *et al.*, 2006).

Contrary to the primary emulsification, the secondary emulsification step should be carried out under mild shear conditions, in order to avoid the breakup of the internal droplets (Dickinson & Akhtar, 2001). Muschiolik *et al.* (2006) advised that a conventional high-pressure homogeniser is not suitable for dispersing the W_1/O emulsion into W_2, as it leads to very low yield (~55 %) of the dye encapsulated in the inner water phase.

Novel methods of duplex emulsion manufacture, based on individual formation of droplets (drop-by-drop), have been proposed. These include microchannel emulsification (Sugiura *et al.*, 2004b), microcapillary device (Utada *et al.*, 2005), microfluidic device (Okushima *et al.*, 2004) and membrane emulsification (Mine *et al.*, 2000; Vladisavljević *et al.*, 2006b). These methods were described in more detail in Section 2.3.2.2. It has been suggested, that membrane technology ensures mild-shear environment (van der Graaf *et al.*, 2005), crucial for the secondary emulsification step in duplex emulsion formation.

There is no comprehensive study on the effect the secondary emulsification step in the production of duplex $W_1/O/W_2$ emulsions has on the encapsulation efficiency of the entrapped addenda measured directly after emulsion preparation and during prolonged storage. Those issues will be addressed in this thesis.

2.5.2 Formulation and stability aspects of duplex emulsions

The issue of duplex emulsion stability is more complex than that of simple emulsions (Jiao & Burgess, 2008). This is because the composition of duplex emulsions, *i.e.* two distinctively different emulsifiers, concentration and composition of the lipid phase will have an effect on the stability of these complex structures (Garti, 1997a). Also the nature of the entrapped materials (encapsulant) is particularly important if such encapsulants are small electrolyte molecules that can rapidly diffuse across the oil layer (Dickinson *et al.*, 1994).

Since the curvatures of the two types of interfaces are opposite, two different types of emulsifiers are required in formulation of duplex emulsions; one that is predominantly oil-soluble and second that is predominantly water-soluble (Jiao & Burgess, 2008). This, in the case of water-in-oil-in water emulsions ($W_1/O/W_2$), involves formulating of the primary

emulsion (W_1/O) using an emulsifier of low HLB* number (*e.g.* Span) and then dispersing it into external water phase (W_2) with the high HLB emulsifier (*e.g.* Tween). In the case of oil-in-water-in-oil emulsions ($O_1/W/O_2$) the formation of primary O_1/W emulsion requires high HLB emulsifiers and then low HLB one in the second step of the emulsification. The presence of two distinctive surfactants is a major cause of instability of multiple emulsions, as the surfactants tend to migrate from one interface to another, thus considerably shortening the emulsion lifetime (Garti, 1997b; Michaut *et al.*, 2004).

The main focus of this thesis is the production and formulation of $W_1/O/W_2$ emulsions therefore the following considerations of duplex emulsion stability will be based on these types of emulsions as an example. The main instability mechanisms occurring in duplex $W_1/O/W_2$ emulsions are schematically presented in Figure 2-8.

Coalescence instability in duplex $W_1/O/W_2$ emulsions can happen on many different levels (Figure 2-8). Firstly, the inner droplets of the primary emulsion may coalesce leading to an increase in the size of the primary water droplets (W_1). Secondly, oil globules may coalesce and this shows as coarsening of the duplex emulsion. Both types of droplet coalescence however, will not directly lead to release of the entrapped in W_1 material. Thirdly, when the thin film of oil between internal (W_1) and external (W_2) water phases ruptures, the inner droplets are completely delivered to the external continuous phase. This collapse in duplex $W_1/O/W_2$ emulsion structure results in a simple O/W_{1+2} emulsion (Ficheux *et al.*, 1998). The third coalescence mechanism is reported to be correlated with the ratio of concentrations of both emulsifiers; for example, by increasing the hydrophilic emulsifier concentration, the

* HLB (Hydrophilic Lipophilic Balance) value is a measure of the balance of the hydrophobic and hydrophilic parts of the surfactant molecule (Walstra, 2003).

destabilisation of duplex structure may occur during few minutes up to several months (Ficheux *et al.*, 1998).

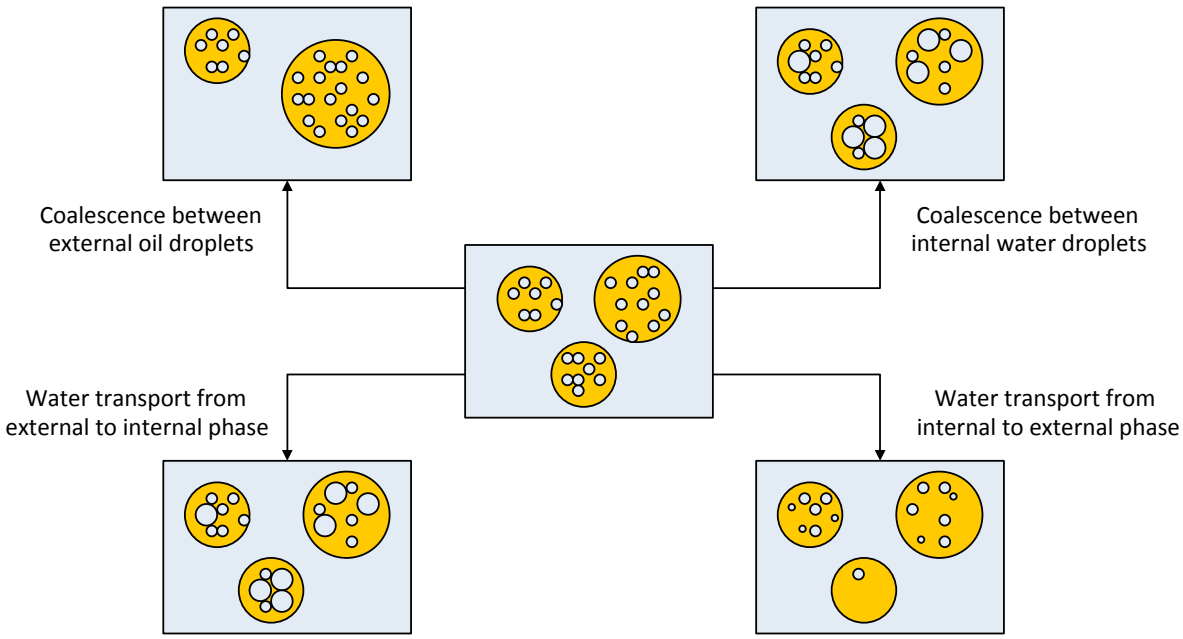

Figure 2-8 Schematic representation of the main instability mechanisms occurring in duplex $W_1/O/W_2$ emulsions.

In addition to coalescence, *the osmotic pressure imbalance* between the internal water droplets (W_1) and the external continuous water phase (W_2) may compromise the stability of duplex $W_1/O/W_2$ emulsions (Figure 2-8). If the osmotic pressure is higher in the internal water phase W_1 than in the external W_2 phase, water will pass through the oil membrane into the W_1. This will lead to internal droplets swelling and possible rupture with release of the encapsulated water phase (W_1) into the external phase (W_2). If the opposite happens, and the osmotic pressure is higher in the external water phase than the internal one, transport of water from W_1 to W_2 may lead to emulsion shrinkage. Both mechanisms, generally termed *compositional ripening* (Pays *et al.*, 2002), can in extreme cases lead to collapse of the duplex structure and a resultant simple O/W_{1+2} emulsion. The mechanisms of compositional ripening are further discussed in Section 2.5.2.4.

The stability of duplex emulsions is highly dependent on type and concentration of emulsifiers used and the control of the osmotic pressures. Table 2-1 gives examples of different formulations and processing techniques used by researchers for the primary and secondary emulsification, in relation to encapsulation efficiency measured after emulsification (yield) and during prolonged storage. In the following sections, emulsions stabilised with different type of emulsifiers have been reviewed alongside reported transport mechanisms.

Table 2-1 Encapsulation stability of duplex emulsions prepared with range of emulsifiers and range of emulsifying techniques.

Encapsulated active	Hydrophobic emulsifier (method of preparation)	Hydrophilic emulsifier (method of preparation)	Yield of emulsification [%]	Encapsulation efficiency on storage [%]	Authors
Glucose	PGPR (Ultra Turrax + HPH)	WPI-XG (HPH with"dual feed cell")	90% at low pH 15% at high pH	90% at pH < 4.4 30 days	Benichou *et al*., 2007
NaCl	Polymeric emulsifier (Couette-type mixer)	Polymeric emulsifier (laminar and turbulent method)		95% 30 days	Pays *et al*., 2002
NaCl	PGPR (rotor-stator mixer)	Tween 80 (rotor-stator mixer)		94-95% 30 days	Sapei *et al*., 2012
$MgCl_2$	PGPR (Couette cell)	Sodium caseinate (Couette cell)	99%	70-92% at 4*C 60-82% at 25*C 30days	Bonnet *et al*., 2009
$MgSO_4$	Polymeric surfactant High speed agitator	PEG 20 Soya sterol + POE-20 cetyl alcohol Low speed stirring		More than 90% 1 day	Geiger *et al*., 1998
Water-soluble dye	PGPR (two stage HPH)	Modified gum arabic (two stage HPH)	> 90%	> 90% 30 days	Su *et al*., 2008
Water-soluble dye	PGPR (two stage HPH)	Sodium caseinate (two stage HPH)	> 90%	> 90% 30 days	Su *et al*., 2006

2.5.2.1 Monomeric surfactants in duplex emulsions

Early studies of multiple emulsions used monomeric surfactants for emulsion stabilisation (Matsumoto *et al.*, 1976; Magdassi *et al.*, 1984). Those studies looked for the best ratios of low and high HLB surfactants for best stabilisation. An experimental weight ratio of 10 for the low HLB surfactant to the high HLB surfactant was recommended (Matsumoto *et al.*, 1976), alongside with the "effective HLB value" of surfactant (Garti, 1997b). Garti (1997a) reported that the concentration of the primary emulsifier has to be high (10 – 30 % of the

primary emulsion) by which the swelling capacity of the oil phase increases (Geiger *et al.*, 1998), while the concentration of the secondary one should stay low (0.5 – 5 %). On the other hand, their earlier work (Garti *et al.*, 1985) suggested, that increased concentration of low HLB surfactant leads to faster water transport across the oil phase leading to emulsion deterioration. This was associated with increased number of reversed mixed micelles, with both high and low HLB surfactants, which acted as carriers for water across the oil phase.

In the food industry, sorbitan monoesters are frequently used as high HLB surfactants (*e.g.* Tween(s)) and amongst low HLB surfactants Span(s) and polyglycerol polyricinoleate (PGPR) are the most common (Mezzenga, 2007). PGPR is a non-ionic surfactant that is permitted for use in a number of food products in many countries and has been frequently used in studies of duplex $W_1/O/W_2$ emulsions. It can be used alone (Weiss *et al.*, 2005) or in combination with other emulsifiers such as sodium caseinate or gum arabic (Su *et al.*, 2006 & 2008). Su *et al.* (2006) reported that the entrapment yield of polymeric dye was mostly dependent on the coalescence stability of the inner water droplets, which is controlled by PGPR concentration. The yield value of > 90 % could be achieved with 4 % PGPR in the oil phase and when the PGPR concentration increases to 8 %, the yield was almost 100 %. They have also suggested a possible synergistic effect between PGPR and sodium caseinate, preparing high yield, stable multiple emulsions with reduced PGPR concentration (2 %) and sodium casinate (0.5 %) added to the inner aqueous phase.

The main applications of PGPR are in the rheological control of chocolate and in the production of low-fat spreads which have a high water and protein content (Hasenhuettl & Hartel, 2008). Such usage is tempered by European rules (EC directive 95/2/EC), that state PGPR is allowed for use in low-fat formulations with 41 % fat or less in a maximum daily

intake of $4g \cdot kg^{-1}$ (Hasenhuettl & Hartel, 2008). Although the usage of PGPR is increasing, there is little scientific understanding of how it behaves at an interface and in the presence of other additives. There is some debate about the role of electrolytes in the stability of PGPR stabilised emulsions. For example, researchers state that a coalescence-stable oil continuous dispersion emulsified by PGPR can only be obtained in the presence of salt in the internal water phase (Fechner *et al.*, 2007), whereas others were able to prepare stable dispersions without salt in the water phase (Su *et al.*, 2006). Moreover, Su *et al.* (2008) claimed that a small addition, and an increasing concentrations, of sodium phosphate buffer or NaCl in the internal aqueous phase would destabilise emulsions, with phase separation proportionally related to the concentration of ions.

2.5.2.2 Hybrids of natural polymers in duplex emulsions

Due to the limitations of small molecular weight surfactants, polymeric emulsifiers have been used to improve stability and to control sustained and prolonged release of active materials (Benichou *et al.*, 2007; Mezzenga *et al.*, 2004; Su *et al.*, 2006). Both, naturally occurring and tailor-made polymeric emulsifiers have been reported to provide better interfacial coverage during emulsification and steric stabilisation against coalescence (Benichou *et al.*, 2004). Moreover, replacing the monomeric surfactants by proteins and polysaccharides appears to be beneficial, since they will not form reversed micelles transporting water, and water soluble material, across the oil phase (Garti, 1997a).

By employing PGPR and sodium caseinate for stabilisation of the primary and secondary interfaces, respectively, Bonnet *et al.* (2009) showed that both primary and secondary emulsions were stable against coalescence for a month. Also bovine serum albumin has been

used in mixtures with monomeric surfactants (Tween 20 and Span 80) resulting in the enhanced stability of $W_1/O/W_2$ emulsions (Garti, 1997a).

2.5.2.3 Solid particles as emulsifiers

It has been well referred in the literature that solid particles of colloidal size can, like surfactant molecules, be employed to kinetically stabilize emulsions (Pickering, 1907). Unlike low molecular weight surfactants, solid particles in Pickering emulsions are thought to be irreversibly adsorbed at the oil-water interface, providing a mechanical barrier against coalescence (Arditty *et al.*, 2004). Once adsorbed on the oil-water interface, the energy required to remove the particle from the interface is very high (~2750 k_BT). Therefore migration of particles from inner to outer interface or vice versa, in duplex emulsions, is expected to be minimal after emulsion formation, thus the major cause of instability occurring in surfactant stabilised emulsions can be eliminated and such emulsions can be stable to coalescence (Binks, 2002). Both $W_1/O/W_2$ and $O_1/W/O_2$ emulsions stabilised solely with solid particles have been made and claimed to be stable against coalescence for over a year (Barthel *et al.*, 2003)

2.5.2.4 Control of Osmotic Pressure

The large Laplace pressure of small water droplets (W_1) (see Eq. 2-3) encapsulated in duplex $W_1/O/W_2$ emulsions is one of the major sources of their instabilities leading to water diffusion from the internal to the external water compartment. As already mentioned, there are two possible mechanisms suggested in the literature for delivering water and water-soluble addenda through the oil phase: swelling-breakdown mechanism and diffusion and/or permeation through the oil membrane (by reverse micellar transport and diffusion across the

very thin lamellae of surfactant phase formed in areas where the oil layer is very thin). It was also proposed that water could migrate *via* hydrated surfactants (Cheng *et al.*, 2007; Wen & Papadopoulos, 2001). All mechanisms are schematically presented in Figure 2-9.

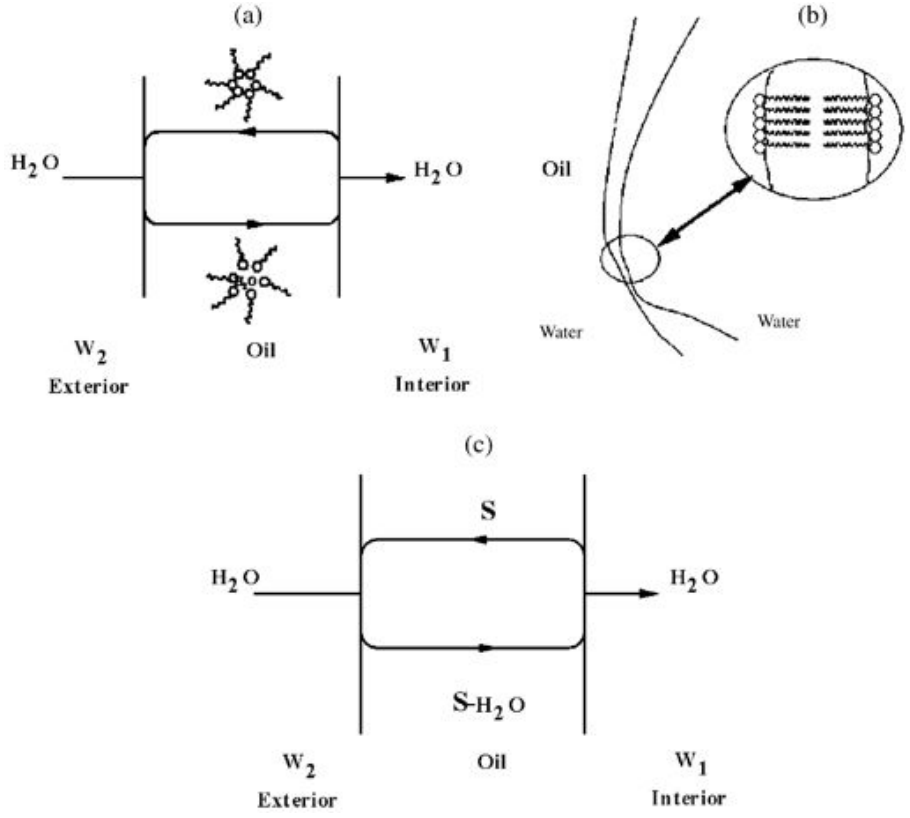

Figure 2-9 Mechanisms of mass transport across the oil membrane in duplex $W_1/O/W_2$ emulsions: (a) reverse micellar transport, (b) permeation through thin lamella of oil, (c) transport *via* hydrated surfactant (image taken from Benichou *et al.*, 2004).

The effect of the osmotic pressure gradients on the water transport rates in $W_1/O/W_2$ double emulsions, especially when the water migration is controlled by different mechanisms as described above, is rather complicated and to some extent still not completely clarified. Wen & Papadopoulos (2001) showed, by observing single $W_1/O/W_2$ globules through capillary video microscopy, that only water may permeate through the oil phase while salt stays entrapped in water compartments. The authors proposed, that transport *via* a hydrated ion mechanism occurred when the oil membrane was sufficiently thin or both interfaces were

visually contacting; with water transport rates increasing with the concentration of salt in one of the water phases. When two water compartments were visually non-contacting, water transport occurred *via* reversed micelles and was independent of the osmotic pressure gradient for a significant range of salt concentrations. In their later study Cheng *et al.* (2007), through the same visual study method found for the first time that ions of NaCl and $AgNO_3$ can migrate through thick oil films. The transport significantly slows when the oil film thickness is less than 1 μm and the transport of ions mainly takes place *via* reverse micelles instead of direct diffusion, and depends on the ion Pauling's radius. Jager-Lezer *et al.* (1997) found that there was no net transport of either water or electrolyte ($MgSO_4$) under iso-osmotic conditions in $W_1/O/W_2$ emulsions. On the contrary, according to Garti (1997b), release of electrolytes takes place even if droplets are stable to coalescence and the osmotic pressures of two phases have been equilibrated. Muscholik (2007) stated that the stability of very small inner droplets and the right concentration of salt or other ingredients are essential to control the osmotic balance in multiple emulsions.

It is apparent that the knowledge of the relationship between water transport rates and the important system parameters is still insufficient for controlling water and encapsulant migration in multiple emulsions (Wen & Papadopoulos, 2001). This thesis aims to address the issue of surfactant concentration and osmotic pressure imbalance on the transport of electrolyte between the two water compartments in duplex $W_1/O/W_2$ emulsions.

3 Materials and Methods

3.1 Materials

The oil soluble emulsifier Admul WOL 1408 (polyglycerol polyricinoleate, PGPR, HLB = 1.5 ± 0.5) was kindly provided by Kerry Bio-Science (The Netherlands). Tween 20 (Sorbitan Monolaurate, HLB = 16.7), glucose, sucrose, fructose, NaCl, KCl and Xanthan Gum (from *Xanthomonas campestris*) were purchased from Sigma Aldrich (UK). Food grade, dry Whey Protein Isolate with 95 % of globular protein content was kindly provided by DAVISCO Foods International, Inc. (Switzerland). Sunflower oil (with ~11 % of saturated fat) and soybean oil (with ~16 % saturated fat) were purchased from the local supermarket. All experiments were performed using distilled water (conductivity 1.3 – 1.5 $\mu S \cdot cm^{-1}$, pH = 6.8). All materials were used without further purification or modification. The percentages of emulsion components were calculated as the weight of the individual component per weight of a final emulsion discussed in the particular section (*i.e.* either W/O, O/W or W/O/W emulsion), unless stated otherwise. All experiments were repeated at least three times and a mean (average) value was reported (*i.e.* sum of all samples divided by the number of samples). Statistical error was calculated and reported as one standard deviation in text and two standard deviations on the graphs.

3.2 Methods

In the subsequent sections the formulation and techniques used in the preparation of primary W_1/O emulsions are described (Section 3.2.1), followed by simple O/W emulsions (Section 3.2.2) and duplex $W_1/O/W_2$ emulsions (Section 3.2.3). The analytical methods used for microstructural characterisation are then presented in Section 3.2.4.

3.2.1 Preparation of simple (primary) W_1/O emulsions

3.2.1.1 Formulation

10 % to 50 % water-in-oil (W_1/O) emulsions were formulated. Commercially available sunflower oil (SF) and soybean oil (SB) were used. Oil-soluble emulsifier polyglycerol polyricinoleate (PGPR) was used at concentrations between 0.5 % and 7 %. Water-soluble materials: NaCl and KCl were used at concentrations between 0.25 % and 2 %.

Prior to emulsification, the desired amount of components were dissolved/dispersed in either the aqueous or fat phase:

(i) PGPR was added to the oil phase and stirred with a high-shear mixer at 2000 rpm for 10 min, at 25 ± 3 °C,

(ii) NaCl and KCl were dissolved in the aqueous phase by mixing with a magnetic stirrer at ambient temperature.

3.2.1.2 Processing – high-shear mixer

A rotor-stator mixer (Silverson L4RT, impeller diameter 28 mm) was used for emulsification of primary W_1/O emulsions. Rotational velocity and mixing time were varied from 2000 rpm to 10,000 rpm and from 2 min to 20 min, respectively. During the initial experiments, that

aimed at understanding factors contributing to W_1/O emulsion stability, a 150 g batch size emulsion was prepared (Section 4.2). Later, when W_1/O emulsions were manufactured in larger quantities for the subsequent duplex emulsion production (Section 4.3 and Chapter 5), a 300 g batch size emulsion was mixed at 10,000 rpm for 10 min. The water phase (with or without salt) was added drop-wise to the oil mixture containing the emulsifier, while homogenising. Shear-induced heating of the sample (up to ~70 °C) resulted in faster water evaporation, therefore the system was cooled during the homogenisation (to ~20 °C) by means of an ice bath. After preparation, emulsions were analysed and then stored either at the temperature of 25 ± 3 °C or at 5 ± 2 °C.

3.2.2 Preparation of simple O/W emulsions

3.2.2.1 Formulation

All raw material solutions described in this section were prepared at the temperature of 21 ± 1 °C. An overhead stirrer (IKA Eurostar Digital) equipped with a pitch blade turbine impeller (50 mm in diameter) was used for preparing the desired dispersions prior to emulsification.

The dispersed phase (sunflower oil) volume was set at 2 % and then from 10 % to 60 % (in a 10 % increment) of the total emulsion volume. When the dispersed phase volume in emulsion was varied, Tween 20 was used at the concentration of 2 %, with the respect to the oil phase.

The concentration of Xanthan Gum (XG) in the aqueous phase was altered between 0 % and 0.5 %. Firstly, a batch of 3 L containing 0.5 % XG in water was mixed vigorously for 4 h using the overhead stirrer. When all XG was dispersed, part of the solution was diluted 50:50 with distilled water, forming a 0.25 % XG dilution. Then again, part of the 0.25 % dilution

was further diluted 50:50 with water forming a 0.125 % XG solution. This was repeated until 0.0156 % XG in water was obtained. 1 % of Tween 20 was added to each of the dilutions and stirred for additional 15 min.

The water-soluble emulsifier Tween 20 content was varied between 0.0005 % and 2 %. A series of Tween 20 solutions in water were prepared by dilution. Firstly, a batch of 4 L containing 2 % Tween 20 was mixed vigorously for 15 min using the overhead stirrer. Then, part of the solution was diluted 50:50 with distilled water, forming a 1 % Tween 20 dilution. This was repeated until 0.0005 % Tween 20 in water was obtained.

Whey Protein Isolate (WPI) solution in water (1:99) was prepared in a batch of 3 L. The solution was mixed vigorously for 4 h using the overhead stirrer. Distilled water with pH = 6.8 was used. The iso-electric point for WPI is at pH = 5.3 (Klein *et al.*, 2010), therefore it could be assumed that, at such experimental conditions, WPI is slightly negatively charged.

3.2.2.2 Processing – rotating membrane emulsification

Shirasu Porous Glass (SPG) hydrophilic membranes with 2.8 μm and 6.1 μm mean pore diameters were purchased from SPG Technology Co. (Japan). The SPG membranes are tubular, 10 mm in outer diameter, 250 mm in length, giving a surface area of ~78 cm^2. The membranes were cut with a diamond blade into 50 mm long pieces and then attached, using suitable commercial glue, to a female threaded metal ferrule on one end and a closing metal cap on the other end. Next, the membrane was mounted on a male threaded shaft of an IKA Eurostar Digital overhead stirrer. The rotating membrane apparatus is shown in Figure 3-1.

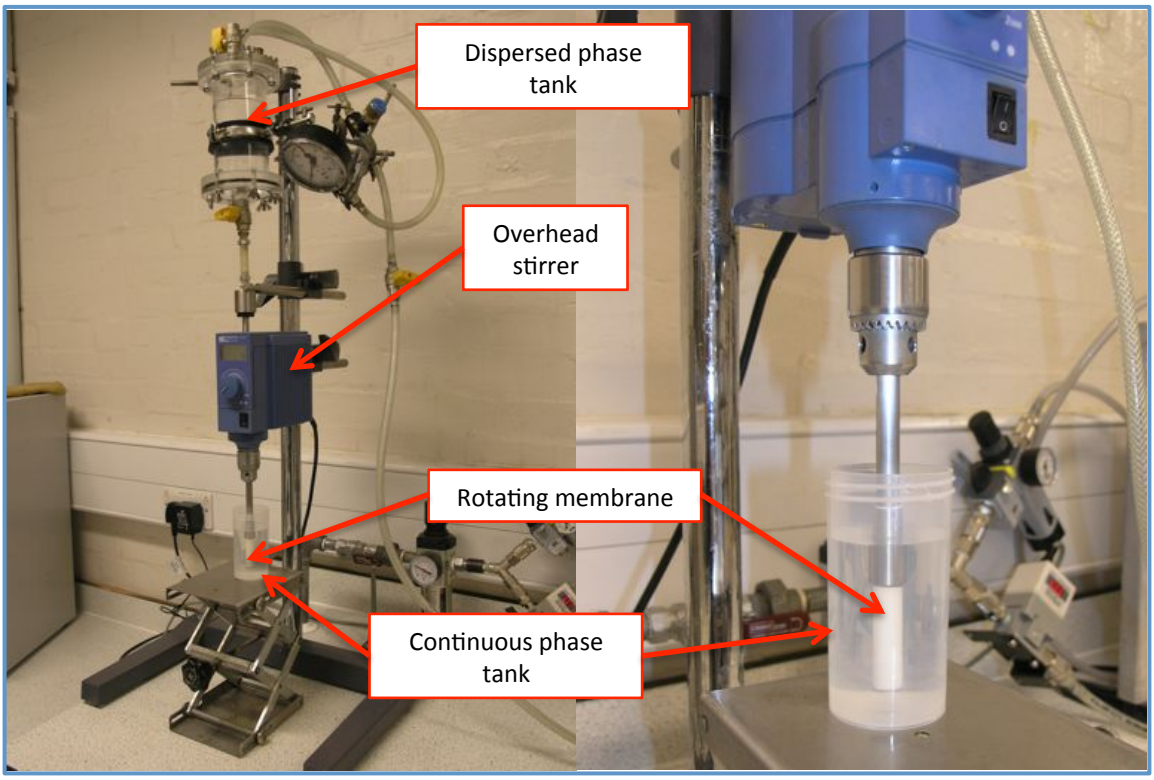

Figure 3-1 The rotating membrane system (Left) with a close-up onto the membrane (Right).

Prior to emulsification, all membranes were pre-wetted with the continuous phase (distilled water) and treated in an ultrasonic bath (Bransonic B2210E, Ultrasonic Cleaner) for 3 h to remove residual air and enable micropores to be filled with the continuous phase. After emulsification, membranes were cleaned with a soap solution in the ultrasonic batch (until the solution was clean), and then sonicated again with ethanol for 3 h. After rinsing with distilled water, membranes were dried in the oven at 60 °C for 12 h and then soaked in the continuous phase while sonicated.

Cleaning of the membranes was conduced as follows. A given membrane was used to produce one emulsion for all combinations of emulsification parameters (*i.e.* rotational velocity and trans-membrane pressure, later referred to as a "*single experimental run*"). Then, the membrane was detached from the stirrer and cleaned as described above. After the

cleaning process, the *single experimental run* was repeated twice (with cleaning in-between), to obtain a total of three samples for all emulsification parameters combinations, for the statistical analysis. Between each batch emulsifications, during the *single experimental run*, the membrane surface was rinsed with distilled water to remove all the residual droplets that may contaminate the next sample.

The range of applied rotational velocities (RV) was determined by the intrinsic limitations of the overhead stirrer (*i.e.* minimum of 50 rpm and maximum of 2000 rpm), but also the design of the rotating membrane. More specifically, at very high RVs, the membrane vibrated intensively, which was especially significant when the metal ferrule and the glass part of the membrane were not connected together (as described above) perfectly in-line. Such vibrations could potentially lead to: (i) inconsistent shear force for different membranes used for the experiments, and (ii) membrane cracking. Consequently, the speed of the membrane rotation was set at 300, 500, 700, 900, 1100, 1300 and the maximum of 1500 rpm. The shear rates and shear stresses at the surface of the rotating membrane (presented in Table 3-1) were calculated for each RV as described in Section 8.2 (Appendix).

Table 3-1 Shear rate and shear stress values corresponding to the rotational velocity [rpm].

Rotational velocity [rpm]	**Shear rate at membrane surface R_i** [s^{-1}]	**Shear stress at membrane surface R_i** [Pa]
300	65	0.05
500	109	0.09
700	146	0.12
900	196	0.16
1100	239	0.20
1300	283	0.23
1500	326	0.27

The dispersed phase (*i.e.* sunflower oil) was pressurised through the membrane pores by compressed air at: (i) 25, 40, 60, 80 and 100 kPa trans-membrane pressure (TMP) for the 2.8 μm pore diameter membrane, and (ii) 10, 20, 30 and 40 kPa TMP for the 6.1 μm pore diameter membrane. The range of TMP was chosen for a given membrane so that: (i) the minimum TMP was a value ~5 kPa above the critical trans-membrane pressure[*] (CTMP), and (ii) the maximum TMP was set at a value ~20 kPa below the pressure, at which spots of the dispersed phase could be observed on the surface of the emulsion. These spots of the dispersed phase were assumed to be as a result of *jetting* (*i.e.* continuous outflow from the membrane pores) as described in Section 2.3.2.3.2. *Jetting* has been reported (Charcosset, 2009) to cause coalescence of oil droplets in the close vicinity to the membrane surface. The maximum TMP was smaller for the 6.1 μm membrane than for the one with 2.8 μm pores, due to the lower hydrodynamic resistance of the former. The CTMP of the 2.8 μm membrane was empirically identified to be ~20 kPa and for the 6.1 μm membrane ~5 kPa.

Membrane emulsification is a semi-batch process, thus the desired dispersed volume fraction was assessed by weighing the emulsion throughout the emulsification process (with a laboratory scale), and terminating the disperse phase flow at a required weight. 100 mL of a sunflower-oil-in-water (O/W) emulsion was made in a plastic beaker of a 180 mL volume capacity (with 52 mm inner diameter).

[*] *i.e.* a minimum pressure at which the dispersed phase passes through a given membrane (as described in Section2.3.2.3.3).

3.2.3 Preparation of duplex $W_1/O/W_2$ emulsions

3.2.3.1 Formulation

To construct duplex $W_1/O/W_2$ emulsions, 30 % of the primary W_1/O emulsion (prepared as described in Section 3.2.1) was dispersed in 70 % of the external water phase (W_2). The primary emulsion contained 0.28 M NaCl in the internal water phase (W_1) and between 1 % and 4 % PGPR dissolved in sunflower oil (with the respect to the primary emulsion). Glucose, sucrose and fructose at different concentrations (0.14 M, 0.28 M, 0.57 M and 0.86 M) were placed in the external water phase (to induce osmotic imbalance between W_1 and W_2) and stirred for 10 min at ambient temperature using a magnetic stirrer. Then, 2 % of a secondary emulsifier - Tween 20 was added to the sugar solution and mixed for additional 10 min.

3.2.3.2 Processing – high-shear mixer

The primary W_1/O emulsion (prepared as described in Section 3.2.1) was placed on the top of the water phase and homogenised at 10,000 rpm for 2, 5 and 10 min using a Silverson mixer (model SL2T, impeller diameter 21 mm) and a 150 g batch size. All duplex emulsions described in this thesis were analysed immediately after preparation and then in regular intervals during storage (in a refrigerator at 5 ± 2 °C).

3.2.3.3 Processing - rotating membrane emulsification

The SPG hydrophilic rotating membrane (Figure 3-1, p.49) with a pore size of 2.8 μm was used to produce duplex $W_1/O/W_2$ emulsions. Prior to emulsification the membrane was cleaned and prepared as described in Section 3.2.2.2.

The rotational velocity was set at 300, 600, 900 and 1200 rpm. The dispersed phase (W_1/O emulsion) was pressurised through the membrane pores by compressed air at the TMP of 40, 60, 80 and 100 kPa. 150 g of 30 %-primary-(W_1/O)-emulsion-in-70 %-water-(W_2) was made in a plastic beaker of 180 mL volume capacity (with 52 mm inner diameter).

3.2.3.4 Processing - cross-flow membrane emulsification

SPG hydrophilic membranes, 250 mm in length and the pore size of 3.9 μm, 6.1 μm and 10 μm were used for the preparation of $W_1/O/W_2$ duplex emulsions in cross-flow membrane emulsification. The membrane apparatus is presented in Figure 3-2.

Prior to emulsification, the membranes were cleaned as described in Section 3.2.2.2. When the desired trans-membrane flux was not obtained by washing with the soap and the solvent, membranes were baked in the muffle furnace at 500 °C for 24 h, to burn all the residual oils (Nakashima *et al.*, 1991). After the heat treatment, to restore hydrophilicity, the membranes were soaked in 2 M HCl at 70 °C for 2 h and finally rinsed with distilled water.

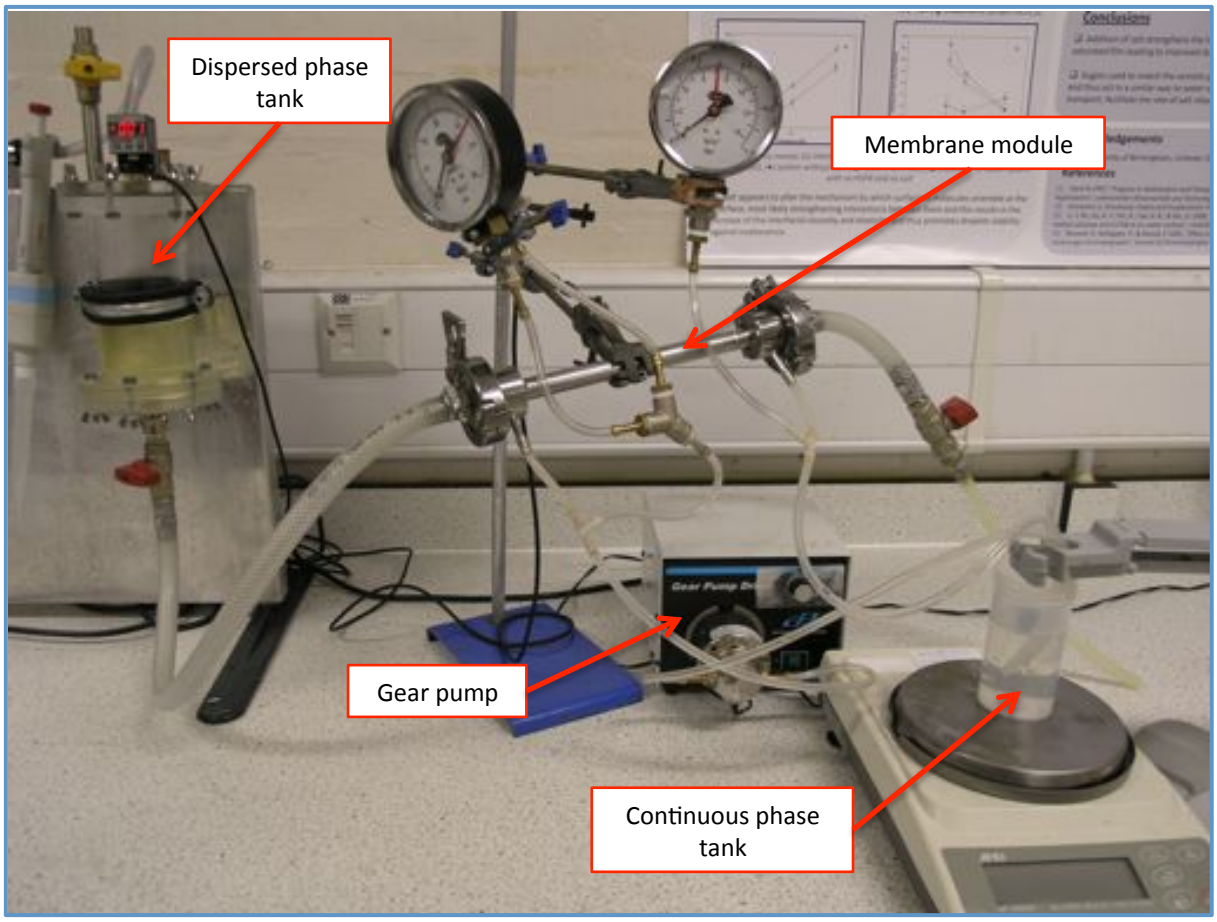

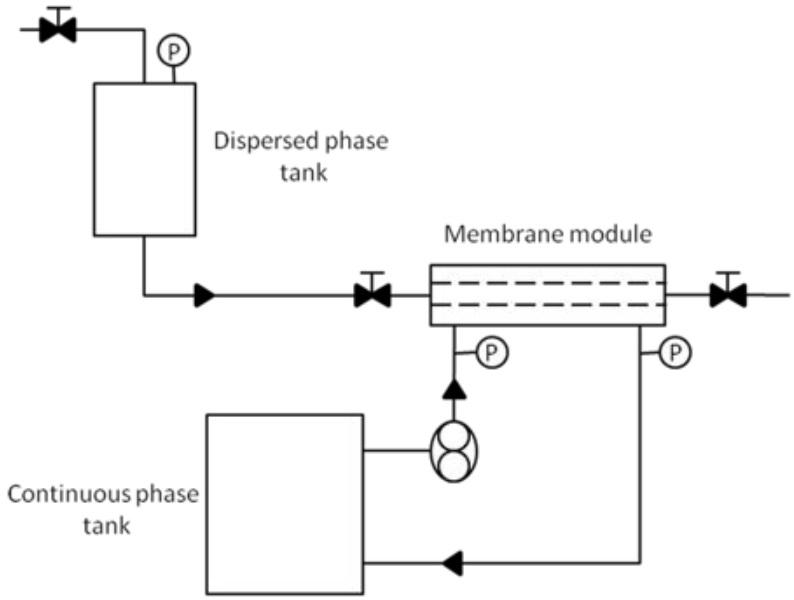

Figure 3-2 (Top) Picture and (Bottom) schematic diagram of the cross-flow membrane system.

Continuous emulsion phase (W_2) with additives (*i.e.* 2 % Tween 20 and 0.14 M glucose), was pumped across the outer surface of the membrane by a gear pump (Micropump, Cole-Palmer, USA; flow rate 2.5 – 5450 $mL \cdot min^{-1}$). The reason behind this rather unconventional design of the direction of the dispersed phase flow through the membrane (*i.e.* inside-out) was to minimise droplets collisions (hence coalescence) in the mainstream of the continuous phase, but also ensure laminar flow conditions, as the gap between the membrane and the module enclosing it was small (2 mm). At three chosen pump flow rates, the pressure exerted by the continuous phase on the membrane surface was measured to be 10, 30 and 50 kPa. The maximum continuous phase pressure was determined by the properties of the pump; *i.e.* the maximum flow rate obtained for a particular formulation (*e.g.* viscosity) of the continuous phase. The dispersed phase, in this case – W_1/O emulsion pressurised in the vessel, was forced (from the inside if the membrane) through the membrane pores at the TMP of 20, 40 and 80 kPa. TMP was calculated as a difference between the dispersed phase pressure and the pressure exerted on the membrane by the continuous phase. One range of TMP was chosen for all three membranes: (i) the minimum TMP was a value ~5 kPa above the CTMP for the membrane with the smallest pores (3.9 μm), and (ii) the maximum TMP was set at a value ~20 kPa below the pressure at which *jetting* could be observed, using membrane with the largest pore diameter (10 μm).

The batch size for the cross-flow membrane emulsification, identically to the high-shear and rotating membrane emulsification (of $W_1/O/W_2$ emulsions) was 150 g, 30 % of which was the dispersed phase (W_1/O). The desired dispersed phase volume fraction was assessed by weighing the emulsion, as described in Section 3.2.2.2.

For further analysis, cross-flow velocities (CFV) were calculated from volumetric flow rates of the emulsion in the membrane module. This was done for each continuous phase pressure (Table 3-2). As mentioned earlier, membrane emulsification is a semi-batch process and the dispersed phase volume fraction increases with emulsification progression. This leads to an increase in the overall viscosity of the emulsion, thus an increase in the pressure exerted by the continuous phase on the membrane, and by extension a drop in the effective TMP. To maintain constant TMP it was decided for practical reasons, to manually reduce the CFV by controlling the pump speed. Due to the increasing viscosity of the produced emulsion, two situations have been considered for velocity calculations: (i) $T_{0\%}$ when the dispersed phase volume is 0 % (start of the emulsification process), and (ii) $T_{30\%}$ when the dispersed phase volume is 30 % (end of the emulsification process). To simplify the way the CFV is referenced in further text, an average of $T_{0\%}$ and $T_{30\%}$ was calculated and used consequently for the respective continuous phase pressure.

Table 3-2 Cross-flow velocities at respective continuous phase pressures; $T_{0\%}$ is for 0 % dispersed phase volume and $T_{30\%}$ is for 30 % dispersed phase volume.

Continuous phase pressure [kPa]	**Cross-flow velocity** [$m \cdot s^{-1}$]		
	$T_{0\%}$	**$T_{30\%}$**	**Average**
10	0.16	0.06	0.11
30	0.23	0.11	0.17
50	0.29	0.15	0.22

3.2.4 Emulsion characterisation

3.2.4.1 Droplet size and microscopic observation

Droplet size distribution of the primary W_1/O emulsions was determined just after preparation and then at weekly intervals by a Malvern Mastersizer 2000 (Malvern Instruments, UK) with a Hydro SM manual small volume sample dispersion unit attached. The scattered intensity as a function of the angle was transformed into size distribution using the Mie theory (Bonnet *et al.*, 2009). Primary emulsion droplet size was determined using relevant refractive index for sunflower oil (*i.e.* 1.4729) as the dispersing medium.

Duplex emulsions were analysed using the same apparatus and measurements were performed in distilled water. Here, it is important to stress that in the special case of duplex emulsions, the scattering objects are optically non-uniform as the oil droplets contain small water droplets. The scattering properties of such structures are more complex, however, as previously proposed by Pays *et al.* (2001) an assumption can be made that the primary emulsion behaves like a simple droplet with the same refractive index as the oil phase. The average droplet size measured by microscopy correlated well with Mastersizer data (*e.g.* droplet size measured by Mastersizer 12.3 μm and microscopic technique 13.1 μm ± 1.2 μm).

The droplet size was reported as a surface-weighted diameter (Sauter diameter), $D_{3,2}$. The mean Sauter diameter is the diameter of a spherical droplet having the same area per unit volume as that of the total collection of droplets in the emulsion. The droplet uniformity was expressed as the span of droplet size distribution:

$$span = D_{90} - D_{10} / D_{50} \qquad \text{Eq. 3-1}$$

where D_{90}, D_{50} and D_{10} are the particle sizes at which 90%, 50% and 10% of the distribution lies below in a cumulative undersize figure.

Images of duplex emulsions were taken just after preparation and regularly during storage on a light microscope (Olympus CH2, Japan, with CCD video camera).

3.2.4.2 Interfacial properties

Interfacial tension. Equilibrium interfacial tensions of surfactant/sugar/salt solutions were measured using a pendant drop method on an EASYDROP Contact Angle Measuring System from Krüss GmbH, Hamburg (Germany). In this method, a drop of aqueous solution (with or without water-soluble components) was formed at the tip of a syringe needle, immersed in a cuvette containing sunflower oil (with or without oil-soluble surfactant). By analysing the shape of the drop, the software calculates the interfacial tension (McClements, 2005). Measurements were performed at 25 ± 3 °C.

Interfacial rheology. Profile Analysis Tensiometer (PAT-1) from Sinterface Technologies (Germany) was used for the determination of dilatational rheological properties of the interfacial layers. The volume of droplet was subjected to small sinusoidal oscillations (0.05 - 0.5 Hz) and fitting the Laplace equation to the resulting drop shape gives an interfacial dilatational modulus. The volume of a drop was always approximately 3.5 μL, with controlled interfacial area of 10 mm^2, which was expanded and compressed, with the amplitude of 0.5 mm^2. The temperature was held constant at 25 °C by the use of a water bath. The storage and loss modulus of interfacial layer was calculated from a Fourier analysis of the measured signal (Leser *et al.*, 2005).

3.2.4.3 Zeta potential

Zeta potential was determined using a Zetamaster from Malvern Instruments (UK). Measurements were performed at 25 ± 3 °C on freshly made emulsions diluted to a phase volume well below 1 %. Dilutions were made using the continuous phase composition.

3.2.4.4 Rheology

Bulk viscosity was measured using a Bohlin Gemini HR Nano from Malvern Instruments (UK), with "PP 60 acrylic" geometry at 25 °C. Viscosity measurements of XG solutions were performed by applying range of shear rates ranging from 0.16 s^{-1} to 790 s^{-1}. Such range of shear rates corresponds to the shear rates generated by the rotation of the membrane, which varies between 65 s^{-1} at 300 rpm and 326 s^{-1} at 1500 rpm (Table 3-1, p.50).

3.2.4.5 Conductivity

The conductivity of duplex emulsions, during the emulsification process (or immediately after) and storage, was measured by a direct current conductivity meter S30 SevenEasy™ fitted with an InLab®710 platinum 4-plate electrode (Mettler Toledo, UK), which had a measurement range of 0.01 $\mu S \cdot cm^{-1}$ - 500 $mS \cdot cm^{-1}$. The conductivity meter was connected to a PC equipped with a RS323 DataLogger and measurements recorded every 1.25 s.

A model (Eq. 3-2) developed by Meredith & Tobias (1960) for describing the conductivity changes of an emulsion (k_e) was used to fit the data obtained from experiments and calibrations. According to this method, conductivity of an emulsion is related to the volume fraction of dispersed phase and conductivity of the continuous phase. If the conductivity of

the dispersed phase (k_d) is much lower than the conductivity of the continuous phase (k_c), conductivity of an emulsion can be described by:

$$k_e = 8k_c \frac{(2-\varphi)(1-\varphi)}{(4+\varphi)(4-\varphi)} \quad \text{Eq. 3-2}$$

where k_e is the conductivity of the bulk emulsion and φ is the dispersed phase volume fraction. The conductivity of the included water phase was measured before primary emulsion formation and assumed not to change on further processing.

Simple emulsions were used to check the model equation. Conductivity of 30 % oil-in-70 % water emulsions, with constant amount of glucose and Tween 20, was recorded as a function of NaCl concentration (Figure 3-3a). The experimental data agreed well with the model prediction for this situation (R^2 = 0.9989). The above model was then used to characterise the behaviour of the more complex duplex emulsions.

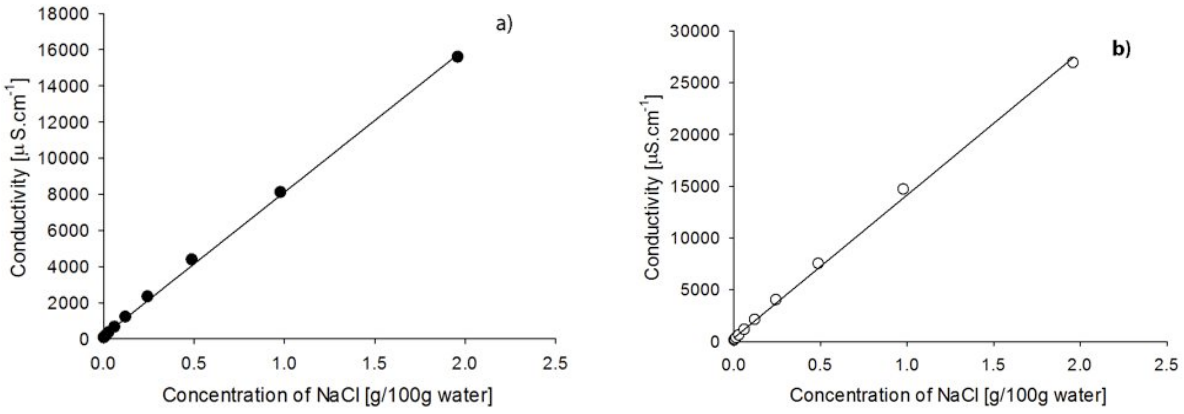

Figure 3-3 (a) Model fitting (Eq. 3-2) to a simplified system of O/W emulsions, R^2 = 0.9989; (b) an example of the calibration curve for the conductivity of glucose (0.14 M) and Tween 20 (2 %) with respect to NaCl concentration, R^2 = 0.998.

The conductivity of a duplex emulsion's external water phase was calculated from the adopted model equation (Eq. 3-1) and the measured conductivity of the $W_1/O/W_2$ emulsion. External water phase before emulsification was also taken into account during calculations. From the linear calibration curve for the conductivity of glucose and Tween 20 solutions with varying NaCl concentration (Figure 3-3b), the amount of salt released from the internal to external water phase was determined. The encapsulation was then expressed as a percentage of salt still retained (encapsulated) in the internal water phase:

$$Encapsulation = \frac{100 \times (M_t - M_r)}{M_t} \qquad \text{Eq. 3-3}$$

where M_t is a total original mass of salt present in the internal water phase and M_r is a mass of NaCl that migrated to the external water phase.

4 Formulation and processing of primary W_1/O emulsions and duplex $W_1/O/W_2$ emulsions with different osmotic pressures

4.1 Introduction

In this Chapter parameters that impact the stability and encapsulation properties of duplex $W_1/O/W_2$ emulsions containing marker compound were investigated.

Initial experiments were carried out to determine the formulation space and process parameters for simple water-in-oil (W_1/O) emulsions (Section 4.2). This was assessed by particle sizing techniques, analysis of the interfacial properties of adsorbed emulsifiers and visual/microscopic observations. Factors investigated in this section can be summarised as:

(i) Concentration of an oil-soluble emulsifier: polyglycerol polyricinoleate (PGPR) was used at range of concentrations (from 0.5 % to 7 %) to stabilise the emulsion droplets,

(ii) Dispersed phase volume: concentration of the internal water phase was altered between 10 % and 50 %,

(iii) Type of the oil phase: commercially available sunflower oil and soybean oil were compared,

(iv) Effect of NaCl and KCl on the stability of emulsions was investigated.

In the following experiments (Section 4.3), PGPR-stabilised W_1/O emulsions, where salt was placed in the internal water phase (W_1), were processed to construct duplex $W_1/O/W_2$

emulsions. Different concentrations of sugars (glucose, fructose and sucrose) were used to induce an osmotic pressures imbalance and the release of salt from the internal water phase during high-shear emulsification and storage has been investigated. The conductivity method assisted by an emulsion conductivity model for direct and online monitoring of salt encapsulation within the duplex emulsions during preparation and storage was used.

In Section 4.4, the effects of the primary W_1/O emulsion composition on the salt entrapment in the produced duplex emulsions were studied. To do that, the PGPR concentration in the primary W_1/O emulsion was varied between 1 % and 4 %. These simple emulsions, with salt enclosed in the internal water phase, were then used to make duplex $W_1/O/W_2$ emulsions. Mixing time of high-shear emulsification (10,000 rpm with a Silverson mixer) was adjusted to 2, 5 and 10 min, to investigate the effect of the secondary emulsification time on the emulsion droplet size and the release of salt from the internal water phase.

4.2 Primary W_1/O emulsions

The purpose of the following experiments was to identify a suitable emulsifier concentration and the emulsifying process for the production of stable primary W_1/O emulsions. Firstly, in Section 4.2.1 factors determining long-term stability of emulsions with PGPR were studied. In Section 4.2.2 the interfacial properties of adsorbed emulsifiers were investigated.

4.2.1 Formulation and processing aspects

Initial experiments were carried out to determine the formulation space and process parameters for the simple primary emulsions. PGPR was used at concentrations of 0.5 – 7 % to stabilise 10 %, 20 % and 30 % W_1/O emulsions, as described in Section 3.2.1.1. High-shear

mixer (Silverson L4RT) was used at different rotational velocities (between 2000 and 10,000 rpm) and samples were emulsified from 2 to 20 min, as described in Section 3.2.1.2.

All produced emulsions had limited stability (maximum of 2 weeks when stored at 5 ± 2 °C) and phase separation was visually detected as a layer of water on the bottom of storage vessels. For example, 20 %-water-in-80 %-oil emulsions with various concentrations of PGPR were stored up to 3 weeks in low and high temperature environment (Table 4-1). The Table shows, that emulsions droplet size measured after emulsification is sub-micron (between 0.15 μm and 0.20 μm) and after 1 week of storage at low temperature (5 ± 2 °C), all emulsions remained stable. However, amongst samples kept at higher temperature (25 ± 3 °C), formulations with the two lowest PGPR concentrations (0.5 % and 1 %), phase separated during the first week. Up to 2 weeks of storage, in all remaining samples (*i.e.* 2 – 7 % PGPR) kept at elevated temperature and in samples with 0.5 – 3 % PGPR stored in the fridge, a layer of water sedimented on the bottom of the storage vessels. Formulations with 4 – 7 % PGPR kept at low temperature remained stable over 2 weeks nevertheless, they phase separated up to 3 weeks of storage.

Table 4-1 Stability of W_1/O emulsions with 20% water phase and PGPR at various concentrations (with no salt in the W_1), stored at 25 ± 3 °C and at 5 ± 2 °C; (ps) phase separation.

PGPR [%]	**$D_{3,2}$** [μm] **after preparation**	**$D_{3,2}$** [μm] 1 week of storage at 25 ± 3 °C	**$D_{3,2}$** [μm] 1 week of storage at 5 ± 2 °C	**$D_{3,2}$** [μm] 2 weeks of storage at 25 ± 3 °C	**$D_{3,2}$** [μm] 2 weeks of storage at 5 ± 2 °C	**$D_{3,2}$** [μm] 3 weeks of storage at 5 ± 2 °C
0.5	0.20	ps	0.22	-	ps	-
1	0.16	ps	0.20	-	ps	-
2	0.18	0.20	0.18	ps	ps	-
3	0.15	0.21	0.21	ps	ps	-
4	0.20	0.19	0.21	ps	0.22	ps
5	0.19	0.19	0.19	ps	0.23	ps
6	0.18	0.20	0.22	ps	0.23	ps
7	0.18	0.18	0.20	ps	0.24	ps

Laser diffraction measurements revealed substantial change in the droplet size distribution with time. Figure 4-1 shows evolution of the droplet size of 10:90 emulsion stabilised with 7 % PGPR, as an example. It shows that the initial monomodal droplet size distribution became bimodal after a week of storage and multimodal after 2 weeks. Such changes are a consequence of *Ostwald ripening* and/or droplet coalescence (as described in Section 2.4), and resulted in phase separation of the sample.

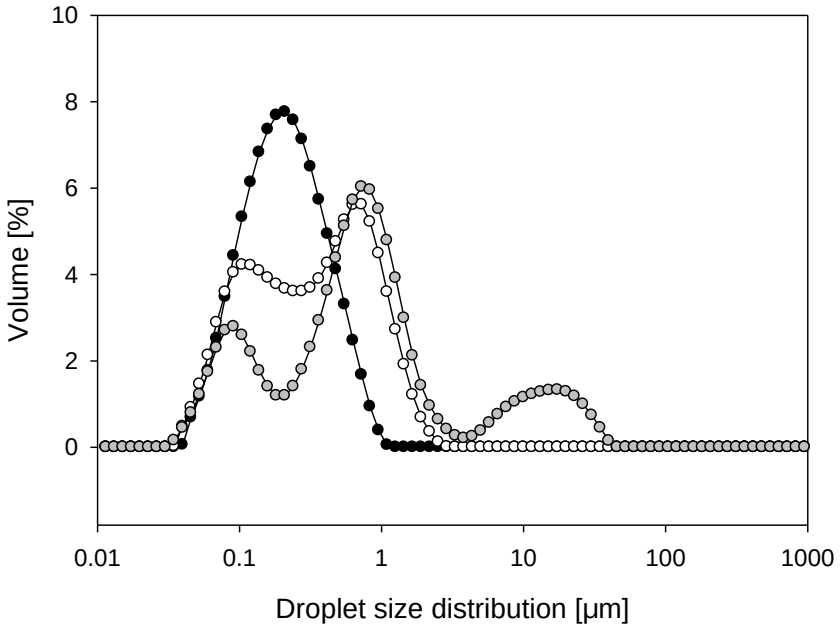

Figure 4-1 Droplet size distribution of 10:90 W_1/O emulsions with 7 % PGPR (with no salt in the W_1), stored at 25 ± 3 °C: (●) just after preparation, (○) 1 week of storage, (●) 2 weeks of storage.

According to research referred to by Muschiolik (2007), coalescence stable W_1/O emulsions with PGPR can be obtained in the presence of salt in the internal water phase. Therefore, in the following set of experiments, W_1/O emulsions with salt dissolved in the water phase were formulated and prepared using the high-shear mixer, as described in Section 3.2.2.2. Emulsion stability was investigated as a function of: (i) oil phase type, (ii) PGPR concentration, (iii) type and concentration of salt in the internal water phase, (iv) dispersed

phase volume, and (v) storage temperature. The variety of applied modifications to the W_1/O emulsion formulation are summarised in Table 4-2.

Table 4-2 Formulation of W_1/O emulsions A – E. All samples were stored both at 25 ± 3 °C and at 5 ± 2 °C.

Formulation	**Water phase volume fraction** [%]	**PGPR** [%]	**Salt** [%]
A	30 (SB)	2, 4, 6	0.25 (NaCl)
B	30 (SF)	0.5, 1, 2, 4, 6	0.25 (NaCl)
C	30 (SF)	4	0.25, 0.5, 1, 2 (NaCl)
D	30 (SF)	4	0.25, 0.5, 1, 2 (KCl)
E	10, 20, 30, 40, 50 (SF)	4	1 (NaCl)

The initial experiments focused on the oil phase composition (formulations A and B in Table 4-2) and thus W_1/O emulsions (30:70) were formulated with either sunflower oil (SF) or soybean oil (SB). In spite of the fact that, sunflower oil and soybean oil have slightly different oil composition (see Section 3.1), when 0.25 % NaCl was added to the aqueous phase and from 2 % to 6 % PGPR to the oil phase, W_1/O emulsions were stable over 19 weeks of storage, regardless of the type of oil used. The emulsions stored both at ambient (25 ± 3 °C) and low temperature (5 ± 2 °C) had comparable droplet size over the investigated storage period. An example of the droplet size evolution during long-term storage, for a 30:70 emulsion containing 4 % PGPR in sunflower oil, is given in Figure 4-2. It shows that the initial droplet size distribution (with span = 2 and the average $D_{3,2}$ diameter of ~0.2 μm) became narrower after 19 weeks of storage (span = 1), with slight increase in the average droplet size (to ~0.3 μm). This increase in the droplet size is a result of *Ostwald ripening*, which occurs due to an increase in solubility of a substance as the size of the particle containing it decreases (McClements, 2005). Mass transport between the emulsion droplets, induced by the differences in their sizes, over time lead to disappearance of small droplets and overall coarsening of the emulsion, which is evident from Figure 4-2.

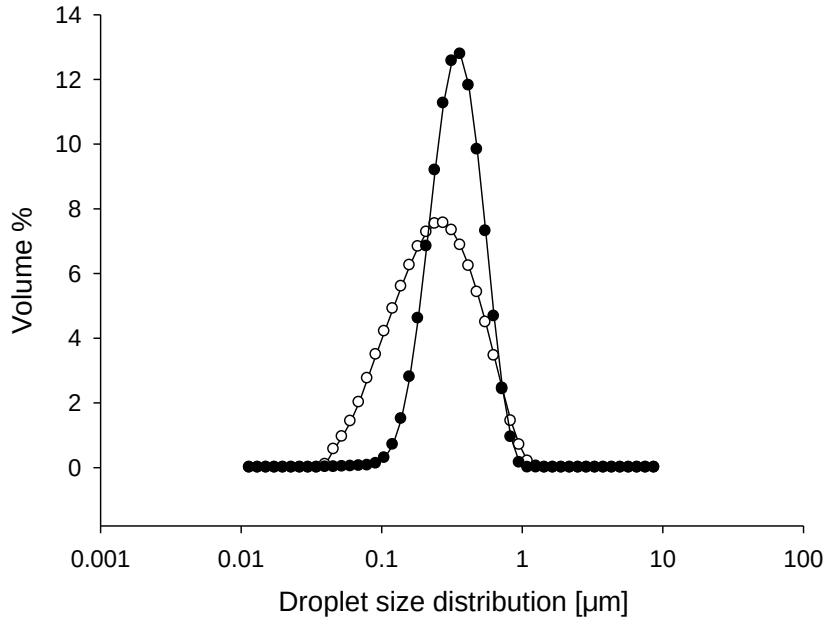

Figure 4-2 Particle size distribution of 30:70 W_1/O emulsions with 4 % PGPR and 0.25 % NaCl, (○) just after preparation and (●) 18 weeks after preparation (stored at 25 ± 3 °C).

To establish the amount of PGPR necessary for long-term emulsion stability, series of 30:70 water-in-SF oil emulsions with 0.5, 1, 2, 4 and 6 % PGPR, and a constant amount of salt in the water phase (0.25 %) were produced and examined over a prolonged storage time of 19 weeks (formulation B, Table 4-2). Emulsions with 0.5 % PGPR showed a bimodal size distribution after preparation and after only a few days a layer of water (roughly 10 % of the total emulsion volume) sedimented at the bottom of the storage container. Formulations with 1, 2, 4 and 6 % PGPR showed a normal size distribution and no significant decrease in their average droplet size (ranging between 0.16 and 0.24 µm, Figure 4-3 left) with increasing concentration of PGPR (*i.e.* from 1 % to 6 %). However, after 2 weeks of storage, water sedimented in the vessels containing 1 % PGPR emulsion (roughly 5 % of the total emulsion volume). Surface coverage calculations (Section 8.1, Appendix) indicate, that 0.6 % PGPR is sufficient to cover the interface of 30 % water-in-oil emulsion with an average 0.2 µm droplet

diameter. However, such calculations have to be treated with caution, as they require certain degree of approximation (*e.g.* average droplet size, molecular weight and hydrodynamic diameter of a polymeric surfactant). From the above experiment it can be concluded that 2 % PGPR or more is necessary to provide long-term stability of the 30:70 primary emulsion.

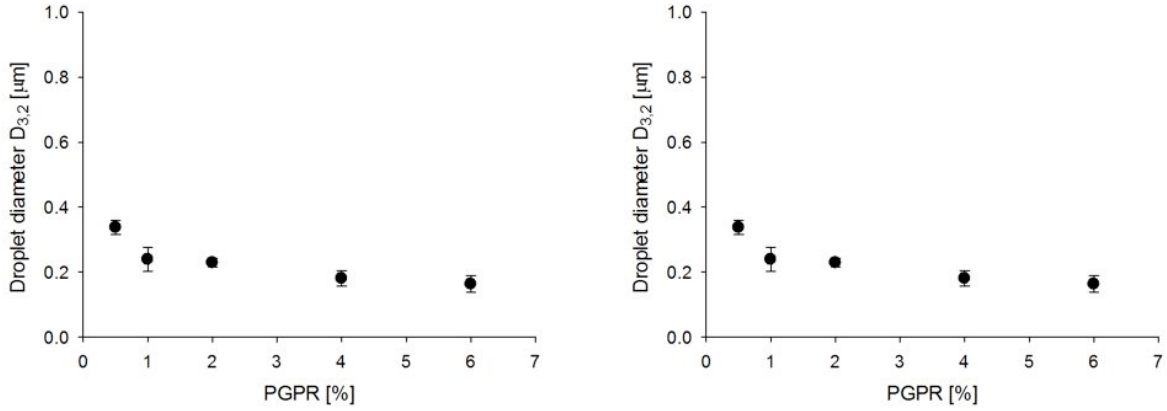

Figure 4-3 Droplet size of W_1/O emulsions: (Left) with 0.25 % NaCl and varied PGPR concentration and (Right) with 4 % PGPR and varied concentration of NaCl.

Further experiments were carried out to determine the minimum level and the type of salt to achieve stability in the system (formulations C, D in Table 4-2). The salt concentration (NaCl or KCl) in the aqueous phase was varied between 0.25 % and 2 % and the concentration of PGPR was kept constant at 4 %. Described here as stable, 30:70 emulsions with similar droplet size of ~ 0.2 µm (Figure 4-3 right) could be produced regardless of the concentration and type of salt used. That is, at a given salt concentration, the emulsions with either NaCl or KCl in the water phase showed very similar droplet size and droplet size distribution immediately after preparation, which remained unchanged during storage period of 4 weeks. A similar trend was observed when, for a given type of salt, its concentration in the aqueous phase was varied.

In the following set of experiments, the effect of the dispersed phase volume fraction on the emulsion stability was analysed (formulation E in Table 4-2). The dispersed phase volume was varied between 10 % and 50 % (in 10 % increments) and the concentration of PGPR was kept constant at 4 %. In order to eliminate the effect of salt on the stability of the emulsion, NaCl was kept at a concentration of 1 %, with the respect to the water phase. All produced emulsions remained stable over the observation period of 19 weeks. However, droplet size and droplet size distribution slightly changed over the storage period. For example, 50:50 emulsions after preparation had the average diameter $D_{3,2}$ of ~0.2 μm and span = 2.2, which then changed to: (i) ~0.4 μm and span of 1 when the samples were refrigerated (at 5 ± 2 °C), and (ii) ~0.5 μm and span of 1.1, when the samples were kept at ambient temperature (25 ± 3 °C). This increase in the average droplet size and narrowing of the droplet size distribution is a result of *Ostwald ripening*. The fact that there was no significant effect of the dispersed phase volume (at concentrations between 10 % and 50 %) on the stability of W_1/O emulsions indicates that the PGPR concentration of 4 % provides a sufficient amount of molecules to stabilise the oil-water interface within the investigated dispersed phase volumes. This is in agreement with the theoretical calculations of surface coverage (Section 8.1 in the Appendix), which indicated that 0.9 % of PGPR is required to stabilise the 50:50 W_1/O emulsion.

4.2.2 Interfacial properties of the adsorbed PGPR layer

As indicated in the previous sections, stable W_1/O emulsions could be produced only when the water phase contained salt. To further understand the mechanisms of the effects exhibited by the addition of NaCl to PGPR stabilised W_1/O emulsions, a study of interfacial tension and interfacial rheology of the adsorbed emulsifier layers was performed (according to the methods described in Section 3.2.4.2).

In Table 4-3 the effect of NaCl on the interfacial tension of PGPR is reported. It shows that the interfacial tension between water and sunflower oil decreased on addition of salt. The measured interfacial tension of a pure water-sunflower oil system was 26.5 ± 0.5 $mN \cdot m^{-1}$, with 4 % PGPR this reduced to 3.5 ± 0.1 $mN \cdot m^{-1}$ and with 0.5 % NaCl this was further reduced to 2.4 ± 0.1 $mN \cdot m^{-1}$. It is unlikely that such a small change in interfacial tension is responsible for the increased stability of the emulsion. The proposed hypothesis is that the change in the interfacial tension is a result of the packing and interaction of the PGPR in the interfacial layer. In order to test this, the interfacial rheology was measured.

Table 4-3 Effect of NaCl on the equilibrium interfacial tension (at 25 ± 3 °C) of water-sunflower oil system, containing PGPR.

Water	**NaCl** [%]	**Oil**	**PGPR** [%]	**Interfacial tension** [$mN \cdot m^{-1}$]
+	-	-	-	71.9 ± 0.2
+	-	+	-	26.4 ± 0.5
+	-	+	4	3.5 ± 0.1
+	0.5	+	4	2.4 ± 0.1

Figure 4-4 shows the results obtained for PGPR with and without NaCl. The results shown are for samples containing 0.125 % PGPR (*i.e.* below CMC[*]) with and without 0.5 % NaCl. As shown in Figure 4-4, the dilatational elasticity of the PGPR adsorbed layers increased with frequency, whereas the dilatational viscosity decreased. This shows that there is a region where the timescale of surfactant diffusion and surface compression/expansion are close (Li *et al.*, 2008). At a frequency of 0.05 Hz the adsorbed layer of PGPR with and without NaCl had a higher loss modulus than storage modulus, whereas for higher frequencies (0.1 and 0.5

[*] CMC (critical micelle concentration) for PGPR was estimated (as described in Section 2.2.2.1) to be between 0.76 % and 1.5 % with the respect to the oil phase.

Hz) it is the other way round. These results are indicative of the absorbed layer having visco-elastic properties (Li *et al.*, 2008).

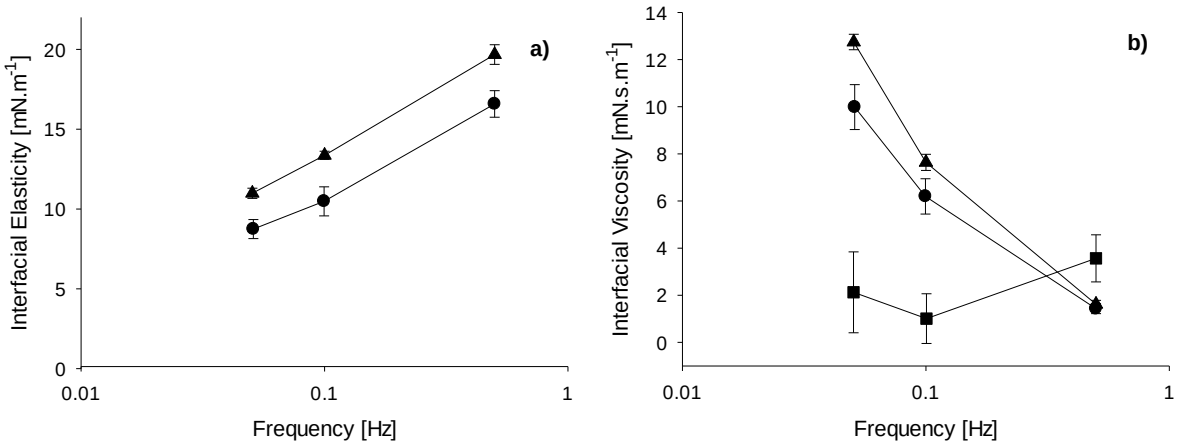

Figure 4-4 Frequency sweep; (a) interfacial elasticity; (b) interfacial viscosity of adsorbed layer of PGPR with NaCl, 0.125 % PGPR (●) system without salt, (▲) system with NaCl, (■) sunflower oil-water system with no PGPR and no salt. Lines are added simply to guide the eye.

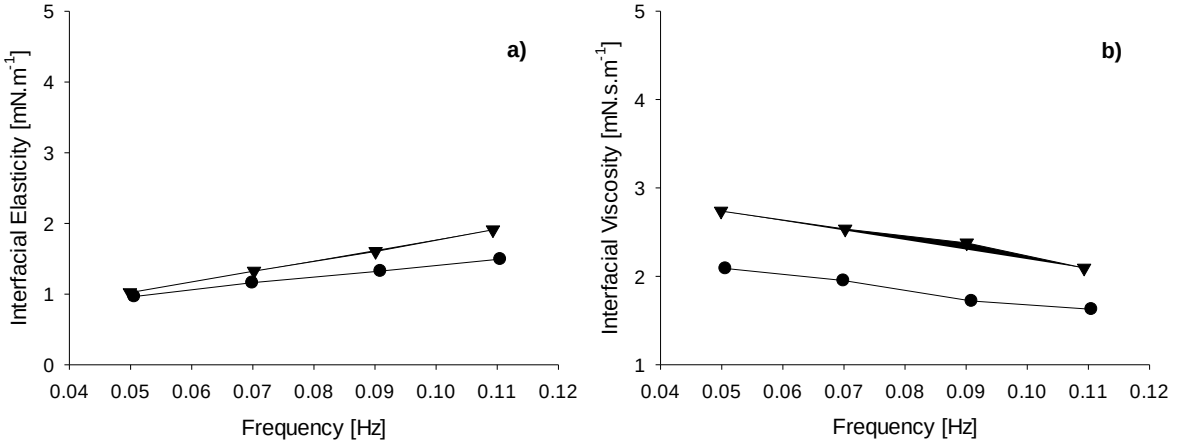

Figure 4-5 Frequency sweep; (a) interfacial elasticity; (b) interfacial viscosity of adsorbed layer of PGPR upon addition of NaCl, 4 % PGPR (●) system without salt, (▼) system with NaCl. Lines are added simply to guide the eye.

Once the PGPR is above the CMC (4 %), the results for interfacial rheology are different. This is shown in Figure 4-5, which demonstrates that when surfactant concentration exceeds

the CMC, both dilatational elasticity and viscosity show much lower dependency on frequency. The changes measured in the interfacial tension during oscillations of a droplet surface area were negligible. This is probably a consequence of the PGPR now being at a concentration, that it can cover the interface during expansion, therefore the loss and storage modulii remained low (Derkach *et al*., 2009).

It is generally thought, that there is a positive relationship between interfacial rheology and emulsion stability (Bos & van Vliet, 2001; Murray, 2002). The observed increase in the elasticity with addition of salt (Figure 4-4a) decreases the interfacial mobility, thus the rate of film drainage between approaching droplets leading to increased emulsion stability against coalescence.

These results (Figure 4-4) are in agreement with the work of Chattopadhyay *et al.* (2002), who reported that surface viscosities of monomolecular films of a series of surfactants increased with the concentration of NaCl. They also suggested that the addition of NaCl increases the hydrophobic cohesion of adsorbed surfactant molecules through possible combined interactions; *i.e.* polar head group-solvent, polar head group-ions and ions-solvent interaction. However, they found this effect to be modified by the nature of the inorganic salt (*Hofmeiseter series*[*]) and specifically the anions. Due to a varied degree of hydration, some anions are more excluded from the interface than others, causing "salting-out" of the surfactant. As a result polar head groups of surfactant are forced from the aqueous phase, which creates "solid-like" domains at the interface.

[*] *Lyotropic* or *Hofmeister* series ranks the relative influence of ions on the physical behaviour of a variety of processes occurring in water (Zhang & Cremer, 2006).

There has been very little work reported on the interactions of surfactant and salt at the oil-water interface. However, Chattopadhyay *et al.* (2002) and Kawashima *et al.* (1992) suggested that partially hydrated anions may migrate to the interface, depleting the hydration shell around the polar group of surfactants. It was hypothesised that this increased the lipophilicity of the polar head groups, leading to a decrease in the HLB value.

4.3 Duplex $W_1/O/W_2$ emulsions

Having established conditions for producing simple W_1/O emulsions (in Section 4.2), duplex $W_1/O/W_2$ emulsions were made, where sugars were used to balance the osmotic pressures. Conductivity method (as described in Section 3.2.4.5) was used to investigate salt release from the internal water phase during emulsification and the subsequent long-term storage.

4.3.1 Composition

In the following experiments, the primary 30:70 W_1/O emulsions were emulsified (as described in Section 3.2.3.2) and: (i) the PGPR concentration was 4 % so that the emulsifier was always in excess, (ii) sunflower oil was used, (iii) the internal water phase (W_1) contained 0.5 % (0.28 M) NaCl, and (iv) all primary emulsions were stored at low temperatures (5 ± 2 °C). 30 % of the W_1/O emulsion was homogenised with 70 % of the external water phase to construct duplex $W_1/O/W_2$ emulsions (according to the method described in Section 3.2.3.2).

It has been reported that the mechanism of molecular transport through the lipid layer can be influenced by factors such as: molecule's partition coefficient, ionisation, charge density,

molecular weight, mobility *etc.* (Aserin, 2008). Here, using an ideal solution approximation* (after Bonnet *et al.*, 2009), it has been assumed that the osmotic pressure is proportional to the concentration of ions in both water phases. Therefore, the concentration of glucose (C_g) in the external water phase, to counterbalance the osmotic pressure of the NaCl in the internal water phase, was calculated as:

$$C_g = C_{Na+} + C_{Cl-} \qquad \text{Eq. 4-1}$$

Where C_{Na+} and C_{Cl-} are molar concentrations of Na^+ and Cl^- ions present in the internal water phase.

Table 4-4 shows the composition of the four duplex $W_1/O/W_2$ emulsions used. Different concentrations of glucose (from 0.14 M to 0.86 M) were placed in the external water phase to balance the osmotic pressures, in order to test how it affects the release of salt from the internal water phase. The formulation where the osmotic pressures were balanced was the formulation III. Formulations I and II included 75 % and 50 % less glucose (respectively), in the external water phase, than required for the osmotic equilibrium. In formulation IV glucose was in a 50 % excess as compared to the osmotically balanced formulation III.

Table 4-4 Formulation of duplex $W_1/O/W_2$ emulsions I – IV.

Formulation	**NaCl in W_1** [M]	**W_1** [%]	**Oil** [%]	**PGPR** [%]	**Glucose in W_2** [M]	**W_2** [%]	**Tween 20** [%]
I	0.28	9	19.65	1.2	*0.14*	68	2
II	0.28	9	19.65	1.2	*0.28*	68	2
III	0.28	9	19.65	1.2	*0.57*	68	2
IV	0.28	9	19.65	1.2	*0.86*	68	2

* where the osmotic pressure of two diluted solutions of the same molarity are proportional to the van't Hoff factor, *i.e.* the ratio of actual concentration of dissociated molecules to the concentration of solute as calculated from the mass.

4.3.2 Emulsification salt release

In Figure 4-6 changes in the conductivity of duplex emulsions during their preparation are shown. It can be seen that for all four conductivity curves the emulsification process can be divided into three regions. The first region, before the mixing starts, is essentially the conductivity of the solution of glucose and Tween 20. The second region starts when the conductivity reduces due to the introduction of the non-conducting primary W_1/O emulsion, but then the conductivity increases linearly due to shear-induced breakdown of the primary emulsion and release of the internal water with NaCl. The third region begins when the homogenisation stops and the curves flatten. The increase at the beginning of the third region seemed to be the consequence of a small amount of creaming (with no mixing applied), creaming was observed almost instantly due to the very low viscosities and relatively large droplet size of the emulsions. Similar conductivity curves for simple emulsions have been reported by Azzam & Omari (2002).

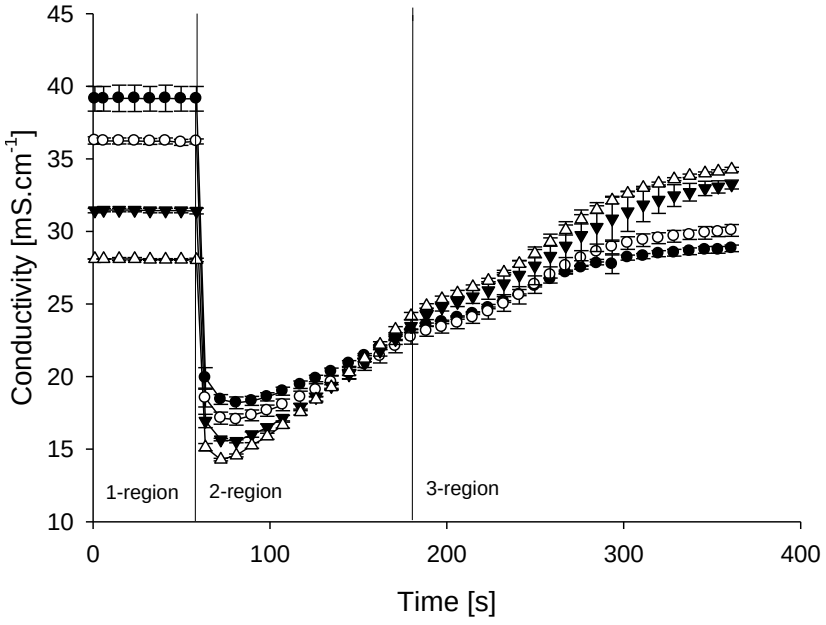

Figure 4-6 Conductivity curves of $W_1/O/W_2$ emulsions during homogenisation process in the presence of 2% Tween 20 and: (●) 0.14 M, (○) 0.28 M, (▼) 0.57 M, (Δ) 0.86 M of glucose in the external water phase.

Figure 4-6 also shows some variation in the conductivity in the first region for all four curves, with lower conductivity for higher glucose concentration. To determine the cause of these variations, five solutions of Tween 20 and different concentrations of glucose were prepared and their conductivity measured. The results are given in Table 4-5. As expected, the glucose has no conductivity and Tween 20, although being a non-ionic molecule, increases the conductivity, probably due to contamination within the emulsifier or/and interactions between polyoxyethylene chains of Tween 20 and water (Hsu & Nacu, 2003). Indeed, whenever glucose was mixed into the 2 % surfactant solution, the conductivity decreased to the level determined by the glucose; the more glucose added the lower the conductivity of solution (Table 4-5). The same was true for emulsions made with sucrose or fructose in the external aqueous phase (Table 4-6). One explanation is that glucose reduces the conductivity due to an increase in bulk viscosity of the solution, thus reduced ionic velocity to the electrodes of the conductivity meter. The viscosities of the samples were measured to test this (Table 4-5). As can be seen the measured viscosities of solutions with varied glucose level, although very low, do differ.

Table 4-5 Effect of glucose concentration and Tween 20 on the conductivity and viscosity of solutions.

Water	+	+	+	+	+	+
Tween 20 (%)	-	-	2	2	2	2
Glucose [M]	-	0.28	-	0.14	0.28	0.57
Viscosity [mPa·s]	-	-	-	0.83	0.91	0.94
Conductivity [$\mu S \cdot cm^{-1}$]	1.2 ± 0.3	1.3 ± 0.2	37.8 ± 0.8	35.3 ± 0.3	33.0 ± 0.5	29.2 ± 0.2

Table 4-6 Encapsulation of salt in W_1 of duplex emulsions during emulsification, with 2% Tween 20 and Fructose or Sucrose in the external water phase (W_2).

	Encapsulation [%]	
Concentration [M]	**Fructose**	**Sucrose**
0.14	99.75 ± 0.02	99.73 ± 0.01
0.28	99.64 ± 0.02	99.59 ± 0.01
0.57	99.44 ± 0.01	99.47 ± 0.02

Figure 4-7 shows the percentage of salt that remains encapsulated in the internal phase of the duplex emulsion with time. The encapsulation was calculated from the measured conductivity using Eq. 3-2. As can be seen from the Figure, there are only low levels of release with the highest at around 0.8 % for the maximum concentration of glucose. The same effect was seen when the glucose was substituted with sucrose and fructose at the same molar concentration (Table 4-6). Again a possible explanation for the observed differences in encapsulation is that the four emulsions had different viscosities, which may have an impact on the conductivity. Therefore, viscosities of all duplex emulsions were measured immediately after preparation, indicating that formulations with 0.86 M and 0.58 M glucose had similar viscosity, whereas those with lower glucose concentration showed a slightly higher viscosity (Table 4-7).

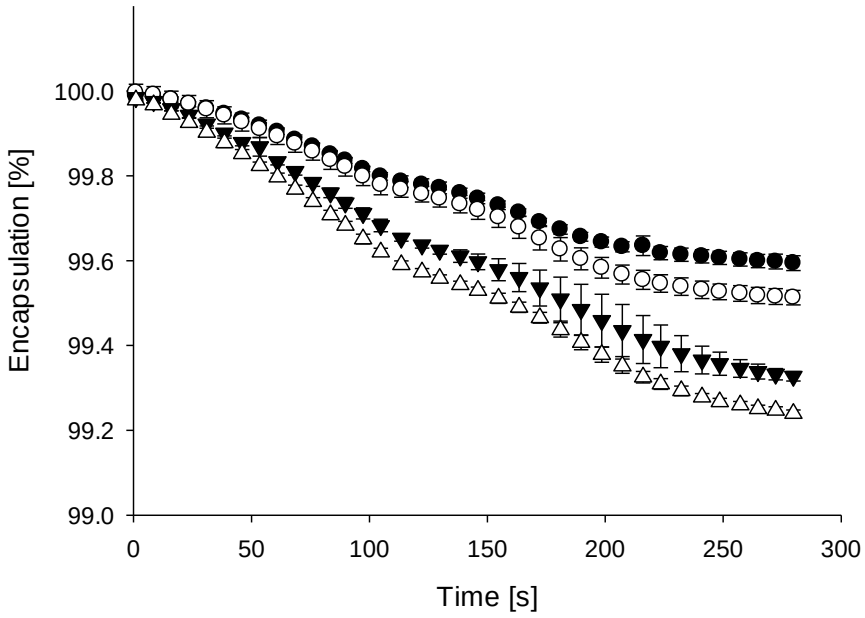

Figure 4-7 Encapsulation of salt in the internal water phase of $W_1/O/W_2$ emulsions during homogenisation process in the presence of 2 % Tween 20 and: (●) 0.14 M, (○) 0.28 M, (▼) 0.57 M, (Δ) 0.86 M of glucose in the external water phase.

Table 4-7 Droplet size evolution and viscosities of formulations I – IV (as described in Table 4-4). All samples showed Newtionian behaviour.

Formulation	**$D_{3,2}$** [μm] **day 1**	**$D_{3,2}$** [μm] **day 60**	**Viscosity** [mPa·s]
I	14.3 ± 0.5	16.2 ± 0.2	6.59
II	12.7 ± 0.2	15 ± 0.9	4.19
III	10.9 ± 0.1	12.9 ± 0.6	3.32
IV	9.9 ± 0.4	12 ± 0.9	3.10

To exclude the effect of particle size related viscosity changes, droplet size measurements on freshly made duplex emulsions were made. However, it was found that the formulations with the highest viscosity (0.14 M glucose) had also the largest external droplet size ($D_{3,2}$ = 14.3 ± 0.5 μm) and vice versa, the smallest size ($D_{3,2}$ = 9.9 ± 0.4 μm) was found for the emulsion with the highest glucose concentration (0.86 M) and consequently lowest viscosity (Table 4-7). Interestingly, when no glucose was present in the external water phase,

the emulsion had a viscosity of 2.05 Pa·s at a shear rate of 10 s^{-1}. One reason for such an increase in viscosity could be, as mentioned earlier, a low level of charged impurities introduced by Tween 20, inducing electrostatic interactions between emulsion droplets. The question is then, what is the magnitude of this charge on the emulsion droplets and how this changes with the addition of glucose. To answer this question, simple O/W emulsions containing a constant concentration of Tween 20 (2 %), PGPR (4 %), but varying levels of glucose were formulated and their zeta potential was measured (Table 4-8).

Table 4-8 Zeta potential of simple O/W emulsions with 4 % PGPR in the oil phase, stabilised by Tween 20 (2 %) and its dependence on the addition of glucose.

Glucose [M]	**Zeta potential** [mV]	**% Change**
0	-22.5 ± 1.3	-
0.14	-21.1 ± 3.1	6.0
0.28	-19.5 ± 2.1	13.2
0.57	-18.5 ± 2.6	17.5
0.86	-16.2 ± 2.0	27.8

It can be seen that the charge on droplets decreased with glucose concentration from -22.5 ± 1.3 mV (no glucose) to -16.2 ± 2.0 mV (0.86 M glucose). From the viscosity and zeta potential observations, it was concluded that the impurities from the Tween 20 introduced some charges onto the emulsion droplets, thus increasing the emulsion viscosity due to electrostatic repulsions between droplets. Even though there is no direct evidence here, when sugar is present in the system, it may bind to the impurity and reduce the charge on the droplets and therefore bulk viscosity of the emulsion. This finding is in agreement with the decrease in the conductivity of Tween 20 solutions with increasing sugar concentration (Table 4-5 and Table 4-6). Another explanation for the observed changes in the zeta potential of the simple emulsions could be the mobility issue. Increasing the concentration of a solute

(glucose) increases the viscosity of the solution, obstructing particles in their migration between electrodes, thus resulting in reduced mobility and hence zeta potential. However, it is likely that the changes in the zeta potential are affected by the combination of the two mechanisms mentioned above.

4.3.3 Storage salt release

The duplex emulsions were stored for 60 days during which their conductivity and droplet size were measured. Figure 4-8 shows the encapsulation of emulsions with varying levels of glucose in the external aqueous phase. It can be seen that the transport of salt over the two months differs significantly. The trend in glucose-dependent-salt-release, observed just after emulsification, continued over the long-term storage. That is, increasing levels of glucose in the external water phase lead to higher release of salt. Such differences could be as a result of interfacial area difference in formulations with different glucose concentrations. In order to test this, droplet size measurements were performed (in 1-week intervals) during sample storage.

During the 60 days of storage the average droplet size of the duplex emulsions increased by approximately 2 μm in each formulation (Table 4-7). Micrographs were taken directly after duplex emulsification and then after 2 months of storage but these showed no appreciable difference in the morphology of duplex emulsions (Figure 4-9). No visible increase in the size of primary emulsion droplets was seen, although some bigger coalesced droplets of the internal phase could occasionally be observed in all emulsions. It was therefore concluded, that there was no significant diffusion of water from or to the internal water phase. This suggests that the release of salt is driven by a chemical potential gradient between the water

phases rather than by osmotic pressures; and did not involve a swelling-breakdown mechanism for the duplex structures.

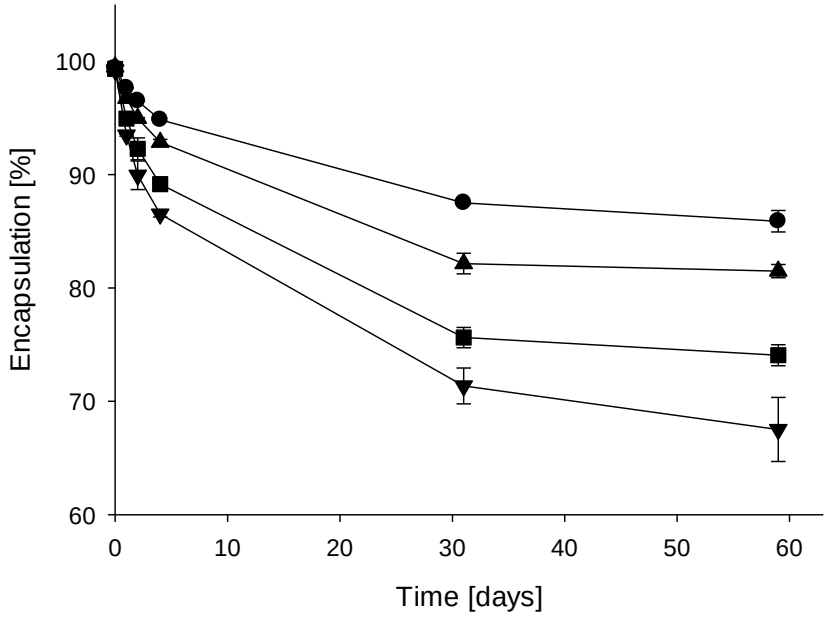

Figure 4-8 Storage encapsulation of salt in the internal water phase of $W_1/O/W_2$ emulsions: formulations I – IV (Table 4-4). Duplex emulsions with 2% Tween 20 and: (●) 0.14 M, (▲) 0.28 M, (■) 0.57 M, (▼) 0.86 M of glucose in the external water phase.

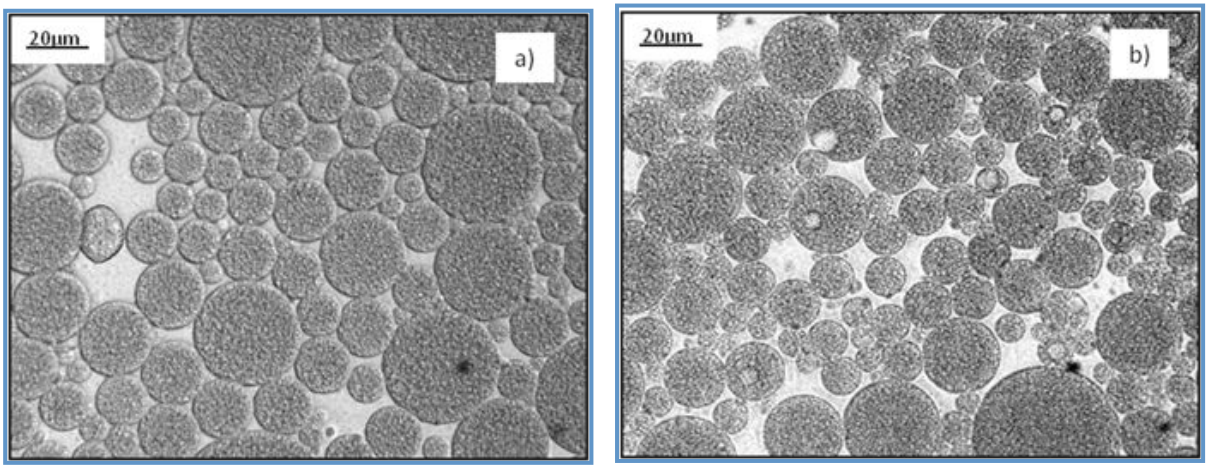

Figure 4-9 Micrographs of typical changes occurring during storage of duplex emulsions (formulation III; 0.57 M glucose); (a) just after preparation, (b) after 2 months of storage.

4.3.4 Effect of sugar

The decreased encapsulating properties of the duplex formulations with addition of glucose suggest, that sugar molecules add to the salt transport over the lipid layer. To investigate how sugars alone or in combination with surfactants (PGPR and Tween 20) modify the interfacial properties of the system, the pendant droplet measurements were performed, as described in Section 3.2.4.2. Figure 4-10 shows the interfacial tension between water and sunflower oil, which contains a very low concentration of PGPR (0.125 %). The interfacial tension decreased on the addition, and the increasing concentration, of glucose.

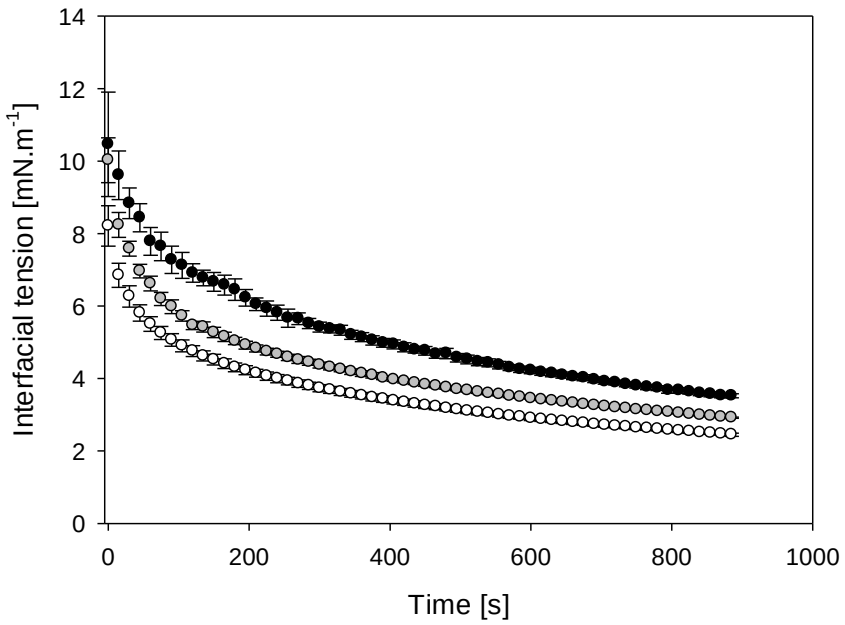

Figure 4-10 Interfacial tension of suflower oil (with 0.125 % PGPR) and glucose solutions; (●) no glucose, (●) 0.28 M glucose, (○) 0.57 M glucose; measurements performed at 25 ± 3 °C.

Figure 4-11 shows the variation of interfacial tension with sugar (glucose, fructose and sucrose) concentration with and without 3 % of Tween 20. In all the cases investigated, increasing the sugar concentration lead to a decrease in the interfacial tension. For example, on increasing glucose concentration (from 0 to 0.86 M) the interfacial tension decreases from

26.8 ± 0.1 to 13.3 ± 1.8 $mN \cdot m^{-1}$. When 3 % Tween 20 is present in the system, the same increase in glucose level reduces the interfacial tension from 4.3 ± 0.1 to 2.5 ± 0.01 $mN \cdot m^{-1}$.

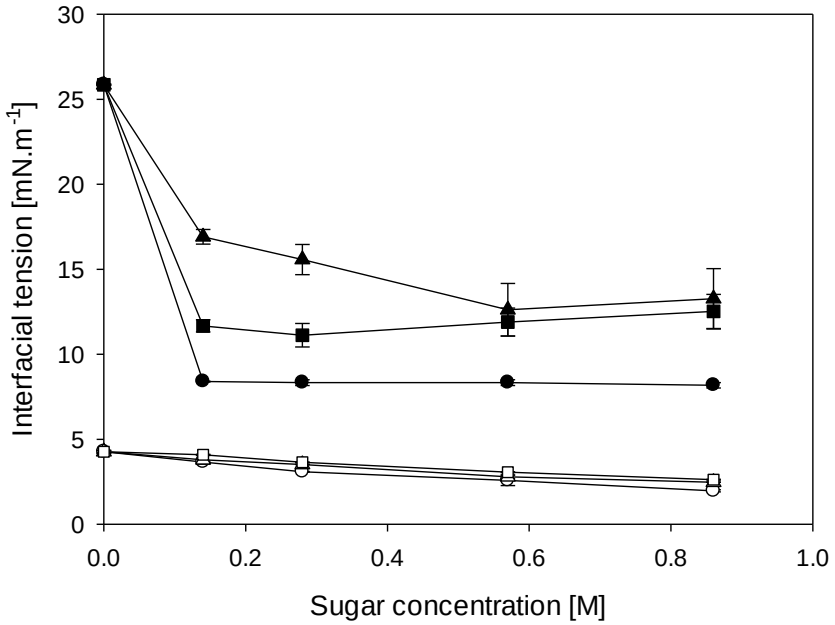

Figure 4-11 Interfacial tension of sunflower oil (no PGPR) and solutions of (▲) glucose, (■) fructose, (●) sucrose, (Δ) glucose with 3 % Tween 20, (□) fructose with 3%Tween 20, (○) sucrose with 3 %Tween 20; measurements performed at 25 ± 3 °C.

Previous research reported that sucrose either does not significantly alter the surface tension (Adhikari *et al.*, 2009; Hutteau *et al.*, 1998; Lindfors, 1924) or slightly decreases the interfacial tension (by around 9 %) between water and olive oil (Howard & Sollman, 1924). However, it has been shown (Giangiacomo, 2006), that sugars at relatively low concentrations (up to 20 %) behave as structure breakers of water clusters. The solvation of sugar molecules (bigger than water molecules) leads to the breaking of a number of H-bonds in the cluster, increasing distances between molecules and number of free molecules. Therefore, one hypothesis for increased salt transport with sugar concentration is that the sugars change the structure of water by increasing the number of monomeric water molecules (*i.e.* decreasing the number of H bonds), which subsequently leads to reduced cohesive water-water

interactions and a decrease in the interfacial tension. According to Giangiacomo, (2006) sugars (glucose, sucrose, fructose) introduce similar modifications to NIR* band of water to the effect of the increase in temperature.

One explanation for the enhanced salt movement with the increasing concentration of glucose is that sugars change the solubility of surfactant molecules, allowing more micelles to be formed. When sugars are introduced to the surfactant solution, their OH groups bind *via* hydrogen bonding with water molecules. This reduces the number of free water molecules available for hydration of the surfactant's head group, which results in their increased association into micelles to reduce unfavorable interactions. However, such an explanation may be not plausible if, as mentioned above, structure-breaking sugars introduce many unbounded water molecules, which would be readily available for the hydration of the surfactant.

Another explanation for the observed phenomenon might be that sugars are (or become) surface active in this specific system and so facilitate the salt transport between water compartments. Rousset *et al*. (2002) have previously reported that PGPR increases the lipophilicity of sucrose, thus making it surface active. It has been argued by Garti (1997b), that an increase in the concentration of a water soluble emulsifier in duplex $W_1/O/W_2$ emulsions has a negative effect on the flux of water (and water soluble components) from the inner to outer dispersion phases That is, at higher concentration more water is "solubilised" by the surfactant (incorporated into the mixed† reversed micelles in the oil phase), which enhances the overall mass transfer rate. Additionally, low HLB surfactant may be incorporated into the micelles of high HLB surfactant in the external water phase leading to

* Near Infrared Spectroscopy
† Composed of both low and high HLB surfactants

its reduced concentration at the primary W_1/O interface. The data here suggests that the glucose behaves like a water-soluble emulsifier facilitating the micellar transport of hydrated ions across the oil layer of duplex emulsions. In summary, increasing the sugar concentration results in greater micellar transport of salt and, therefore, lower encapsulation properties of duplex emulsions.

4.4 Effect of PGPR concentration and processing time

The overall stability of duplex emulsions essentially depends on the stability of the primary emulsion (Su *et al.*, 2006), which, in turn is determined, amongst others, by the type and concentration of the emulsifiers used. It is also thought, that the concentration of the primary emulsifier has to be high enough to provide the primary emulsion stability during the secondary emulsification step, but at the same time not too excessive so that the transport of molecules *via* reversed micelles between the two water compartments is minimal (Garti *et al.*, 1985). In order to investigate the effect of oil-soluble emulsifier (PGPR) concentration on the duplex $W_1/O/W_2$ emulsions droplet size and the release of salt from the internal water phase, primary (30:70) W_1/O emulsions were constructed with 1, 2 and 4 % PGPR (with respect to the primary W_1/O emulsion) and constant amount of NaCl (0.28 M) in the W_1 water phase. Average droplet size of the produced W_1/O emulsions, measured immediately after emulsification, was between 0.19 and 0.24 μm (as shown in Figure 4-3, p.68). Duplex emulsions were formulated with 30 % primary (W_1/O) emulsion and 70 % of the external water phase (W_2), where 2 % Tween 20 and 0.14 M glucose were placed. A low glucose level was chosen to ensure slower rate of salt release, as determined in Section 4.3.3. $W_1/O/W_2$ emulsions were prepared as described in Section 3.2.3.2 and different mixing times (2, 5 and 10 min) were applied in order to find the optimal emulsion droplet size for the studied system. All duplex emulsions were stored at 5 ± 2 °C.

4.4.1 Droplet size

The effects of PGPR concentration and the duration of high-shear mixing were investigated in relation to duplex emulsion droplet size. Table 4-9 shows emulsions droplet diameter ($D_{3,2}$) as a function of PGPR concentration and mixing time. Additionally, the droplet size evolution during storage for 17 weeks (for emulsion with 1 % PGPR) and 14 weeks (for emulsions with 2 % and 4 % PGPR) is shown. It can be seen that, when emulsions were stabilised with 1 % and 2 % PGPR, the duplex emulsion droplet size was 15.9 ± 0.7 μm and there was no significant effect of the mixing time on the droplet diameter. For the emulsions with 4 % PGPR and homogenised for 2, 5 and 10 min the droplet size distribution curves are given in Figure 4-12. It shows that there is no appreciable difference between the three curves, *i.e.* comparable average droplet sizes for all emulsions (13.6 ± 0.6 μm) and similar size distributions (span = ~1.2). This means that the droplet size obtained after 2 min of high-shear mixing cannot be further reduced by longer application of shear (*i.e.* 5 and 10 min). These data suggest, that the droplet size between ~14 and ~16 μm is the minimum droplet size that can be obtained for these specific formulations within the investigated emulsification conditions.

Table 4-9 Droplet size evolution in duplex $W_1/O/W_2$ emulsions as a function of PGPR concentration during storage for: (a) 17 weeks, (b) 14 weeks. All samples contain 0.28 M NaCl in the W_1 and 2 % Tween 20 and 0.14 M glucose in the W_2.

PGPR [%]	**Mixing time** [min]	**$D_{3,2}$** [μm] **after preparation**	**$D_{3,2}$** [μm] **during storage**
1	2	16.5 ± 0.5	15.4 [a]
	5	16.2 ± 0.2	15.1 [a]
	10	15.5 ± 0.2	15.3 [a]
2	2	17.0 ± 0.7	16.7 [b]
	5	15.5 ± 0.1	16.6 [b]
	10	15.0 ± 0.3	17.0 [b]
4	2	14.3 ± 0.5	16.5 [b]
	5	13.2 ± 0.2	15.7 [b]
	10	13.4 ± 0.2	16.2 [b]

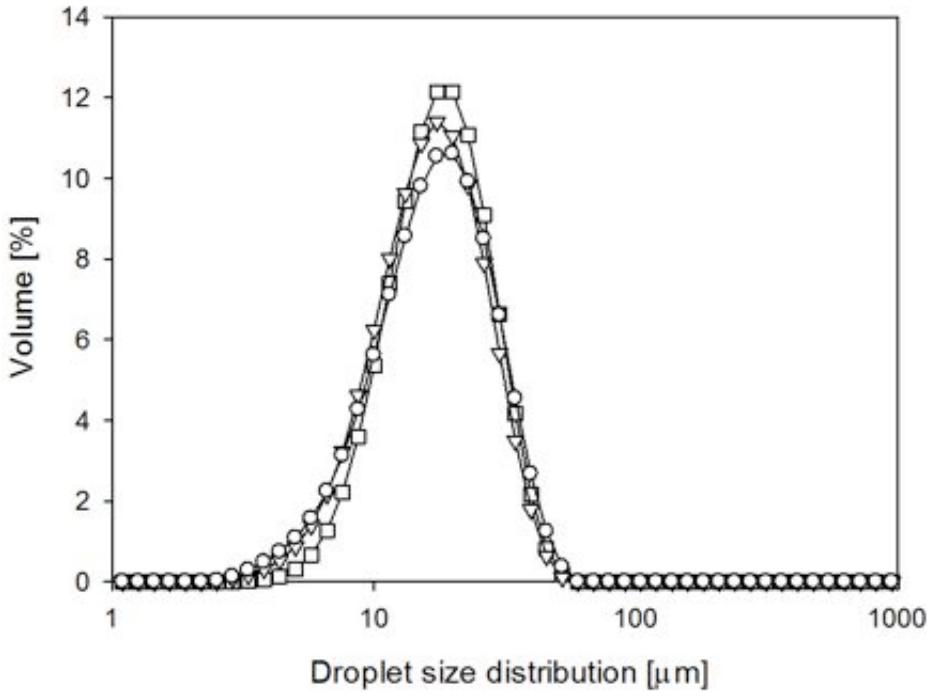

Figure 4-12 Droplet size of duplex $W_1/O/W_2$ emulsions with 0.28 M NaCl in the W_1, 4 % PGPR in oil, 0.14 M glucose and 2 % Tween 20 in the W_2, homogenised in the high shear mixer at 10,000 rpm for: (□) 2 min, (∇) 5 min and (○) 10 min.

Duplex emulsions were stored for 17 weeks (1 % PGPR) and 14 weeks (2 % and 4 % PGPR), during which their droplet size was measured. Table 4-9 shows that the droplet size of $W_1/O/W_2$ emulsions does not change significantly during storage. Nonetheless, microscopic analysis revealed that the internal structure of emulsions with 1 % PGPR changed over the storage period. This is shown in Figure 4-13, where typical images of a duplex emulsion microstructure taken just after emulsification (Figure 4-13a) and after 17 weeks of storage (Figure 4-13b) are given. It appears that the aged emulsions contained less internal water droplets (W_1) than the freshly made duplex emulsions. This observation indicates that 1% PGPR is not sufficient to stabilise the duplex emulsion and corresponds well with, previously observed (Section 4.2.1), limited stability of W_1/O emulsions with 1 % PGPR. Poor stability of the primary emulsion results in droplet coalescence during emulsion processing (*i.e.*

secondary emulsification) and storage, causing an increase in the droplet size of the internal water phase (W_1). This would consequently lead to a faster exclusion of W_1 droplets from the oil phase and into the external water phase W_2, as it was shown, that larger droplets are first to be expelled from the oil phase (González-Ochoa *et al.*, 2003). This is because of larger contact area of both W_1/O and O/W_2 interfaces, which increases the coalescence probability.

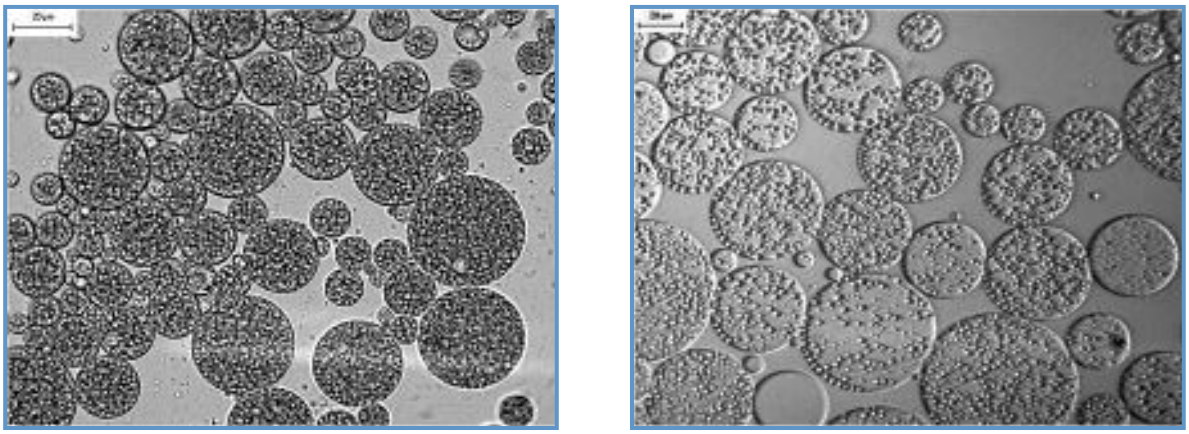

Figure 4-13 Example of microstructural changes during storage of duplex W_1/O/W_2 emulsion stabilised with 1 % PGPR in the oil phase and 2 % Tween 20 in the external water phase: (Left) emulsion immediately after preparation, (Right) emulsion after 17 weeks of storage. Both samples contain 0.28 M NaCl and 0.14 M glucose in the W_1 and W_2, respectively.

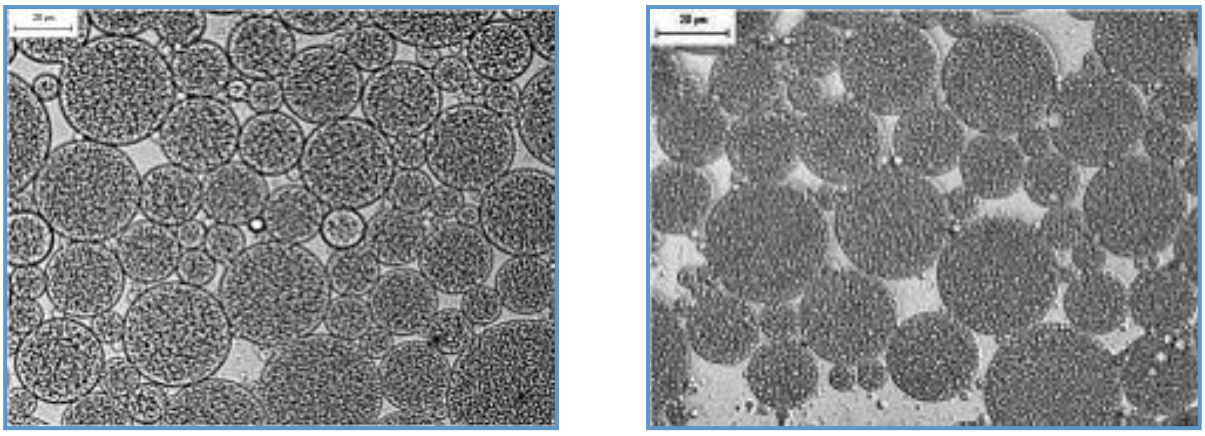

Figure 4-14 Example of microstructural changes during storage of duplex W_1/O/W_2 emulsion stabilised with 4 % PGPR in the oil phase and 2 % Tween 20 in the external water phase: (Left) emulsion immediately after preparation, (Right) emulsion after 14 weeks of storage. Both samples contain 0.28 M NaCl and 0.14 M glucose in the W_1 and W_2, respectively.

The results are different when 2 % and 4 % PGPR were used in the primary emulsion formulation. Figure 4-14 shows an example of typical changes occurring in the microstructure of a duplex emulsion (with 4 % PGPR) during storage. Figure 4-14 left shows that in a freshly made emulsion, the internal water droplets (W_1) are relatively small (below the resolution of the optical microscope) and closely packed within the oil phase. After 14 weeks of storage, some large coalesced W_1 droplets could be detected in the oil phase however, no dramatic change in the size of the internal water droplets (W_1) could be observed (Figure 4-14 right). No appreciable difference in the duplex microstructure over the storage period suggests that, there are enough PGPR molecules in the system (with 2 % and 4 % PGPR) to stabilise all the interfaces formed (see Section 4.2.1) and thus coalescence does not occur.

4.4.2 Emulsification salt release

The conductivity of duplex emulsions with varied PGPR concentration in the oil phase was measured throughout the high-shear emulsification (for 2 min, 5 min and 10 min) and for subsequent 3min, 5 min and 5 min, respectively, after mixing has stopped (as described in Section 4.3.2). Figure 4-15 shows the percentage of salt, that remains encapsulated in the internal water phase (W_1) of the duplex emulsion as a function of PGPR concentration and time of homogenisation. As in Section 4.3, the encapsulation was calculated from the measured conductivity using Eq. 3-2.

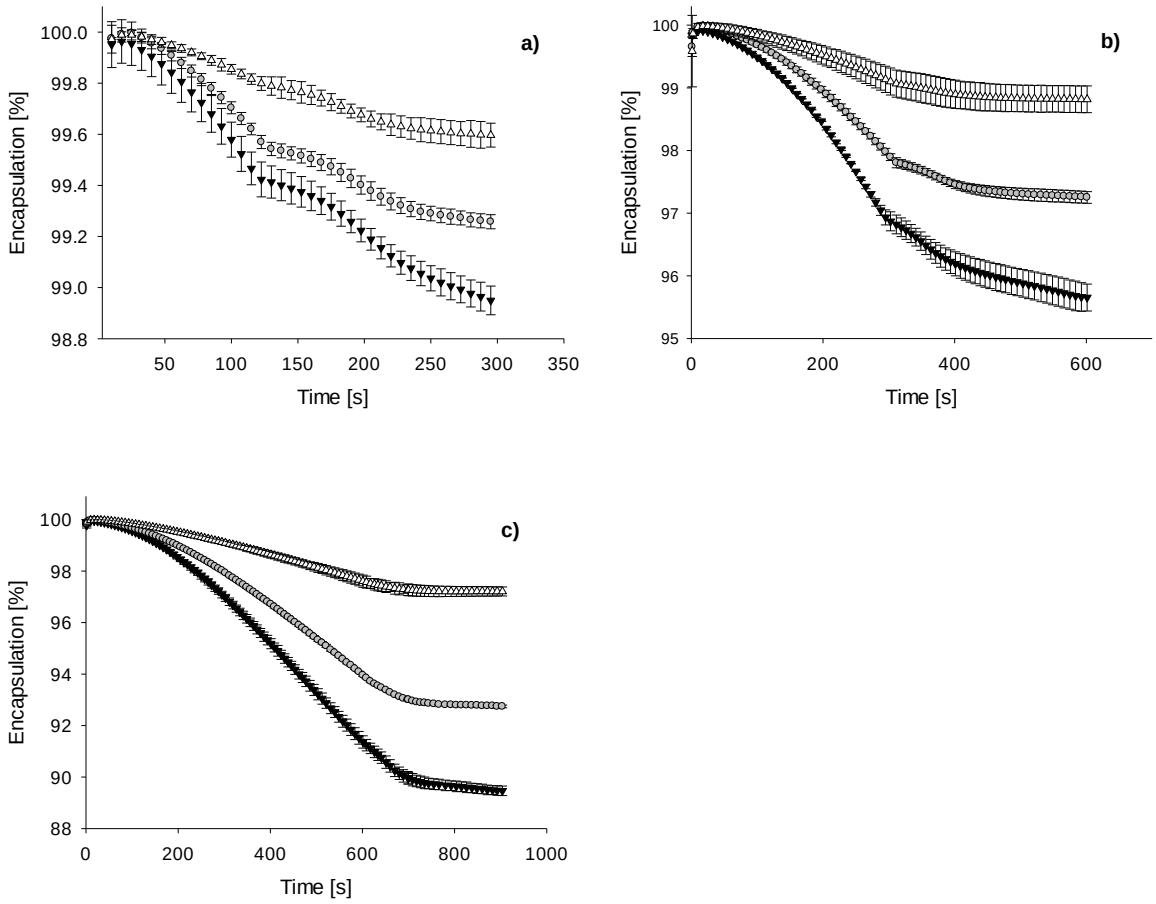

Figure 4-15 Emulsification encapsulation salt (in W_1) of duplex $W_1/O/W_2$ emulsions with 2 % Tween 20 in the external water phase, mixed in the high-shear mixer at 10,000 rpm for (a) 2 min, (b) 5min, (c) 10 min, as a function of PGPR concentration (▼) 1 %, (●) 2 %, (∆) 4 %. All samples contain 0.28 M NaCl and 0.14 M glucose in the W_1 and W_2, respectively.

Figure 4-15 shows, that levels of release are increasing with: (i) decreasing PGPR concentration in the oil phase, and (ii) the duration of high-shear homogenisation. The highest salt encapsulation in duplex emulsions homogenised for 2 min (Figure 4-15a) was observed for the 4 % PGPR formulation (~99.6 %), followed by the 2% PGPR (~99.2 %) and 1 % PGPR (~98.9 %). When the emulsification time increased to 5 min (Figure 4-15b), the overall encapsulation of salt was considerably lower and also decreased when PGPR content reduced, from ~98.8 % to ~95.6 % for 4 % and 1 % PGPR, respectively. Further increase in the high-

shear mixing (to 10 min) resulted in the lowest salt encapsulation of ~89.4 % for the 1 % PGPR, ~92.7 % for the 2 % PGPR and ~97.2 % for the 4 % PGPR stabilised emulsions.

The decrease in salt release with increasing PGPR concentration for a given mixing time could be attributed to a better interfacial membrane stabilisation with higher amount of PGPR molecules present in the bulk phase. This could lead to formation of surfactant multilayers at the interface, resulting in stronger interfacial properties of adsorbed solute (Opawale & Burgess, 1998; for range of Span surfactants), which in turn would hinder coalescence between the internal and external water phases. In addition to better interfacial stability, a higher concentration of PGPR molecules leads to a larger driving force for surfactant adsorption during interface expansion under shear. It has been reported by Surh *et al.*, (2007), that intense mechanical stresses during secondary emulsification have the potential to disrupt the primary W_1/O emulsion droplets. Therefore, when the interface is expanded during emulsification, 2 % PGPR ensures higher gradient of surfactant concentration between the interface and the bulk phase, as compared to 1 %. Resultant rapid adsorption of surfactants ensures that the interface is stabilised faster than the timescale for coalescence between the internal water droplets and/or with the external O/W_2 interface. Additionally, as shown in Table 4-10, the viscosity of the oil phase increases with the PGPR concentration, which results in the increased droplets resistance to the effects of shearing (*i.e.* viscous losses into heat) thus reduced rate of coalescence. This would therefore explain the observed differences in the salt release during emulsification for a fixed mixing time and improved stability of $W_1/O/W_2$ emulsions when the concentration of PGPR is increased.

Table 4-10 Viscosities of W_1/O emulsions (with 0.28 M NaCl) as a function of PGPR concentration. Measurements taken at a share rate of 11 s^{-1}.

PGPR [%]	**1**	**2**	**4**
Viscosity [Pa·s]	0.103	0.113	0.152

The effects of duration of the high-shear homogenisation on salt encapsulation are identical in trend for all PGPR concentrations studied (*i.e.* longer mixing times lead to higher salt release, Figure 4-15). Therefore, as an example the emulsion with 4 % PGPR is discussed below. Figure 4-16 shows the extent of salt release from W_1 during mixing for 2 min, 5 min and 10 min, for the emulsion with 4 % PGPR. It can be seen that the three different mixing times resulted in significant differences in the salt release curves for the respective duplex emulsions. The emulsion mixed for 2 min released less salt (0.4 %) than emulsions subjected to the shearing force for 5 and 10 min, which released considerably more salt (1.2 % and 2.8 %, respectively). This is a consequence of a shear-induced breakage of duplex emulsions structure and subsequent release of the internal water phase with salt. As discussed earlier, during secondary emulsification both W_1/O and O/W_2 interfaces expand in the shear-induced flow. This causes fluctuations in surfactant concentration at the interface (*i.e.* formation of surfactant depleted regions) and may result in coalescence of the internal water droplets and/or with the external water phase (W_2). More coalescence events could be expected as the number of collisions between droplets, and droplets with the O/W_2 interface increases with the duration of mixing. Coalescence between the inner and outer water phases results in a delivery of the internal droplet content (W_1) into the water continuous phase (W_2).

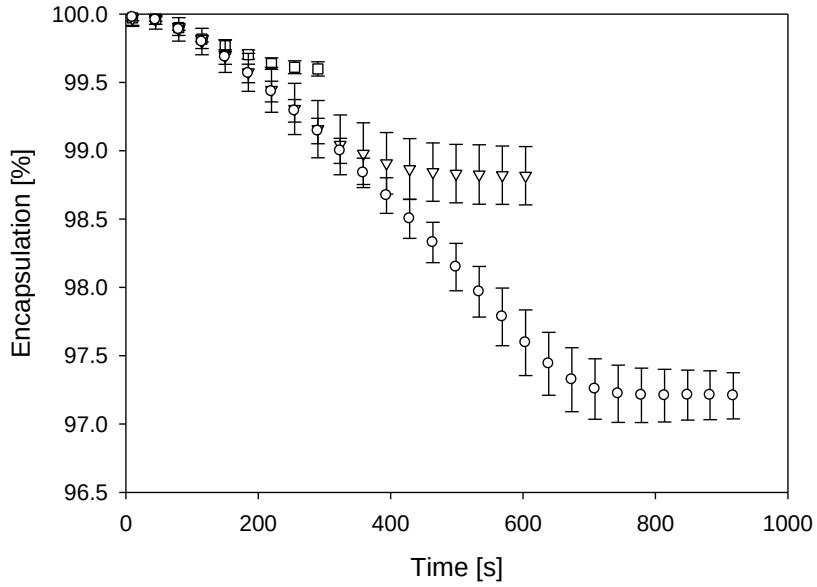

Figure 4-16 Emulsification encapsulation of salt in the internal water phase of $W_1/O/W_2$ emulsions, containing 2 % Tween 20 in the external water phase, mixed in the high-shear mixer at 10,000 rpm for (□) 2 min, (▽) 5 min and (○) 10 min. All samples contain 0.28 M NaCl and 0.14 M glucose in the W_1 and W_2, respectively.

4.4.3 Storage salt release

In order to study the effects of PGPR concentration and homogenisation time on the long-term salt release, duplex emulsions were stored for 17 weeks (1 % PGPR) and 14 weeks (2 % and 4 % PGPR), during which their conductivity was measured. Figure 4-17 shows the % of salt retained in the emulsions with varying levels of PGPR, that were emulsified in the high-shear mixer for 2 min (Figure 4-17a), 5 min (Figure 4-17b) and 10 min (Figure 4-17c). It can be seen that transport of salt during prolonged storage: (i) differs significantly between compositions with different PGPR level for a given mixing time, and (ii) remains very similar for all mixing times, when one PGPR concentration is considered.

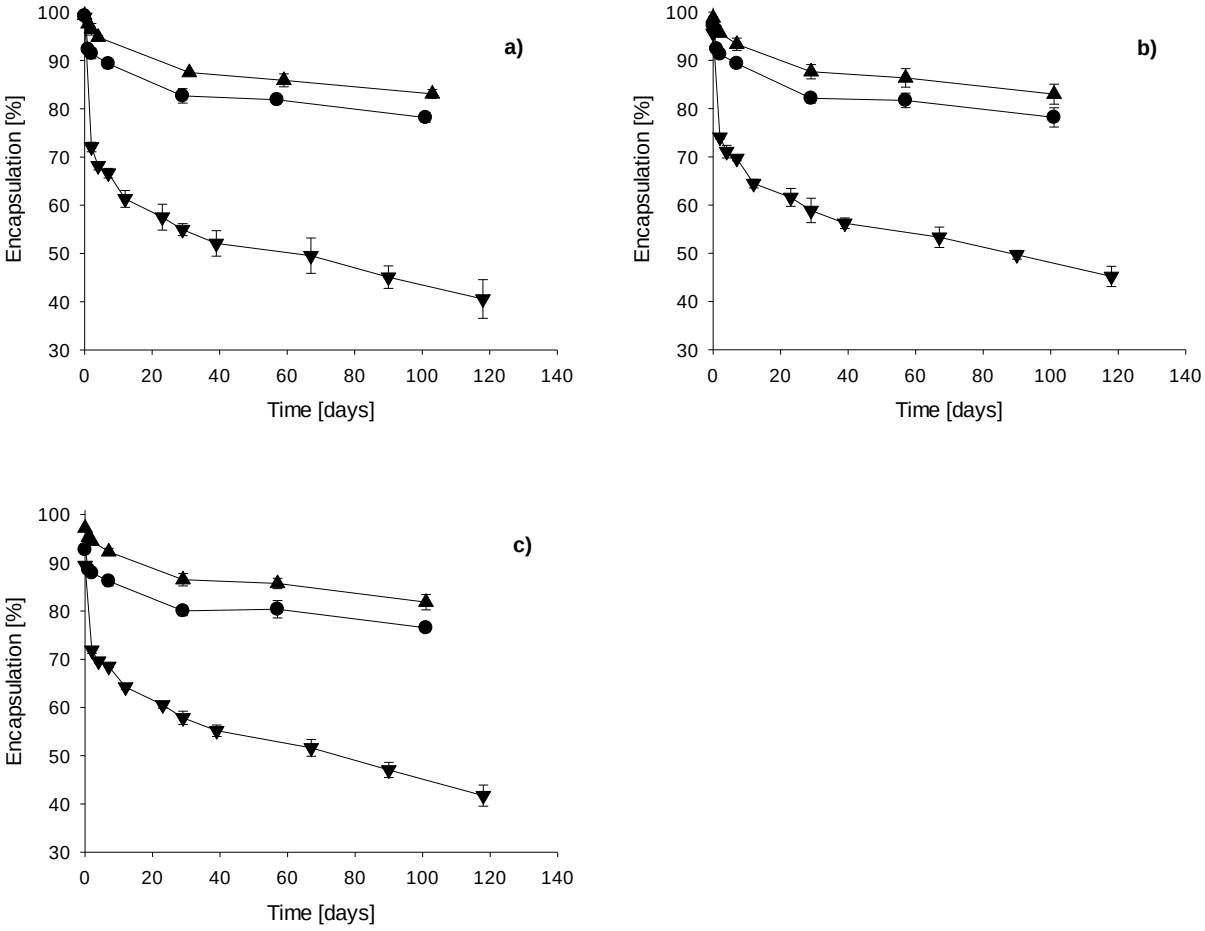

Figure 4-17 Storage release of salt from the internal water phase of duplex $W_1/O/W_2$ emulsions stabilised with 2 % Tween 20 and mixed in the high shear mixer for: (a) 2 min, (b) 5min and (c) 10 min, as a function of PGPR concentration (▼) 1 %, (●) 2 %, (▲) 4 %. All samples were stored at 5 ± 3ºC and contain 0.28 M NaCl and 0.14 M glucose in the W_1 and W_2, respectively.

Firstly, the effect of PGPR concentration is analysed. For a given homogenisation time, for example 2 min (Figure 4-17a), the highest storage salt encapsulation was observed in emulsions with 4 % PGPR (~83 %), followed by 2 % PGPR (~78 %) and the lowest encapsulation in emulsions with 1 % PGPR (~40 %). Markedly higher loss of salt in duplex emulsions with 1 % PGPR and the observed changes in the emulsion morphology during storage (Figure 4-13), both indicate that the concentration of primary surfactant plays a crucial role in duplex emulsion stability. Even though, theoretical calculations of surface coverage (Section 8.1, Appendix) suggest that 0.6 % PGPR is enough to stabilise the primary

W_1/O emulsion*, the effective concentration of surfactant at the primary interface may be lower due to its migration to the secondary interface with the external W_2. This would result in increased coalescence and phase separation with release of encapsulated salt. Reduced stability of primary W_1/O emulsion with 1 % PGPR was also discussed in Section 4.2.1.

When the PGPR concentration is higher (> 1 %), the majority of salt release occurs during the initial stages of storage, where the formulation with 2 % PGPR showed faster release of salt than formulation with 4 % PGPR (Figure 4-17). These initial variations in the rate of release may be again related to different viscosities of both formulations, as shown in Table 4-10. Increasing the viscosity of the primary emulsion is most likely to result in slower molecular/micellar transport of water and water-soluble ingredients across the oil phase. It was suggested by Garti *et al.* (1985) that higher concentrations of the primary emulsion stabiliser (in this case PGPR) increase the micellar transport of water between the two water compartments. However, the obtained data suggest otherwise and a similar rate of salt release was observed for the majority of the storage period. This suggests that at PGPR concentrations that ensure primary emulsion stability, the long-term salt release is not dependent on the concentration of the primary emulsifier.

The effect of mixing time on the long-term salt release is identical for all investigated PGPR concentrations (*i.e.* the loss of salt from emulsions made with a particular PGPR level is comparable on storage for all applied mixing times Figure 4-17). Therefore as an example, the emulsion with 4 % PGPR is discussed further. Figure 4-18 shows salt release profiles for emulsions prepared by mixing at 10,000 rpm for 2, 5 and 10 min, as described in Section 3.2.3.2.

* 30% water-in-70% oil emulsion with an average 0.2 μm droplet size.

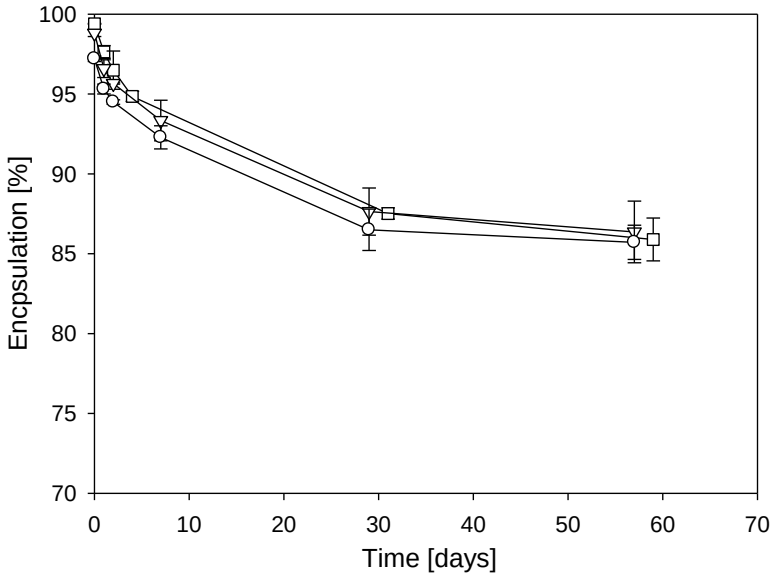

Figure 4-18 Storage encapsulation of salt in the internal water phase of duplex $W_1/O/W_2$ emulsions stabilised with 4 % PGPR in oil and 2 % Tween 20 in the external water phase, mixed in the high shear mixer at 10,000 rpm for (□) 2 min, (∇) 5 min and (○) 10 min. All samples were kept at 5 ± 3ºC and contain 0.28 M NaCl and 0.14 M glucose in the W_1 and W_2, respectively.

It can be seen, that salt release over the storage period was the same for all three mixing times (~12.6 % loss of salt). This is contrary to the encapsulation measured directly after emulsification, when the release of salt varied significantly between emulsions with different mixing times (Figure 4-16). These observations indicate that in this case, long-term salt release from duplex emulsions is not determined by the time droplets are subjected to shearing forces, but rather by the composition of both water phases and the chemical potential gradient between them. Additionally, all three emulsions have similar droplet sizes (Table 4-9), and thus comparable diffusion distances and surface areas available for molecular transport.

4.5 Chapter conclusions

The primary W_1/O emulsions formulated with PGPR are more stable against coalescence and subsequent phase separation when the water phase contains a small amount of salt. NaCl alters the molecular orientation of surfactants at the interface, most likely strengthening interactions between them, which results in an increase of the interfacial viscosity and elasticity and thus promotes droplet stability against coalescence.

In $W_1/O/W_2$ duplex emulsions the majority of salt release from the internal water phase takes place during the initial stages of storage and is proportional to glucose concentration. The lowest salt release rate happens when the concentration of glucose in the external water phase is less than required for balancing the osmotic pressures. No significant change in the droplet size and no swelling-breakdown of the duplex emulsion, suggests that the release of salt is driven by the chemical potential difference between the two water phases rather than the unbalanced osmotic pressures.

Sugars used to match the osmotic pressure, alone and in combination with surfactants, alter the system's interfacial tension. Therefore, it is proposed that sugars act in a similar way to water-soluble emulsifiers, which by increasing micellar transport, increase the rate at which salt is released from the internal aqueous phase.

High-shear secondary emulsification has the potential to damage the structure of duplex emulsions. The extent of this damage depends on the concentration of the primary emulsifier (PGPR) and the duration of the mechanical shear. However, long-term salt release does not depend on the homogenisation conditions but on the formulation, *i.e.* 2 % or more of PGPR is crucial for the long-term stability of the investigated duplex emulsions.

5 Duplex $W_1/O/W_2$ emulsions produced with high-shear, cross-flow and rotating membrane techniques

5.1 Introduction

In the previous Chapter it was shown, that mechanical shear during secondary emulsification leads to a partial breakdown of the duplex structure leading to subsequent release of salt from the internal water phase. The magnitude of salt loss was greater for longer mixing times. In this Chapter, membrane emulsification techniques, alongside the high-shear technique, were used for the secondary emulsification step in duplex $W_1/O/W_2$ emulsion preparation. The need for a mild-shear secondary emulsification in the process of duplex emulsion preparation makes membrane techniques particularly desirable, as it is claimed (Aserin, 2008) to enable high encapsulation yields of the internal droplets in the final product.

This study investigated potential advantages of cross-flow and rotating membrane emulsification in the production of shear-sensitive duplex emulsions. The experimental work aimed at understanding the effects of membrane emulsification parameters: (i) cross-flow velocity (CFV), trans-membrane pressure (TMP) and pore size in cross-flow membrane emulsification, and (ii) rotational velocity (RV) and trans-membrane pressure in rotating membrane emulsification on the microstructure and encapsulation properties of $W_1/O/W_2$ emulsions. Finally, it was investigated whether duplex emulsions prepared with the cross-flow and rotating membranes have different encapsulation properties than duplex emulsions prepared in the high-shear process.

5.2 Formulation and processing

The primary 30 %-water-in-70 %-oil emulsion, containing 0.28 M NaCl in the internal water phase (W_1) and 4 % of an oil-soluble emulsifier (PGPR), was prepared in the high-shear mixer as described in Section 3.2.1. Then, duplex $W_1/O/W_2$ emulsions with 30 % dispersed phase (primary W_1/O emulsion) and the continuous phase (W_2) containing 2 % Tween 20 and 0.14 M glucose were produced. For the secondary emulsification step three techniques were used. Firstly, high-shear mixer as described in Section 3.2.3.2. Secondly, SPG hydrophilic cross-flow membranes with 3.9 μm, 6.1 μm and 10 μm pore diameters were used in the experimental set-up described in Section 3.2.3.4. The applied TMP varied between 20 and 80 kPa and the CFV was altered between 0.11 and 0.22 $m \cdot s^{-1}$ (Table 3-2, p.56). Thirdly, a rotating membrane was prepared and used as described in Section 3.2.3.3. The TMP was altered between 40 and 100 kPa and the RV range was between 300 and 1200 rpm. The extent of the applied RV, TMP and CFV was explained in Sections 3.2.3.3 and 3.2.3.4. All duplex emulsions were analysed for droplet size (according to the method described in Section 3.2.4.1) and encapsulation of salt (as described in Section 3.2.4.5) directly after preparation and then, in regular intervals during storage. All duplex emulsions were stored at 5 ± 2 °C.

5.3 Droplet size and droplet size distribution

High-shear mixer, cross-flow membrane and rotating membrane emulsification techniques were employed to produce duplex $W_1/O/W_2$ emulsions. The effects of emulsification parameters on duplex emulsion droplet size and droplet size distribution were investigated. The droplet size data obtained with the high-shear mixer and referenced in this Chapter were previously discussed in Section 4.4.1 (*i.e*. formulation with 4 % PGPR).

5.3.1 Cross-flow membrane emulsification

In cross-flow membrane emulsification, the effects of TMP, CFV and membrane pore size were investigated in relation to the duplex emulsion droplet size. Figure 5-1 shows changes in the emulsion droplet size with CFV and TMP for cross-flow membranes with 3.9 μm (Figure 5-1a), 6.1 μm (Figure 5-1b) and 10 μm pore diameter (Figure 5-1c). On the Y-axis of the graphs, the average droplet size of emulsions made with the high-shear mixer (~14 μm for all mixing times, as shown in Section 4.4.1) has been plotted as a reference. The effects of TMP, CFV and membrane pore diameter on the droplet size are discussed individually.

5.3.1.1 Effect of cross-flow velocity on droplet size

As shown in Figure 5-1, the mean droplet size $D_{3,2}$ decreases as CFV increases for a given TMP. This trend occurs for all three membranes. For example, for the 3.9 μm membrane at 40 kPa TMP, the droplet size is 35.1 ± 1.5 μm for 0.11 $m \cdot s^{-1}$, 16 ± 0.7 μm for 0.17 $m \cdot s^{-1}$ and 12.7 ± 1.2 μm for 0.22 $m \cdot s^{-1}$ CFV. Similar observations have been previously reported for single (Peng & Williams, 1998) and duplex emulsions (Vladisavljević & Schubert, 2003). A possible explanation for this behaviour comes from the fact, that the flow of the continuous phase generates shear, which is a major driving force for the detachment of droplets from the membrane pores. The sooner the droplet detaches, less dispersed phase flows inside it, and the smaller the final emulsion droplet. It is shown in Table 5-1, that the wall shear stress* at the membrane surface increases from 0.26 to 0.48 Pa when CFV increases from 0.11 to 0.22 $m \cdot s^{-1}$ (for the emulsion with 0 % dispersed phase). Consequently, with increasing CFV, smaller droplets are formed due to larger shear forces.

* Equations used for calculations are summarized in Section 8.2, in the Appendix.

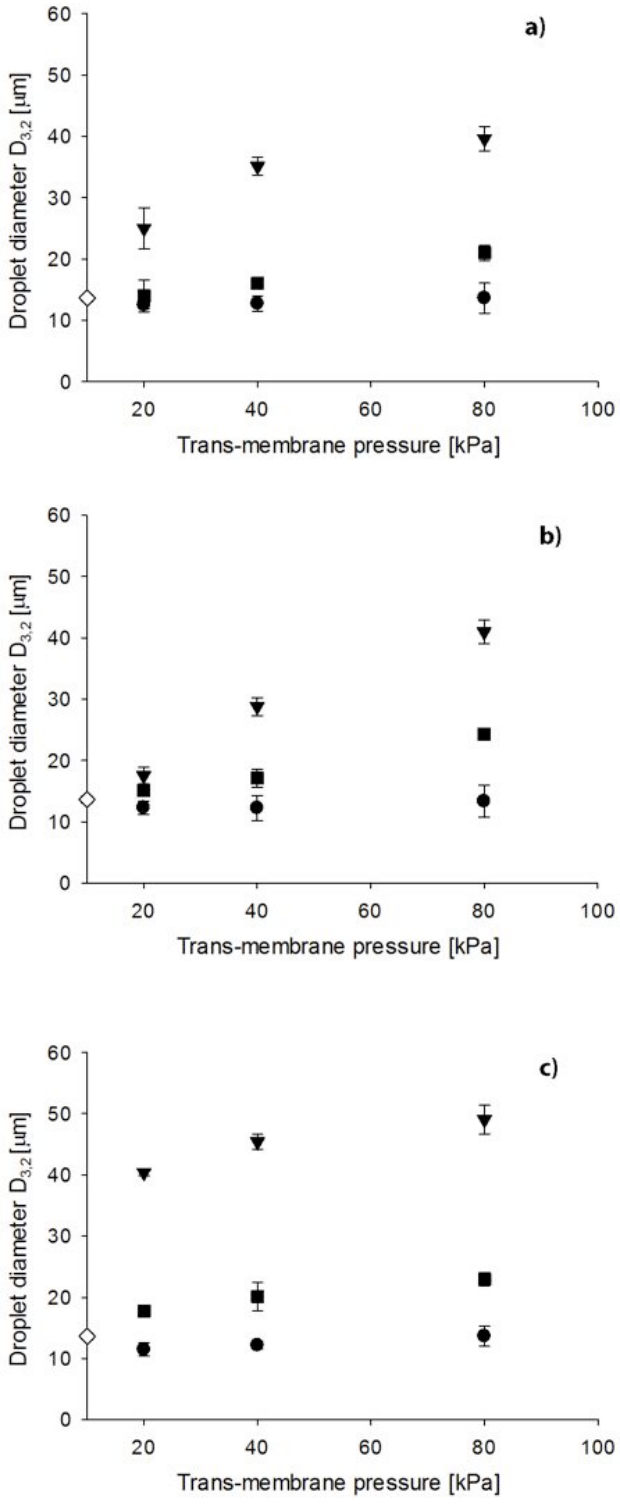

Figure 5-1 Droplet size ($D_{3,2}$) of duplex emulsions made using cross-flow membranes with: (a) 3.9 µm, (b) 6.1 µm, (c) 10 µm pore size. Effect of TMP at various CFV: (▼) 0.11 m·s^{-1}, (■) 0.17 m·s^{-1}, (●) 0.22 m·s^{-1}. Note, on the Y-axis (◇) is the average droplet size for emulsions made with the high-shear mixer.

Table 5-1 Shear stress and shear rate values for all three emulsification processes. Equations used for calculations are given in Section 8.2 in the Appendix. $T_{0\%}$ and $T_{30\%}$ is when the dispersed phase is 0% and 30%, respectively. R_i and R_o denotes that calculations were made for the membrane surface and for the inside wall of the emulsyfying container, respectively.

			Shear rate [s^{-1}]	**Shear stress** [Pa]
High-shear mixer			21980	145
Cross-flow membranes	**Cross-flow velocity** [$m \cdot s^{-1}$]			**Wall shear stress** [Pa]
	0.11	$T_{0\%}$	317	0.26
		$T_{30\%}$	116	1.61
	0.17	$T_{0\%}$	455	0.38
		$T_{30\%}$	212	2.94
	0.22	$T_{0\%}$	576	0.48
		$T_{30\%}$	295	4.10
Rotating Membrane	**Rotational velocity** [rpm]			**Shear stress** [Pa]
	300	$T_{0\%}$ R_i	65	0.054
		$T_{0\%}$ R_o	2.4	0.002
		$T_{30\%}$ R_i	65	0.332
		$T_{30\%}$ R_o	2.4	0.012
	600	$T_{0\%}$ R_i	130	0.108
		$T_{0\%}$ R_o	4.8	0.004
		$T_{30\%}$ R_i	130	0.664
		$T_{30\%}$ R_o	4.8	0.024
	900	$T_{0\%}$ R_i	196	0.162
		$T_{0\%}$ R_o	7.2	0.006
		$T_{30\%}$ R_i	196	0.997
		$T_{30\%}$ R_o	7.2	0.037
	1200	$T_{0\%}$ R_i	261	0.217
		$T_{0\%}$ R_o	9.6	0.008
		$T_{30\%}$ R_i	261	1.329
		$T_{30\%}$ R_o	9.6	0.049

5.3.1.2 Effect of trans-membrane pressure on droplet size

The effect of TMP on the droplet size varies depending on the applied CFV (Figure 5-1). At high CFV (0.22 $m \cdot s^{-1}$), (i) the smallest emulsion droplet sizes are obtained, and (ii) the TMP has no (or only little) effect on the droplet size. For example, for the 3.9 μm membrane, the

emulsion droplet diameter is 12.5 ± 0.6 μm at 20 kPa, 12.7 ± 1.2 μm at 40 kPa and 13.6 ± 0.5 μm at 80 kPa TMP. Similar observations were made for all three membranes. Peng & Williams (1998) reported, that at high CFVs the time the droplets stay attached to the membrane surface is small and thus the effect of TMP on the droplet size was decreasing with increasing CFV. This means that at high CFV of 0.22 $m \cdot s^{-1}$ (Figure 5-1), the drag force quickly overcomes the interfacial tension between the two phases (equilibrium interfacial tension of ~1 $mN \cdot m^{-1}$). As a result, the time of droplet detachment is likely to be very short and droplets break off the pore tip before more liquid is pushed into them, resulting in a relatively small droplet size.

The situation is different when the CFV is lower (*i.e.* 0.11 and 0.17 $m \cdot s^{-1}$). With decreasing CFV, the effect of the dispersed phase flow on the droplet diameter is more significant (especially for the 3.9 μm and 6.1 μm membranes). The diameter of droplets increases with TMP, from 25 ± 3.3 μm at 20 kPa TMP to 39.6 ± 2 μm at 80 kPa TMP (CFV = 0.11 $m \cdot s^{-1}$, 3.9 μm pore size membrane). This observation is supported by previous research by Joscelyne & Trägårdh (2000), who reported that the largest change in droplet size occurs at small wall shear stresses, *i.e.* smallest CFV. There are several possible reasons that alone, or more likely in combination, are responsible for the formation of larger droplets with increasing TMP:

(i) According to Darcy's law, the flow through the pores should increase with TMP (Schroder *et al*., 1998). As a result, more liquid is pumped into the drop, increasing its volume before detachment.

(ii) The increase in droplet diameter may result from the mechanism of droplet formation, which changes with increasing TMP. At low TMP, droplets are created *via a dripping mechanism* (Egidi *et al*., 2008), where as soon as the droplet is formed at the pore tip, the hydrodynamic drag force of the continuous phase helps the droplet to break away

from the membrane. On the contrary, at higher TMPs droplets are formed in *a continuous jetting regime* (Peng & Williams, 1998). This increases the probability of droplet coalescence at the membrane surface (Charcosset, 2009), resulting in a larger mean droplet diameter.

(iii) Larger droplets at higher TMPs could also be as a result of more membrane pores being activated (Lepercq-Bost *et al.*, 2008). In this case, droplets formed at neighbouring pores are likely to touch and coalesce (Abrahamse *et al.*, 2002).

(iv) It has been reported (Lepercq-Bost *et al.*, 2008), that the rate of surfactant adsorption onto the newly formed interface has an effect on the droplet size. When the TMP increases, the rate of the interface formation between the two phases becomes higher, and possibly comparable with the rate of the interfacial tension decrease. Low surfactant coverage would lead to: (i) larger interfacial tension and (ii) droplet coalescence during their formation and in the bulk emulsion. As a consequence, larger droplets are produced (Christov *et al.*, 2002).

5.3.1.3 Effect of membrane pore size on droplet size

The effect of membrane pore size on the emulsion droplet size is given in Figure 5-1. Droplet sizes obtained with all cross-flow membranes are: (i) 13 – 40 μm for the 3.9 μm membrane, (ii) 13 – 41 μm for the 6.1 μm membrane, and (iii) 12 – 49 μm for the 10 μm membrane. It is apparent, that the minimum droplet size for all three membranes remains similar (~12 μm). This, perhaps surprising observation, could be explained by considering the interfacial tension in the presence of both Tween 20 and PGPR in the system. By solubilising PGPR in the oil phase (4 %) and Tween 20 in the water phase (2 %), the interfacial tension was lower than for the systems where Tween 20 or PGPR acted as a sole surfactant, as can be seen in Figure 5-2. The interfacial tension measurements, even though far from the dynamic conditions during

emulsification, suggest that the presence of both emulsifiers is likely to allow a faster decrease of the interfacial tension, enhancing the detachment of droplets from the pore, which ultimately results in the production of small droplets. In addition to the above, it has been reported by Vladisavljević *et al.*, (2006a), that an untreated SPG membrane has a negative inherent surface potential of -15 to -35 mV within the pH range of 2 – 8, due to dissociation of the acid silanol groups. As it was previously shown in Section 4.3.2 (and Pawlik *et al.*, 2010), that the impurities in Tween 20 introduce negative charges onto the emulsion droplets. Electrostatic repulsions between the negatively charged membrane surface and the interface of the forming droplet (with adsorbed Tween 20 molecules carrying charged impurities) would increase the contact angle between the dispersed phases and the membrane (measured in the dispersed phase, see Figure 2-7, p.27). This in turn will reduce the extent to which the dispersed phase wets the membrane surface, resulting in droplets being pushed off the membrane by electrostatic repulsions.

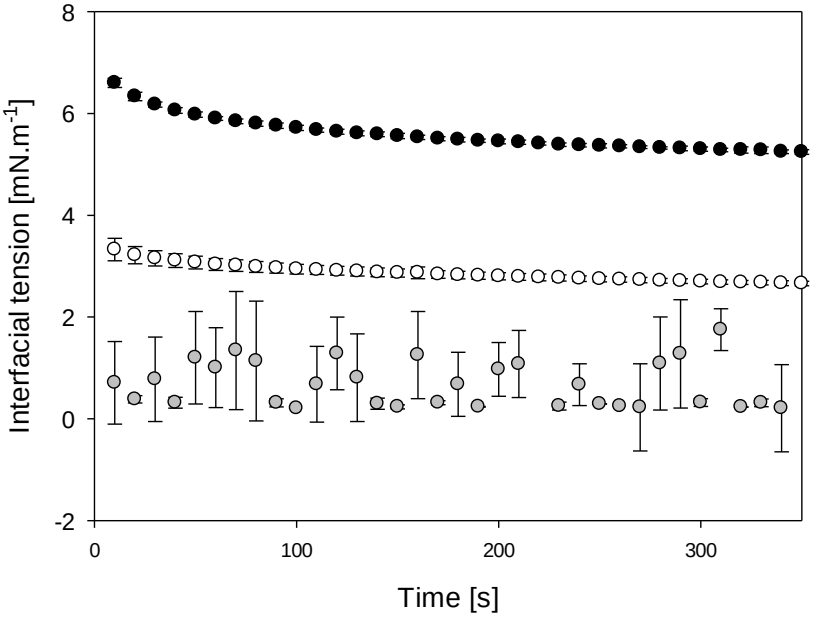

Figure 5-2 Change of the interfacial tension with time (at 21 ± 1 °C) for sunflower oil-water systems with: (●) 2 % Tween 20, (○) 4 % PGPR and (●) 2 % Tween 20 + 4 % PGPR.

In order to correlate the membrane mean pore size (d_p) and the diameter of the produced droplets (d_d), the ratio of d_d/d_p for all the membranes was calculated (Table 5-2). The ratio d_d/d_p is given at a range of values, as it depends on the TMP and CFV, at a given pore size.

Table 5-2 Ratio of d_d/d_p calculated for SPG membranes used. d_d is the diameter of a droplet and d_p is the diameter of a membrane's pore.

	Membrane pore size [μm]	d_d/d_p
Cross-flow membranes	3.9	3 – 10
	6.1	2 – 7
	10.0	1 – 5
Rotating membrane	2.8	3 – 14
Literature		2 – 10

Previous research with SPG cross-flow membranes (Charcosset, 2009; Joscelyne & Trägårdh, 2000; Mine, Shimizu, & Nakashima, 1996; Timgren *et al.*, 2010) indicated, that the droplet diameter is 2 to 10 times bigger than the membrane pore diameter. The data for the 3.9 μm and 6.1 μm membranes fall within this range, while for the 10 μm membrane, the range of d_d/d_p ratios is slightly narrower and at high CFV, the droplet size is very close to the mean pore size, *i.e.* $d_d/d_p = 1$. This shows that, even though the drag force is very high, the droplet will break off the pore only when it reaches a certain equilibrium volume, which is determined by the rate at which interfacial tension decreases, *i.e.* determined by the emulsion formulation. As mentioned above, at high CFV, the droplet size does not depend on the membrane pore size (across the range of processing conditions) and remains constant at ~13 μm; it can be then concluded that, for the formulation and processing parameters considered in this study, the minimum equilibrium droplet diameter size is ~13 μm. This diameter is very similar to the 10 μm membrane pore diameter, which leads to a diameter ratio of $d_d/d_p = 1$.

5.3.1.4 Droplet size distribution

The droplet size distribution of duplex $W_1/O/W_2$ emulsions made with cross-flow membranes was investigated. Span and size distribution curves were analysed in relation to the membrane pore size and the applied trans-membrane pressures and cross-flow velocities.

Figure 5-3a shows that for the 3.9 μm membrane, the highest span (1.6 ± 0.1) is for emulsions made at the TMP of 20 kPa and 0.11 $m \cdot s^{-1}$ CFV. For emulsions made at higher TMPs and CFVs, the span is smaller (between ~1.2 and ~1.4) and remains constant over the range of the investigated TMPs and CFVs. In order to get better understanding of the effects of CFV and TMP on polydispersity of the samples, droplet size distribution curves were plotted for emulsions prepared with the 3.9 μm membrane. This is shown in Figure 5-3b-d, where additionally the average droplet size distribution curve of duplex emulsions made with the high-shear mixer is given for comparison. The Figure shows that at low CFV (0.11 $m \cdot s^{-1}$), the size distribution becomes narrower with the increase in TMP from 20 to 40 kPa, and then it stays constant upon further increase in TMP (Figure 5-3b). It is also shown, that at low CFV the average emulsion droplet size is larger for the emulsions made with the membrane than with the high-shear mixer. When the CFV increases to 0.17 $m \cdot s^{-1}$ (Figure 5-3c), size distribution curves become similar to the emulsions made with the high-shear mixer and shift towards smaller droplet size. At the highest CFV of 0.22 $m \cdot s^{-1}$ (Figure 5-3d), droplet size and droplet size distributions of emulsions made with both emulsification techniques are very similar.

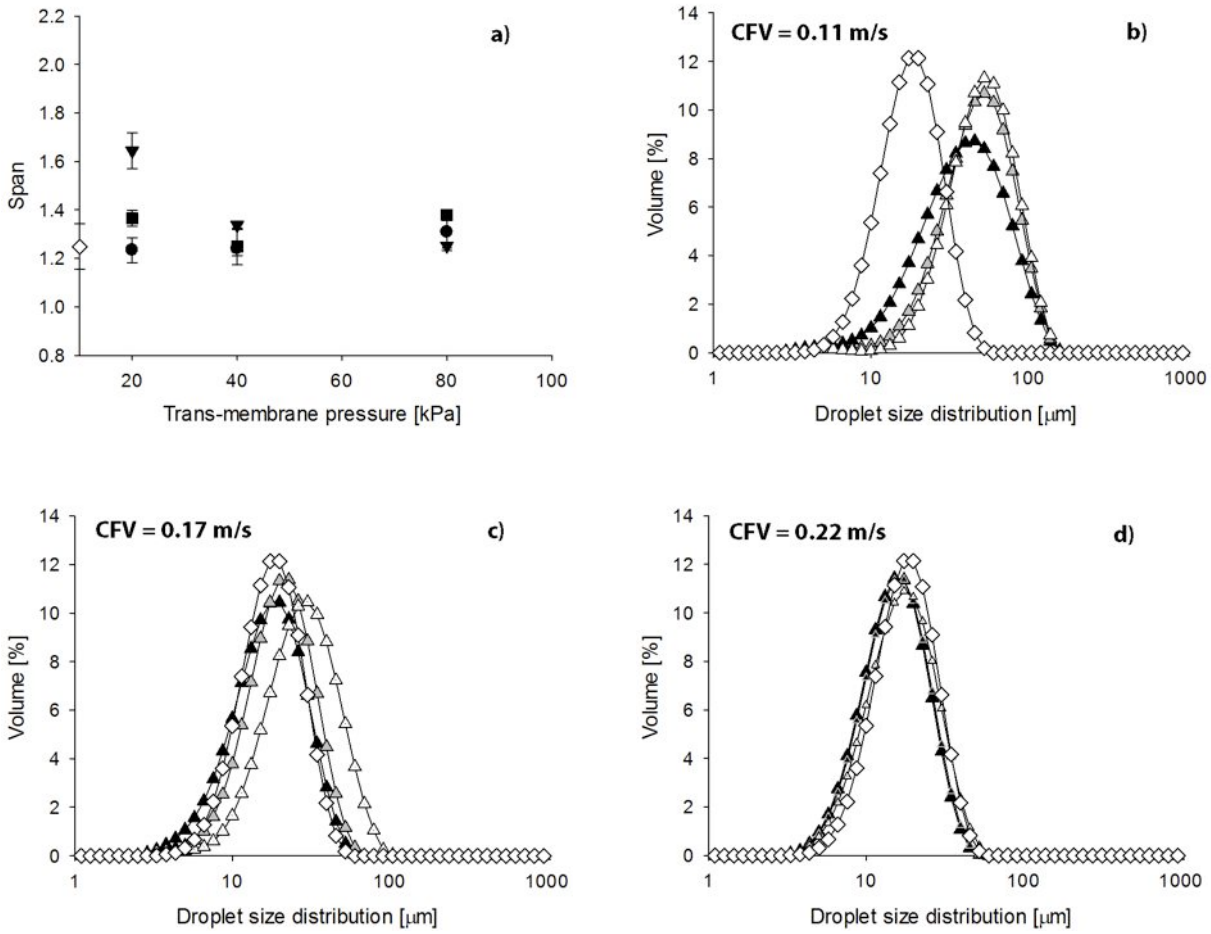

Figure 5-3 (a) Span of duplex emulsions made using the 3.9 μm cross-flow membrane; effect of CFV: (▼) 0.11 m·s^{-1}, (■) 0.17 m·s^{-1}, (●) 0.22 m·s^{-1} and TMP; where (◊) is the mean span of emulsions made witht the high-shear mixer. (b-d) droplet size distributions of duplex emulsions made using the 3.9 μm membrane; effect of TMP: (▲) 20 kPa, (▲) 40 kPa, (△) 80 kPa at various CFVs; where (◊) is the mean droplet size distribution of emulsions made with the high-shear mixer.

The broadest size distribution exhibited by emulsions made at 20 kPa TMP and 0.11 m·s^{-1} CFV could be as a result of the fact, that at low TMP big droplets are produced alongside the small ones due to a range of active pores. It has been reported (Abrahamse *et al.*, 2002), that the number of active pores increases with TMP. Therefore, if at 20 kPa TMP a range of pores is active, the interface formation rate at the small active pores would be relatively low (compared to higher TMPs at a given CFV) and so droplets break off the membrane at smaller volumes. At large active pores, on the other hand, faster interface formation rates and a low

shear force (at 0.11 $m \cdot s^{-1}$) would allow the droplet to stay attached to the pore for longer, thus more dispersed phase flows into it before detachment. When the shear force increases (*e.g.* to 0.17 $m \cdot s^{-1}$ CFV), the drag force of the continuous phase is larger for big droplets than for small ones, leading to faster detachment of the former and thus more uniform droplet size distribution. Similarly, when the TMP increases (*e.g.* to 40 kPa for a given, low CFV) the interface is quickly formed and the interfacial tension is lowered to a smaller extent. Again, large droplets attached to large pores will have bigger drag force acting on them (as compared to droplets formed from the small pores), which helps them to break off the membrane. This results in less polydisperse emulsion with increased overall droplet size (Figure 5-1a).

For the 6.1 μm membrane (Figure 5-4), similarly to the 3.9 μm membrane, the highest span (1.6 ± 0.04) was observed for emulsions made at low TMP and CFV (20 kPa and 0.11 $m \cdot s^{-1}$, respectively). With the increase in TMP and CFV, the span becomes narrower and similar: (i) for all investigated emulsification parameters, and (ii) for emulsions made with the high-shear mixer.

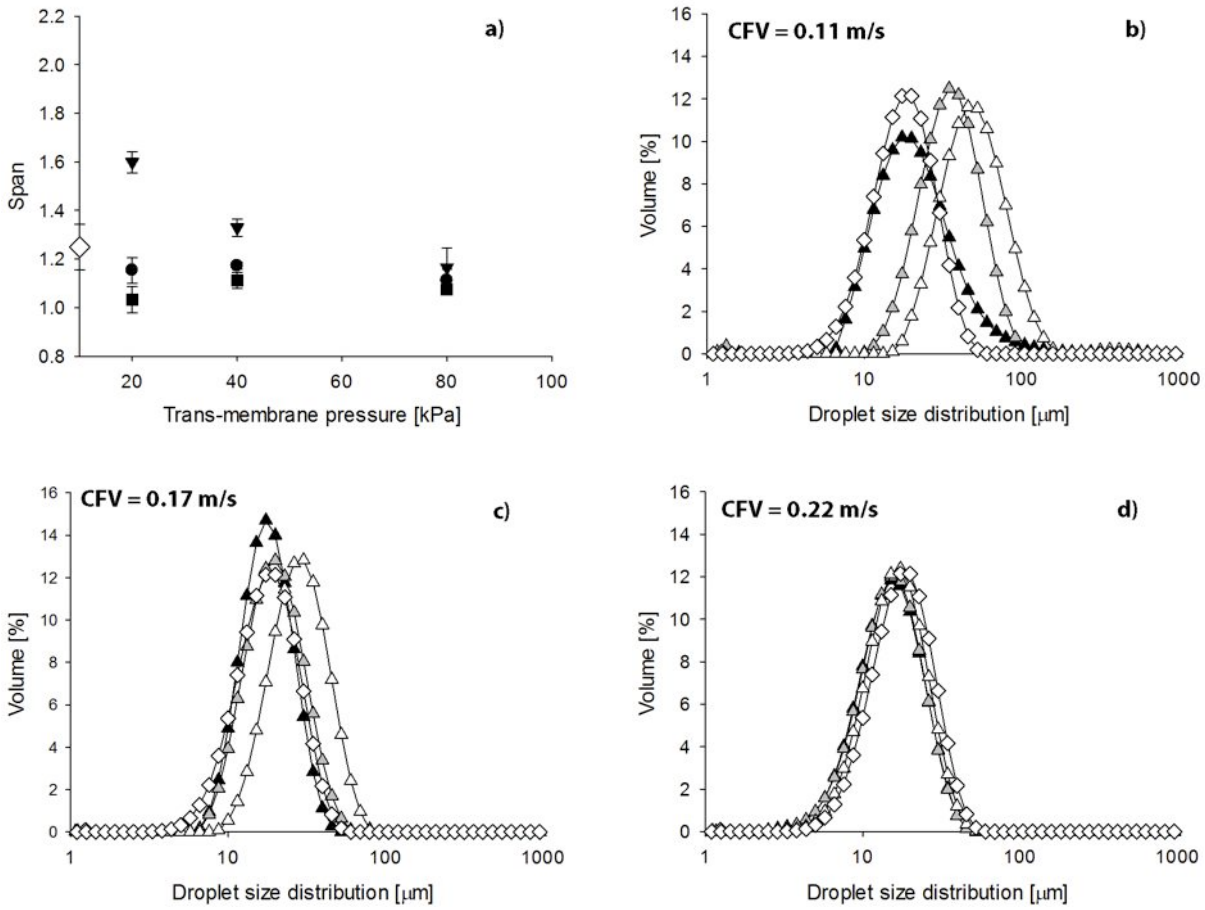

Figure 5-4 (a) Span of duplex emulsions made using the 6.1 μm cross-flow membrane; effect of CFV: (▼) 0.11 m·s^{-1}, (■) 0.17 m·s^{-1}, (●) 0.22 m·s^{-1} and TMP; where (◊) is the mean span of emulsions made witht the high-shear mixer. (b-d) droplet size distributions of duplex emulsions made using the 6.1 μm membrane; effect of TMP: (▲) 20 kPa, (▲) 40 kPa, (△) 80 kPa at various CFVs; where (◊) is the mean droplet size distribution of emulsions made with the high-shear mixer.

For the 10 μm membrane (Figure 5-5), span values are independent of CFV, but somewhat increase with TMP. That is, at 20 kPa TMP span is between ~1.2 and ~1.4, and increases at 80 kPa to a range between ~1.5 and ~1.7. This increase is most probably as a result of a continuous outflow of the dispersed phase at high TMPs, which may lead to droplet coalescence at membrane surface, hence wider size distribution. This phenomenon was not observed for the 3.9 μm and 6.1 μm membranes. It has been previously reported (Charcosset, 2009), that *jetting* of the dispersed phase is more probable for membranes with bigger pore diameters. Droplet size distribution curves of emulsions made with the 10 μm membrane and

the high-shear mixer are given in Figure 5-5. It shows that, for all CFVs, the distribution becomes slightly wider with the increase in TMP. The application of higher CFV reduces droplet size, however the size distribution remains unchanged.

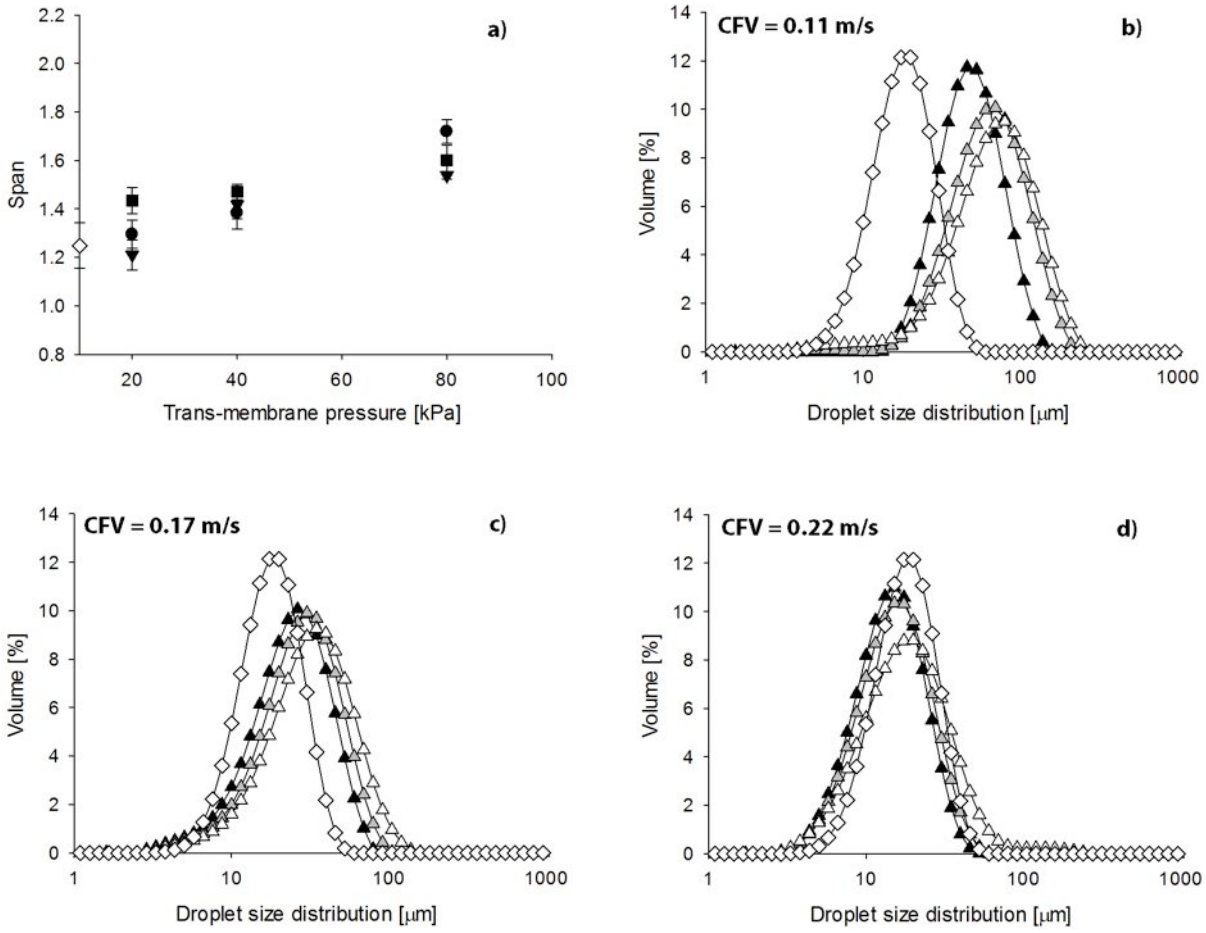

Figure 5-5 (a) Span of duplex emulsions made using the 10 μm cross-flow membrane; effect of CFV: (▼) 0.11 m·s^{-1}, (■) 0.17 m·s^{-1}, (●) 0.22 m·s^{-1} and TMP; where (◊) is the mean span of emulsions made witht the high-shear mixer. (b-d) droplet size distributions of duplex emulsions made using the 10 μm membrane; effect of TMP: (▲) 20 kPa, (▲) 40 kPa, (△) 80 kPa at various CFVs; where (◊) is the mean droplet size distribution of emulsions made with the high-shear mixer.

In summary, increasing CFV makes the droplet size distribution narrower only: (i) at low TMP (20 kPa), and (ii) for the membranes with 3.9 μm and 6.1 μm pore size. Previous research (Charcosset, 2009) showed, that with increasing shear stress the droplet size distribution becomes narrower. This effect however, does not occur with the 10 μm

membrane. It may be due to the fact that higher dispersed phase fluxes (as compared to membranes with smaller pores and thus higher hydrodynamic resistance), do not allow formation of small droplets at low TMP and CFV. This seems to be confirmed by a relatively large mean droplet size (~40 μm, Figure 5-1c) observed at 20 kPa and 0.11 $m \cdot s^{-1}$. Furthermore, the droplet size distribution decreases with the TMP, but only at low CFV and for the 3.9 μm and 6.1 μm membrane. This is due to formation of mainly large droplets at high TMPs. For the 10 μm membrane, the span increases with TMP which may be a consequence of the disperse phase *jetting*.

5.3.2 Rotating membrane emulsification

The rotating membrane technique was used to produce duplex $W_1/O/W_2$ emulsions as described in Section 3.2.3.3. The trans-membrane pressure and rotational velocity were altered, in order to understand their effects on the droplet size and droplet size distribution of duplex emulsions. Changes in the emulsion droplet size with TMP and RV are given in Figure 5-6. On the Y-axis of the graph, the mean droplet size of the emulsions made with the high-shear mixer (~14 μm, Section 4.4.1) has been plotted as a reference. As a general trend, it was observed that the droplet size increases with TMP and decreases with RV. The mechanisms underlying these tendencies are discussed in the following sections.

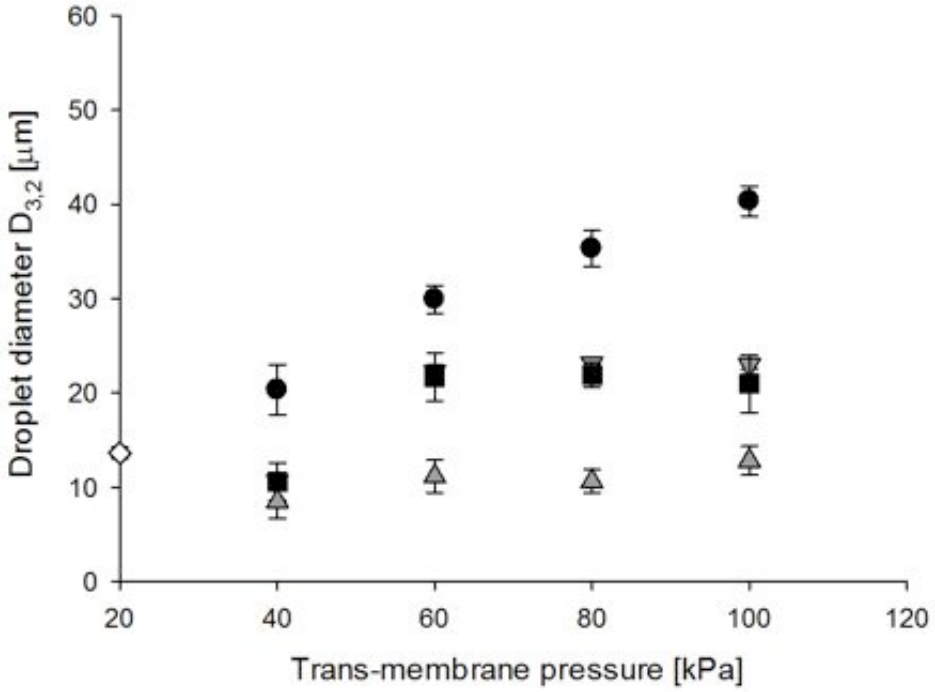

Figure 5-6 Droplet size ($D_{3,2}$) of duplex emulsions made using the 2.8 μm rotating membrane. Effect of TMP and RV: (●) 300 rpm, (▼) 600 rpm, (■) 900 rpm, (▲) 1200 rpm. Note, on the Y-axis (◇) is the average droplet size for all emulsions made with the high-shear mixer.

5.3.2.1 Effect of rotational velocity and trans-membrane pressure on droplet size

The effect of TMP on the emulsion droplet size is considered. It is shown in Figure 5-6, that at low RV (300 rpm), the droplet size increases substantially with TMP, from 20.3 ± 1.7 μm at 40 kPa to 40.3 ± 1.6 μm at 100 kPa. This steady increase is probably due to the mechanisms described in Section 5.3.1.2 for small CFVs in the cross-flow membrane technique. That is: (i) an increase in the dispersed phase flux, (ii) transition from a *dripping* to a *jetting* mechanism of droplet formation, (iii) increased percentage of active pores, and (iv) slower rate of interfacial tension decrease.

The smallest emulsion droplets were obtained at the highest RV (1200 rpm) and showed only little dependency on the changes in TMP (*e.g.* 8.7 ± 0.1 μm at 40 kPa increased to 13.8 ± 0.5 μm at 100 kPa). This corresponds to a trend observed in the droplet size data obtained for the cross-flow membrane (Figure 5-1), and suggests that at high wall shear stresses, RV and CFV have a similar effect on the duplex emulsion droplet size.

At intermediate RVs (600 rpm and 900 rpm), emulsion droplet sizes are comparable over the range of applied TMPs. They initially increase from ~10.5 μm to ~22 μm between 40 kPa and 60 kPa and then remain constant at higher TMPs (~22 μm at 80 and 100 kPa). This suggests, that at the intermediate values of RV, a transition between the two mechanisms determining the emulsion droplet size occurs. This transition occurs between a low-shear mechanism (at 300 rpm), when TMP has a significant effect on droplet size, and a high-shear mechanism (at 1200 rpm), when TMP has very little influence on droplet size.

When the effect of RV on droplet size is considered, Figure 5-6 shows that regardless of the TMP, an increase in RV in general leads to a reduction in emulsion mean droplet size. This can be explained by the fact, that increased rpm of the rotating membrane corresponds to higher shear stresses at the membrane wall (Table 5-1, calculations in Section 8.2 in the Appendix). This creates a stronger detaching force and thus allows formation of smaller droplets.

5.3.2.2 Effect of membrane pore size on droplet size

The calculated d_d/d_p ratio for the 2.8 μm rotating membrane is between 3 and 14, which is slightly higher than the ratio for the cross-flow membranes (Table 5-2, p.106). The d_d/d_p ratios for the rotating SPG membranes have not been reported before. Comparison with the cross-

flow system (Table 5-1, p.102) shows, that the shear stresses for the investigated RVs of the rotating membrane are smaller (max. of ~1.3 Pa at 1200 rpm) than the wall shear stresses calculated for CFVs in cross-flow membrane emulsification (max. of ~4.1 Pa at 0.22 $m \cdot s^{-1}$). Therefore, it could be expected that the average droplet size would be larger for the rotating membrane and consequently the larger d_d/d_p ratio. It was also observed, that during emulsification at 300 rpm, newly created droplets did not detach from the membrane immediately, but rather built up at its surface. Due to a small centrifugal force, a layer of droplets was formed at the membrane wall, and then slowly dispersed into the bulk upon further rotation of the membrane. The thickness of this layer was proportional to the TMP. This behaviour most probably leads to coalescence of droplets in the layer, resulting in bigger average droplet size and d_d/d_p ratio.

5.3.2.3 Droplet size distribution

Span and droplet size distribution curves of emulsions made using the 2.8 μm rotating membrane and the high-shear mixer were compared. Figure 5-7 gives changes in the span of emulsions produced at various RVs and TMPs. On the Y-axis, the average span of the emulsions made with the high-shear mixer has been plotted as a reference. Additionally, in Figure 5-8, changes in droplet size distributions with varying TMP and RV are shown. The mean droplet size distribution of emulsions made with the high-shear mixer has also been plotted for comparison.

It can be seen from Figure 5-7, that for the TMPs of 60 kPa, 80 kPa and 100 kPa, span values: (i) are similar and (ii) increase with RV. More polydisperse emulsions produced at higher RV may be due to satellite droplet formation at higher centrifugal forces. The results are different at the lowest TMP of 40 kPa, where the span decreases from 3 ± 0.2 at 300 rpm to 2.3 ± 0.1 at

600 rpm and then further to 0.8 ± 0.3 at 1200 rpm. Similarly to the cross-flow system, at small TMPs a range of pores with different diameter is active (Lepercq-Bost *et al.* 2008), and so there is a range of droplet inflation rates which results in the production of both relatively small and large droplets (due to low RV, Figure 5-8a). Therefore, the mean $D_{3,2}$ is big (~21 μm, Figure 5-6) and so is span (span = ~3). With the increased shearing force, the effective drag force is larger for the big droplets, causing their relatively fast detachment and thus the average droplet size (Figure 5-6) and droplet size distribution (Figure 5-8b-c) decrease. At 1200 rpm only small droplets are produced (Figure 5-8d), and thus the span is low (~0.8) and $D_{3,2}$ is small (~8.7 μm).

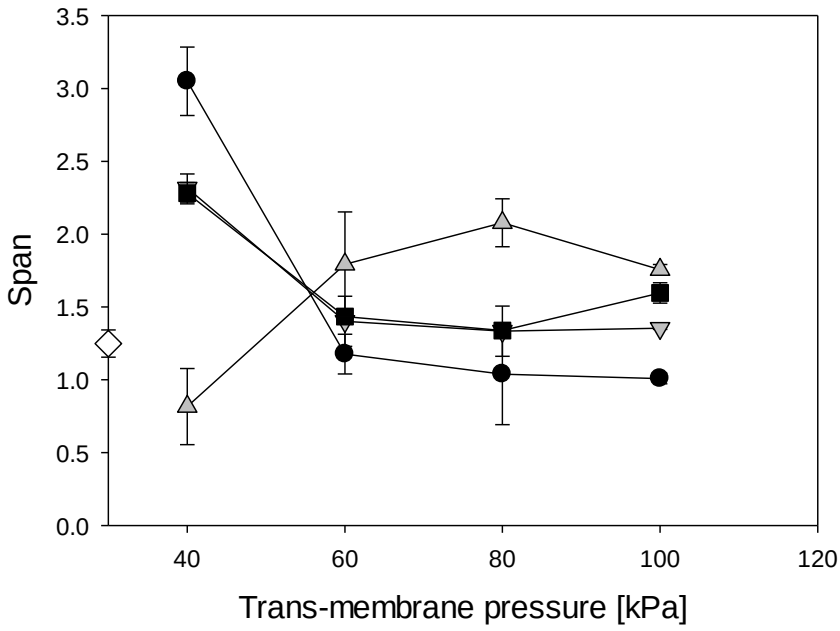

Figure 5-7 Span of duplex emulsions made using the 2.8 μm rotating membrane. Effect of TMP and RV: (●) 300 kPa, (▼) 600 kPa, (■) 900 kPa, (▲) 1200 kPa. Note, on the Y-axis (◇) is the mean span for duplex emulsions made with the high-shear mixer. Lines are drawn simply to guide the eye.

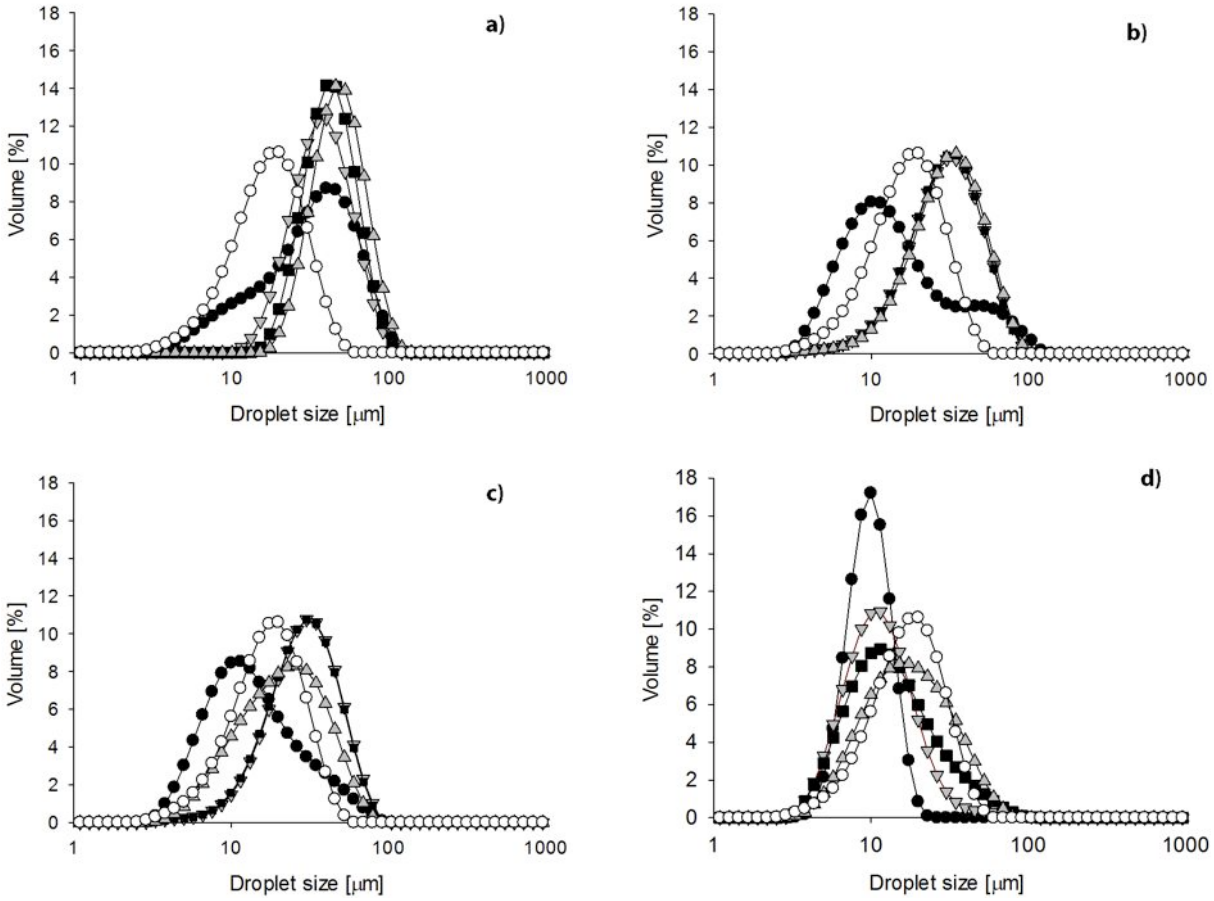

Figure 5-8 Droplet size distributions of duplex emulsions made using the 2.8 μm rotating membrane. Effect of RV: (a) 300 rpm, (b) 600 rpm, (c) 900 rpm, (d) 1200 rpm and TMP: (●) 40 kPa, (▼) 60 kPa, (■) 80 kPa, (▲) 100 kPa. (○) is for duplex emulsions made with the high-shear mixer.

5.3.3 Droplet size - comparison of emulsifying techniques

In summary, the minimum droplet sizes of emulsions obtained with all three emulsification techniques were similar:

- ~14 μm with the high-shear mixer (an average of all emulsions, see Section 4.4.1),
- ~13 μm with the 3.9 μm cross-flow membrane technique (at 0.22 $m \cdot s^{-1}$ CFV),
- ~13 μm with the 6.1 μm cross-flow membrane technique (at 0.22 $m \cdot s^{-1}$ CFV),
- ~12 μm with the 10 μm cross-flow membrane technique (at 0.22 $m \cdot s^{-1}$ CFV),
- ~9 μm with the rotating membrane technique (at 1200 rpm RV).

However, shear forces created in those emulsifying techniques are markedly different (Table 5-1, p.102). All this suggests, that in the high-shear droplet breakup (in the Silverson), the back reaction takes place, which ultimately yields droplets of ~14 μm. The mechanism of droplet breakup in a turbulent flow (*i.e.* in the high-shear mixer) involves instantaneous formation of large interfacial area, which for a finite time stays naked (*i.e*. with no or limited number of surfactant molecules), until the diffusion of surfactant reduces the excess energy (Eq. 2-1). This finite time for surfactant adsorption means that the interface remains "unprotected" and when, for example, two droplets come into contact, they are likely to coalesce. The resultant droplet size depends on how fast surfactant can adsorb at the interface. In membrane emulsification, emulsion droplets are expected to be maintained as they are produced without any further breakage or coalescence (Yuan *et al.*, 2009b). Nevertheless, here the droplet size is also determined by the surfactant adsorption kinetics and the droplets cannot detach from the membrane before the interfacial tension is sufficiently low.

This study has demonstrated, that duplex emulsions made with both membrane techniques have very similar droplet size distributions to the duplex emulsions prepared by the high-shear method (Figure 5-3, Figure 5-4, Figure 5-5 and Figure 5-8). It has been reported (Vladisavljević & Schubert, 2003), that the droplet size distribution of emulsions made with SPG cross-flow membranes is narrow, with spans well below 1. The obtained data indicate that the droplet size distribution for both membrane techniques is wider, with span values between ~1 and ~3. This however, is in agreement with Lepercq-Bost *et al.* (2008), who used an α-Al_2O_3 cross-flow membrane for the production of simple O/W emulsions, and obtained a span of 2 which decreased to 1.3 at high wall shear stresses. The polydispersity was explained in terms of steric hindrance of droplets caused by higher percentage of active pores at higher

dispersed phase fluxes. This could lead to the coalescence of droplets formed at neighbouring pores or/and earlier detachment of some of the droplets (Abrahamse *et al.*, 2002).

Another factor contributing to a broader size distribution of the duplex emulsions could be the fact that in the semi-batch emulsification, the dispersed phase volume fraction increases as the emulsification progresses. As explained in Section 3.2.3.4, the CFV was manually adjusted at the pump, to maintain a constant effective TMP. As a result, the wall shear stress (Table 5-1, p.102) and thus the hydrodynamic drag force of the continuous phase would vary during each semi-batch emulsification. This could lead to wider droplet size distribution of the final product.

Furthermore, polydispersed emulsions can be as a result of the membrane being wetted by the dispersed phase. This may happen when: firstly, the dispersed phase volume in the continuous phase is high and causes deposition of the disperse phase droplets on the membrane surface. As a result the contact area between the forming droplet and the membrane may extend over several pores, subsequently causing the membrane to be wetted with the dispersed phase (Christov *et al.*, 2002; Nakashima *et al.*, 1991). Secondly, the presence of oil soluble emulsifier (PGPR) in the dispersed phase may facilitate the wetting of pores, and consequently the membrane surface, with the primary W_1/O emulsion.

In addition, a broader size distribution of the emulsions may come from inherent membrane properties. It has been reported (Joscelyne & Trägårdh, 2000; Peng & Williams, 1998), that a narrow membrane pore size distribution is the most critical factor for the production of monodisperse emulsions. This means that, if the membrane pore diameter distribution is not sufficiently narrow, the produced emulsion would most probably be polydisperse. It is very

likely, that all the abovementioned factors in combination contribute to a broader size distribution of the investigated duplex emulsions.

5.3.4 Droplet size on storage

During long-term storage all the produced duplex emulsions changed in droplet size by only an average of 1 - 2 μm, which falls within the experimental error (see *e.g.* Figure 5-1, p.101). This was confirmed by microscopic analysis, which showed no significant change in the internal structure of duplex emulsions (Figure 4-9, p.81).

5.4 Emulsification salt release

It was shown in Chapter 4, that long high-shear emulsification time has a negative effect on the encapsulation of salt in duplex emulsions measured during and directly after homogenisation (Section 4.4.2). In this section, the effect of membrane emulsification parameters on the encapsulation of salt in the internal water phase of duplex $W_1/O/W_2$ emulsions was investigated. The conductivity of emulsions was measured immediately after their preparation (according to a method described in Section 3.2.4.5).

5.4.1 Cross-flow membrane emulsification

The effect of CFV and TMP on duplex emulsions stability during the emulsification process was investigated. Figure 5-9 shows salt entrapment in duplex emulsions made with the 3.9 μm membrane (Figure 5-9a), 6.1 μm membrane (Figure 5-9b) and 10 μm membrane (Figure 5-9c), measured just after emulsification. It is evident, that salt release depends on all the investigated parameters, which are further developed below.

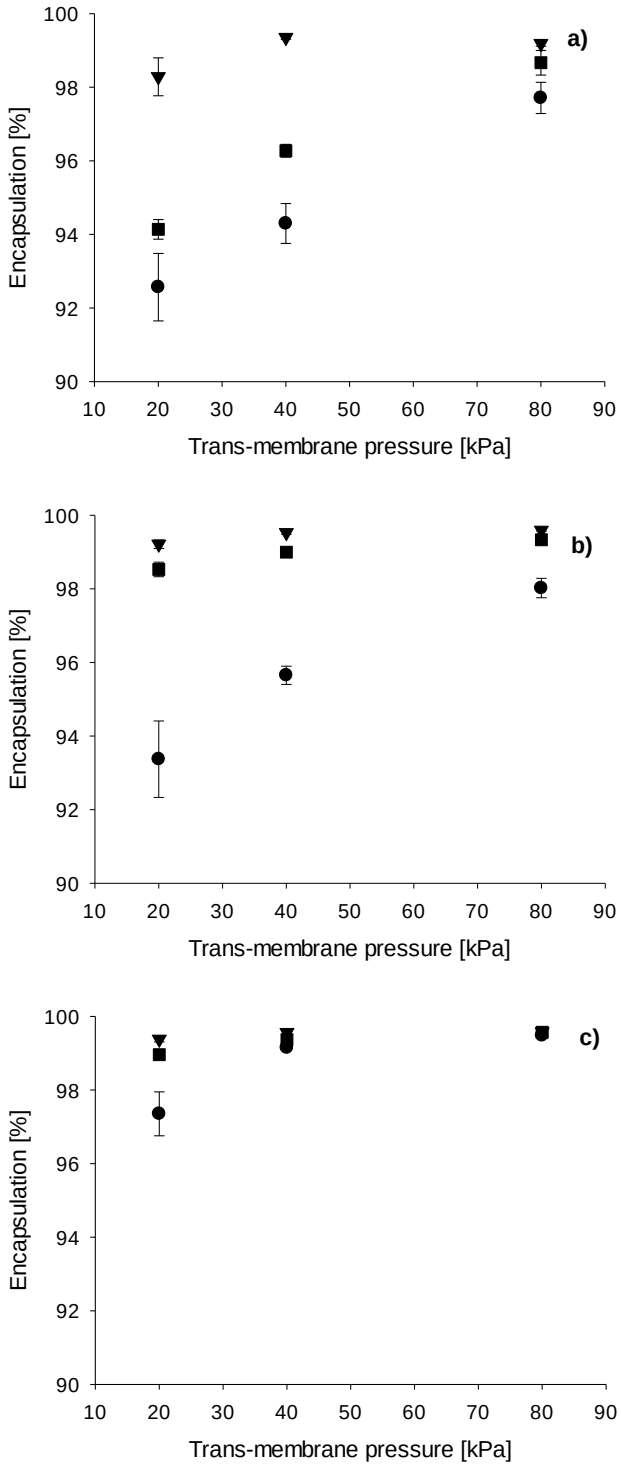

Figure 5-9 Emulsification salt encapsulation in the internal water phase of duplex emulsions made using cross-flow membranes with: (a) 3.9 µm, (b) 6.1 µm and (c) 10 µm pore diameter. Effect of TMP at various CFV: (▼) 0.11 m·s^{-1}, (■) 0.17 m·s^{-1} and (●) 0.22 m·s^{-1}.

5.4.1.1 Effect of cross-flow velocity

It can be seen from Figure 5-9, that for a given TMP the encapsulation efficiency decreases with an increase in the velocity at which the continuous phase flows inside the membrane module. This effect is more significant for the 3.9 μm and 6.1 μm membranes. For example, for the 3.9 μm membrane (Figure 5-9a), at 20 kPa TMP the salt encapsulation decreases from ~98 % at 0.11 $m \cdot s^{-1}$ CFV to ~94 % at 0.17 ms^{-1} and ~93 % at 0.22 $m \cdot s^{-1}$. Similarly for the 6.1 μm membrane (Figure 5-9b), at 20 kPa TMP the salt encapsulation decreases from ~99 % at 0.11 $m \cdot s^{-1}$ CFV to ~98 % at 0.17 $m \cdot s^{-1}$ and to ~93 % at 0.22 $m \cdot s^{-1}$. However, for the 10 μm membrane and 20 kPa TMP (Figure 5-9c), there is only a slight decrease from ~99 % at 0.11 $m \cdot s^{-1}$ CFV to ~97 % at 0.22 $m \cdot s^{-1}$.

The reason for this increase in salt release with the increase in CFV may come from the shear forces inherent to each CFV. As shown in Table 3-2 (p.56), the increase in CFV from 0.11 $m \cdot s^{-1}$ to 0.22 $m \cdot s^{-1}$ causes an increase in the membrane wall shear stress from 1.61 Pa to 4.10 Pa for $T_{30\%}$, and consequently an increase in the shear stress acting on the emulsion droplets in the membrane module and the tubing system. This may result in breakage of shear-sensitive duplex droplets (Vladisavljević *et al.*, 2006a). It has been suggested by van der Graaf *et al.* (2005), that the external phase flow induces internal streaming in the duplex droplets, which increases the frequency of collisions (and thus coalescence) of the internal water droplets with the outer water phase. In addition to the emulsion damage induced by the fluid flow in the membrane module, breakage of duplex droplets may occur in the gear pump, which was used to pressurise the continuous phase through the membrane module. The rotating pump gears transfer the emulsion with a very small mechanical clearance (typically in the order of 10 μm), to the discharge side of the pump. This may result in damage of the larger emulsion droplets during the pumping cycle and subsequent release of the internal water phase.

5.4.1.2 Effect of trans-membrane pressure

Figure 5-9 shows, that there is a strong effect of TMP on the encapsulation of salt. This is especially significant for: (i) CFV of 0.17 $m \cdot s^{-1}$ and 0.22 $m \cdot s^{-1}$, and (ii) membranes with the 3.9 μm and the 6.1 μm pore diameter (Figure 5-9a-b). For example, for the 3.9 μm membrane (Figure 5-9a), at 0.22 $m \cdot s^{-1}$ the salt entrapment is ~93 % at 20 kPa, which increases to ~94 % at 40 kPa, and then further to ~98 % at 80 kPa TMP.

Salt encapsulation at a given CFV increases with TMP and thus, according to Darcy's law, the dispersed phase flux through the micropores. The increase in duplex encapsulation with TMP is most probably a consequence of the emulsification time; that is the time taken to produce a 30 % dispersed phase volume $W_1/O/W_2$ emulsion at a given CFV, TMP and membrane pore size. This time dependence is shown in Figure 5-10, where the emulsification time was plotted as a function of both CFV and TMP for all three membranes. It is shown, that for a given membrane, the emulsification time increases for smaller TMPs. For example, for the 3.9 μm membrane at the CFV of 0.11$m \cdot s^{-1}$ the emulsification takes ~200 s at 80 kPa, which increases to ~300 s at 40 kPa and further to ~1300 s at 20 kPa TMP. Due to the semi-batch emulsification procedure, duplex droplets produced at the beginning of the process continue to re-circulate within the continuous phase through the membrane module, until the desired volume fraction of the dispersed phase is obtained. As a result, some droplets are exposed to the flow induced shear forces for longer, hence greater subsequent breakage of the duplex structure and release of the entrapped internal water phase with salt may occur.

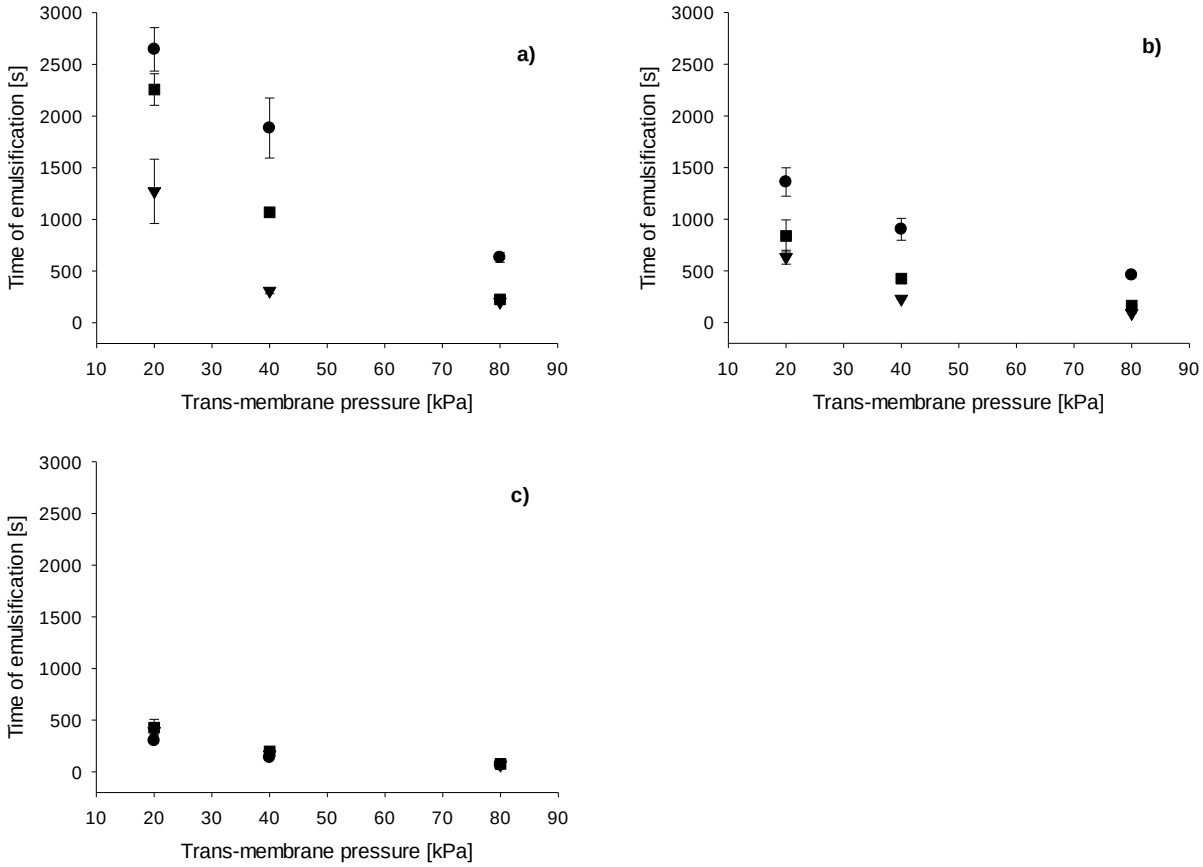

Figure 5-10 Emulsification time of duplex emulsions made using cross-flow membranes with: (a) 3.9 μm, (b) 6.1 μm and (c) 10 μm pore diameter. Effect of TMP at various CFV: (▼) 0.11 m·s^{-1}, (■) 0.17 m·s^{-1} and (●) 0.22 m·s^{-1}.

The dependency of emulsification time on TMP, CFV and membrane pore diameter (as shown in Figure 5-10), corresponds in trend and the magnitude of changes to the dependency of encapsulation on TMP, CFV and membrane pore size (Figure 5-9). That is, salt release from duplex droplets increases at longer emulsification times. It should also be noted, that for a given TMP, the emulsification time increases with CFV, especially for the 3.9 μm and 6.1 μm membranes. This is most probably due to fouling of membranes, which may block the pores and/or reduce pore size, thus resisting flux of the dispersed phase.

5.4.1.3 Effect of membrane pore size

The effect of membrane pore size on the salt entrapment in duplex emulsions is shown in Figure 5-9. It shows that the salt encapsulation is higher in emulsions made with membranes with larger pores. For example, at 20 kPa TMP and 0.22 $m \cdot s^{-1}$ CFV, salt encapsulation is ~94 % for the 3.9 μm membrane (Figure 5-9a), ~96 % for the 6.1 μm membrane (Figure 5-9b) and ~99 % for the 10 μm membrane (Figure 5-9c). This can be explained in terms of the semi-batch emulsification time (Figure 5-10). The smaller the membrane pore size is, the longer it takes to produce 30 % dispersed volume fraction emulsions, hence the longer duplex droplets are subjected to shear forces induced by the continuous phase flow.

5.4.2 Rotating membrane emulsification

The effects of RV and TMP on the salt encapsulation in duplex $W_1/O/W_2$ emulsions produced with the rotating membrane were studied. The conductivity of samples was measured directly after emulsification (as described in Section 3.2.4.5). Figure 5-11 shows changes in the encapsulation of NaCl in duplex emulsions, depending on the applied TMP and RV. These data show, that there are no significant differences in the release of salt within the investigated TMPs and RVs. All emulsions prepared using the rotating membrane released only a small amount of salt (up to 1.2 %) during the emulsification process. This is most probably a result of a very mild emulsification process, with the maximum shear rate of 261 s^{-1} (Table 5-1, p.102).

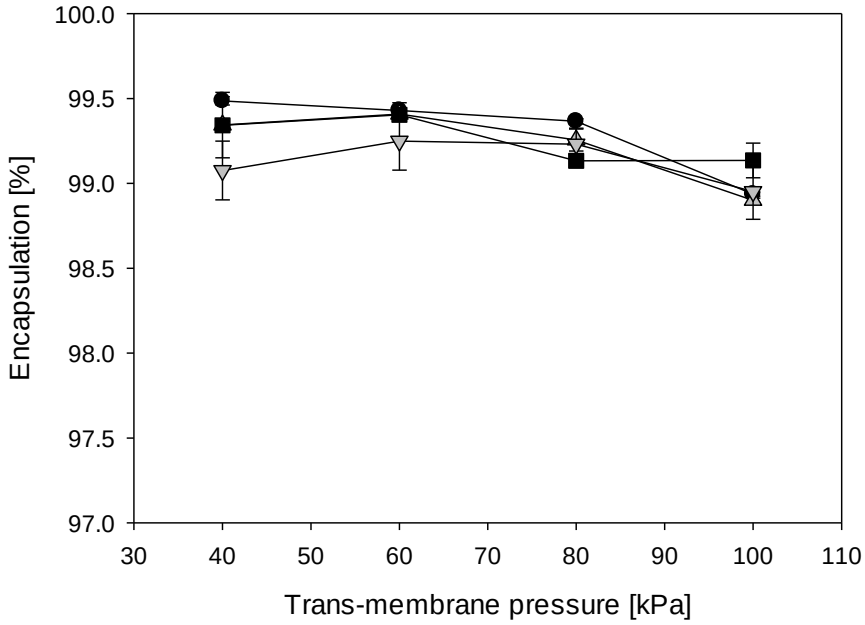

Figure 5-11 Emulsification salt encapsulation in the internal water phase of duplex emulsions made using the 2.8 μm rotating membrane. Effect of TMP at various RV: (●) 300 rpm, (▲) 600 rpm, (■) 900 rpm, (▼) 1200 rpm. The lines are drawn simply to guide the eye.

5.4.3 Emulsification salt release - comparison of emulsifying techniques

Emulsions produced using the rotating membrane released up to 1.2 % of salt during the emulsification process, which is lower than in the high-shear process (up to 2.8 % for 10 min mixing, Section 4.4.2) and in cross-flow emulsification (up to 7.5 % for the 3.9 μm membrane at 20 kPa TMP and 0.22 $m \cdot s^{-1}$ CFV). It can be assumed, that the emulsion droplet size, and thus interfacial area, has no effect on salt release during the emulsification process. This is due to the fact that: (i) in high-shear emulsification, the emulsions mixed for different times released different amounts of salt despite very similar droplet sizes, and (ii) the emulsions prepared with the rotating membrane released similar amounts of salt during emulsification, despite a relatively wide range of droplet sizes (between ~9 μm and ~40 μm). The reason for the observed variations in the encapsulation for emulsions produced using those three

techniques could be the magnitude of shear forces that act on duplex droplets during the emulsification process.

All calculated shear rates and shear stresses for the three emulsifying systems are given in Table 5-1 (p.102). It shows, that the shear forces generated at the gap between the Silverson's rotor and stator are the highest (21,980 s^{-1}), followed by the cross-flow membrane (116 - 576 s^{-1}) and the rotating membrane (2.4 – 261 s^{-1}). In cross-flow membrane emulsification, the shear stress increases with CFV and emulsification progress (from $T_{0\%}$ to $T_{30\%}$), as the viscosity of the emulsion increases. In the emulsifying cylinder (beaker) of the rotating membrane, the shear stress varies depending on the distance to the membrane and progress of emulsification. At the surface of the rotating membrane, the shear stress is highest for the maximum rotational speed (*i.e.* 1200 rpm) and increases with progress of emulsification (from 0.217 Pa at $T_{0\%}$ to 1.329 Pa at $T_{30\%}$, calculated for the surface of the rotating membrane R_i). Additionally, the shear stress acting on duplex droplets in close proximity to the beaker wall is significantly smaller (0.008 Pa at R_o, $T_{0\%}$) than close to the membrane wall (0.217 Pa at R_i, $T_{0\%}$).

Since the release of internal droplets in duplex emulsions is dependent on the applied shear stress (due to droplet elongation, Aserin, 2008), the minimum encapsulation would be expected in emulsions produced by the high-shear process. However, the observed salt encapsulation in emulsions produced using cross-flow membranes is similar or even lower (*e.g.* for 0.22 $m \cdot s^{-1}$ CFV using the 3.9 μm membrane), than in emulsions made using the high-shear mixer. It is therefore likely, that the external phase flow in the semi-batch cross-flow emulsification, and the use of the gear pump, induces destructive shear forces in the system. This will cause duplex droplet damage and a decrease in emulsion quality.

5.5 Storage salt release

In order to evaluate long-term emulsion properties, all duplex emulsions were examined for salt release over the storage period of up to 60 days (for high-shear emulsification and the rotating membrane) and up to 70 days (for cross-flow membranes). Encapsulation data for emulsions made with the high-shear mixer was previously discussed in Section 4.4.3 and given here as a reference.

5.5.1 Cross-flow membrane emulsification

The effects of TMP, CFV and membrane pore size on salt encapsulation were investigated. Table 5-3 shows storage salt encapsulation for all three cross-flow membranes with different pore sizes. Salt encapsulation for emulsions prepared using the 3.9 μm, 6.1 μm, and 10 μm membranes was similar, when compared for the corresponding CFVs and TMPs. This could be explained in terms of droplet size. With similar ranges of duplex droplet sizes produced with all three membranes (Figure 5-1, p.101), and thus comparable interfacial area available for molecular transport, salt release for all the membranes would be comparable. Therefore, for clarity of the discussion the membrane with 3.9 μm mean pore diameter will be considered as an example.

Table 5-3 Storage salt encapsulation in the internal water phase of duplex emulsions made using cross-flow membranes with 3.9 µm, 6.1 µm and 10 µm pore diameter. Emulsions were stored up to 70 days at 5 ± 3 °C.

CFV [m·s^{-1}]	0.11			0.17			0.22		
TMP [kPa]	20	40	80	20	40	80	20	40	80
Membrane [µm]	**Encapsulation** [%]								
3.9	84.7 ±0.8	83.3 ±4.2	91.4 ±0.5	80.4 ±1.6	84.2 ±0.4	89.6 ±0.8	74.1 ±1.2	77.3 ±1.6	81.3 ±0.8
6.1	83.9 ±2.0	88.8 ±0.3	91.0 ±0.3	80.3 ±1.2	84.4 ±0.3	87.8 ±0.9	75.0 ±0.4	78.3 ±1.4	80.8 ±1.4
10.0	81.6 ±1.0	87.0 ±1.2	89.3 ±0.5	80.2 ±0.9	84.9 ±0.4	86.5 ±0.3	77.2 ±1.3	83.4 ±0.9	85.8 ±0.6

Figure 5-12 shows storage encapsulation for emulsions produced using the 3.9 µm cross-flow membrane at various TMPs and the CFV of 0.11 m·s^{-1} (Figure 5-12a), 0.17 m·s^{-1} (Figure 5-12b) and 0.22 m·s^{-1} (Figure 5-12c). The data show, that the release of salt over the storage period was higher for low TMPs and high CFVs. For example, after 70 days of storage, emulsions made at CFV of 0.11 m·s^{-1} retained ~85 % salt when produced at 20 kPa TMP. This (i) increased to ~91 % when TMP increased to 80 kPa and (ii) decreased to ~74 % when CFV increased to 0.22 m·s^{-1}. This trend is similar to the encapsulation measured immediately after emulsification (Figure 5-9a, p.121). A possible explanation for this might be that at high CFVs and low TMPs, the emulsion droplets are smaller than those produced at lower CFVs and higher TMPs (Figure 5-1a, p.101). As a result, a larger interfacial area is created, which facilitates molecular transport between the two water phases.

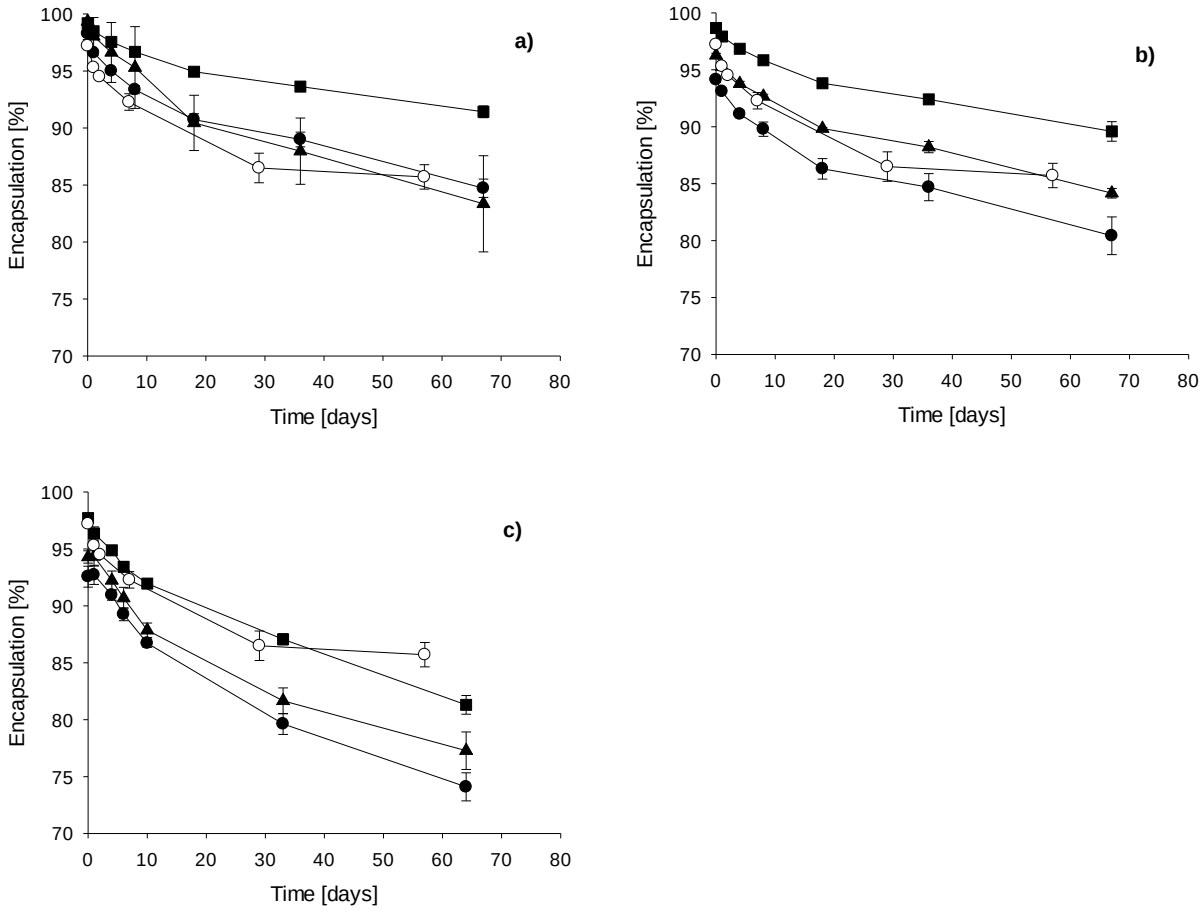

Figure 5-12 Storage encapsulation of salt in the internal water phase of duplex emulsions prepared using (○) high-shear mixer and 3.9 µm cross-flow membrane at TMP of (●) 20 kPa, (▲) 40 kPa and (■) 80 kPa; and CFV of: (a) 0.11 m·s^{-1}, (b) 0.17 m·s^{-1} and (c) 0.22 m·s^{-1}.

Figure 5-12 also includes the storage encapsulation curve of emulsions prepared with the high-shear mixer. For the CFV of 0.11 m·s^{-1} and 0.17 m·s^{-1}, the storage salt release in the Silverson-made emulsions is similar to emulsions made by the cross-flow system. However, salt release in emulsions prepared at the highest CFV (0.22 m·s^{-1}) is somewhat higher than the release in emulsions made with the high-shear mixer. This is quite unexpected as membrane emulsification is commonly considered advantageous (Charcosset *et al.*, 2004) for the production of shear-sensitive duplex emulsions. This phenomenon is further explained in Section 5.5.3.

5.5.2 Rotating membrane emulsification

Figure 5-13 shows the data on the storage salt release from duplex emulsions made with the SPG rotating membrane at 40 - 100 kPa TMP and 300 - 1200 rpm RV. The encapsulation of salt in emulsions prepared with the high-shear mixer has also been plotted on the Figure, for reference. It can be seen that over the storage period, the release of salt differs significantly between emulsions prepared by the two methods. With no considerable influence of processing parameters (TMP and RV) on the salt release, all emulsions prepared with the rotating membrane showed higher entrapment of salt during 60 days of storage (~92 %) than emulsions prepared with the high-shear mixer (~87 %). This is further discussed in Section 5.5.3.

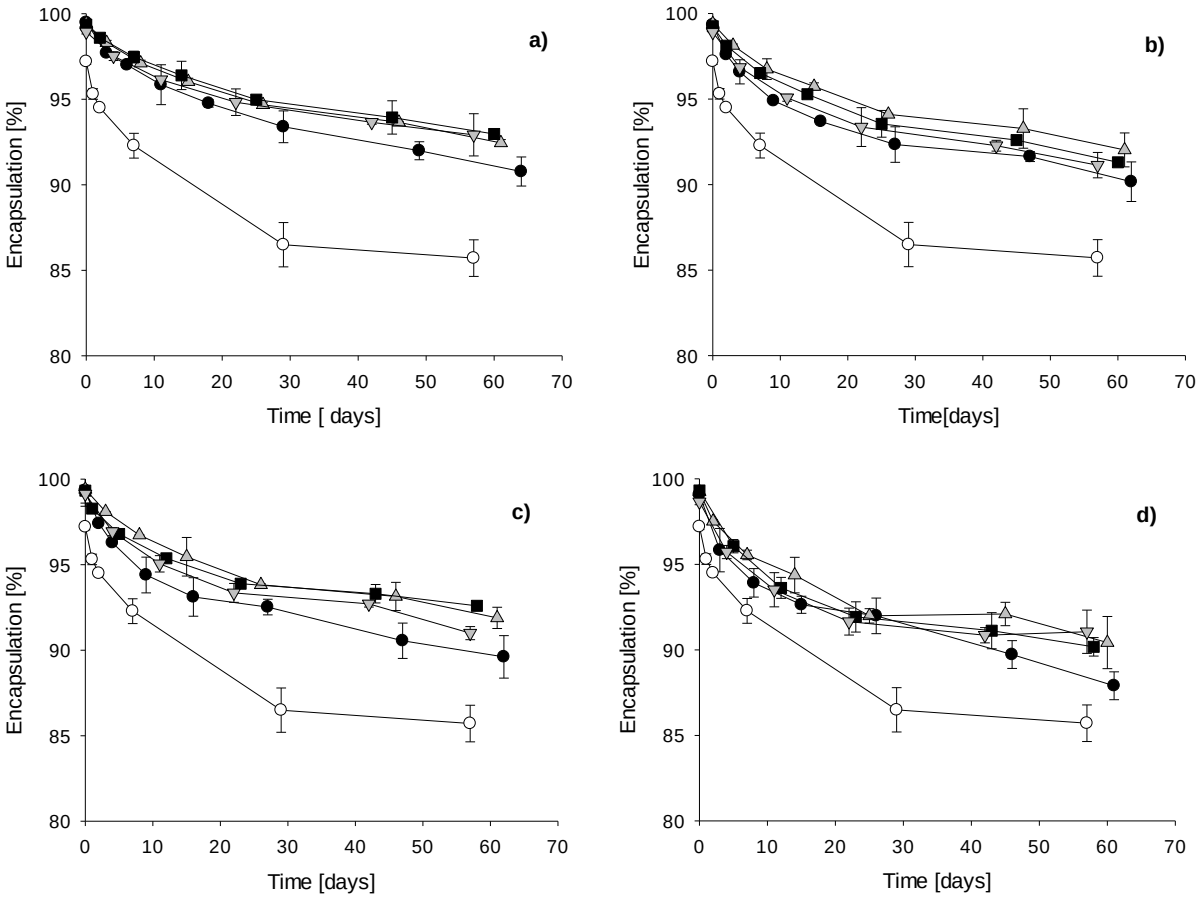

Figure 5-13 Storage encapsulation of salt in the internal water phase of duplex emulsions prepared using (○) the high-shear mixer and rotating membrane at TMP of: (●) 40 kPa, (▲) 60 kPa, (■) 80 kPa and (▼) 100 kPa and RV of: (a) 300 rpm, (b) 600 rpm, (c) 900 rpm and (d) 1200 rpm.

5.5.3 Storage salt release - comparison of emulsifying techniques

Differences in performance between emulsions produced with the high-shear mixer, cross-flow membranes and the rotating membrane may be explained in terms of: (i) emulsion droplet size, and (ii) the shear forces that duplex droplets were subjected to during emulsification. Table 5-4 summarises the data presented so far. It can be seen that droplet sizes of emulsions prepared with the high-shear mixer (~14 μm) are comparable to the minimum droplet size obtained with cross-flow membranes (~13 μm for 0.22 $m \cdot s^{-1}$ CFV) and the rotating membrane (~9 μm for 1200 rpm RV).

Table 5-4 Summary of the droplet size and encapsulation data for all three processing techniques. *range of values reflects different encapsulation for emulsions mixed for 2, 5 and 10 min, **range of values reflects different encapsulation for emulsions with varied TMP, CFV and RV.

	High-shear mixer	**Cross-flow membrane 3.9 μm**	**Rotating membrane**
Droplet size [μm]	13.6 ± 0.6	12.6 – 40**	8.5 – 40.3**
Salt encapsulation during emulsification [%]	99.4 – 97.2*	99.3 – 92.5**	99.5 – 98.6**
Loss of salt on storage [%]	12.6 ± 0.9	7.8 – 19.9**	7.9 ± 1.1

Salt encapsulation measured directly after emulsification is highest for the rotating membrane (99.5 - 98.6 %; a range that depends on the applied TMP and RV, Figure 5-11). The encapsulation of emulsions made with the high-shear mixer is slightly lower (99.4 – 97.2 %, Section 4.4.3), with the lowest salt entrapment for emulsions made with the 3.9 μm cross-flow membrane (99.3 – 92.5 %, Figure 5-9a). As explained in Section 5.4.3, this is probably a

consequence of the magnitude and duration of shear forces acting on duplex droplets during the emulsification process.

The percentage decrease in salt encapsulation during the storage period was also calculated.. As seen from Table 5-4 the % loss of salt from the internal water phase is largest for the 3.9 μm cross-flow membrane (7.8 – 19.9 %), followed by high-shear emulsification (12.6 ± 0.9 %), and lowest for the rotating membrane (7.9 ± 1.1 %).

Due to the fact that: (i) the minimum droplet size and droplet size distribution obtained by all emulsifying techniques are similar, and (ii) there is no visible difference in morphology of the internal water droplets (W_1) between the analysed samples, the interfacial area is unlikely to be the only factor causing markedly different encapsulation properties of these duplex emulsions. Therefore, the reason for this behaviour could be associated with the emulsification process and interfacial properties of the system. It has been reported by Okochi & Nakano (1997), that the release of a series of drugs from duplex $W_1/O/W_2$ emulsions was slower when emulsions were prepared by the membrane as compared to a stirring method. This was explained by the surface properties of droplets, and a distinctively different way of emulsifier deposition and orientation at the interface in these two methods. Using small angle X-ray scattering, it was established that during membrane emulsification surfactants adsorb at the interface in a homogenous manner. As a result, a densely packed layer of surfactant molecules with an isotropic orientation is created, which then is claimed to provide a mechanical barrier against molecular transport across the interface. This does not happen in the stirring process.

This hypothesis, however thermodynamically surprising, would correspond to the data on the storage salt release. In the case of cross-flow emulsification, a homogenous and dense layer of surfactant molecules forms at the interface during droplet formation at the tip of the membrane pore. However, subsequent intensive processing inside the membrane module and the gear pump leads to droplet deformation (and/or break-up), which disturbs the isotropic molecular orientation at the interface. This may lead to an irregular film of surfactants, and thus a weaker barrier for the migration of ions. In the high-shear mixer, due to a random deposition of surfactant molecules during emulsification, an anisotropic layer of surfactant is created. This "leaky" interface and similar droplet size for all emulsions prepared with this technique would lead to a comparable release of salt over the storage period. Finally, for the rotating membrane, mildness of the emulsification process (*i.e.* no significant post-formation droplet processing) ensures that the densely packed layer of surfactant is not further disturbed during semi-batch emulsification, and thus the rate of salt release is slower than for emulsions made with the high-shear mixer and the cross-flow membrane. As mentioned earlier, differences in the salt release resulting from the process of emulsion preparation are surprising. This is because low molecular weight surfactants are highly dynamic and they would be expected to quickly return to their most favourable conformation(s) at the interface. This transition however, can be affected by low storage temperature (~4°C), but also the influence of other components of the complex duplex emulsion formulation. Firstly, two different types of surfactants are present at the O/W_2 (*i.e.* secondary) interface. It was discussed in Section 4.2.2, that PGPR exhibits viscoelastic properties and by forming "solid-like" domains at the interface restricts droplet coalescence and molecular transport. Secondly, sugars present in the external water phase (W_2) showed surface activity (Section 4.3.4), which may affect surfactant mobility at the interface. However, further work is required to investigate the suggested phenomenon.

5.6 Industrial application

From the perspective of industrial technology, SPG membrane emulsification has been reported (Gijsbertsen-Abrahamse *et al*., 2004) to have low dispersed phase flux. This is due to the fact that, even though SPG membranes have high porosity (50 – 60 %), there is only up to 2.6 % active pores (Vladisavljević & Schubert, 2002). However, maximising the dispersed phase throughput has to be considered carefully in order to avoid *jetting* from the pores.

In order to compare the dispersed phase throughputs obtained with the membranes used in this study with the existing data, the dispersed phase fluxes (J_d) through membranes were calculated according to:

$$J_d = Q_d / \rho_d A_m \qquad \text{Eq. 5-1}$$

where Q_d is the mass flow rate of the dispersed phase, ρ_d is the dispersed phase density and A_m is the membrane surface area. Figure 5-14 shows J_d obtained for cross-flow membranes with pore size of 3.9 μm (Figure 5-14a), 6.1 μm (Figure 5-14b), 10 μm (Figure 5-14c) and the rotating membrane with 2.8 μm pore size (Figure 5-14d).

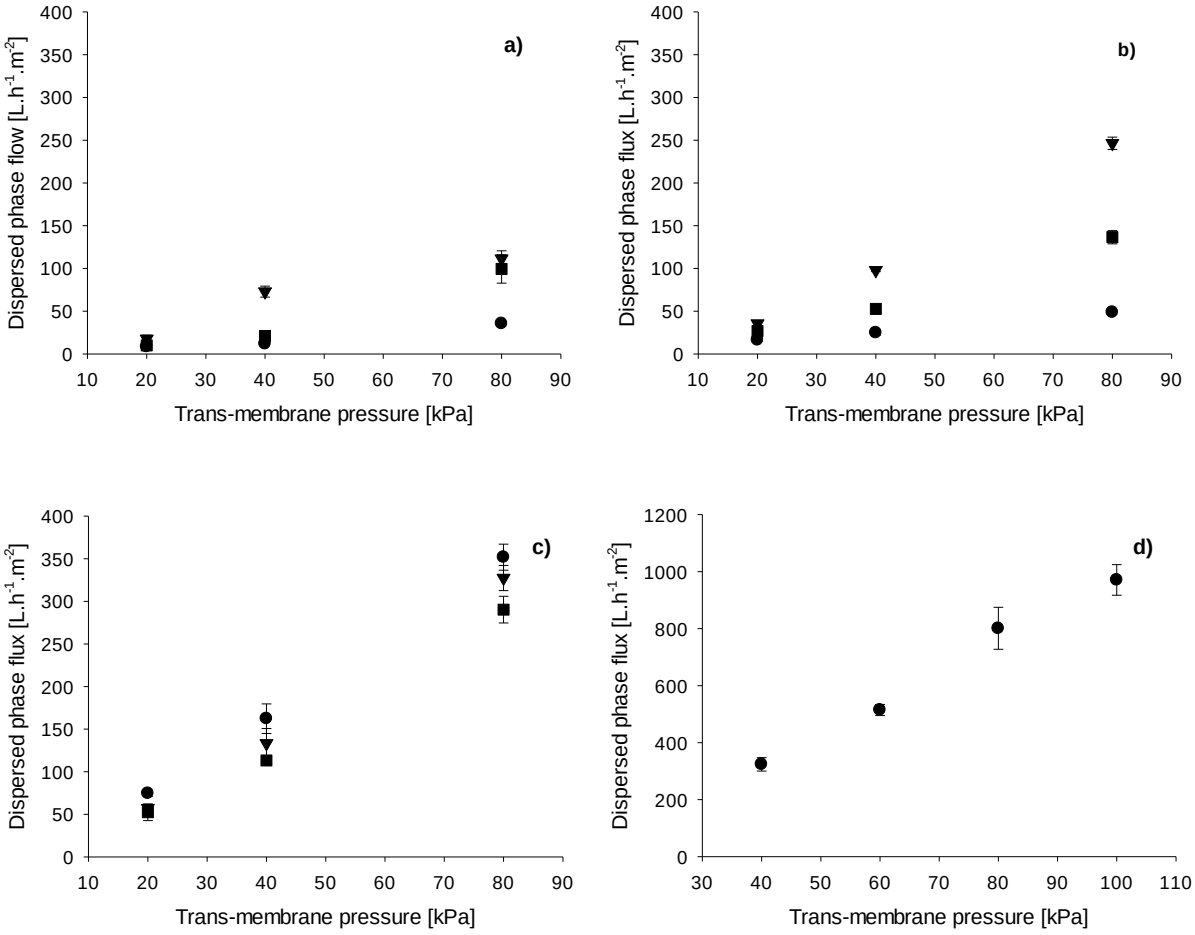

Figure 5-14 Dispersed phase flux in cross-flow membranes with pore diameters of: (a) 3.9 µm (b) 6.1 µm, (c) 10 µm and (d) 2.8 µm rotating membrane. Effect of TMP at various CFV: (▼) 0.11 m·s^{-1}, (■) 0.17 m·s^{-1} and (●) 0.22 m·s^{-1}.

It can be seen that in the cross-flow system, within the explored TMPs (20 – 80 kPa), the flux of the dispersed phase increases with membrane pore size. That is, the lowest flux was obtained for the 3.9 µm membrane (8 – 111 L·m^{-2}·h^{-1}), followed by the 6.1 µm membrane (16 – 246 L·m^{-2}·h^{-1}), with the highest flux achieved for the 10 µm membrane (52 – 352 L·m^{-2}·h^{-1}). This increase in the dispersed phase flow with the diameter of membrane pores is expected due to the Darcy's law correlation. Theoretically, J_d is expected to be comparable for a fixed TMP regardless the CFV. The observed variation in J_d between different CFVs and one TMP could be consequence of membrane fouling (as shown in Section 5.4.1.2).

Several studies have attempted to correlate membrane characteristics and processing parameters with the dispersed phase flux (Katoh *et al.*, 1996; Kukizaki & Goto, 2007; Scherze et al., 1999). Similarly to the work of Katoh *et al*. (1996), the formulation presented in this work contains oil soluble emulsifier (PGPR) in the dispersed phase (*i.e.* W_1/O emulsion), and water soluble emulsifier (Tween 20) in the continuous phase. PGPR's presence in the disperse phase could facilitate membrane wetting by the W_1/O emulsion and thus reduce the hydrodynamic resistance of the inherently hydrophilic SPG membrane. Membranes used in this work have larger pore diameters than those referenced in the aforementioned research review. This explains the higher fluxes achieved (Figure 5-14).

Now considering the rotating SPG membrane, Figure 5-14d shows that the dispersed phase flux increases linearly with the applied TMP. At 100 kPa TMP the J_d was found to be ~970 $L \cdot m^{-2} \cdot h^{-1}$. Similarly, high dispersed phase fluxes of 187 – 3190 $L \cdot m^{-2} \cdot h^{-1}$ were obtained by Dragosavac *et al*. (2008) on a Nickel membrane (d_p = 19 μm and d_p = 40 μm) in the stirred cell emulsification set-up. Even though the rotating membrane used has a smaller pore size (2.8 μm) than the cross-flow systems (3.9 μm, 6.1 μm and 10 μm), fluxes of the dispersed phase were three times bigger than the highest throughput for the 10 μm membrane (352 $L \cdot m^{-2} \cdot h^{-1}$). This is most probably as a result of: (i) static fluid pressure resulting from the design of the rotating membrane apparatus (Figure 3-1) and (ii) centrifugal force inherent to the method.

The output capacity of a typical industrial homogeniser varies between 100 and 20,000 $L \cdot h^{-1}$ and the production of 1000 L of O/W emulsion containing 10 % of oil will typically take an hour (Joscelyne & Tragardh, 2000). With 1 m^2 of SPG membrane surface, such a production rate can be obtained (depending on the required droplet size) by both cross-flow (Figure

5-14a-c) and the rotating membrane (Figure 5-14d). The scale-up has been claimed to be easy, involving multiplication of many small processes (*i.e.* adding more membranes to a device) (Charcosset, 2009; Vladisavljević & Williams, 2005). Additionally, for the commercial production the cost, lifespan of membranes and the membrane apparatus have to be considered, as well as the membrane properties. The lifespan of the membrane will be determined by its resistance to fouling and the cleaning agents used. All employed SPG membranes fouled after certain time of operation, in which case the whole apparatus had to be dismantled and the cleaning process was performed as described in Section 3.2.3.4. In the case of more severe fouling, the membranes were heat-treated. This was impossible to perform for the rotating membrane due to its specific design (see Section 3.2.3.3).

5.7 Chapter conclusions

The droplet size of emulsions produced with both membrane techniques decreases with the shear force generated by either CFV or RV. Droplet size increases with the applied TMP due to: (i) increase in the dispersed phase flux, (ii) transition from a *dripping* to a *jetting* mechanism of droplet formation, (iii) increased percentage of active pores, and (iv) slower rate of interfacial tension decrease. Similar minimum droplet size could be obtained by all three emulsifying techniques, it is suggested that at the highest shear forces generated in each emulsification technique, the droplet size is primarily determined by the rate of the interfacial tension decrease.

Duplex emulsions made with the rotating membrane released least salt during storage (7.9 ± 1.1 % loss of salt), followed by high-shear emulsification (12.6 ± 0.9 %) and the cross-flow membrane (7.8 – 19.9 %). This was due to a combined effect of: (i) emulsion droplet size, thus the interfacial area available for molecular transport, and (ii) the effect of shear

forces applied in each emulsification process and thus different interfacial properties of adsorbed surfactants.

SPG rotating membrane emulsification is a promising technique in the secondary emulsification step in duplex emulsions manufacture. As a low shear process it offers higher salt encapsulation in the internal water phase of duplex emulsions than both the cross-flow membrane and the high-shear techniques. This is due to: (i) homogenous and isotropic layer of surfactant deposited on the interfaces and (ii) absence of repeated droplet breakup after their formation at the membrane surface. Moreover, the emulsion production rate is higher than for the cross-flow system.

6 Simple O/W emulsions produced using SPG rotating membranes.

6.1 Introduction

It was highlighted in the previous Chapter, that the rotating membrane technique is a promising tool for the secondary emulsification step in the manufacture of duplex $W_1/O/W_2$ emulsions. However, the area of rotating membrane emulsification remains scarcely explored, and more specifically SPG (Shirasu Porous Glass) membranes have not previously been used as rotating devices for emulsification. Therefore, there is a need to study how processing parameters and formulation can influence the properties of both O/W and W/O emulsions manufactured using the SPG rotating membranes. This would help assessing the effectiveness of the technique in the area of duplex emulsion formation by considering it as a tool for both primary and secondary emulsification step. Due to the hydrophilic nature of the native SPG membranes used in this study, the work in this Chapter focuses on O/W emulsions alone.

The aim of this Chapter, was to understand the effect of rotating membrane emulsification parameters, SPG membrane properties and emulsion formulation on the properties of simple O/W emulsions. This was assessed by measuring emulsions droplet size and size distribution span. Parameters investigated in this Chapter can be summarised as:

(i) Membrane pore size: 2.8 μm and 6.1 μm mean pore diameter membranes were compared,

(ii) Trans-membrane pressure (TMP) and rotational velocity (RV): applied at ranges of 10 – 100 kPa and 300 – 1500 rpm, respectively,

(iii) Dispersed phase volume: concentration of the oil phase was altered between 2 % and 60 %,

(iv) Viscosity of the continuous phase: from 0 % to 0.5 % of Xanthan Gum (XG) was used to modify the viscosity of the aqueous phase,

(v) Concentration of a low molecular weight surfactant: from 0.0005 % to 1 % of Tween 20 was used to stabilise emulsion droplets,

(vi) Whey Protein Isolate (WPI) was used as an emulsifier: 1 % WPI solution was used at the range of applied TMPs and RVs,

(vii) Emulsifier adsorption kinetics: comparison of WPI and Tween 20 as emulsion stabilisers.

6.2 Membrane pore size

To study the effect of membrane pore size on the emulsion droplet size and size distribution, membranes with 2.8 μm and 6.1 μm average pore diameter were used. For both membranes the TMP and RV were varied in order to understand their effects on the properties of the produced emulsions. 2 % oil-in- 98 % water emulsions with 1 % Tween 20 were made as described in Section 3.2.2.1. The RV was varied between 300 and 1500 rpm and the TMP between 25 and 100 kPa for the 2.8 μm membrane, and between 10 and 40 kPa for the 6.1 μm membrane (according to a method described in Section 3.2.2.2). Different nominal range of TMP for both membranes is applied because, according to the capillary pressure equation (Eq. 2-4), smaller pressure is required to force a liquid through larger pores.

6.2.1 Droplet size

In this section, the effect of RV and TMP on the emulsion droplet size was investigated. Figure 6-1 gives the evolution of the droplet diameter $D_{3,2}$ as a function of TMP and RV for emulsions made with the 2.8 μm membrane. It appears from the Figure, that the effect of TMP on the droplet size depends on the applied RV. At low RV, the average emulsion droplet size increased with increasing TMP. For example, at 300 rpm, the diameter $D_{3,2}$ changed from 8.2 ± 1.1 μm at 25 kPa to 30.4 ± 5.5 μm at 100 kPa TMP. According to Darcy's law (Section 2.3.2.3.2), the dispersed phase flux through the membrane pores is proportional to the pressure applied across the membrane. Therefore, the water-oil interface formation rate will increase with the TMP. A finite time for surfactant adsorption means that the droplet will stay attached to the pore until the interfacial tension is low enough so that the applied hydrodynamic drag can detach it. The longer the droplet stays attached to the membrane, the more oil is pumped into it, increasing its volume before detachment. This explains why increasing TMP leads to formation of bigger droplets.

At high RV, the effect of TMP on the droplet size becomes less significant. For example at the RV of 1500 rpm, the droplet diameter increases from 7 ± 0.3 μm to 16 ± 3.4 μm. This phenomenon is similar to the one observed in cross-flow membrane emulsification (see Section 5.3.1.2), where the biggest change in droplet size occurred at low membrane shear stresses (CFVs). This suggests that at high RV, shear and centrifugal forces are high enough to quickly overcome the interfacial tension even at higher interface formation rates (high TMPs). As a result, droplets stay attached to the membrane pores for shorter time and thus less dispersed phase is forced into the droplet before it detaches.

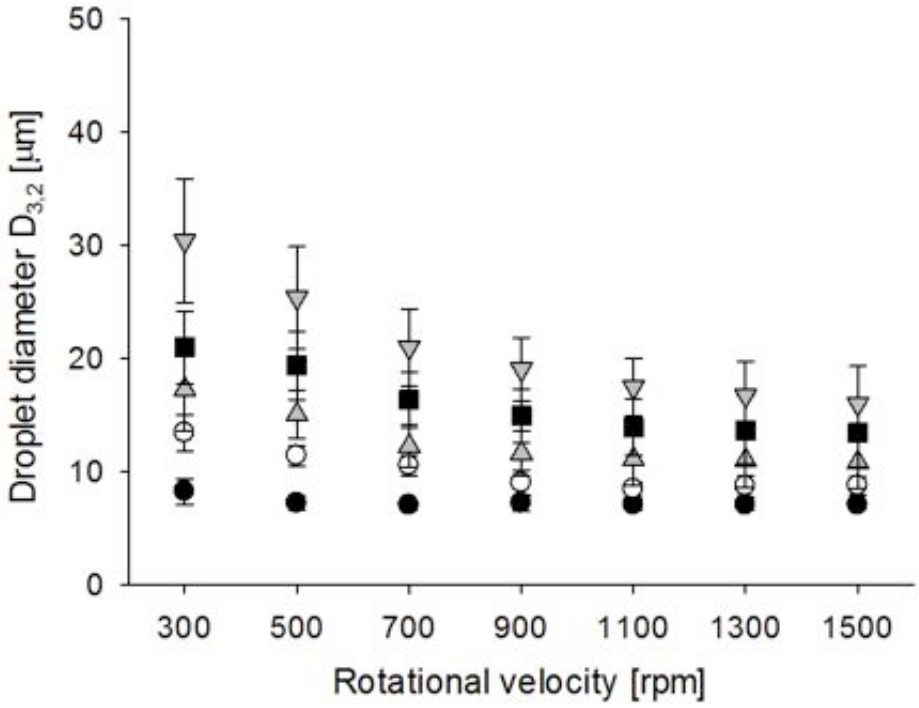

Figure 6-1 Droplet size of O/W (2:98) emulsions with 1 % Tween 20, made with the 2.8 µm rotating membrane. Effect of RV at various TMPs: (●) 25 kPa, (○) 40 kPa, (▲) 60 kPa, (■) 80 kPa and (▼) 100 kPa.

Rotations of the membrane generate the drag force, which is considered to be the main detaching force in membrane emulsification (Timgren *et al*., 2009). Therefore, higher values of shear stress at the membrane surface are assumed to lead to smaller average droplets being produced (Vladisavljević & Williams, 2006). As shown in Table 3-1 (p.50), increasing RV results in higher shear stress at the membrane surface (*e.g.* from 0.05 Pa at 300 rpm to 0.27 Pa at 1500 rpm). Figure 6-1 shows however, that the effect of RV on the emulsion droplet size varies with the applied TMP. At low TMP (*e.g*. 25 kPa), the droplet size does not change with increasing RV (8.2 ± 1.1 µm at 300 rpm and 7 ± 0.3 µm at 1500 rpm; 25 kPa). This is due to the fact, that at low TMPs the rate of interface formation of the inflating droplet is slow, and most likely slower than the rate at which surfactants adsorb at the expanding oil-water interface. Relatively high concentration (1 %) of low molecular weight Tween 20 (~1227

$g \cdot mol^{-1}$) ensures rapid molecules adsorption onto the newly formed interface and quick reduction of the interfacial tension. Then, even the smallest applied drag force (at *e.g.* 300 rpm) detaches the droplet at its minimum, for this system, volume.

At high TMP (*i.e.* above 60 kPa) the droplet size decreases with the RV. For example, at 100 kPa, the diameter $D_{3,2}$ decreases from 30 ± 5.5 μm at 300 rpm to 16 ± 3.4 μm at 1500 rpm. Fast interface formation at high TMP allows the droplets to grow in size before the interfacial tension decreases to the point, that the applied drag force can shear them off the membrane surface. This results in general increase in the droplet size. Therefore, when the RV increases, the resultant drag force is much higher than for small droplets, which manifest itself in their larger susceptibility to the effect of RV; *i.e.* droplet size significantly reduces with increasing RV. This happens until the RV is 1000 rpm, when a further increase in the RV does not affect the droplet size. At this point onwards, even though the drag force is large, the droplets detach only after reaching a volume dictated by the rate of interfacial tension decrease at a given interface expansion rate.

Similar observations were made for the 6.1 μm membrane. The range of the obtained droplet sizes varies between 21 ± 2.5 and 61.2 ± 0.7 μm (Figure 6-2). It can be seen that the droplet size of emulsions made at 10 kPa and 20 kPa does not change significantly with RV. However, at higher applied TMP of 30 kPa and 40 kPa the droplet size decreases with RV. For example, at 40 kPa, the diameter $D_{3,2}$ decreases from 61.2 ± 0.7 μm at 300 rpm to 41.4 ± 2.8 μm at 1500 rpm. It is also clear that, for a given RV, the droplet size increases with the TMP. This is similar in trend to the observations made for the 2.8 μm membrane.

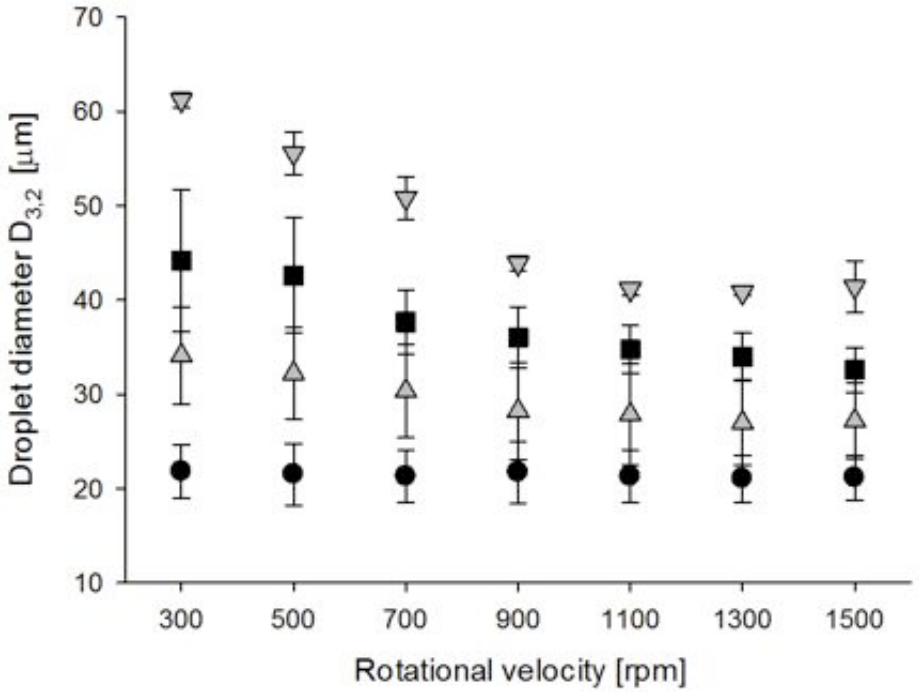

Figure 6-2 Droplet size of O/W (2:98) emulsions with 1 % Tween 20, made with the 6.1 µm rotating membrane. Effect of RV at various TMPs: (●) 10 kPa, (▲) 20 kPa, (■) 30 kPa and (▼) 40 kPa.

6.2.2 Droplet size distribution

In this section the effects of RV and TMP on the emulsion droplet size distribution were investigated. The span of each size distribution was plotted as a function of RV for various TMPs. Figure 6-3 shows changes in span with RV and TMP, for O/W emulsions prepared using the 2.8 µm rotating membrane. It can be seen from the Figure, that for a given RV, span increases with TMP in the following order: 25 < 60 < 80 < 100 < 40 kPa. The Figure also shows, that the span remains independent of RV (within the experimental error) for the TMPs of 25, 60, 80 and 100 kPa. The exception is the TMP of 40 kPa, where the span halves with the increase in RV (from 3.2 ± 0.6 at 300 rpm to 1.7 ± 0.2 at 1500 rpm). The effects of TMP and RV are explained by considering the mechanism of droplet formation schematically shown in Figure 6-4.

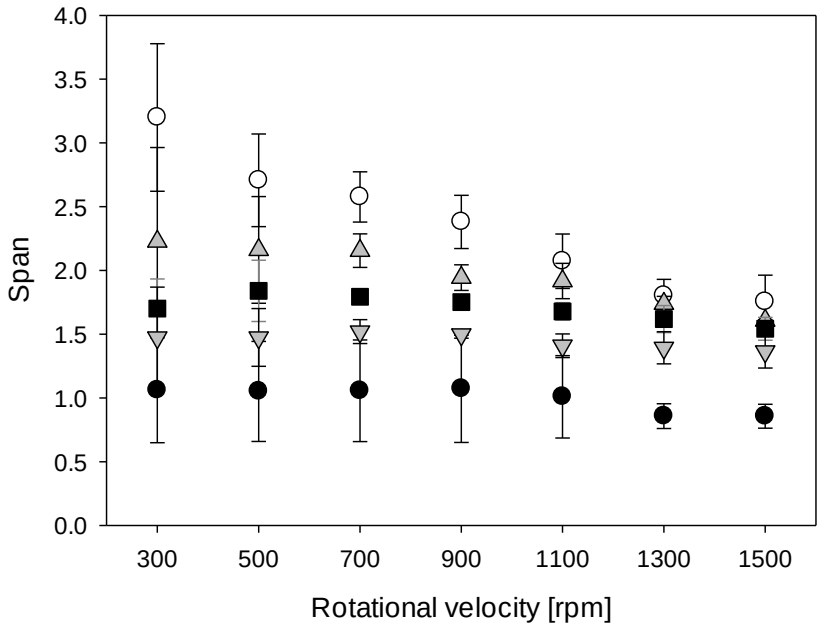

Figure 6-3 Span of O/W (2:98) emulsions with 1 % Tween 20, made with the 2.8 µm rotating membrane. Effect of RV at various TMPs: (●) 25 kPa, (○) 40 kPa, (▲) 60 kPa, (■) 80 kPa and (▼) 100 kPa.

At 25 kPa TMP span is the lowest (1.1 ± 0.4). Even though there is no evidence here, it has been reported (Abrahamse *et al.*, 2002), that more pores become activated as the TMP increases. It is therefore probable, that at low TMP only big pores are active as, according to the capillary pressure equation (Eq. 2-4), larger pores (*i.e.* d_{p1} in Figure 6-4) require lower pressure to become wetted by the dispersed phase. This situation is shown in Figure 6-4A. Low interface formation rate and abundance of surfactant ensures, that even the smallest applied shear force detaches the droplet at a volume dictated by the relatively low interfacial tension. This results in small (Figure 6-1) and narrowly distributed droplets. Therefore, a subsequent increase in the drag force (with increasing RV) has no effect on span (1.1 ± 0.4 at 300 rpm and 0.8 ± 0.1 at 1500 rpm) or the droplet size.

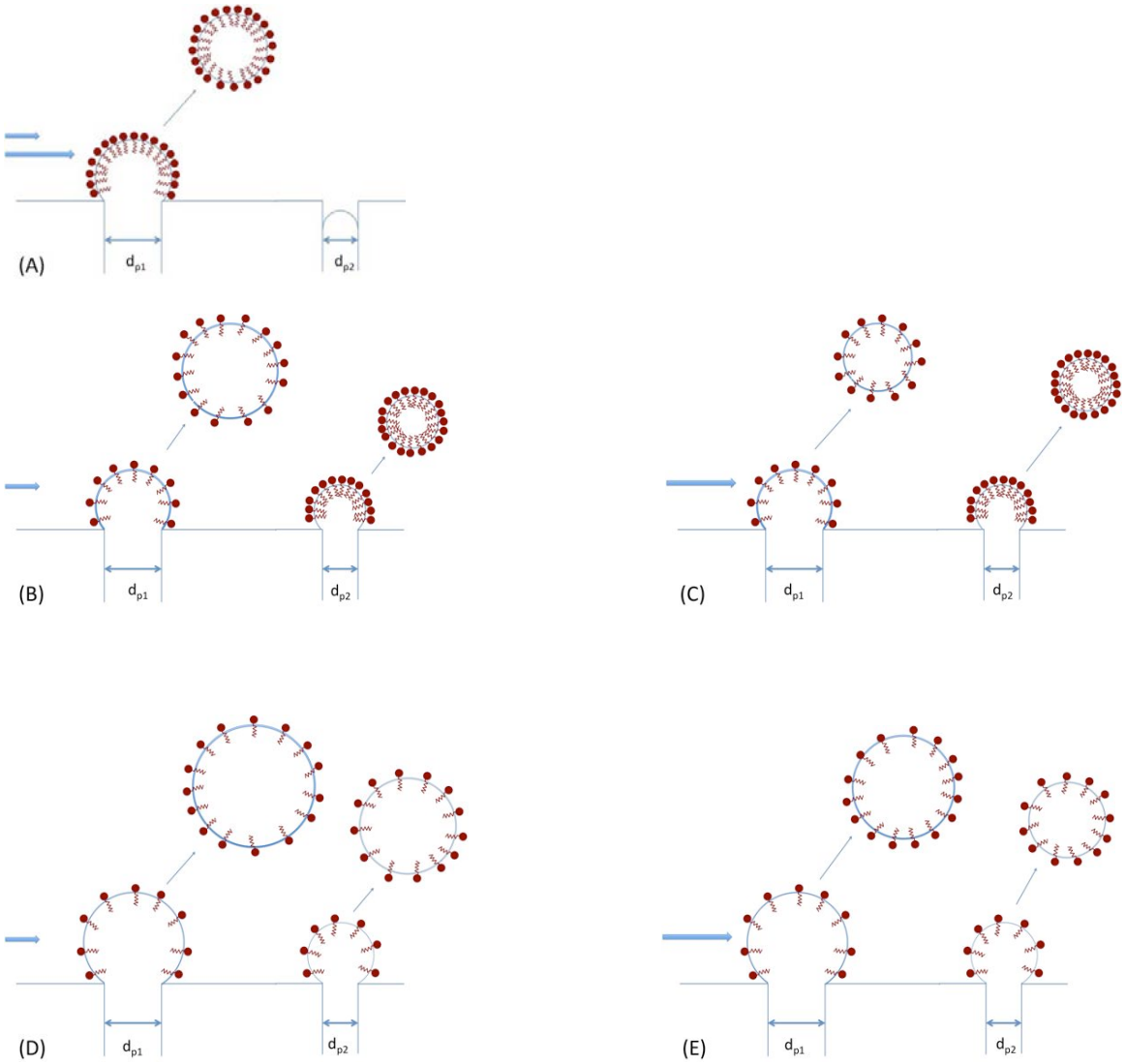

Figure 6-4 Schematic diagram of mechanism of droplet formation in the rotating membrane technique. (A) at low TMP, small droplets with low span are produced for low and high RV, (B) at intermediate TMP and low RV, polydisperse droplet are formed, (C) at intermediate TMP increase in RV reduces both droplet size and span, (D) at high TMP and low RV large droplets with small span are formed, and (E) at high TMP increase in RV decreses droplet size but span remains unchanged. d_p is a pore diameter and $d_{p1} > d_{p2}$.

When the flux of the dispersed phase increases at 40 kPa TMP, more pores become activated (Figure 6-4B). The flow of the dispersed phase through the newly activated pores (such as

d_{p2}) will be slower (due to higher pressure drop across the pore as compared to the pores already activated at 25 kPa TMP). This will lead to uneven rate of interface formation across the range of active pores, leading to a polydisperse emulsion (span of 1.7 – 3.2). Increasing RV causes larger increase in the drag force acting on bigger droplets (*i.e.* produced at d_{p1}) than smaller droplet (*i.e.* produced at d_{p2}), leading to a quicker detachment of the former. As a result, initial (at low RV) large difference in the droplet sizes produced from d_{p1} and d_{p2} pores diminishes and so their distribution becomes narrower.

When the TMP is further increased (to 60, 80 and 100 kPa), the droplet interface formation rate is high for all the active pores (Figure 6-4D). Due to a high interfacial tension at the point of droplet detachment, the average droplet diameter is relatively large (Figure 6-1). Reduced span is a result of the fact that the drag force acting on the droplet increases with their size, therefore larger drag acting on larger droplets (produced at d_{p1}) ensures their faster detachment at the size similar to the droplets produced from smaller pores (d_{p1}). When the RV increases, the drag force causes faster detachment of all droplets, leading to the reduction in the average size (Figure 6-1), but their relative size (*e.g.* droplet produced from d_{p1}/ droplet produced prom d_{p2}) remains similar to that at low RV.

The same mechanism of droplet formation is valid for the 6.1 μm membrane; the effects of RV and TMP on the width of droplet size distribution are given in Figure 6-5. It can be seen that span is the lowest (0.7 ± 0.01) for the lowest TMP (10 kPa), and is not influenced by the changes in RV. Emulsions produced at the intermediate TMP (*i.e.* 20 kPa) have the widest size distribution at the lower end of the RV range (3.3 ± 1.1 at 300 rpm), followed by emulsions made at 30 kPa (~2.6 at 300 rpm). The initial span values for these TMPs decrease

when RV is increased (to 0.8 ± 0.1 and 1 ± 0.3 at 1500 rpm respectively). For 40 kPa TMP span somewhat decreases with RV; from 1.7 ± 0.2 at 300 rpm to 1.1 ± 0.1 at 1500 rpm. These trends are in line with the observations made for the 2.8 μm membrane.

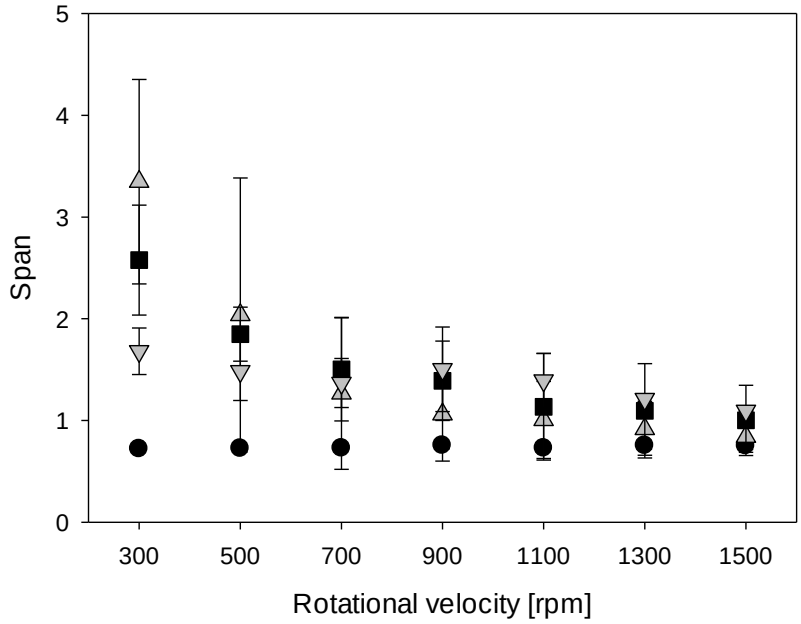

Figure 6-5 Span of O/W (2:98) emulsions with 1 % Tween 20, made with the 6.1 μm rotating membrane. Effect of RV at various TMPs: (●) 10 kPa, (▲) 20 kPa, (■) 30 kPa and (▼) 40 kPa.

6.2.3 Comparison of the 2.8 μm and 6.1 μm membrane

In order to understand the effect of the rotating SPG membrane average pore diameter on the emulsion properties, droplet size and size distribution spans are compared for emulsions produced with the 2.8 μm and the 6.1 μm membrane.

Table 6-1 summarises the data obtained with both membranes. Smaller droplets could be produced with the 2.8 μm membrane compared to the 6.1 μm membrane, however the droplet size distribution was similar for both systems. Larger range of the d_d/d_p ratios for the 2.8 μm

membrane suggests that for the investigated conditions (RVs and TMPs), more significant modification in the droplet size was possible when the 2.8 μm membrane was used. This is also shown in Figure 6-6, where the extent of the effects that RV and TMP have on the droplet size for both membrane is plotted. Figure 6-6 (right) gives a % decrease in the emulsion droplet size with increasing RV, calculated for each TMP and membrane pore size. Figure 6-6 (left) gives % decrease in droplet size with decreasing TMP, calculated for each RV and both membranes. It can be seen that:

- The maximum effect of the RV increase (from 300 to 1500 rpm) on the droplet size was observed at the highest TMP: (i) 100 kPa for the 2.8 μm membrane (47 % decrease in the droplet size) and, (ii) 40 kPa for the 6.1 μm membrane (32 % decrease in the droplet size).
- The maximum effect of the TMP decrease on the droplet size was observed at 300 rpm: (i) for the 2.8 μm membrane; a 73 % decrease in droplet size with TMP decrease (from 100 to 25 kPa) and, (ii) for the 6.1 μm membrane, a 64 % decrease in droplet size with TMP decrease (from 40 to 10 kPa).

Table 6-1 Comparison between 2.8 μm and 6.1 μm membranes. (d_d) – droplet diameter, (d_p) – pore diameter.

Membrane [μm]	**$D_{3,2}$ diameter** [μm]		**Span**		d_d/d_p
	min.	*max.*	*min.*	*max.*	
2.8	7 ± 0.3	30.4 ± 5.5	0.8 ± 0.1	3.2 ± 0.6	2.5 – 11
6.1	21 ± 2.5	61 ± 0.7	0.7 ± 0.02	3.3 ± 1	3.5 – 10

Larger reduction in droplet size with modification of TMP rather than RV suggests, that surfactant adsorption is a crucial factor in controlling the droplet size in rotating membrane emulsification.

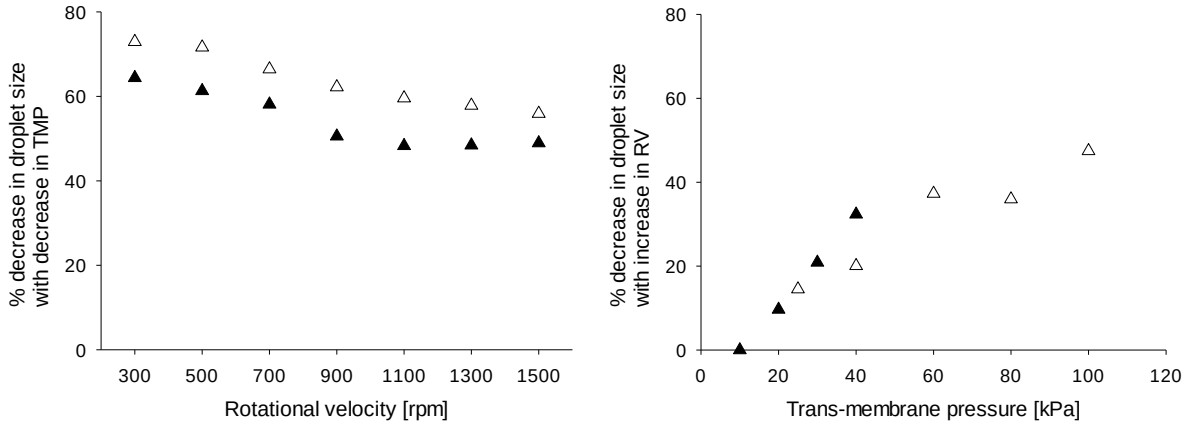

Figure 6-6 Potential of TMP and RV to modify emulsion droplet size. % decrease in the droplet size with: (Left) decrease in the TMP (from 100 to 25 kPa for the 2.8 µm membrane and from 40 to 10 kPa for the 6.1 µm membrane); (Right) increase in RV (from 300 to 1500 rpm) for: (△) 2.8 µm membrane and (▲) 6.1 µm membrane.

Due to a different hydrodynamic resistance of both membranes, 40 kPa is the only TMP crossing-over the two membrane systems. When the droplet size data versus RV for the 40 kPa TMP is plotted for both membranes (Figure 6-7), it can be seen that at 300 rpm, the average emulsion droplets produced with the 6.1 µm membrane (61 ± 0.7µm) are about six times bigger than the droplets made with the 2.8 µm membrane (13.4 ± 1.6 µm). This is a consequence of faster wetting of larger pores than small ones (*vide* capillary pressure Eq. 2-4) and thus faster flow of the dispersed phase and the interface formation. Subsequently, high interfacial tension retains droplets longer at the pore opening and their size increases. It is also shown that for the 2.8 µm membrane, the droplet size decreases only marginally with increasing the RV (to 8.7 ± 0.8 µm at 1500 rpm). The droplet size of emulsions prepared with the 6.1 µm membrane was reduced significantly as the RV was increased (to 41.4 ± 2.8 µm at 1500 rpm). This is because, as explained in Section 6.2.1, the TMP of 40 kPa causes

relatively slow interface formation at the 2.8 μm pores. The resultant low interfacial tension allows droplet detachment even at very low shear rates of the membrane. However, this does not happen for relatively high droplet inflation rates at the 6.1 μm pores. Instead, the droplet can detach from the membrane only when the drag force exceeds the interfacial tension; with increasing RV the drag force acting on droplets increases faster for bigger droplets, and so the effect of RV is more pronounced for the 6.1 μm membrane.

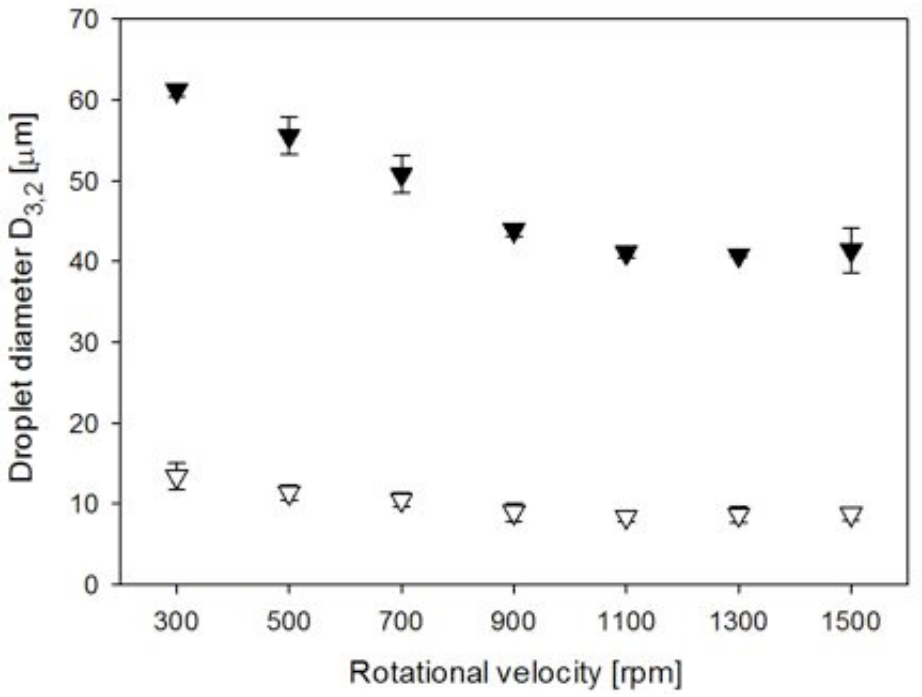

Figure 6-7 Droplet size of O/W (2:98) emulsions with 1 % Tween 20, made at 40 kPa TMP. Effect of RV and membrane pore size: (▽) 2.8 μm and (▼) 6.1 μm.

Now, the question is whether the similar trends exist when the effective TMP for both membranes is compared. To do that, the TMP was normalised over the CTMP* for both systems. Figure 6-8 shows two cases where the ratio of TMP/CTMP was close for both membranes: *i.e.* ~1.3 in Figure 6-8 (left) and ~2.9 in Figure 6-8 (right). It is evident that, regardless of the difference in the membrane pore sizes, when the similar effective TMP was

* Critical trans-membrane pressure (CTMP) - experimentally established minimum pressure at which the dispersed phase could be pushed through a given membrane.

applied, the particle size of the emulsions does not significantly change with the increasing RV. This again means, that the droplets break off the membrane only after the shear force overcomes the interfacial tension. This highlights the significance of the dynamics of interfacial tension decrease as an important factor for controlling droplet size in membrane emulsification. As explained in Section 6.2.1, at slow interface formation rates (Figure 6-8 left), low interfacial tension allows the droplets to be detached at their minimum volume even at low shear rates (*i.e*. 300 rpm). It is evident from Figure 6-8 (left), that such a volume, for similar hydrodynamic conditions (RV and TMP/ CTMP ratio) essentially depends on the membrane pore size. As expected, larger droplets could be obtained at faster interface formation rates (from ~11 to ~31 µm, Figure 6-8 right) than at slow interface formation rate (from ~7 to ~21 µm, Figure 6-8 left). The issue of data reproducibility is discussed later in this Chapter (Section 6.6).

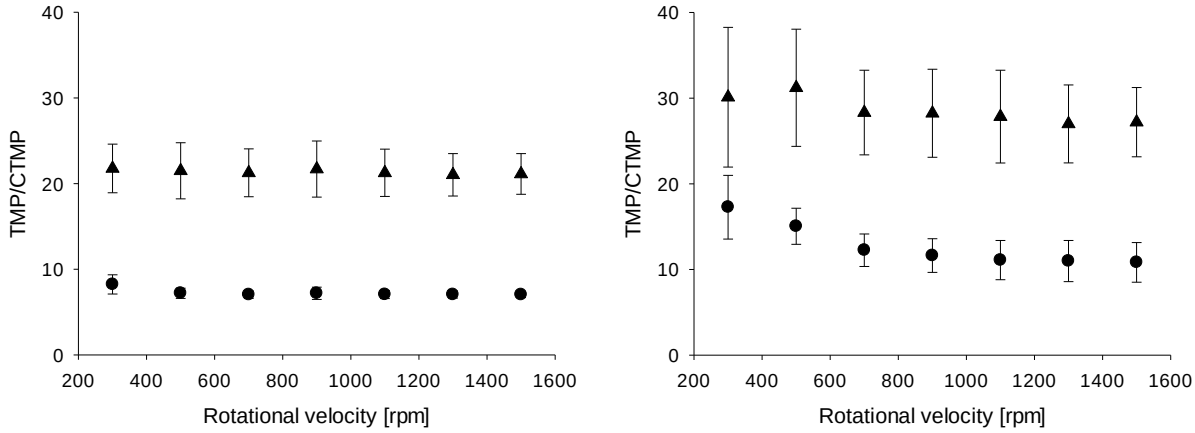

Figure 6-8 Droplet size as a function of RV and TMP/CTMP for the (●) 2.8 µm and (▲) 6.1 µm membrane: (Left) slow interface formation where TMP/CTMP ≅ 1.3, and (Right) fast interface formation where TMP/CTMP ≅ 2.9.

6.3 Dispersed phase volume

In this section the effect of the dispersed phase volume on the emulsion droplet size and droplet size distribution have been studied. The emulsions were produced using the 2.8 µm

pore size membrane (as described in Section 3.2.2.2), at 40 kPa TMP and 1500 rpm RV. Based on results of Section 6.2, a moderate value of TMP was chosen to provide a relatively slow increase in the interfacial area, but also sufficiently high throughput of the dispersed phase. High RV was applied to ensure high drag and centrifugal forces. The concentration of Tween 20 was kept constant at 2 % with the respect to the oil phase. The dispersed phase volume was adjusted to 2, 10, 20, 30, 40, 50 and 60 %.

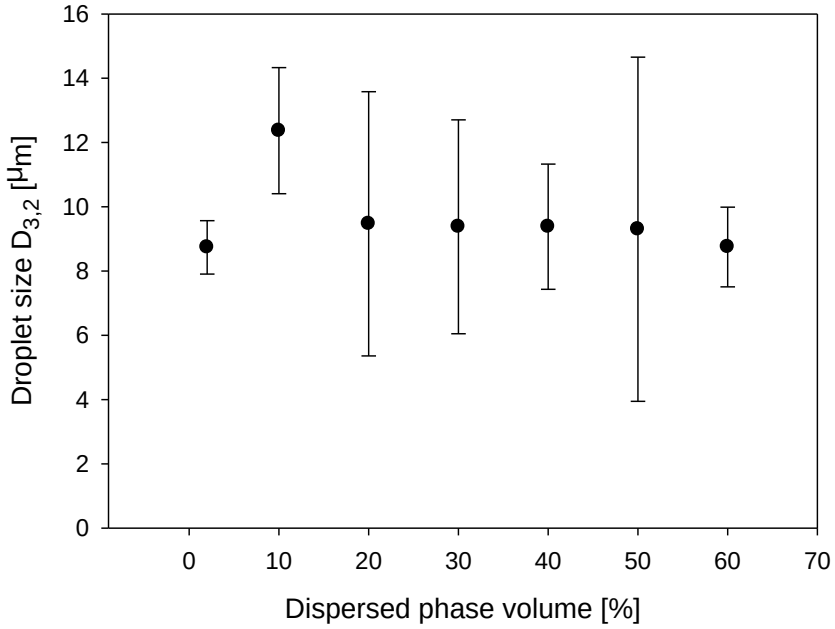

Figure 6-9 Droplet size as a function of dispersed phase volume. O/W emulsions stabilised with 2 % Tween 20 (with the respect to the oil phase) were made using the 2.8 μm rotating membrane at 40 kPa TMP and 1500 rpm RV.

The effect of the oil volume on the emulsion droplet size is given in Figure 6-9. It can be seen, that the average droplet size is similar (9.5 ± 1.3 μm) for all produced emulsions, regardless of the dispersed phase volume. It could be expected, that the viscosity of the continuous phase would change with the dispersed phase volume, which in turn would affect the drag force and the size of the produced droplets. In order to test this, the viscosities of the emulsions were measured (by a method described in Section 3.2.4.4) at the shear rate of 328 s^{-}

[1], which was chosen in order to relate it to the shear rate induced by membrane rotation at the applied RV of 1500 rpm (Table 3-1, p.50). It should be noted that, due to the fact that emulsification is a semi-batch process, the viscosity of the emulsion changes as the dispersed phase increases during emulsification.

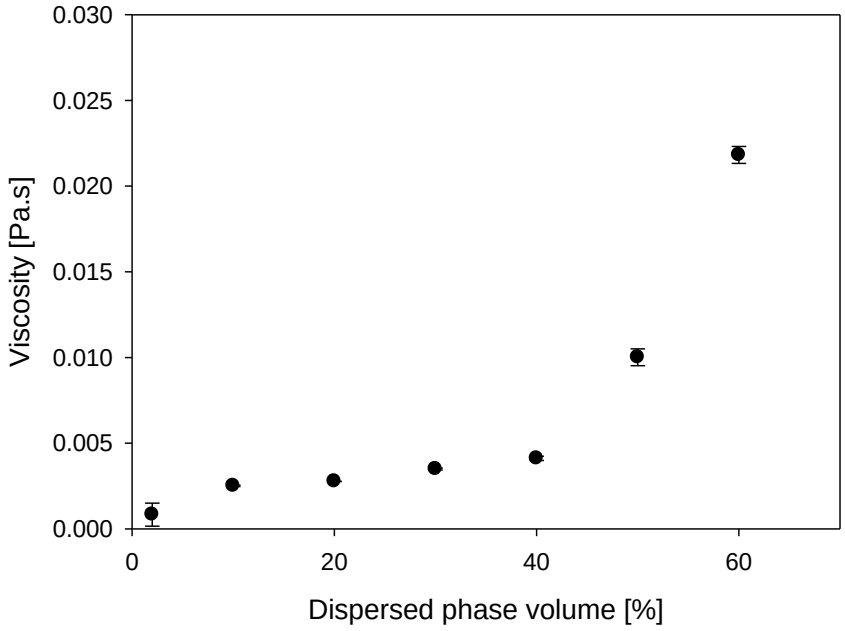

Figure 6-10 Viscosity of O/W emulsions as a function of the dispersed phase volume; values taken at a shear rate of 328 s^{-1} and 25 °C. Tween 20 concentration was kept at 2 % with the respect to the oil phase.

As expected, the viscosity of an emulsion increases with the dispersed phase volume as the increasing number of droplets disturbs local fluid velocity gradients increasing its resistance to flow (McClements, 2005). This is shown in Figure 6-10, where changes in the viscosity of an emulsion with the percentage of the dispersed phase are given. Up to 40 % of the oil phase, emulsion viscosity does not change significantly. When the concentration of droplets further increases (to 50 % and 60 % phase volume), the viscosity rises more sharply (up to 22 mPa·s at 60 %) as closely packed droplets start interacting with each other. Despite a relatively large increase in the disperse phase volume (up to 60 %), no phase inversion (from O/W to W/O

emulsion) was observed (*i.e.* all emulsions had measurable conductivity). This may be associated with limited mixing in the vessel and high concentration of the high HLB surfactant (Tween 20), which, due to steric requirements, tends to bend the interface in the way that favours the formation of an O/W emulsion.

Both Figure 6-9 and Figure 6-10 suggest that, under the applied emulsification parameters the viscosity of the emulsion has no (or very little) effect on the droplet size. This happens despite the increase in the drag force[*] caused by the increase in viscosity when the percentage of oil changed from 2 to 60. Similar results were presented by Schadler & Windhab (2006), who found that there was no change in droplet size and distribution when the dispersed phase volume was increased from 5 % to 30 % at the applied RV of 8000 rpm. One explanation for no difference in the droplet size with increasing viscosity may be that the viscosity affects the kinetics of surfactant adsorption. An increase in the viscosity of the continuous phase will decrease the diffusion coefficient (Eq. 2-2) of surfactant molecules/micelles. The aspect of viscosity-related-changes in the surfactant adsorption process at different hydrodynamic conditions is further investigated in Section 6.4.

Evolution of droplet size distribution span with the dispersed phase volume are given in Figure 6-11. It shows that there is no significant effect of the concentration of the dispersed phase on the polydispersity of the emulsion. The average span for all emulsions is ~1.6 and falls within the range of spans obtained with the 2.8 μm membrane (between ~0.85 and ~3.5) and the 6.1 μm membrane (between ~0.7 and ~3.4) for diluted emulsions (2 % oil in 98 % water emulsions).

[*] The drag force could not be calculated due to complex (*i.e.* non-laminar) flow conditions.

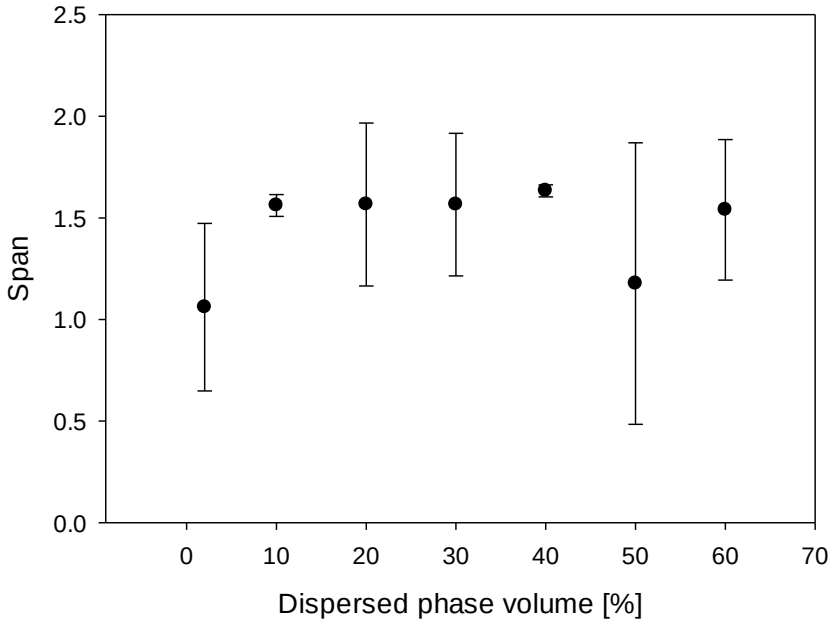

Figure 6-11 Effect of the dispersed phase volume on span of O/W emulsions with Tween 20, made using the 2.8 µm membrane at 40 kPa TMP and 1500 rpm RV.

6.4 Viscosity of the continuous phase

It was shown in the previous section, that increasing the viscosity of the emulsion (by increasing the dispersed phase volume) does not have a significant effect on either the droplet size or droplet size distribution of the produced O/W emulsions. In this section, the effect of the continuous phase viscosity, resulting from the presence of a thickener in the aqueous phase, on emulsion droplet size and droplet size distribution was investigated. Low dispersed phase volume (2 %) was chosen to limit the effect of semi-batch emulsification system, *i.e.* in-process viscosity increase. O/W emulsions were produced with the 2.8 µm hydrophilic SPG rotating membrane, at 25 kPa TMP and a range of RV from 300 rpm to 1500 rpm. Low TMP was maintained to ensure slow interface formation, resulting in a relatively low interfacial tension at the droplet detachment point, regardless of the RV as shown in Section 6.2.1. The continuous phase viscosity was modified by adding Xanthan Gum (XG). It was

assumed that anionic structure of XG and its very low solubility in oil ensures no adsorption onto the negatively charged SPG membrane or the oil/water interface.

Solutions of XG at various concentrations (0.0156 %, 0.0312 %, 0.0625 %, 0.125 %, 0.25 % and 0.5 %), each containing 1 % Tween 20, were prepared as described in Section 3.2.2.1. The viscosity of each solution was measured (as described in Section 3.2.4.4), by applying a range of shear rates from 0.16 s^{-1} to 790 s^{-1}, in order to cover the range of shear rates generated by the rotation of the membrane (Table 3-1, p.50). Results are given in Figure 6-12. The viscosity of the continuous phase with no XG (Newtonian fluid behaviour) was averaged to 0.9 mPa·s throughout the applied shear rates. Due to low dispersed phase volume (2 %), the emulsion viscosity is assumed to be the same as the viscosity of the continuous phase, *i.e.* the viscosity of the Xanthan Gum-Tween 20-water solution.

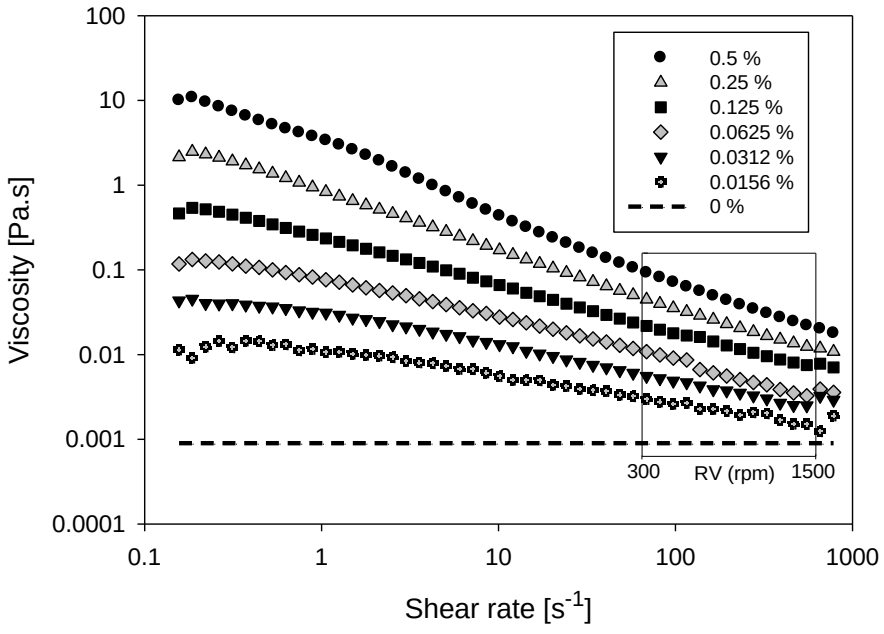

Figure 6-12 Viscosity curves of XG solutions at different concentrations (0 – 0.5 %), measured at shear rates corresponding to rotational velocity [rpm] of the membrane (*i.e.* the range highlighted in the frame) at 25°C.

Figure 6-13 demonstrates the evolution of emulsion droplet size as a function of: (i) various concentrations of XG in the continuous phase, and (ii) rotational velocity of the membrane. Firstly, Figure 6-13 shows that for a given RV: (i) droplet size increases with XG concentration in the continuous phase, and (ii) the most significant change in the droplet size happens at small rotational velocity. For example, increasing the XG concentration from 0 to 0.5 % leads to an increase in the droplet size from 8.2 ± 1.1 µm to 23.4 ± 4.3 µm at 300 rpm, while at 1500 rpm the droplet size only slightly increases from 7 ± 0.3 µm to 11.4 ± 2.7 µm. These changes in droplet size can also be related to the modification of the viscosity of the aqueous phase in the presence of XG. As can be seen, by increasing XG concentration from 0 % to 0.5 %, at low RV (300 rpm), *i.e.* at low shear rate (65 s^{-1}), the viscosity increases from 0.9 mPa.s to 92.5 mPa.s (0.5 % XG, Figure 6-12), while at high RV (1500 rpm), *i.e*. at high shear rate (325 s^{-1}), the viscosity increases from 0.9 mPa·s (no XG) to 30.7 mPs·s (0.5 % XG).

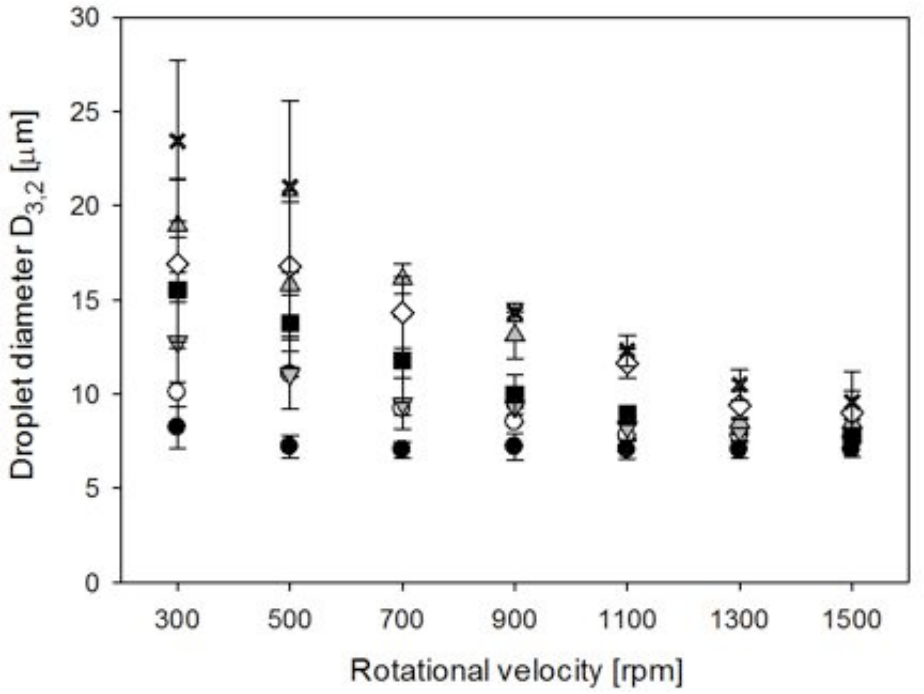

Figure 6-13 Droplet size of O/W (2:98) emulsions stabilised with 1 % Tween 20, made with the 2.8 µm rotating memrane at 25 kPa TMP. Effect of RV and XG concentration: (●) 0 %, (○) 0.0156 %, (▼) 0.0312 %, (■) 0.0625 %, (▲) 0.125 %, (◇) 0.25 % and (×) 0.5 %.

Secondly, Figure 6-13 shows that the effect of RV on the droplet size depends on the XG concentration. The percentage decrease in the droplet size resulting from increasing the RV (from 300 to 1500 rpm) was calculated for each concentration of XG, and shown in Table 6-2. It is evident, that up to 0.125 % XG, the more viscous the aqueous phase is the more significant is the decrease in droplet size with RV. Further increase in viscosity (up to 0.5 % XG) results in constant decrease in droplet size with RV.

Table 6-2: Percentage decrease of the droplet size over the range of rotational velocity (300 – 1500 rpm) as a function of XG concentration.

XG [%]	0	0.0156	0.0312	0.0625	0.125	0.25	0.5
Percentage decrease [%]	15	24	39	45	52	43	51

It appears from the above data analysis that increasing the continuous phase viscosity tends to yield bigger emulsion droplets. The question is then, how this change in viscosity impacts: (i) the drag force and, (ii) the interfacial tension force acting on the droplet during its detachment.

Due to the complexity of the flow in the rotating membrane system (*i.e.* formation of Taylor vortices, Schadler & Windhab, 2006), the hydrodynamic drag force could not be calculated. However, it can be expected that the drag force increases with the RV and the viscosity of the XG solutions. Nevertheless, due to shear-thinning properties of XG, for a given XG concentration, the potential increase in the drag force resulting from the increase in RV could be neutralised/balanced out by the shear-induced reduction in the continuous phase viscosity and consequently the drag force acting on the droplets. This means that the effect of the drag

force may not have a major influence on the size of the produced droplets and thus the surfactant adsorption needs to be considered.

The adsorption rate of surfactants depends on the molecular characteristics of the surfactant (*e.g.* size, interactions *etc.*), the nature of the bulk liquid (*e.g.* polarity, viscosity) and the environmental conditions (*e.g.* flow pattern, temperature) (McClements, 2005). As discussed in Section 2.2.2.1, there are three steps identified (Padron-Aldana, 2005) in the emulsifier adsorption onto the interface: (i) disintegration of micelles, (ii) transport of surfactant molecules from the bulk to the sub-surface[*], and (iii) the actual adsorption of molecules onto the interface. Consequently, the effects of XG concentration (thus continuous phase viscosity) and RV on the droplet size, as given in Figure 6-13, could be explained in terms of viscosity-induced changes in surfactant adsorption kinetics.

At very low or zero concentration of XG, the viscosity of the continuous phase is low (0.9 mPa·s for 0 % XG) and the fluid flow in the gap between the membrane and inner wall of the beaker is most likely to be transitional to turbulent. The Reynolds numbers were calculated as follows:

$$Re = \omega R_i \delta / \upsilon \qquad \text{Eq. 6-1}$$

where ω is angular velocity, R_i is the radius of the membrane, δ is the gap width and υ is the kinematic viscosity. For 0 % XG solution the Reynolds number increases from 3284 at 300 rpm to 16,419 at 1500 rpm. At such hydrodynamic conditions, surfactant molecules (and micelles) are very quickly transported, mainly due to advection, to the proximity of the interface. As a result, the interfacial tension is being quickly reduced, possibly down to the

[*] *i.e.* the region of the bulk phase, with a thickness of a few molecular diameters, immediately next to the interface

value of the equilibrium interfacial tension, as the interface expansion rate is relatively slow at the TMP of 25 kPa. Such quick decrease in the interfacial tension ensures that: (i) the droplet size distribution of the emulsion with 0 % XG is relatively narrow (span = 1 in Figure 6-15) and monomodal (Figure 6-14), with the mean droplet size of ~8 μm and, (ii) the RV has negligible effect on the droplet size (Figure 6-13).

At high concentration of XG (*i.e.* for 0.5 % XG) the Reynolds numbers are reduced (between 35 and 536, for 300 and 1500 rpm respectively), due to a general increase in fluid viscosity. At low RV (*i.e.* 300 rpm) the flow pattern is most likely laminar or with onset of first vortices, and thus molecular diffusion is the dominant transport mechanism in the surfactant adsorption. The diffusion coefficient of Tween 20 molecules[*], calculated using Eq. 2-2, decreases with the increase in XG concentration; from 1×10^{-11} to 0.5×10^{-11} m^2 s^{-1}, for 0.25 % and 0.5 % XG respectively. This leads to a slow rate of interfacial tension decrease, resulting in: (i) larger average droplet size (Figure 6-13), and (ii) possible coalescence of oil droplets at the membrane surface and in the bulk (Figure 6-14a). When the RV increases (for high XG concentrations), the viscosities of the shear thinning XG solutions decrease and thus the fluid flow becomes more transitional to turbulent (Re = 536 at 1500 rpm, 0.5 % XG). In such hydrodynamic conditions the molecular transport of surfactant would be controlled mainly by advection. Assuming that surfactant mass transport due to advection is proportional to velocity of the fluid in contact with the membrane surface, for a given XG concentration, the dynamic interfacial tension at the point of droplet detachment will be smaller at higher RV.

[*] Tween 20 molecule's hydrodynamic radius of 4.7×10^{-10} m was used after Owusu & Zhu, (1996).

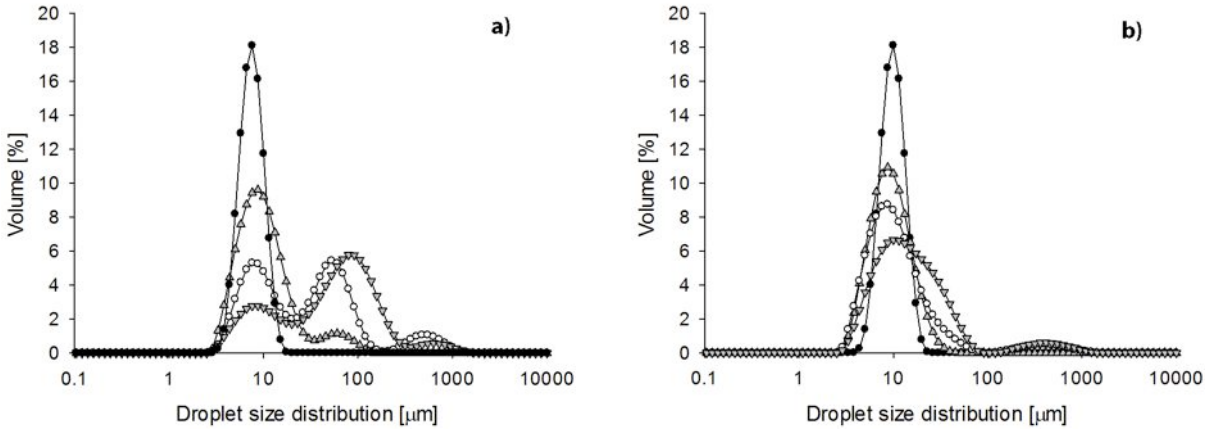

Figure 6-14 Droplet size distribution curves of O/W (2:98) emulsions stabilised with 1 % Tween 20, as a function of XG concentration: (▼) 0.25 %, (○) 0.0625 %, (▲) 0.0156 % , (●) 0 %; and rotational velocity of: (a) 300 rpm and (b) 1500 rpm.

For a given RV, an increase in the viscosity of the continuous phase leads to a slower decrease in the interfacial tension due to: (i) slow disintegration of micelles, and/or (ii) hindered diffusion of surfactant molecules from the bulk water phase, as the importance of diffusion in molecular transport will be increasing with viscosity. This would result in low surfactant coverage of newly formed interfaces, which may lead to droplet coalescence. The presence of coalescence in the solutions with higher XG concentration seems to be confirmed by a bimodal and multimodal droplet size distributions given in Figure 6-14a. It shows the droplet size distribution of emulsions produced at 300 rpm, where the viscosity of the continuous phase is 44.9 mPa·s (0.25 % XG), 10.8 mPa·s (0.0625 % XG), 3 mPa·s (0.0156 % XG) and 0.9 mPa·s (0 % XG).

A similar effect of the continuous phase viscosity was observed by Vladisavljević *et al.* (2002), who used a polypropylene hollow fibres membrane for the production of W/O emulsions. They reported, that an increase in the viscosity of oil slowed down the stabilisation of newly formed droplets and thus coalescence of water droplets could not be avoided. The

authors claimed, that coalescence was limited at higher continuous phase velocity. The data presented here for 1500 rpm (Figure 6-14b) also show a shift in the size distribution towards monomodal, especially for lower concentrations of XG (0.0156 % and 0.0625 %). This is also shown in Figure 6-15, where the span of droplet size distribution is presented as a function of RV and XG concentration. Due to some multimodal distribution curves, the graph shows scattered data with large error bars. However, it appears that at the RV of 1300 rpm and 1500 rpm the span is the smallest. This could be as a result of the hindered coalescence due to (i) stronger centrifugal force that pushes droplets away from the membrane into the bulk phase, and/or (ii) lower dynamic interfacial tension resulting from faster surfactant adsorption resulting from the advective transport.

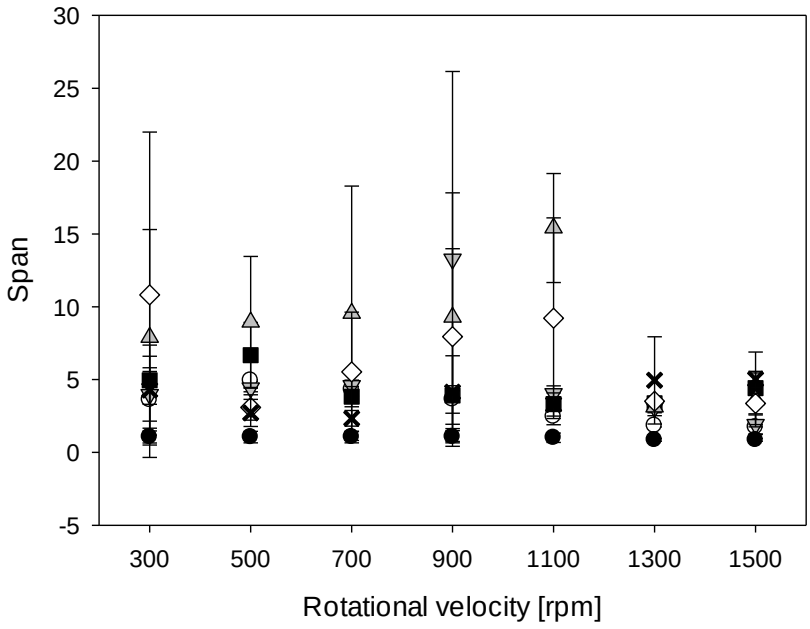

Figure 6-15 Span of O/W (2:98) emulsions stabilised with 1 % Tween 20, made with the 2.8 µm rotating memrane at 25 kPa TMP. Effect of RV and XG concentration: (●) 0 %, (○) 0.0156 %, (▼) 0.0312 %, (■) 0.0625 %, (▲) 0.125 %, (◇) 0.25 % and (×) 0.5 %.

In summary, increasing the continuous phase viscosity results in higher drag force acting on the droplets at the membrane surface, but this does not ensure reduction in droplet size. This

is down to hindered adsorption of surfactant from the viscous media. The surfactant adsorption phenomenon is further investigated in Section 6.5 where the concentration and type of emulsifier were varied.

6.5 Emulsifier type and concentration

In membrane emulsification, the size of the droplets depends on the interfacial tension force acting on the inflating droplet. It is well established (McClements, 2005), that both the type and the concentration of the emulsifier present in the system affect the oil-water interfacial tension. In this section, two emulsifiers, Tween 20 (low molecular weight surfactant) and Whey Protein Isolate (WPI), were used to stabilize O/W (2:98) emulsions (formulation in Section 3.2.2.1). Emulsions were produced using the 2.8 μm pore size membrane, at different RVs and TMPs. Firstly, the effects of Tween 20 concentration on the emulsion droplet size and droplet size distribution were investigated at various RVs and discussed as a function of the interfacial tension measured at different surfactant concentrations (Section 6.5.1). Then the effect of Whey Protein Isolate on the droplet size of emulsions prepared at different RVs and TMPs was studied (Section 6.5.2). Lastly, both emulsifiers, Tween 20 and WPI, were compared in terms of their role in determining emulsion droplet size during membrane emulsification (Section 6.5.3).

6.5.1 Tween 20

To begin with, equilibrium interfacial tension was measured at various Tween 20 concentrations, using pendant drop method described in Section 3.2.4.2. The interfacial tension data is presented in Figure 6-16; the values were taken after 30 min of equilibrating.

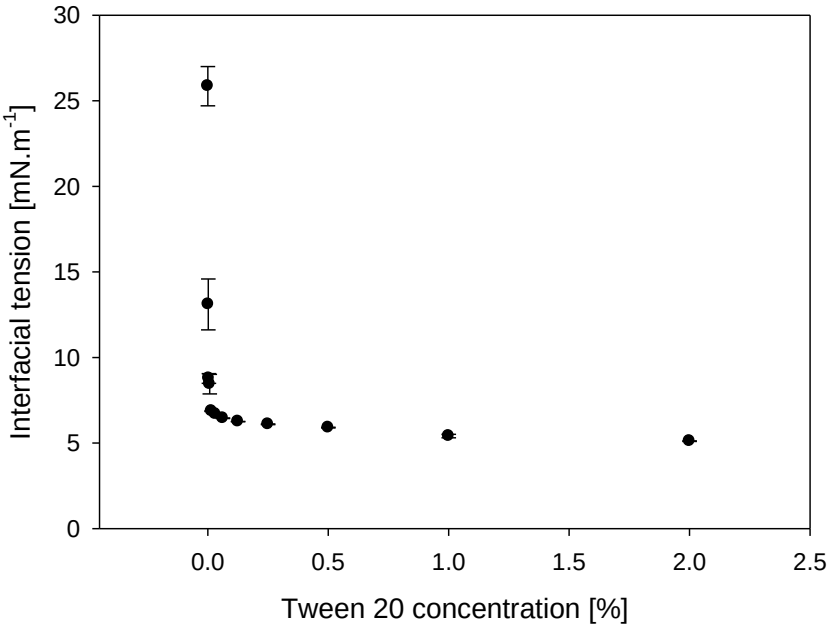

Figure 6-16 Equilibrium interfacial tension (at 21 ± 1 °C) of Tween 20 solutions with concentrations ranging between 0 % and 2 %.

The CMC value of Tween 20 was obtained (as theoretically discussed in Section 2.2.2.1) from Figure 6-16. It shows, that the interfacial tension initially sharply decreases with Tween 20 concentration from the initial value of ~26 $mN \cdot m^{-1}$, that was measured for surfactant-free oil-water interface. Between 0.0156 % and 0.0078 % of Tween 20, interfacial tension levels off, indicating full surfactant coverage of the interface and formation of micelles. These two concentrations of Tween 20 correspond to 1.27×10^{-4} M and 6.36×10^{-5} M, respectively. Taking the average of both values gives the CMC of 9.5×10^{-5} M. For further experiments, five solutions across the concentration range were chosen: two above the CMC (1 % and 0.125 %), one near to the CMC (0.0156 %) and two below the CMC (0.0019 % and 0.0005 %). Theoretical calculations of surface coverage (performed using the same method as for PGPR in Section 8.1, Appendix) showed, that the minimum amount of Tween 20[*] needed to stabilize the 2 % O/W emulsion is 0.000025 %. Therefore, in the present experimental

[*] The interface covered by a hydrophilic head of a Tween 20 molecule was taken as ~70 A^2 after Owusu & Zhu (1996).

conditions, even the lowest concentration of Tween 20 should ensure full surface coverage of the emulsion droplets.

O/W (2:98) emulsions were prepared using the 2.8 μm pore size membrane at the Tween 20 concentrations mentioned above. The TMP was kept constant at 25 kPa and the RV was varied from 300 rpm to 1500 rpm. Emulsifications with 0.0019 % and 0.0005 % Tween 20 solutions yielded phase separated samples at the RV of 300 rpm. This is most probably due to a very small shear stress and relatively slow reduction of the interfacial tension (at low Tween 20 concentrations), which both resulted in the membrane being wetted with the dispersed phase and thus subsequent coalescence of the oil droplets. For these Tween 20 concentrations the lower limit of RV range was kept at 500 rpm.

Changes in the emulsion droplet size with the RV and Tween 20 concentration are given in Figure 6-17. It can be seen that, regardless of the rotational velocity, the droplet size increases as the concentration of Tween 20 decreases from 1 % to 0.0019 %, and then stays unchanged upon further decrease to 0.0005 %. At 500 rpm, for example, the average droplet diameter varies from 8.2 ± 1.1 μm for 1 % Tween 20, to 37.7 ± 3 μm for 0.125 %, to 74.8 ± 14.6 μm for 0.0156 % and to 94 ± 10 μm for both 0.0019 % and 0.0005 %. This can be explained by considering surfactant adsorption kinetics, which depends on the flow characteristics in the membrane system. The calculated Reynolds numbers (Eq. 6-1)[*] varied between 3283 (for 300 rpm) and 16,419 (for 1500 rpm), which indicates turbulent or transitional flow in the annular gap between the membrane and the inner wall of the emulsification beaker. In turbulent/transitional conditions, transport of surfactant to the interface occurs *via* convection,

[*] Kinematic viscosity for all solutions was assumed to be equal to that for water (*i.e.* 1.004×10^{-6} $m^2 \cdot s^{-1}$)

which is a sum of molecular diffusion and advection*. Nonetheless, the advective transport has been reported (Walstra, 1983) to be the dominant mechanism.

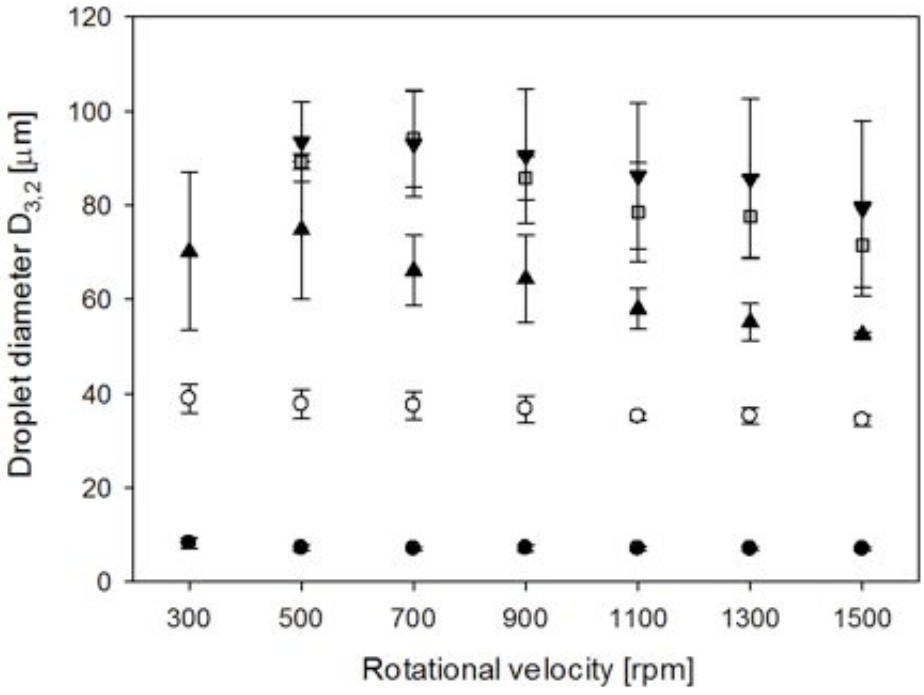

Figure 6-17 Droplet size of O/W (2:98) emulsions made with the 2.8 μm rotating memrane at 25 kPa TMP. Effect of RV and Tween 20 concentration: (●) 1 %, (○) 0.125 %, (▲) 0.0156 %, (■) 0.0019 % and (▼) 0.0005 %.

The magnitude of surfactant mass transport due to advection in one spatial direction would be proportional to fluid velocity in this specific direction, and the mass concentration of molecules/micelles (Roberts & Webster, 2002). This means that, for a given RV, surfactant mass transport in turbulent/transitional conditions existing in the gap between the membrane and the beaker would be proportional to the concentration of surfactant molecules/micelles. Therefore, increased concentration of Tween 20 would result in: (i) higher advective mass transport due to larger amount of available molecules/micelles in the bulk phase, and (ii) faster adsorption due to larger concentration gradient between the sub-surface and the interface. This will increase the rate of interfacial tension reduction and thus smaller final

* *i.e.* movement due to the bulk fluid motion

droplets volume at the detachment point. It was assumed here, that surfactant molecules are adsorbed at the interface as soon as they reach the sub-surface. However, it could be expected (Padron-Aldana, 2005), that adsorption rate slows down as the interface becomes saturated with surfactant, but this will occur for all concentrations of Tween 20.

At constant Tween 20 concentration, the RV has little or no effect on the emulsion droplet size (Figure 6-17). Since the advective mass transport is proportional to fluid velocity and solute concentration (Roberts & Webster, 2002), and yet the data do not show droplet size reduction with increase in membrane RV, it means that the adsorption of surfactant is slower for lower Tween 20 concentration due to smaller number of Tween 20 molecules present in the bulk. Therefore, even high advective transport supplies only limited number of molecules/micelles to the vicinity of the sub-surface, which then creates lower chemical potential gradient between the sub-surface and the interface.

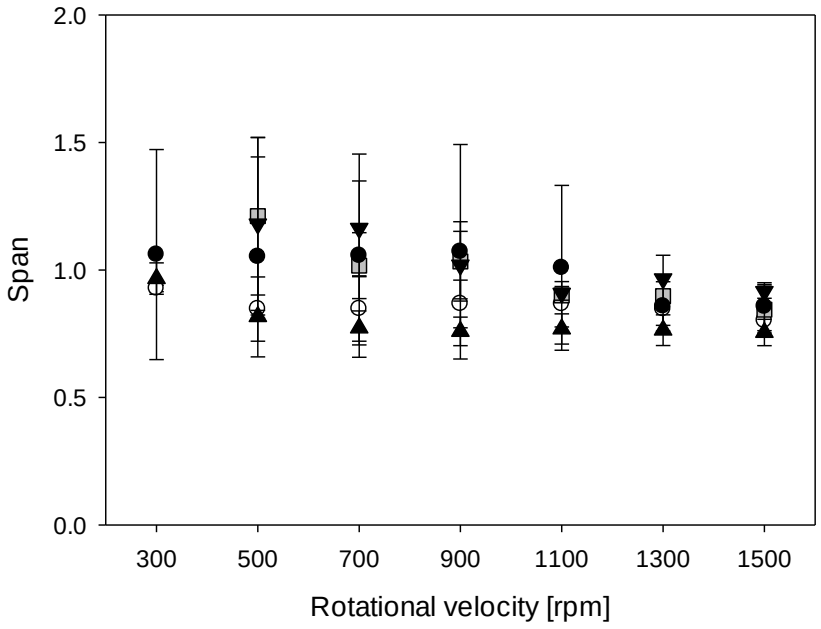

Figure 6-18 Span of O/W (2:98) emulsions made with the 2.8 µm rotating memrane at 25 kPa TMP. Effect of RV and Tween 20 concentration: (●) 1 %, (○) 0.125 %, (▲) 0.0156 %, (■) 0.0019 % and (▼) 0.0005 %.

In summary, the droplets cannot be detached from the membrane sooner than after reaching a volume which is dictated by: (i) the concentration of surfactant molecules in the bulk and, (ii) their flow dependent transport from the bulk and to the interface.

The effects of RV and Tween 20 concentration were analysed in relation to the droplet size distribution. Figure 6-18 shows span of droplet size distribution of O/W emulsions prepared with the 2.8 μm membrane, where RV and the concentration of Tween 20 in the continuous phase were altered. It can be seen that the span is independent of RV and surfactant concentration. This indicates that there is no evidence of coalescence and the few active pores (as discussed in Section 6.2.2 for low TMP) ensure that the droplets are relatively homogeneous in size.

6.5.2 Whey Protein Isolate

Contrary to low molecular weight surfactants, proteins have been reported (Bos & van Vliet, 2001; Rodriguez-Patino *et al.*, 1999) to form strong viscoelastic films around the droplets *via* non-covalent intermolecular interactions and covalent disulphide cross-linking, which are generally thought to be linked (Tadros, 1994) to stability of colloidal dispersions. The protein adsorption process is complex and involves several steps/mechanisms (Rodriguez-Patino *et al.*, 1999) including: (i) transport of protein from the bulk phase into the droplet sub-surface (*via* molecular diffusion and/or advection), (ii) actual adsorption and unfolding at the interface and, (iii) protein rearrangement at the interface. Murray *et al.* (1998) additionally pointed out, that when the interface expands new protein molecules are attached to the interface, but also parts of the molecules already adsorbed at the interface.

In this section, the effects of RV and TMP on the droplet size and the droplet size distribution of emulsions stabilised with Whey Protein Isolate (WPI) were investigated. O/W (2:98) emulsions were prepared using the 2.8 μm pore size membrane, as described in Section 3.2.2.2. The concentration of WPI was kept constant at 1 % throughout the experiments (solutions preparation is Section 3.2.2.1. It is worth noting that, in the present experimental conditions (pH = 6.8), WPI is slightly negatively charged, which is assumed to ensure repulsive electrostatic interactions between the negatively charged membrane surface and the protein molecules. The TMP and the applied RVs were varied from 25 kPa to 100 kPa and from 300 rpm to 1500 rpm, respectively.

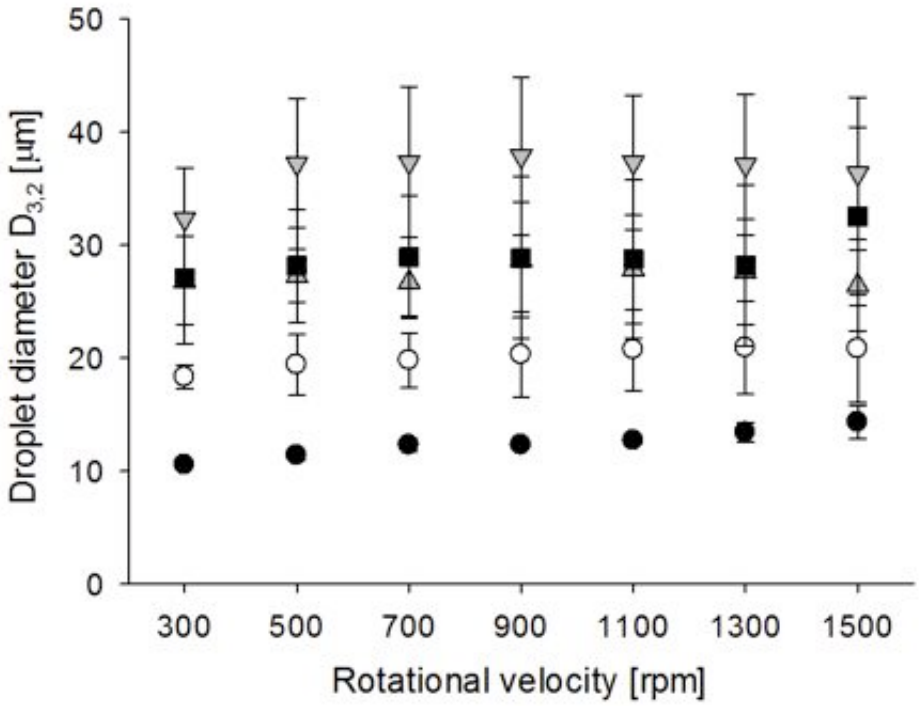

Figure 6-19 Droplet size of O/W (2:98) emulsions stabilised with 1 % WPI and made with the 2.8 μm rotating memrane. Effect of RV and TMP: (●) 25 kPa, (○) 40 kPa, (▲) 60 kPa, (■) 80 kPa and (▼) 100 kPa.

The effect of RV and TMP on emulsion droplet size is given in Figure 6-19. It shows, that the droplet size increases with the applied TMP. For example, at 700 rpm $D_{3,2}$ is 12.3 ± 0.6 μm at

25 kPa TMP, 19.9 ± 4.4 μm at 40 kPa, 26.7 ± 3 μm at 60 kPa, 28.9 ± 7.4 μm at 80 kPa and 37.3 ± 9.7 μm at 100 kPa. This is due to the fact, that for a given RV, the rate of oil-water interface formation increases with TMP, as well as the flux of the dispersed phase, according to the Darcy's law. This means that the interfacial tension reduction caused by WPI adsorption would be slower at higher interfacial expansion rates.

Considering now the effect of rotational velocity, Figure 6-19 shows, that for a given TMP the increase in RV, resulting in higher drag force, does not cause significant changes in the droplet size. For example, at the TMP of 40 kPa, the diameter $D_{3,2}$ is 18 ± 1 μm at 300 rpm, 20 ± 4 μm at 900 rpm and 21 ± 5 μm at 1500 rpm. This means that, since WPI is in abundance, and the increase in the advective transport (with increasing RV) does not affect the droplet size, it is the adsorption from the sub-surface to the interface that is the rate-limiting step in the interfacial tension decrease. It can be assumed that, at relatively short timescales of interface formation at the membrane surface, the rearrangement of the protein molecules at the interface does not play a significant role in the interfacial tension decrease at the point of droplet detachment. It can also be assumed, that there is a barrier to molecular adsorption created by electrostatic interactions between negatively charged WPI molecules. This means that when the interface expands, the first protein molecules initially adsorb onto the interface, and thus the interface becomes negatively charged. Electrostatic repulsions will consequently hinder further adsorption of the approaching charged protein molecules. As a result, the interfacial tension does not decrease with the increase in the advective transport of protein molecules, and the volume of droplets will depend primarily on the applied TMP.

The effects of RV and TMP were analysed in relation to the droplet size distribution of emulsions stabilised with WPI. Figure 6-20 shows the span of droplet size distributions at

various TMPs and RVs. It shows, that for the lowest TMP of 25 kPa, the emulsions are largely polydisperse but with increasing RV their size distributions become narrower. Coalescence of oil droplets does not seem to be the reason for a wider droplet size distribution at low TMP, as it would be more probable to happen at higher interface expansion rates (higher TMPs). However, Figure 6-20 shows that this is not the case, as at 100 kPa larger droplets with relatively small span are formed. Instead, this is similar to situation described in Section 6.2.1 for Tween 20 at 40 kPa TMP, where the range of active pores leads to uneven interfacial tension decrease and thus polydispersed emulsions. Here, this happens at lower TMP of 25 kPa due to slower adsorption of WPI (discussed in detail in the next Section).

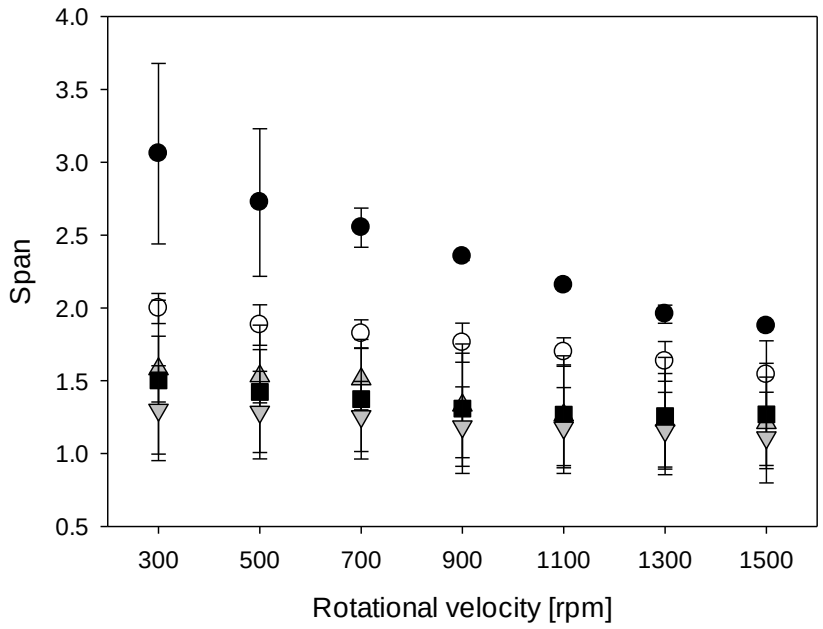

Figure 6-20 Span of O/W (2:98) emulsions stabilised with 1 % WPI and made with the 2.8 µm rotating memrane. Effect of RV and TMP: (●) 25 kPa, (○) 40 kPa, (▲) 60 kPa, (■) 80 kPa and (▼) 100 kPa.

6.5.3 Comparison of WPI and Tween 20 as emulsifier

Low molecular weight surfactants and proteins are both surface active*. However, the adsorption of protein is considered slower than low molecular weight surfactants due to high molecular weight of the former. Now, the question is how this affects the droplet size of emulsions produced with the rotating membrane. Figure 6-21 shows the droplet size of emulsions produced with the 2.8 μm pore size membrane, where the interface was stabilised with either 1 % WPI (Figure 6-21a, described in detail in Section 6.5.2) or 1 % Tween 20 (Figure 6-21b, described in detail in Section 6.2.1). In both systems: (i) TMP was altered between 25 kPa and 100 kPa, and (ii) RV was altered between 300 rpm and 1500 rpm. By comparing both Figures it can be observed that droplet size of emulsions stabilised with Tween 20 is slightly smaller (a range between 7 ± 0.3 μm and 30.4 ± 5.5 μm) than emulsions stabilised with WPI (a range between 10.5 ± 0.1 μm and 37.8 ± 9.8 μm). The above observation is somewhat unusual, as there are several possible reasons why larger droplet size could be expected in the formulation with WPI as compared with the formulation with Tween 20.

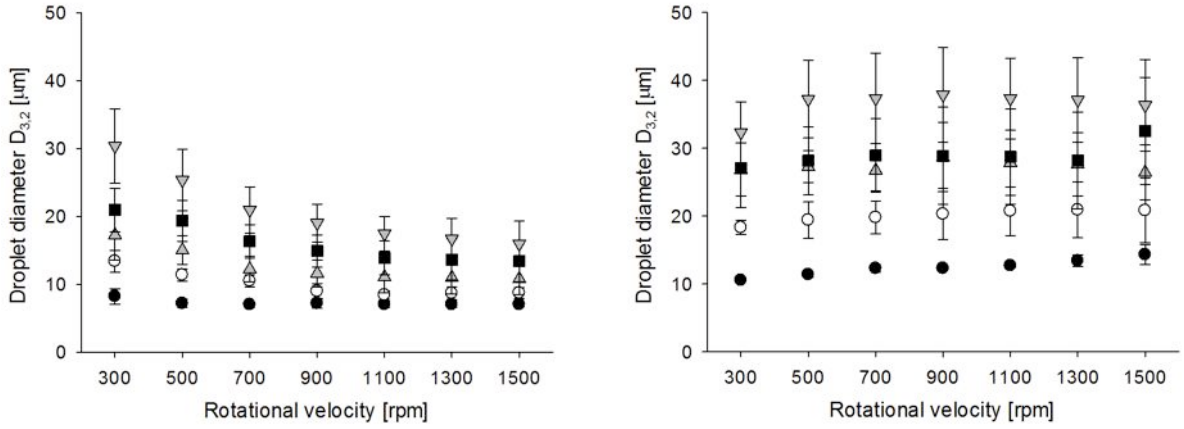

Figure 6-21 Droplet size of O/W (2:98) emulsions stabilised with: (Left) 1 % Tween 20 and (Right) 1 % WPI; as a function of RV and TMP: (●) 25 kPa, (○) 40 kPa, (▲) 60 kPa, (■) 80 kPa and (▼) 100 kPa.

* *i.e.* they lower the interfacial tension of fluid interfaces

Firstly, the WPI monomer is significantly bigger than the Tween 20 molecule. WPI has an average protein concentration of 90 % with β-lactoglobulin, as a major component. This relatively small globular protein (mass of a monomer – 18,300 $g \cdot mol^{-1}$) consists of 162 amino acids and in the pH range of 5 – 8 exists as a dimer (Rodriguez-Patino *et al.*, 1999). Due to a markedly higher molecular weight of WPI than Tween 20 (molecular mass = 1227 $g \cdot mole^{-1}$), it would be expected that in laminar conditions (or when molecular diffusion significantly contributes to the molecular transport), the adsorption of protein would be slower than low molecular weight surfactant such as Tween 20. The diffusion coefficient for both molecules was calculated (Eq. 2-2) giving: 0.76×10^{-10} $m^2 \cdot s^{-1}$ for the WPI dimer* and 5.2×10^{-10} $m^2 \cdot s^{-1}$ for the Tween 20 molecule.

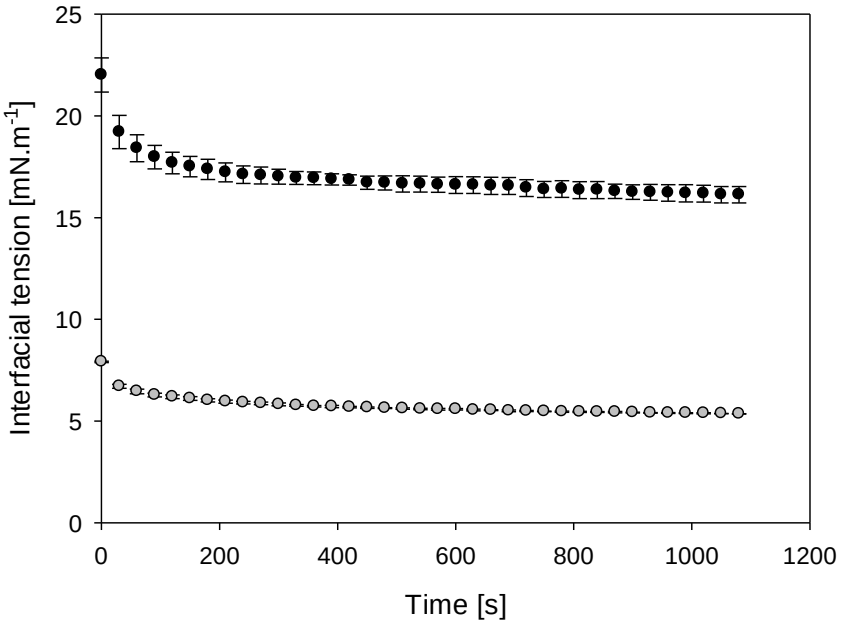

Figure 6-22 Interfacial tension evolution with time in: (●) 1 % WPI and (●) 1 % Tween 20 solution.

Secondly, low molecular weight surfactants usually reduce the interfacial tension to a greater extent as they have higher adsorption energies (Bos & van Vliet, 2001). This is shown in

* The hydrodynamic diameter of a WPI dimer was taken from Noisuwan *et al.*, (2009).

Figure 6-22, where the interfacial tension of 1 % WPI and 1 % Tween 20 solutions was measured over time, according to the method described in Section 3.2.4.2. It can be seen, that the first measured point after the formation of a pending droplet with Tween 20 gives a much lower value (~8 $mN \cdot m^{-1}$), than any point during the measurement of the WPI system (with the minimum at ~17 $mN \cdot m^{-1}$). Therefore, at the short timescale of droplet inflation at the membrane surface, Tween 20 would be expected to lower interfacial tension faster than WPI and thus facilitate droplet detachment due to the smaller Laplace pressure inside the droplet.

Lastly, slower adsorption of protein may arise from the repulsive interactions between the molecules already adsorbed at the interface and those approaching the interface. These repulsions originate from: (i) negative charge of protein at the pH = 6.8 and (ii) steric repulsions due to the size of WPI molecules.

However, despite the reasons mentioned above, the emulsion droplet size in the system with Tween 20 is only marginally smaller than emulsions produced with WPI as an emulsifier (Figure 6-21). This may be resulting from the fact, that under turbulent conditions, adsorption rate increases when the size of the emulsifier molecule increases, relative to the size of the droplets (McClements, 2005). Additionally, due to the fact that protein molecules are charged, there are no net attractions between molecules in the bulk and therefore, transport of molecules is not hindered by finite protein disassociation time. On the contrary, above the CMC most of the low molecular weight Tween 20 molecules in the bulk exist in the form of micelles. Therefore, when the gradient of surfactant is created between the interface and the bulk, the finite time for micelle disintegration would slow down the adsorption process (McClements, 2005). Finally, electrostatic repulsions between the negatively charged membrane surface and the interface of the droplet (with WPI molecules carrying negative

charges) forming at the pore opening would increase the contact angle between the disperse phases and the membrane (measured in the dispersed phase, see Section 2.3.2.3.3). This in turn will reduce the extent to which the dispersed phase wets the membrane surface resulting in droplets being almost "repelled" from the membrane thus their faster detachment and smaller average droplet size.

6.6 Rotating membrane technique – data repeatability

To assess the statistical significance of the data obtained with the rotating membrane, three membranes with 2.8 μm pore diameter and three membranes with 6.1 μm pore diameter were used for the experiments. It was observed, that repeatability of results (*i.e.* variations in produced emulsions) during the rotating membrane emulsification was affected by: (i) the membrane used, and (ii) membrane's wear due to its usage and/or cleaning. It was observed, that when 250 mm long membrane was cut into the 50 mm tubes and mounted on the metal collar, they performed in a different way (the emulsification procedure and sample formulation were kept strictly constant in all repeatability trials). This also happened when the membranes were used for the first time (*i.e*. after heat-treatment and regeneration in acid, performed before attaching to the metal ferrule) and therefore considered clean. This may suggest that, the 250 mm tubular membranes do not have a homogenous structure throughout their length, and as a consequence big experimental errors were observed when different membranes with the same nominal pore size were used. Similar discrepancies in performance were observed between the emulsions prepared with a given membrane during its usage/lifespan. For example, the standard deviation for three subsequent *single experimental runs* that were performed on the same membrane (with washing procedure applied after each *single experimental run*), was similar to the standard deviation between three *single experimental runs* which were performed each on a different membrane (with the same

nominal pore diameter). Additionally, after a prolonged membrane usage (more than approximately 500 runs), standard deviation for the produced emulsions started to increase. This is most probably due to: (i) membrane fouling and/or insufficient/inappropriate cleaning process applied, and (ii) micro-cracks in the membrane structure. Therefore, for the purpose of this work, only the emulsions produced during the first 500 emulsification runs of the particular membrane were considered.

6.7 Chapter conclusions

O/W emulsions with range of droplet sizes could be produced using SPG rotating membranes. The size of the produced droplets can be manipulated by changes is TMP and RV. However, within the applied spectrum of hydrodynamic conditions, more significant decrease in droplet size could be obtained by decreasing the TMP, rather than by increasing the RV. This indicated the importance of the balance between the rate of interface formation and surfactant adsorption on the size of the produced droplets. Smallest droplets with relatively narrow droplet size distribution (span = 1) could be obtained when TMP was just above the membrane's CTMP. Under similar hydrodynamic conditions, the droplet size depends on the membrane pore size.

Viscosity of the continuous phase affects the droplet size and size distribution span through a complex mechanism. Increase in the viscosity increases the drag force of the continuous phase, but at the same time slows down the adsorption of surfactant onto the newly formed interfaces. To what extent viscosity modifies the adsorption, depends also on the fluid flow in the membrane system, affecting surfactant transport to the interface. Smallest droplets can be obtained when the continuous phase viscosity is lowest and/or at high RV. In both cases advective transport of surfactant molecules ensures rapid decrease in the interfacial tension.

Emulsion droplet size can be controlled through a choice of the emulsifier type and concentration. Larger droplets are formed when the concentration of Tween 20 decreases, and no reduction in droplet size could be obtained by changing the RV. This means, that even high advective transport in turbulent conditions supplies only as much surfactant, as available in the bulk continuous phase.

WPI at 1 % can stabilize O/W emulsions produced using the rotating membrane. Electrostatic repulsions of the negatively charged protein molecules slow down the adsorption process, making it independent of the applied RV. Despite relatively large size of WPI molecules, the protein could stabilize droplets of a similar size to those stabilized with Tween 20. This may come from electrostatic repulsions between the membrane surface and the protein.

7 Conclusions and Future work

The aim of this thesis was to investigate the stability criteria of duplex $W_1/O/W_2$ emulsions. More specifically, this work focused on the following objectives:

- Production of duplex $W_1/O/W_2$ emulsions using food grade materials,
- Formulation and processing parameters determining stability of the primary W_1/O emulsions,
- Formulation of duplex $W_1/O/W_2$ emulsions with structured water phases (*e.g.* to induce the osmotic pressures imbalance) to study the release of the encapsulated marker compound during processing and storage (under usage conditions),
- Influence of the secondary emulsification process on the short- and long-term stability of duplex emulsions (*i.e.* stability that is measured by changes in emulsions droplet size and encapsulation properties); high shear mixer and two membrane techniques as a probe,
- Novel routes for the production of emulsions; membrane emulsification.

7.1 Conclusions

Primary W_1/O emulsions formulated with PGPR are more stable against coalescence and subsequent phase separation when the water phase contains small amount of NaCl. Salt alters the mechanism by which surfactant molecules orientate at the interface, most likely strengthening interactions between them and resulting in an increase of the interfacial viscosity and elasticity, and thus promoting droplet stability.

In $W_1/O/W_2$ duplex emulsions the majority of salt release from the internal water phase takes place during the initial stages of storage and is proportional to the glucose concentration. The lowest salt release rate occurs when the glucose concentration in the external water phase is lower than required for balancing the osmotic pressures. With no significant change in the droplet size and no swelling-breakdown of the duplex emulsion, the release of salt is driven by the chemical potential difference between the two water phases rather than the unbalanced osmotic pressures.

Sugars used to match the osmotic pressure, alone and in combination with surfactants, structure water and alter the system's interfacial tension. This suggests, that sugars act in a similar way to water-soluble emulsifiers, which, by increasing micellar transport, increase the rate at which salt is released from the internal aqueous phase.

High-shear secondary emulsification has the potential to damage the structure of duplex emulsions. The extent of this damage depends on the concentration of the primary emulsifier (PGPR) and the duration of the mechanical shear. Long-term salt release does not depend on the homogenisation conditions but on the emulsion droplet size (thus interfacial area) and formulation, *i.e.* 2 % or more of PGPR is crucial for the long-term stability of the investigated duplex emulsions.

Duplex emulsion droplet size produced with cross-flow and rotating membrane techniques decreases with the drag force generated by either CFV or RV, whilst the droplet size increases with the applied TMP. The effect of TMP is associated with: (i) the increase in the dispersed phase flux, (ii) the transition from a *dripping* to a *jetting* mechanism of droplet formation, (iii) an increased percentage of active pores, and (iv) slower rate of the interfacial tension

decrease. A similar minimum droplet size (~12 μm) obtained by all three techniques indicate, the droplet size is primarily determined by the rate of the interfacial tension decrease.

Salt release from the internal water phase of duplex $W_1/O/W_2$ emulsions varies between the three emulsifying techniques used. The slowest release rate is when the duplex emulsions are made with the rotating membrane, followed by high-shear emulsification and the highest release for the cross-flow membrane. These differences are due to: (i) the emulsion droplet size, thus the interfacial area available for molecular transport, and (ii) the effect of shear forces applied in each emulsification process and thus different interfacial properties of adsorbed surfactants. It is proposed, that during droplet formation in both membrane techniques, a homogenous deposition of surfactant molecules at the interface results in a dense and isotropic layer of surfactant. This layer is likely to provide a stronger mechanical barrier against ionic diffusion between the two water phases of duplex emulsions, thus resulting in slower salt release. However, during cross-flow emulsification, shear forces generated in the membrane system disturb the homogenously packed surfactant molecules, creating a “leaky” interface.

SPG rotating membrane is a promising technique for the secondary emulsification step in duplex emulsions manufacture. As a low shear process it offers higher salt encapsulation in the internal water phase of duplex emulsions than both the cross-flow membrane and the high-shear techniques. This is probably due to homogenous and isotropic layer of surfactant deposited on the interfaces.

When the rotating membrane device was used to produce O/W emulsions, the droplet size could be controlled by the choice of membrane pore size, rotational velocity and trans-

membrane pressure. Decreasing the TMP is more effective in reducing the droplet size than an increase in the RV. This highlights the significance of the rate of surfactant adsorption to the newly formed interface. Smallest and relatively homogenous droplets can be produced at low TMP, regardless of the applied RV. Under similar hydrodynamic conditions, the droplet size depends on the membrane pore size.

The emulsion droplet size is also dependent on the viscosity of the continuous phase. When viscosity increases, it increases the drag force that acts on the emulsion droplets at the membrane surface, but at the same time hinders surfactant adsorption onto the newly formed oil/water interface. The magnitude of viscosity-modified-surfactant-adsorption depends on the fluid flow in the membrane module. Smallest droplets can be produced when the continuous phase viscosity is lowest and /or at high RV. In both cases, the advective transport of surfactant molecules ensures rapid decrease in the interfacial tension.

Finally, the droplet size can be controlled by the choice of an emulsifier and its concentration. By reducing the concentration of Tween 20, larger droplets are formed and changing RV has no effect on the droplet size. When 1 % of WPI is used, it can stabilise O/W emulsions produced with the rotating membrane. The electrostatic repulsions between the negatively charged protein molecules and the membrane surface are the main reason for: (i) slow adsorption process and thus no effect of RV on the droplet size, and (ii) relatively fast detachment of droplets and thus similar average droplet size to Tween 20 stabilised emulsions made in the same hydrodynamic conditions.

7.2 Future work

Based on this work, the following areas merit future examination:

- **Formulation of the primary W_1/O emulsions**

It was observed, that PGPR is an excellent emulsifier for the oil continuous emulsions. Nevertheless, PGPR is allowed in limited concentrations ($4g \cdot kg^{-1}$) in some countries but not the others. Therefore, it would be beneficial to substitute (or partially substitute) PGPR with other food-grade emulsifiers such as lecithin, solid particles or mixtures of these.

The effect of salts on the properties of PGPR-stabilised emulsions deserves more work to determine the ion specific interactions, *i.e. Hofmeister* series.

It would also be interesting to study the use of a gelling agent for structuring the water phase and its effects on the stability of W_1/O emulsions. The preliminary experiments revealed limited stability of agarose structured internal water phase (up to 1% agarose) even though Muschiolik *et al.*, (2006) reported, that instead of salt the presence of gelled gelatin prevents water coalescence in PGPR-stabilised emulsions.

- **Sugars surface activity and molecular transport**

It was found that sugars modify the interfacial tension between oil and water. To better understand the effect of sugar on the transport of material across the interface, the interfacial rheology of adsorbed emulsifiers in the presence of sugar could be investigated.

Additionally, interactions of sugar and individual components of the formulation as well as the transport of sugar molecules between the two water compartments should be looked into. Even though Dickinson *et al.* (1991) claimed that glucose is an oil phase impermeant compound, elsewhere it was suggested (Magdassi & Garti, 1984), that glucose is more easily

solubilised in the oil phase than ions of inorganic salts. Any possible changes in glucose concentration need to be appropriately monitored in terms of osmotic pressure control.

- **Effect of emulsifying technique on the encapsulation properties of duplex $W_1/O/W_2$ emulsions**

The data in Chapter 5 suggest, that there is a difference in encapsulation properties between duplex emulsions made with different techniques. This was associated with the way surfactant deposits and orientates itself at the interface. To further study the phenomena, the enthalpy of surfactant reorganisation at the interface could be measured with micro DSC. Also, the interface could be visualised by X-ray small angle scattering, as suggested by Okochi & Nakano (2000). If such differences in emulsifier orientation are indeed a cause of leaky interface, the rearrangement of molecules at the interface would be more feasible to study in less dynamic systems. For instance, using proteins as emulsifiers. Rearrangement of protein molecules at the interface takes longer than low molecular weight surfactants and thus the measured differences in enthalpy could be more pronounced.

- **Cross-flow membrane emulsification**

It was found, that a semi-batch process of the cross-flow membrane emulsification has a consequence in the enhanced release of salt from duplex emulsions during the secondary emulsification step. It would be of a great interest to construct a continuous process, with a low shear pump to minimise duplex droplets breakup in the bulk phase.

To further improve trans-membrane fluxes, premix emulsification could be potentially beneficial (van der Graaf *et al*., 2005). Coarse duplex emulsion prepared by gentle mechanical stirring would be passed through the SPG membrane at hypothetically higher rates, thus

limiting duplex processing time in the membrane system (particularly advantageous for the cross-flow system).

- **Rotating membrane emulsification**

Rotating membrane showed to be a promising emulsification device, with a relatively high throughput. It would be interesting to establish whether droplet size, polydispersity can be better controlled by:

1. Using membranes with different surface properties (wall contact angle, porosity, shape of pore opening).
2. Modification of viscosities of both dispersed and continuous phases.
3. Using a range of emulsifiers (*e.g.* solid particles) in the dispersed phase and/or continuous phase.

Additionally, investigation of the mechanism(s) of droplet formation/detachment at the membrane pore would help to better understand the relative significance of forces acting on the droplet. By employing a suitable imaging technique and developing a robust theoretical model (based on a force balance) a better control over emulsion droplet size could be achieved. This is essential to successfully scale up the membrane emulsification process and assess its industrial viability. Currently, the Microstructure Group in Chemical Engineering (University of Birmingham, UK) is undertaking work addressing these issues.

8 Appendix

8.1 Surface coverage calculations

In order to calculate surface load at saturation in PGPR stabilised W_1/O emulsions, several assumptions had to be made. These include:

a) Determination of the structure of the PGPR molecule.

Polyglycerol polyricinoleate (PGPR) consists of polyglycerol as the hydroplilic group and interestrified ricinoleic fatty acids as the hydrophobic group. Chemical structure of PGPR is given in Figure 8-1. The polyglycerol part of PGPR is a mixture of di- tri- and tetraglycerol (min 75%) and maximum of 10% as heptaglycerol or higher. Here, the fraction consisting of tri-glycerol tri-ricinoleate is shown.

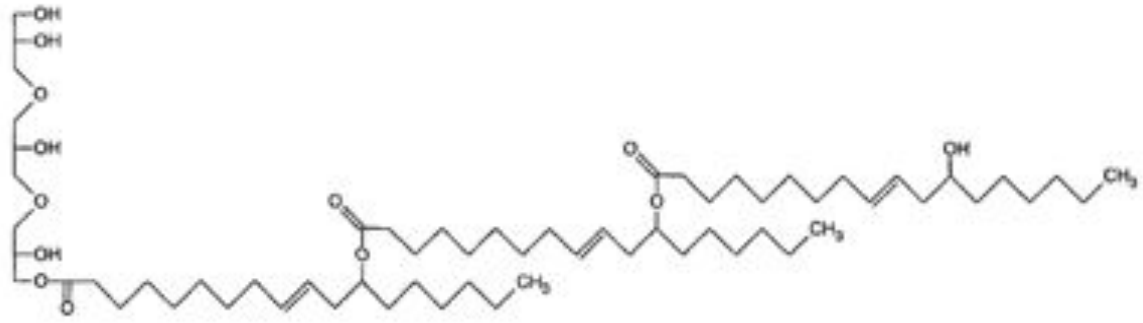

Figure 8-1 Average chemical structure of polyglycerol polyricinoleate (PGPR): tri-glycerol tri-ricinoleate (GRAS Notification for Polyglycerol Polyricinoleate (PGPR)(2008), viewed on September 2011, http://www.accessdata.fda.gov/scripts/fcn/gras_notices/grn000266.pdf.

According to Gunes at al (2010) the molecular weight distribution of PGPR (characterised by Size Exclusion Chromatography) ranges from 200 to 2000 g·mol^{-1}, with a maximum at 500 g·mol^{-1}. Also the hydrodynamic radius of PGPR in oil can be roughly estimated to be of the order of 1 nm. The molecular weight of PGPR was taken as 1200 g·mol^{-1}, as advised by its manufacturer – Kerry BioScience (personal communication).

b) Interfacial area in model emulsion was calculated as:

$$\frac{A}{V} = \frac{6\,\varphi}{D_{3,2}} \qquad \text{Eq. 8-1}$$

Where A is the interfacial area, φ is dispersed volume fraction (0.3), $D_{3,2}$ is average droplet diameter (~0.2 μm) and V is unit volume [100 cm^3].

$$A = 900 \text{ m}^2$$

c) Number of PGPR molecules (N) was obtained by dividing the interfacial area A by the area occupied by one PGPR molecule (*i.e.* its oil immersed part):

$$N = 2.87 \times 10^{20} \text{ molecules of PGPR}$$

From Avogadro constant (6.022×10^{23}), number of moles of PGPR (n) was calculated:

$$n = 4.7 \times 10^{-4} \text{ mol PGPR}$$

d) Taking 1200 g·mol^{-1} as the average molecular mass of PGPR the required amount of PGPR (m) to stabilise 100 cm^3 of:

- 30:70 emulsion is: m = 0.6 g,
- 50:50 emulsion is: m = 0.9 g.

8.2 Shear calculations

In order to compare the three emulsification techniques described above, relative shear stresses that the emulsion droplets are subjected to during each emulsification process were calculated. The analysis is given in Table 5-1.

8.2.1 High-shear mixer

For the high-shear mixer, the shear rate was calculated from the gap between rotor and stator where the highest energy dissipation occurs (Utomo *et al.*, 2008):

$$\dot{\gamma} = \frac{\pi N D}{\delta} \qquad \text{Eq. 8-2}$$

where $\dot{\gamma}$ is the shear rate at the gap, N is the agitation speed, D is the diameter of an impeller, and δ is the gap between the impeller and the screen. The shear stress τ was obtained from the following relationship with viscosity η for Newtonian fluids:

$$\tau = \eta \dot{\gamma} \qquad \text{Eq. 8-3}$$

8.2.2 Cross-flow membrane system

For the cross-flow membrane, $\dot{\gamma}$ was calculated from a wall shear stress (τ_w) and Eq. 7-3 for each CFV, as shown in Chapter 5. Due to the batch nature of the emulsification process, as

explained in Section 3.2.3, calculations were performed for both limiting conditions: at the beginning ($T_{0\%}$) and at the end ($T_{30\%}$) of the emulsification process.

$$\tau_w = 0.5\, f_F\, \rho_c v^2 \qquad \text{Eq. 8-4}$$

$$f_F = \frac{16}{Re}, \qquad \text{for Re} < 2000 \qquad \text{Eq. 8-5}$$

$$Re = \frac{\rho_c\, v D_h}{\eta_c} \qquad \text{Eq. 8-6}$$

where f_F is the Fanning friction factor, $\rho_c$is the continuous phase density, v is the CFV, Re is the Reynolds number, D_h is the hydraulic diameter of the cross-flow membrane annulus and is η_c the dynamic viscosity.

8.2.3 Rotating membrane system

For the rotating membrane, the shear rate was estimated in the same way as for the cross-flow emulsification, at $T_{0\%}$ and $T_{30\%}$ and all RVs. It was based on a Taylor-Couette model of concentric cylinders with a wide gap between them. Due to the width of the gap, the simple shear between the cylinders is disturbed by the secondary flow induced by the formation of Taylor vortices. Shear rate at the surface of the membrane (at R_i) is expressed by:

$$\dot{\gamma}_i = \frac{2\,\omega\, a^2}{a^2 - 1} \qquad \text{Eq. 8-7}$$

Shear rate at the wall of an emulsification beaker (at R_o) can be written as:

$$\dot{\gamma}_o = \frac{2\,\omega}{a^2 - 1}, \qquad \text{where} \quad a = \frac{R_o}{R_i} \qquad \text{Eq. 8-8}$$

where ω is the RV , R_o is the radius of the beaker (external cylinder) and R_i is the radius of the rotating membrane (internal cylinder).

9 List of references

Abrahamse, A.J., van der Padt, A., Boom, R.M., & de Heij, W.B.C. (2001). Process fundamentals of membrane emulsification: Simulation with CFD. *AIChE Journal*, 47, 1285-1291

Abrahamse, A.J., van Lierop, R., van der Sman, R.G.M., van der Padt, A., & Boom, R.M. (2002). Analysis of droplet formation and interactions during cross-flow membrane emulsification. *Journal of Membrane Science*, 204, 125-137

Adhikari, B., Howes, T., Wood, B.J., & Bhandari, B.R. (2009). The effect of low molecular weight surfactants and proteins on surface stickiness of sucrose during powder formation through spray drying. *Journal of Food Engineering*, 94, 135-143

Aguilera, S. (1999). Microstructural principles of food processing and engineering, (2 ed.) Gaithersburg, Md

Arditty, S., Schmitt, V., Giermanska-Kahn, J., & Leal-Calderon, F. (2004). Materials based on solid-stabilized emulsions. *Journal of Colloid and Interface Science*, 275, 659-664

Aryanti, N., Hou, R., & Williams, R.A. (2009). Performance of a rotating membrane emulsifier for production of coarse droplets. *Journal of Membrane Science*, 326, 9-18

Aryanti, N., Williams, R.A., Hou, R., & Vladisavljević, G.T. (2006). Performance of rotating membrane emulsification for o/w production. *Desalination*, 200, 572-574

Aserin, A. (2008). Multiple Emulsions, Technology and Applications John Wiley & Sons, Inc.

Azzam, M.O.J. & Omari, R.M. (2002). Stability of egg white-stabilized edible oil emulsions using conductivity technique. *Food Hydrocolloids*, 16, 105-110

Barthel, H., Binks, B. P., Dyab, A., & Fletcher, P. (2003). Multiple Emulsions, 10/376,811[US2003/0175317 A1] (patent)

Benichou, A., Aserin, A., & Garti, N. (2004). Double emulsions stabilized with hybrids of natural polymers for entrapment and slow release of active matters. *Advances in Colloid and Interface Science*, 108-109, 29-41

Benichou, A., Aserin, A., & Garti, N. (2007). W/O/W double emulsions stabilized with WPI-polysaccharide complexes. *Colloids and Surfaces A: Physicochemical and Engineering Aspects*, 294, 20-32

Benjamins, J., Lyklema, J., & Lucassen-Reynders, E.H. (2006). Compression/Expansion Rheology of Oil/Water Interfaces with Adsorbed Proteins. Comparison with the Air/Water Surface. *Langmuir*, 22, 6181-6188

Binks, B. (2002). Particles as surfactants − similarities and differences. *Current Opinion in Colloid & Interface Science*, 7, 21-41

Bonnet, M., Cansell, M., Berkaoui, A., Ropers, M.H., Anton, M., & Leal-Calderon, F. (2009). Release rate profiles of magnesium from multiple W/O/W emulsions. *Food Hydrocolloids*, 23, 92-101

Bos, A. & van Vliet, T. (2001). Interfacial rheological properties of adsorbed protein layers and surfactants: a review. *Advances in Colloid and Interface Science*, 91, 437-471

Charcosset, C., Limayem, I., & Fessi, H. (2004). The membrane emulsification process - a review. *Journal of Chemical Technology & Biotechnology*, 79, 209-218

Charcosset, C. (2009). Preparation of emulsions and particles by membrane emulsification for the food processing industry. *Journal of Food Engineering*, 92, 241-249

Chattopadhyay, A.K., Ghaicha, L., Oh, S.G., & Shah, D.O. (2002). Salt effects on monolayers and their contribution to surface viscosity. *The Journal of Physical Chemistry*, 96, 6509-6513

Cheng, J., Chen, J.F., Zhao, M., Luo, Q., Wen, L.X., & Papadopoulos, K.D. (2007). Transport of ions through the oil phase of W1/O/W2 double emulsions. *Journal of Colloid and Interface Science*, 305, 175-182

Cheng, C.J., Chu, L.Y., Xie, R., & Wang, X.W. (2008). Hydrophobic Modification and Regeneration of Shirasu Porous Glass Membranes on Membrane Emulsification Performance. *Chemical Engineering & Technology*, 31, 377-383

Christov, N.C., Ganchev, D.N., Vassileva, N.D., Denkov, N.D., Danov, K.D., & Kralchevsky, P.A. (2002). Capillary mechanisms in membrane emulsification: oil-in-water emulsions stabilized by Tween 20 and milk proteins. *Colloids and Surfaces A: Physicochemical and Engineering Aspects*, 209, 83-104

Danov, K.D., Danova, D.K., & Kralchevsky, P.A. (2007). Hydrodynamic forces acting on a microscopic emulsion drop growing at a capillary tip in relation to the process of membrane emulsification. *Journal of Colloid and Interface Science*, 316, 844-857

Derkach, S., Kragel, J., & Miller, R. (2009). Methods of measuring rheological properties of interfacial layers (Experimental methods of 2D rheology). *Colloid Journal*, 71, 1-17

Dickinson, E., Evison, J., Owusu, R.K., (1991). Preparation of fine protein-stabilized water-in-oil-in-water emulsions. *Food Hydrocolloids*, 5, 481-484

Dickinson, E. (1992). An Introduction to Food Colloids Oxford University Press.

Dickinson, E., Evison, J., Owusu, R. K., & Williams, A. (1994), Protein-Stabilized water-in-oil-in-water emulsions, in: Gums and Stabilisers for the Food Industry 7, G. O. Philips & P. A. Williams, Eds., Oxford: Oxford University Press, pp. 91-101

Dickinson, E. & Akhtar, M. (2001), Water-in-oil-in-water multiple emulsions stabilized by polymeric and natural emulsifiers, in: Food Hydrocolloids, Fundamentals of Formulation, E. Dickinson & R. Miller, Eds., Cambridge: The Royal Society of Chemisty, pp.133-144

Dickinson, E. (2009), Hydrocolloids and emulsion stability, in: Handbook of Hydrocolloids (2nd ed.), G. O. Phillips & P. A. Williams, Eds., Woodhead Publishing, pp. 23-49

Dragosavac, M.M., Sovilj, M.N., Kosvintsev, S.R., Holdich, R.G., & Vladisavljević, G.T. (2008). Controlled production of oil-in-water emulsions containing unrefined pumpkin seed oil using stirred cell membrane emulsification. *Journal of Membrane Science*, 322, 178-188

Egidi, E., Gasparini, G., Holdich, R.G., Vladisavljević, G.T., & Kosvintsev, S.R. (2008). Membrane emulsification using membranes of regular pore spacing: Droplet size and uniformity in the presence of surface shear. *Journal of Membrane Science*, 323, 414-420

Fechner, A., Knöth, A., Scherze, I., & Muschiolik, G. (2007). Stability and release properties of double emulsions stabilised by caseinate-dextran conjugates. *Food Hydrocolloids*, 21, 943-952

Fellows, P.J. (2000). Food Processing Technology - Principles and Practice, (2nd ed.) Woodhead Publishing.

Fennell, E. & Wennerstrom, H. (1994). The colloidal domain: where physics, chemistry, biology and technology meet. VCH Publishers.

Ficheux, M.F., Bonakdar, L., Leal-Calderon, F., & Bibette, J. (1998). Some Stability Criteria for Double Emulsions. *Langmuir*, 14, 2702-2706

Garti, N., Magdassi, S., & Whitehill, D. (1985). Transfer phenomena across the oil phase in water-oil-water multiple emulsions evaluated by Coulter counter: 1. Effect of emulsifier 1 on water permeability. *Journal of Colloid and Interface Science*, 104, 587-591

Garti, N. (1997a). Double emulsions: scope, limitations and new achievements. *Colloids and Surfaces A: Physicochemical and Engineering Aspects*, 123-124, 233-246

Garti, N. (1997b). Progress in Stabilization and Transport Phenomena of Double Emulsions in Food Applications. *Lebensmittel-Wissenschaft und-Technologie*, 30, 222-235

Geiger, S., Tokgoz, S., Fructus, A., Jager-Lezer, N., Seiller, M., Lacombe, C., & Grossiord, J.L. (1998). Kinetics of swelling-breakdown of a W/O/W multiple emulsion: possible mechanisms for the lipophilic surfactant effect. *Journal of Controlled Release*, 52, 99-107

Georgieva, D., Schmitt, V., Leal-Calderon, F., & Langevin, D. (2009). On the Possible Role of Surface Elasticity in Emulsion Stability. *Langmuir,* 25, 5565-5573

Giangiacomo, R. (2006). Study of water-sugar interactions at increasing sugar concentration by NIR spectroscopy. *Food Chemistry*, 96, 371-379

Gijsbertsen-Abrahamse, A.J., van der Padt, A., & Boom, R.M. (2004). Status of cross-flow membrane emulsification and outlook for industrial application. *Journal of Membrane Science*, 230, 149-159

González-Ochoa, H., Ibarra-Bracamontes, L., & Rauz-Lara, J.L. (2003). Two-Stage Coalescence in Double Emulsions. *Langmuir*, 19, 7837-7840

Gunes, D.Z., Clain, X., Breton, O., Mayor, G., & Burbidge, A.S. (2010). Avalanches of coalescence events an local extensional flows-Stabilisation or destabilisation due to surfactant. *Journal of Colloid and Interface Science*, 343, 79-86

Hasenhuettl, G.L. & Hartel, R.W. (2008). Food Emulsifiers and Their Applications, (2nd ed.) Springer.

Hiemenz, P. (1977). Principles of colloid and surface chemistry, Marcel Dekker.

Howard, R.L. & Sollman, T. (1924). The Interfacial Tension of Some Aqueous Solutions against Oils, as corrected for Specific Gravity. *The Journal of Physical Chemistry*, 28, 1291-1296

Hsu, J.P. & Nacu, A. (2003). Behavior of soybean oil-in-water emulsion stabilized by nonionic surfactant. *Journal of Colloid and Interface Science*, 259, 374-381

Hunter, R.J. (1987). Foundations of colloid science. Vol 1., Oxford: Clarendon.

Hutteau, F., Mathlouthi, M., Portmann, M.O., & Kilcast, D. (1998). Physicochemical and psychophysical characteristics of binary mixtures of bulk and intense sweeteners. *Food Chemistry*, 63, 9-16

Israelachvili, J.N. (2011). Intermolecular and surface forces, (3rd ed.), Academic Press.

Jager-Lezer, N., Terrisse, I., Bruneau, F., Tokgoz, S., Ferreira, L., Clausse, D., Seiller, M., & Grossiord, J.L. (1997). Influence of lipophilic surfactant on the release kinetics of water-soluble molecules entrapped in a W/O/W multiple emulsion. *Journal of Controlled Release*, 45, 1-13

Jiao, J. & Burgess, D. J. (2008), Multiple Emulsion Stability: Pressure Balance and Interfacial Film Strength, in: Multiple Emulsions, Technology and Applications, A. Aserin, ed., Wiley & Sons, Inc., pp. 1-28

Joscelyne, S.M. & Trägårdh, G. (1999). Food emulsions using membrane emulsification: conditions for producing small droplets. *Journal of Food Engineering*, 39, 59-64

Joscelyne, S.M. & Trägårdh, G. (2000). Membrane emulsification -- a literature review. *Journal of Membrane Science*, 169, 107-117

Kabalnov, A. (1998). Thermodynamic and theoretical aspects of emulsions and their stability. *Current Opinion in Colloid & Interface Science*, 3, 270-275

Kabalnov, A.S. & Shchukin, E.D. (1992). Ostwald ripening theory: applications to fluorocarbon emulsion stability. *Advances in Colloid and Interface Science*, 38, 69-97

Kargar, M., Fayazmanesh, K., Alavi, M., Spyropoulos, F., & Norton, I.T. (2011). Investigation into the potential ability of Pickering emulsions (food-grade particles) to enhance the oxidative stability of oil-in-water emulsions. *Journal of Colloid and Interface Science*, 357, 527-533

Katoh, R., Asano, Y., Furuya, A., Sotoyama, K., & Tomita, M. (1996). Preparation of food emulsions using a membrane emulsification system. *Journal of Membrane Science*, 113, 131-135

Kawakatsu, T., Trägårdh, G., Trägårdh, C., Nakajima, M., Oda, N., & Yonemoto, T. (2001). The effect of the hydrophobicity of microchannels and components in water and oil phases on droplet formation in microchannel water-in-oil emulsification. *Colloids and Surfaces A: Physicochemical and Engineering Aspects*, 179, 29-37

Kawashima, Y., Hino, T., Takeuchi, H., & Niwa, T. (1992). Stabilisation of Water/Oil/Water Multiple Emulsion With Hypertonic Inner Aqueous Phase. *Chemical & Pharmaceutical Bulletin*, 40, 1240-1246

Kim, H.J., Decker, E.A., & Julian McClements, D. (2006). Preparation of multiple emulsions based on thermodynamic incompatibility of heat-denatured whey protein and pectin solutions. *Food Hydrocolloids*, 20, 586-595

Klein, M., Aserin, A., Ishai, P.B., & Garti, N. (2010). Interactions between whey protein isolate and gum Arabic. *Colloids and Surfaces B: Biointerfaces*, 79, 377-383

Kobayashi, I., Nakajima, M., Chun, K., Kikuchi, Y., & Fujita, H. (2002). Silicon array of elongated through-holes for monodisperse emulsion droplets. *AIChE Journal*, 48, 1639-1644

Kobayashi, I., Nakajima, M., & Mukataka, S. (2003). Preparation characteristics of oil-in-water emulsions using differently charged surfactants in straight-through microchannel

emulsification. *Colloids and Surfaces A: Physicochemical and Engineering Aspects*, 229, 33-41

Kukizaki, M. & Goto, M. (2007). Preparation and characterization of a new asymmetric type of Shirasu porous glass (SPG) membrane used for membrane emulsification. *Journal of Membrane Science*, 299, 190-199

Kukizaki, M. (2009). Shirasu porous glass (SPG) membrane emulsification in the absence of shear flow at the membrane surface: Influence of surfactant type and concentration, viscosities of dispersed and continuous phases, and transmembrane pressure. *Journal of Membrane Science*, 327, 234-243

Leal-Calderon, F., Thivilliers, F., & Schmitt, V. (2007). Structured emulsions. *Current Opinion in Colloid & Interface Science*, 12, 206-212

Lepercq-Bost, E., Giorgi, M.L., Isambert, A., & Arnaud, C. (2008). Use of the capillary number for the prediction of droplet size in membrane emulsification. *Journal of Membrane Science*, 314, 76-89

Leser, M.E., Acquistapace, S., Cagna, A., Makievski, A.V., & Miller, R. (2005). Limits of oscillation frequencies in drop and bubble shape tensiometry. *Colloids and Surfaces A: Physicochemical and Engineering Aspects*, 261, 25-28

Lesmes, U. & McClements, D.J. (2009). Structure-function relationships to guide rational design and fabrication of particulate food delivery systems. *Trends in Food Science & Technology*, 20, 448-457

Li, Y.M., Xu, G.Y., Xin, X., Cao, X.R., & Wu, D. (2008). Dilational surface viscoelasticity of hydroxypropyl methyl cellulose and CnTAB at air-water surface. *Carbohydrate Polymers*, 72, 211-221

Lindfors, K.R. (1924). Surface Tension of Sugar Factory Products. *Industrial & Engineering Chemistry*, 16, 813-816

Malone, M.E., Appelqvist, I.A.M., Norton, I.T. (2003). Oral behaviour of food hydrocolloids and emulsions. Part 2. Taste and aroma release. *Food Hydrocolloids*, 17, 775-784

Magdassi, S., Garti, N. (1984). Release of electrolytes in multiple emulsions: Coalescence and breakdown or diffusion through oil phase? *Colloids and Surfaces*, 12, 367-373

Magdassi, S., Frenkel, M., Garti, N., & Kasan, R. (1984). Multiple emulsions II: HLB shift caused by emulsifier migration to external interface. *Journal of Colloid and Interface Science*, 97, 374-379

Matsumoto, S., Kita, Y., & Yonezawa, D. (1976). An attempt at preparing water-in-oil-in-water multiple-phase emulsions. *Journal of Colloid and Interface Science*, 57, 353-361

McClements, D.J. & Decker, E.A. (2000). Lipid Oxidation in Oil-in-Water Emulsions: Impact of Molecular Environment on Chemical Reactions in Heterogeneous Food Systems. *Journal of Food Science*, 65, 1270-1282

McClements, D.J. (2005). Food Emulsions; Principles, Practices and Techniques, (2nd ed.) CRS Press.

Meredith, R.E. & Tobias, C.W. (1960). Conductivities in emulsions. *Journal of the Electrochemical Society*, 108, 286-290

Mezzenga, R., Folmer, B.M., & Hughes, E. (2004). Design of Double Emulsions by Osmotic Pressure Tailoring. *Langmuir*, 20, 3574-3582

Mezzenga, R. (2007). Equilibrium and non-equilibrium structures in complex food systems. *Food Hydrocolloids*, 21, 674-682

Michaut, F., Perrin, P., & Hébraud, P. (2004). Interface Composition of Multiple Emulsions: Rheology as a Probe. *Langmuir*, 20, 8576-8581

Miller, R. & Kretzschmar, G. (1991). Adsorption kinetics of surfactants at fluid interfaces. *Advances in Colloid and Interface Science*, 37, 97-121

Mine, Y., Shimizu, M., & Nakashima, T. (1996). Preparation and stabilization of simple and multiple emulsions using a microporous glass membrane. *Colloids and Surfaces B: Biointerfaces*, 6, 261-268

Murray, B.S., Ventura, A., & Lallemant, C. (1998). Dilatational rheology of protein+non-ionic surfactant films at air-water and oil-water interfaces. *Colloids and Surfaces A: Physicochemical and Engineering Aspects*, 143, 211-219

Murray, B.S. (2002). Interfacial rheology of food emulsifiers and proteins. *Current Opinion in Colloid & Interface Science*, 7, 426-431

Muschiolik, G., Scherze, I., Preissler, P., Weiss, J., Knoth, A., & Fechner, A. (2006). Multiple Emulsions – Preparation and Stability. In proceedings of IUFoSt, downloaded July 2011, http://iufost.edpsciences.org/index.php?option=com_article&access=doi&doi=10.1051/IUFoST:20060043&Itemid=129.

Muschiolik, G. (2007). Multiple emulsions for food use. *Current Opinion in Colloid & Interface Science*, 12, 213-220

Myers, D. (1992). Surfactant science and technology, (2nd ed.) VCH Publishers.

Nakashima, T., Shimizu, M., & Kukizaki, M. (1991). Membrane Emulsification Operation Manual, (1st ed.) Japan, Industrial Research Institute of Miyazaki Prefecture.

Nakashima, T., Shimizu, M., & Kukizaki, M. (2000). Particle control of emulsion by membrane emulsification and its applications. *Advanced Drug Delivery Reviews*, 45, 47-56

Noisuwan, A., Hemar, Y., Wilkinson, B., & Bronlund, J.E. (2009). Dynamic rheological and microstructural properties of normal and waxy rice starch gels containing milk proteins. *Starch/Stärke*, 61, 214-227

Norton, I., Fryer, P., & Moore, S. (2006). Product/Process integration in food manufacture: Engineering sustained health. *AIChE Journal*, 52, 1632-1640

Okochi, H. & Nakano, M. (1997). Comparative study of two preparation methods of w/o/w emulsions: stirring and membrane emulsification. *Chemical & Pharmaceutical Bulletin*, 45, 1323-1326

Okochi, H. & Nakano, M. (2000). Preparation and evaluation of w/o/w type emulsions containing vancomycin. *Advanced Drug Delivery Reviews*, 45, 5-26

Okushima, S., Nisisako, T., Torii, T., & Higuchi, T. (2004). Controlled Production of Monodisperse Double Emulsions by Two-Step Droplet Breakup in Microfluidic Devices. *Langmuir*, 20, 9905-9908

Opawale, F.O. & Burgess, D.J. (1998). Influence of Interfacial Properties of Lipophilic Surfactants on Water-in-Oil Emulsion Stability. *Journal of Colloid and Interface Science*, 197, 142-150

Owusu, R.K. & Zhu, Q-H. (1996). Interfacial parameters for selected Spans and Tweens at the hydrocarbon-water interface, *Food Hydrocolloids*, 10, 27-30

Padron-Aldana, G. (2005). Effect of surfactants on droplet size distribution in a batch, rotor-stator mixer. PhD University of Maryland.

Palzer, S. (2009). Food structures for nutrition, health and wellness. *Trends in Food Science & Technology*, 20, 194-200

Patist, A., Kanicky, J.R., Shukla, P.K., & Shah, D.O. (2002). Importance of Micellar Kinetics in Relation to Technological Processes. *Journal of Colloid and Interface Science*, 245, 1-15

Pawlik, A., Cox, P.W., & Norton I.T. (2010). Food grade duplex emulsions designed and stabilised with different osmotic pressures. *Journal of Colloid and Interface Science*, 352, 59-67

Pays, K., Giermanska-Kahn, J., Pouligny, B., Bibette, J., & Leal-Calderon, F. (2001). Coalescence in Surfactant-Stabilized Double Emulsions. *Langmuir*, 17, 7758-7769

Pays, K., Giermanska-Kahn, J., Pouligny, B., Bibette, J., & Leal-Calderon, F. (2002). Double emulsions: how does release occur? *Journal of Controlled Release*, 79, 193-205

Peng, S.J. & Williams, R.A. (1998). Controlled Production of Emulsions Using a Crossflow Membrane: Part I: Droplet Formation from a Single Pore. *Chemical Engineering Research and Design*, 76, 894-901

Pickering, S.U. (1907). CXCVI.-Emulsions. *Journal of the Chemical Society, Transactions*, 91, 2001-2021

Roberts, P. J. W. & Webster, D. R. (2002), Turbulent diffusion, in: Environmental fluid mechanics: theories and applications, H. H. Shen, Ed., American Society of Civil Engineers, pp. 7-45

Rodriguez-Patino, J.M., Rodriguez Nino, M.R., & Sanchez, C.C. (1999). Adsorption of Whey Protein Isolate at the Oil-Water Interface as a Function of Processing Conditions: A Rheokinetic Study. *Journal of Agricultural and Food Chemistry*, 47, 2241-2248

Rousset, P., Sellappan, P., & Daoud, P. (2002). Effect of emulsifiers on surface properties of sucrose by inverse gas chromatography. *Journal of Chromatography* A, 969, 97-101

Sapei, L., Naqvi, M.A., Rousseau, D., (2012). Stability and release properties of double emulsions for food applications. *Food Hydrocolloids*, 27, 316-323

Schadler, V. & Windhab, E.J. (2006). Continuous membrane emulsification by using a membrane system with controlled pore distance. *Desalination*, 189, 130-135

Scherze, I., Marzilger, K., & Muschiolik, G. (1999). Emulsification using micro porous glass (MPG): surface behaviour of milk proteins. *Colloids and Surfaces B: Biointerfaces*, 12, 213-221

Scherze, I., Knöfel, R., & Muschiolik, G. (2005). Automated image analysis as a control tool for multiple emulsions. *Food Hydrocolloids*, 19, 617-624

Schramm, L. & Stasuik, E. (2006), Emulsions: Overview, in: Finely dispersed particles, Micro-, Nano-, and Atto-Engineering, A. M. Spasic & J. P. Hsu, Eds., CRC Taylor & Francis, pp. 79-112

Schroder, V., Behrend, O., & Schubert, H. (1998). Effect of Dynamic Interfacial Tension on the Emulsification Process Using Microporous, Ceramic Membranes. *Journal of Colloid and Interface Science*, 202, 334-340

Schubert, H. & Engel, R. (2004). Product and Formulation Engineering of Emulsions. *Chemical Engineering Research and Design*, 82, 1137-1143

Seifriz, W. (1923). Studies in emulsions. *American Journal of Physiology*, 66, 738-749

Su, J., Flanagan, J., Hemar, Y., & Singh, H. (2006). Synergistic effects of polyglycerol ester of polyricinoleic acid and sodium caseinate on the stabilisation of water-oil-water emulsions. *Food Hydrocolloids*, 20, 261-268

Su, J., Flanagan, J., & Singh, H. (2008). Improving encapsulation efficiency and stability of water-in-oil-in-water emulsions using a modified gum arabic (Acacia (sen) SUPER GUM(TM)). *Food Hydrocolloids*, 22, 112-120

Sugiura, S., Nakajima, M., Oda, T., Satake, M., & Seki, M. (2004a). Effect of interfacial tension on the dynamic behavior of droplet formation during microchannel emulsification. *Journal of Colloid and Interface Science*, 269, 178-185

Sugiura, S., Nakajima, M., Yamamoto, K., Iwamoto, S., Oda, T., Satake, M., & Seki, M. (2004b). Preparation characteristics of water-in-oil-in-water multiple emulsions using microchannel emulsification. *Journal of Colloid and Interface Science*, 270, 221-228

Surh, J., Vladisavljević, G.T., Mun, S., & McClements, D.J. (2006). Preparation and Characterization of Water/Oil and Water/Oil/Water Emulsions Containing Biopolymer-Gelled Water Droplets. *Journal of Agricultural and Food Chemistry*, 55, 175-184

Tadros, T. & Vincent, B. (1983), Emulsion Stability, in: Encyclopedia of emulsion technology, Vol. 1, Basic Theory, P. Becher, Ed., Marcel Dekker, Inc., pp. 129-285

Tadros, T. (1994). Fundamental principles of emulsion rheology and their applications. *Colloids and Surfaces A: Physicochemical and Engineering Aspects*, 91, 39-55

Taylor, P. (1998). Ostwald ripening in emulsions. *Advances in Colloid and Interface Science*, 75, 107-163

Timgren, A., Trägårdh, G., & Trägårdh, C. (2009). Effects of cross-flow velocity, capillary pressure and oil viscosity on oil-in-water drop formation from a capillary. *Chemical Engineering Science*, 64, 1111-1118

Timgren, A., Trägårdh, G., & Trägårdh, C. (2010). A model for drop size prediction during cross-flow emulsification. *Chemical Engineering Research and Design*, 88, 229-238

Timgren, A., Rayner, M., Sjöö, M. and Dejmek, P. (2011). Starch particles for food based Pickering emulsions, Procedia Food Science, 1, 95 – 103

Unilever, Nutrition; Diet, health & the fight against obesity company's mission (2012), viewed January 2012, http://www.unilever.co.uk/brands/nutrition/diethealthandthefightagainstobesity/.

Utada, A.S., Lorenceau, E., Link, A.R., Kaplan, D.R., Stone, H.A., & Weitz, D.A. (2005). Monodisperse double emulsions generated from a micocapillary device. *Science*, 308, 537-541

Utomo, A.T., Baker, M., & Pacek, A.W. (2008). Flow pattern, periodicity and energy dissipation in a batch rotor-stator mixer. *Chemical Engineering Research and Design*, 86, 1397-1409

van der Graaf, S., Schroen, C.G.P.H., & Boom, R.M. (2005). Preparation of double emulsions by membrane emulsification--a review. *Journal of Membrane Science*, 251, 7-15

van der Ven, C., Gruppen, H., de Bont, D.B.A., & Voragen, A.G.J. (2001). Emulsion Properties of Casein and Whey Protein Hydrolysates and the Relation with Other Hydrolysate Characteristics. *Journal of Agricultural and Food Chemistry*, 49, 5005-5012

Vladisavljević, G.T. & Schubert, H. (2002). Preparation and analysis of oil-in-water emulsions with a narrow droplet size distribution using Shirasu-porous-glass (SPG) membranes. *Desalination*, 144, 167-172

Vladisavljević, G.T., Tesch, S., & Schubert, H. (2002). Preparation of water-in-oil emulsions using microporous polypropylene hollow fibers: influence of some operating parameters on droplet size distribution. *Chemical Engineering and Processing*, 41, 231-238

Vladisavljević, G.T. & Schubert, H. (2003). Influence of process parameters on droplet size distribution in SPG membrane emulsification and stability of prepared emulsion droplets. *Journal of Membrane Science*, 225, 15-23

Vladisavljević, G.T., Shimizu, M., & Nakashima, T. (2004). Preparation of monodisperse multiple emulsions at high production rates by multi-stage premix membrane emulsification. *Journal of Membrane Science*, 244, 97-106

Vladisavljević, G.T., Shimizu, M., & Nakashima, T. (2005). Permeability of hydrophilic and hydrophobic Shirasu-porous-glass (SPG) membranes to pure liquids and its microstructure. *Journal of Membrane Science*, 250, 69-77

Vladisavljević, G.T. & Williams, R.A. (2005). Recent developments in manufacturing emulsions and particulate products using membranes. *Advances in Colloid and Interface Science*, 113, 1-20

Vladisavljević, G.T. & Williams, R.A. (2006). Manufacture of large uniform droplets using rotating membrane emulsification. *Journal of Colloid and Interface Science*, 299, 396-402

Vladisavljević, G. T., Nakashima, T., Shimizu, M., Schubert, H., & Nakajima, M. (2006a), Production of monodispersed emulsions using Shirasu Porous Glass Membranes, in: Finely dispersed particles. Micro-, Nano-, and Atto-Engineering, A. M. Spasic & J. P. Hsu, Eds., CRC Press, Taylor & Francis Group, pp. 396-429

Vladisavljević, G.T., Shimizu, M., & Nakashima, T. (2006b). Production of multiple emulsions for drug delivery systems by repeated SPG membrane homogenisation: Influence of mean pore size, interfacial tension and continuous phase viscosity. *Journal of Membrane Science*, 284, 373-383

Vladisavljević, G.T., Kobayashi, I., Nakajima, M., Williams, R.A., Shimizu, M., & Nakashima, T. (2007). Shirasu Porous Glass membrane emulsification: Characterisation of membrane structure by high-resolution X-ray microtomography and microscopic observation of droplet formation in real time. *Journal of Membrane Science*, 302, 243-253

Walstra, P. (1983), Formation of Emulsions, in: Encyclopedia of Emulsion Technology, P. Becher, Ed., Marcel Dekker, Inc., pp. 57-128

Walstra, P. (2003). Physical Chemistry of Foods, Marcel Dekker Inc.

Wang, Z. & Wang, S. (2000). Effect of continuous phase viscosity on membrane emulsification. *Chinese Journal of Chemical Engineering*, 8, 108-112

Ward, A.F.H. & Tordai, L. (1946). Time-Dependence of Boundary Tensions of Solutions I. The Role of Diffusion in Time-Effects. *The Journal of Chemical Physics*, 14, 453-461

Weiss, J., Scherze, I., & Muschiolik, G. (2005). Polysaccharide gel with multiple emulsion. *Food Hydrocolloids*, 19, 605-615

Wen, L. & Papadopoulos, K.D. (2001). Visualization of water transport in $W_1/O/W_2$ emulsions. *Colloids and Surfaces A: Physicochemical and Engineering Aspects*, 174, 159-167

World Health Organization (WHO), 10 facts on obesity (2010), viewed June 2011, http://www.who.int/features/factfiles/obesity/en/.

Williams, R.A., Peng, S.J., Wheeler, D.A., Morley, N.C., Taylor, D., Whalley, M., & Houldsworth, D.W. (1998). Controlled Production of Emulsions Using a Crossflow Membrane: Part II: Industrial Scale Manufacture. *Chemical Engineering Research and Design*, 76, 902-910

Xu, J.H., Luo, G.S., Chen, G.G., & Wang, J.D. (2005). Experimental and theoretical approaches on droplet formation from a micrometer screen hole. *Journal of Membrane Science*, 266, 121-131

Yasuno, M., Nakajima, M., Iwamoto, S., Maruyama, T., Sugiura, S., Kobayashi, I., Shono, A., & Satoh, K. (2002). Visualization and characterization of SPG membrane emulsification. *Journal of Membrane Science*, 210, 29-37

Yuan, Q., Aryanti, N., Hou, R., & Williams, R.A. (2009a). Performance of slotted pores in particle manufacture using rotating membrane emulsification. *Particuology*, 7, 114-120

Yuan, Q., Williams, R.A., & Biggs, S. (2009b). Surfactant selection for accurate size control of microcapsules using membrane emulsification. *Colloids and Surfaces A: Physicochemical and Engineering Aspects*, 347, 97-103

Zhang, Y., and Cremer, P.S. (2006). Interactions between macromolecules and ions: the Hofmeister series. *Current Opinion in Chemical Biology*, 10, 658-663